NUREG/IA-0084
NT 163 (90)

International Agreement Report

Relevant Results Obtained in the Analysis of LOBI/MOD2 Natural Circulation Experiment A2-77A

Prepared by
F. D'Auria, G. M. Galassi

Universita' Degli Studi Di Pisa
Dipartimento Di Costruzioni Meccaniche E Nucleari
Pisa, Italy

Office of Nuclear Regulatory Research
U.S. Nuclear Regulatory Commission
Washington, DC 20555

April 1992

Prepared as part of
The Agreement on Research Participation and Technical Exchange
under the International Thermal-Hydraulic Code Assessment
and Application Program (ICAP)

Published by
U.S. Nuclear Regulatory Commission

Available from

Superintendent of Documents
U.S. Government Printing Office
P.O. Box 37082
Washington, D.C. 20013-7082

and

National Technical Information Service
Springfield, VA 22161

NUREG/IA-0084
NT 163 (90)

International Agreement Report

Relevant Results Obtained in the Analysis of LOBI/MOD2 Natural Circulation Experiment A2-77A

Prepared by
F. D'Auria, G. M. Galassi

Universita' Degli Studi Di Pisa
Dipartimento Di Costruzioni Meccaniche E Nucleari
Pisa, Italy

Office of Nuclear Regulatory Research
U.S. Nuclear Regulatory Commission
Washington, DC 20555

April 1992

Prepared as part of
The Agreement on Research Participation and Technical Exchange
under the International Thermal-Hydraulic Code Assessment
and Application Program (ICAP)

Published by
U.S. Nuclear Regulatory Commission

NOTICE

This report documents work performed under the sponsorship of the Italian Conitato Nazionale Per La Ricerca e Per Lo Sviluppo Dell' Energia Nucleare e Delle Energie Alternative (ENEA) of Italy. The information in this report has been provided to the USNRC under the terms of an information exchange agreement between the United States and Italy (Technical Exchange and Cooperation Agreement Between the United States Nuclear Regulatory Commission and the Conitato Nazionale Per La Ricerca e Per Lo Sviluppo Dell' Energia Nucleare e Delle Energie Alternative (ENEA) of Italy in the field of reactor safety research and development, April 1, 1981). Italy has consented to the publication of this report as a USNRC document in order that it may receive the widest possible circulation among the reactor safety community. Neither the United States Government nor Italy or any agency thereof, or any of their employees, makes any warranty, expressed or implied, or assumes any legal liability of responsibility for any third party's use, or the results of such use, or any information, apparatus, product or process disclosed in this report, or represents that its use by such third party would not infringe privately owned rights.

Abstract

The present document describes the activities carried out at Pisa University to assess the RELAP5/MOD2 performance in the application to the natural circulation test A2-77A performed in LOBI/MOD2 facility.

Sensitivity calculations have been performed in this context, with the attempt to distinguish the code limitations from the uncertainties of the measured conditions.

The characterization of instabilities in two-phase natural circulation and the evaluation of the user effect upon the code results are special goals achieved in the frame of the A2-77A analysis. Both of these are discussed in sect. 5.

TABLE OF CONTENTS

LIST OF FIGURES IN THE TEXT

LIST OF TABLES IN THE TEXT

ACKNOWLEDGEMENTS

Part of the work has been carried out in the framework of the European Community Shared Cost Action Program (contract 2996-06 EL ISP I).

The CEC contribution is gratefully acknowledged.

The authors wish to acknowledge the stimulating discussions with LOBI researchers Mrs. G. De Santi, L. Piplies, H. Stadtke, and B. Worth and with Prof. Mazzini of DCMN.

Mr. G. Fantappiè contributed to the analysis with basic models, and Mr. P. Lombardi performed most of the work related to the evaluation of user effect on the results.

1. INTRODUCTION

In the frame of the system codes assessment activities /1/,/2/, the DCMN of Pisa University performed the post test analysis, by RELAP5/MOD2 code, of the A2-77A test carried out in the LOBI/MOD2 experimental facility.

LOBI/MOD2 is a PWR experimental simulator installed at JRC of Ispra.

A2-77A is a natural circulation test including 1-phase, 2-phases and reflux condensing modes of natural circulation.

Actually the experiment consists of two parts wich differentiate owing to the pressures of primary and secondary sides (9.0 and 7.5 MPa for the PS pressure in two cases, respectively). Having been recognized that measured phenomena are essentially the same in the two parts of the test, it has been decided to analyze only the former part of the test (PS pressure equal to 9.0 MPa) in the present framework.

The purpose of the analysis is to assess the capabilities of an advanced code in predicting the various phases of natural circulation in a typical PWR situation; in particular mechanical non equilibrium phenomena (CCFL, stratification, etc.) are important in the test together with asymmetries in geometric and boundary conditions of the loops connected with the RPV. Besides, the values of fluid velocities and of temperature differences among the various zones of the loop, are relativelly small (much lower than typical values characterizing the nominal condition of the loop with pumps in operation) making very critic the achievement of steady conditions in the code calculations.

The instabilities occurring in the main quantities during the two-phase period and the influence of user upon the code results are discussed into detail.

2. EXPERIMENT DESCRIPTION

2.1 - LOBI/MOD2 test facility

The LOBI facility simulates the KWU PWR plant of Biblis (FRG). The facility (LOBI-MOD1) was built in the frame of a R&D contract between BMFT and CEC; at present it is operated by CEC.

The primary circuit is approximately 1/700 scale model of the four loops of Biblis reactor and consists of the vessel and of two loops: the triple (intact) loop representing three loops and the single loop (broken), representing one loop of the reference plant. The facility is schematically shown in Fig. 1.

The core simulator is constituted by 64 directly heated rods, arranged in a 8x8 square matrix, having the same geometrical dimensions of that in real plant: nominal heating power is 5.3 Mw.

The operating conditions (PS and SS pressures and temperatures, fluid velocities inside the bundle and the SG tubes, etc.), are typical of PWR systems.

HPIS and accumulator injections are provided in both HLs and CLs; AFW and further plant specific features (PRZ sprays and heaters, etc.), are included in the facility.

Almost 50 experiments, comprising LBLOCAs, SBLOCAs and Special Transients, have been performed up to now, roughly in ten years of operation.

A2-77A is one of the characterization tests of the facility.

2.2 - Test objectives and system configuration

The main objectives of the test are /3/:

a) to investigate the LOBI-MOD2 test facility characteristics during natural circulation conditions;
b) to analyze how the different energy transport modes of natural circulation settle in LOBI i.e:
   - subcooled single-phase natural circulation;
   - satured single-phase natural circulation;
   - two-phase natural circulation;
   - reflux condenser mode;
c) to determine the transitions between the various modes as a function of primary system mass inverntory;
d) to investigate the instrumentation capability to detect low natural circulation mass flow rates, small differential pressures and temperatures;
e) to compare LOBI results with that of other natural circulation experiments, such as those performed in PKL, Semiscale, Flecht.

Test A2-77A was performed with the integral two-loop configuration.

The main data on the system configuration are summarized in Tab. I.

In particular it should be noted that PRZ was used only to achieve the initial conditions; afterward it was valved out. Similarly, UH was removed mainly to avoid condensation in structures due to heat losses during the draining periods.

MCP were at zero speed during the whole test; no pump seal water was applied during the test. In order to limitate the asymmetries between the two loops, a "locked rotor resistance simulator" was inserted in the BL, downstream the MCP. The hydraulic characteristics of this simulator are shown in Tab. II.

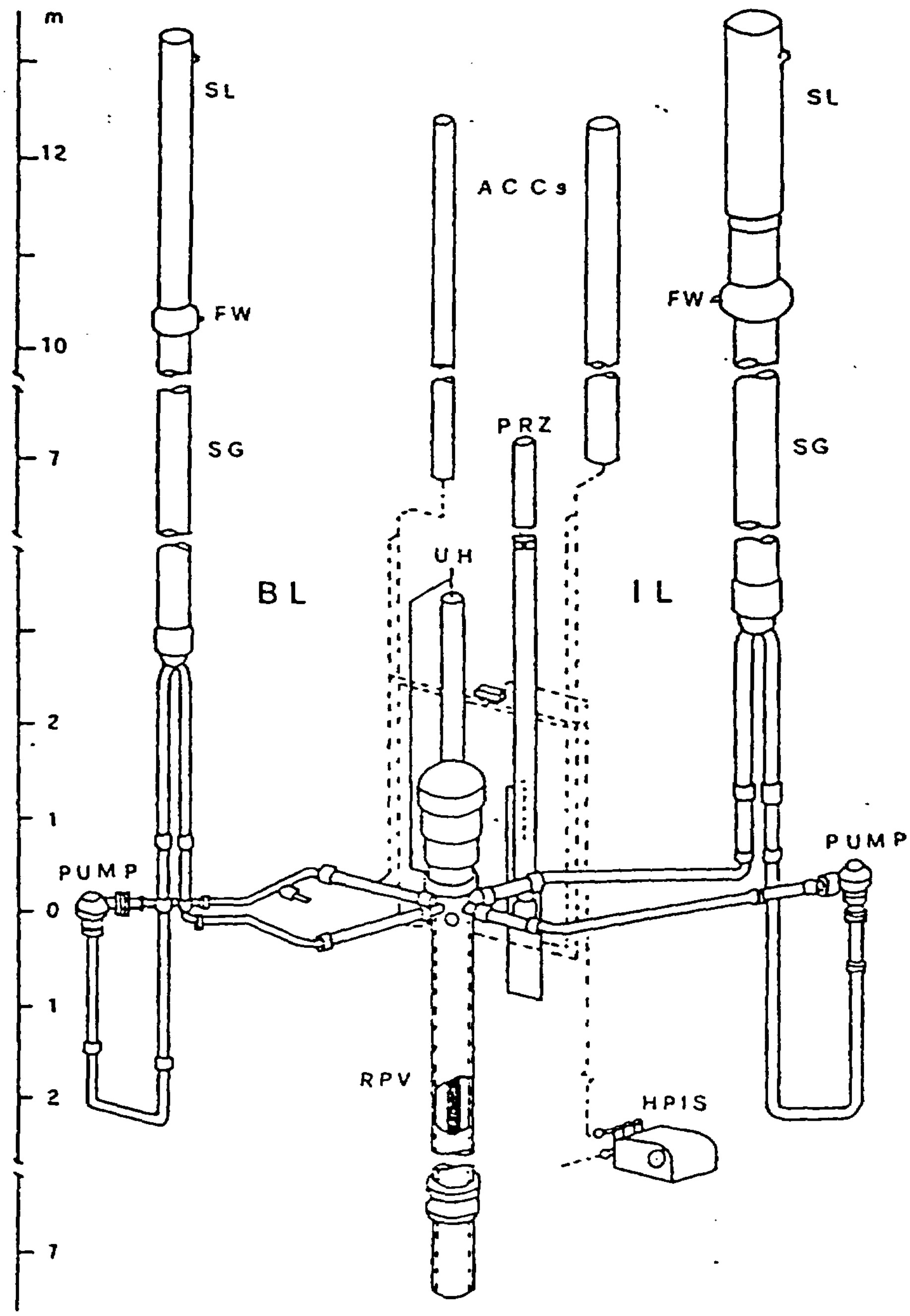

Fig. 1 - Scheme of LOBI-MOD2 facility

Break Position	**No break assembly was used in this test**
Upper Head	Not used in this test
Pressurizer	Connected to triple loop hot leg (only for steady state n° 1, see Chapter 4.2)
High pressure Injection System (HPIS)	Not used in this test
Accumulator Injection System	Not used in this test
Pump Seal Water	Not used in this test
Simulation of Pump Locked Rotor Resistance	Obtained via orifices inserted in a two-way valve located at the discharge side of the main coolant pump Triple loop: Valve always in the "full-open" position Single loop: Valve always in the "resistance" position
Auxiliary Feedwater (AFW)	used with the "feed and bleed" procedure controlled to maintain a constant secondary water level in the steam generators throughout the test.

Tab. I - LOBI/MOD2 system configuration for A2-77 test

The resistance simulates together with the resistance of the pump at zero speed, the total locked rotor resistance.

Information on resistance characteristics of this additional "Locked Rotor Resistance Simulator" is given in the following.

Δp-measurements were performed with water ($t = 22$ to $25\,^\circ C$, $\rho = 997\ kg/m^3$).

The results are:

Measurement No.	Re	ζ
1	$0.716 \cdot 10^5$	73.1
2	$1.13 \cdot 10^5$	69.7
3	$1.55 \cdot 10^5$	68.3
4	$1.77 \cdot 10^5$	66.3
5	$1.99 \cdot 10^5$	65.3

With $\Delta p = \zeta \dfrac{\rho}{2} w^2$ $\qquad$ $Re = \dfrac{w \cdot Di}{\nu}$

w ... mean velocity in the broken loop

Di ... inner diameter of broken loop (46.1 mm)

Tab. II - Hydraulic characteristics of BL "locked rotor resistance simulator"

2.3 - Initial and boundary conditions

The test started with PS pressure at 14. MPa and SS pressure at 8.65 MPa. Draining of water from LP was necessary to evaluate the loop behaviour in several natural circulation conditions. In particular, the SS pressure led to a PS pressure of about 9.0 MPa when saturation conditions where reached in PS (Fig. 2).

After each draining step the primary system was allowed to stabilize at the new conditions. The primary pressure decreased rapidly and after few draining steps reached the foreseen value of 90 bar. The test continued through saturated single-phase and two-phase natural circulation and it terminated with reflux condenser mode. The test was finished when dry-out phenomena in the uppermost sections of the core occurred, due to low level (52% of primary inventory) in the RPV.

The complete list of initial conditions for the test is given in Tab. III.

Further boundary conditions are ad follows:

a) the heating power remained constant at about 183 Kw; the axial distribution is given in Fig. 3.
b) the triple and single loop SGs were isolated throughout the test; "feed and bleed" procedure was adopted to control the secondary pressure and steam generator water level; the water level in the SG steam dome was regulated to remain costant at the initial nominal elevation by using the AFW system; the SS pressure relief valves acted at about 8.65 MPa for Part 1. The pressure was kept costant during each single part of the test via the secondary relief valves; the PS pressure stabilized out at about 9.0 MPa;
c) as already mentioned, transition between the various modes of natural circulation (single-phase, two-phase, reflux condensation) was obtained by reducing stepwise the primary inventory. Discrete amounts of water were drained from the vessel lower plenum for each step, condensed and measured in a catch tank. The system mass inventory was varied in increments of about 1% to 3% of the total initial system mass. After each draining step sufficient time was given to the primary system to stabilize out. The time duration of each cycle (including the draining period, the stabilization period and the steady state period) varied between 25 and 30 minutes. The draining mass flow was about 1 kg/min which represented a compromise between technical requirements of a slow draining process and a limitation of the test time duration.

The PS was affected by a small amount of continuous fluid leakage. This leakage could not be visually observed during the test.

To quantify the total amount of fluid lost by the primary loop, the primary system was completely refilled after the end of the test. Two independent methods were used to quantify this originally unknown mass leak /3/. On this basis the overall mass inventory decrease from the PS (drained water plus leaks) was estimated and the results are shown in Tab. IV /4/; in particular the sum of the values included in columns A and B of Tab. IV have been used as input for code calculation (17 time steps).

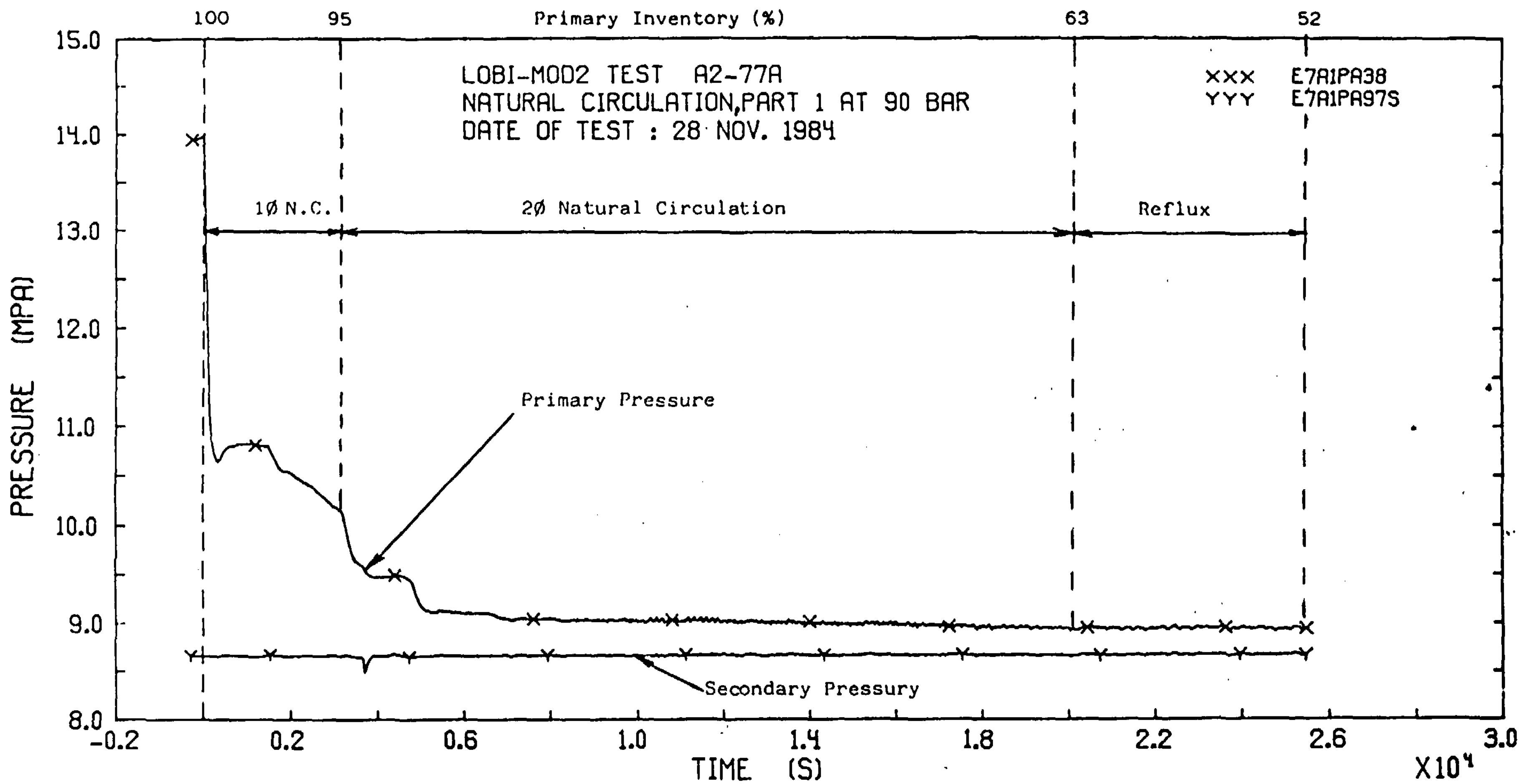

Fig. 2 - Primary and Secondary Pressure during Part 1

		Specified	Actual	Units
Primary System				
Mass flow:	– Triple Loop	(c. 1.05)	0.95	kg/s
	– Single Loop	(c 0.35)	0.3	kg/s
Pressure:	– Upper Plenum	14.0	14.0	MPa
Fluid temperatures:				
Vessel outlet	– Triple Loop	318	321	°C
	– Single Loop	318	319	°C
Vessel inlet	– Triple Loop	300	300	°C
	– Single Loop	300	296	°C
Pressurizer:		336	336	°C
Core Power:		0.17(3%)	0.183	MW
Liquid mass without pressurizer and upper head			373	kg
Liquid volume without pressurizer and upper head			0.522	m^3
Secondary System				
Auxiliary Feedwater mass flow:				
	– Triple Loop	c. 0.037	–	kg/s
	– Single Loop	c. 0.012	–	kg/s
Pressure:	– Steam Line	8.6	8.65	MPa
Temperatures:				
Steam Generator Inlet	– Triple Loop	c. 30	25	°C
	– Single Loop	c. 30	25	°C
Steam Generator Outlet	– Triple Loop	300	300	°C
	– Single Loop	300	300	°C
Downcomer Water Level:	– Triple Loop	8.33	c. 8.6	m
	– Single Loop	8.23	c. 8.9	m

Tab. III - Initial conditions for test A2-77

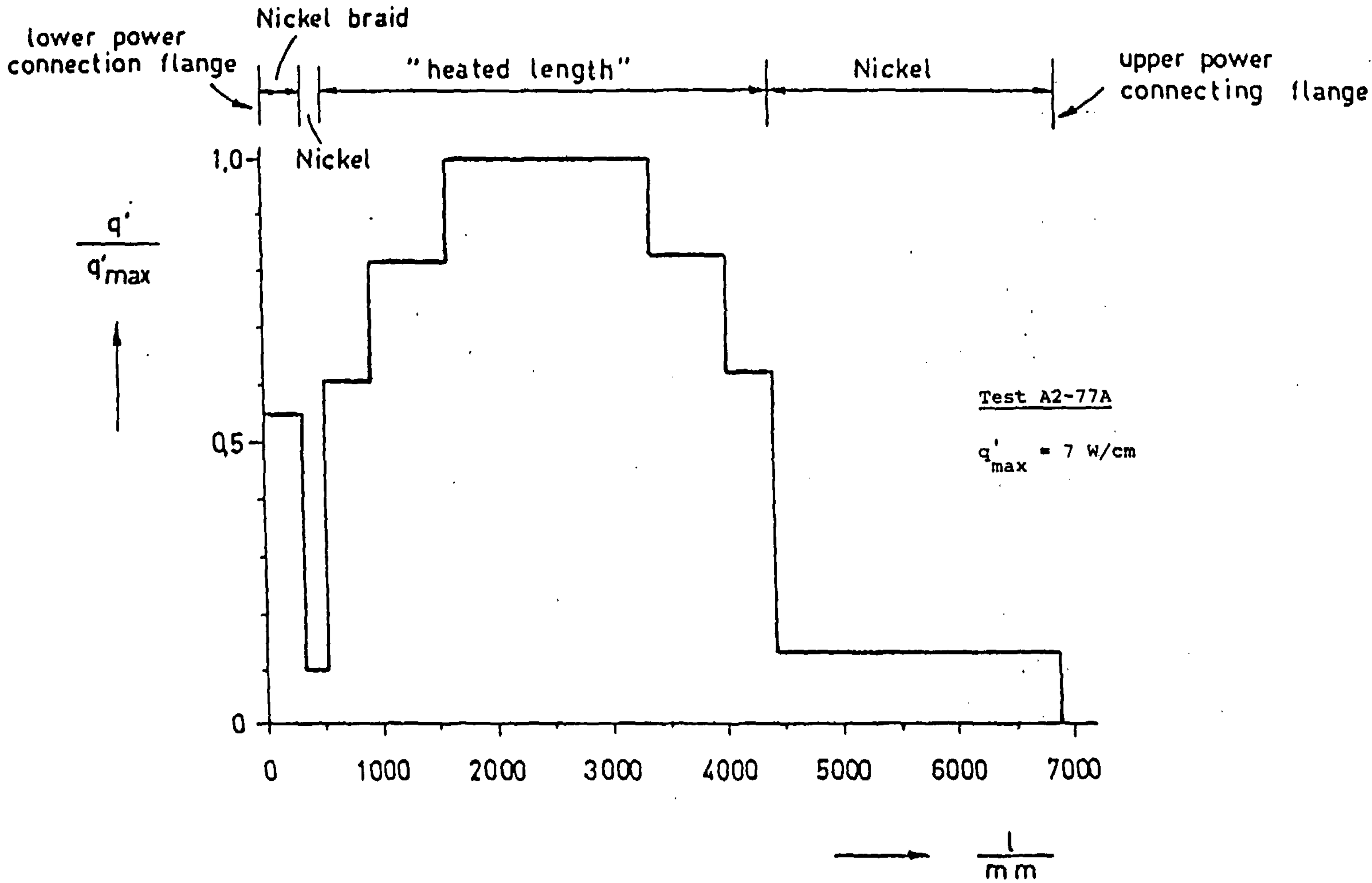

Fig. 3 - Axial Power Distribution prior to Initiation of Test

Steady state number	Last data point on tape before end of steady state. Seconds (point #)	Start of draining after steady state [Secs].	Amount water drained before steady state [kg]. Specified	Measured	Accumulated measured amount drained before steady state [kg].	Accumulated leakage estimated before steady state [kg].	Primary fluid inventory estimated [kg].	Remarks*
1	-12.8 (11)	0	0	0	0	0	370.0	Single phase subcooled natural circulation
2	1468.0 (68)	1500	6.0	6.02	6.02	3.5	360.5	Single phase saturated natural circulation
3	3158.4 (133)	3180	3.0	2.97	8.99	7.0	354.0	
4	4770.4 (195)	4800	3.0	2.94	11.93	10.2	347.9	Two phase natural circulation
5	6564.0 (264)	6599	10.0	9.93	21.86	13.6	334.5	
6	8072.0 (332)	8100	10.0	9.92	31.78	16.32	321.9	
7	9944.0 (394)	9958	10.0	10.35	42.13	15.9	312.0	
8	11686. (461)	11700	10.0	9.93	52.06	21.5	296.4	
9	13532. (532)	13560	10.0	9.88	61.94	23.0	285.1	
10	15456. (606)	15480	10.0	9.88	71.82	24.6	273.6	
11	17068. (668)	17100	10.0	9.94	81.76	26	262.2	
12	18576. (726)	18600	10.0	9.91	91.67	27	251.3	
13	20084. (784)	20099	10.0	9.92	101.59	28	240.4	
14	21566. (841)	21600	10.0	9.96	111.55	29	229.5	Reflux
15	23074. (899)	23099	10.0	9.93	121.48	30	218.5	
16	24582. (957)	24599	10.0	9.95	131.43	31	207.6	
17	25466. (991)	-	10.0	9.90	141.33	32	196.7	

*Subject to further analysis, see /1/.

Tab. IV - History of drainage from LP during A2-77 test

3. ADOPTED NODALIZATIONS AND PERFORMED SENSITIVITY ANALYSES

3.1 - Nodalization

The basic nodalization is the one adopted for ISP 18 post test calculation /5/ (Fig. 4). A further nodalization has been specifically set up including two different U-tubes in order to assess the influence of differential elevations of U-tubes in SGs, considering some conclusions from experimental data analysis /6/, /7/. The main characteristics of the nodalizations are summarized in Tab. V.

Few aspects are common to the performed sensitivity calculations:

- 17 main "draining steps" are included in the code input: during each of them the same amount of water is drained from the lower plenum as in the experiment; nevertheless the time duration of each "steady state" period is lower than in the test owing to the need to save CPU time; obviously it has been checked that a reasonable steady situation was reached in the code calculation after the end of the various "steady state" periods (the observation of some experimental boundary conditions, e.g. vessel wall temperature, also suggested this choice);
- additional "draining steps" were added in the code input in order to arrive at dryout conditions in core rods, so that the overall time duration of the calculated test was more than 4000 seconds; in Tab. VI the draining steps used ad input to the code are specified (the comparison between data in Tabs. IV and VI allows one to fix the corresponding periods in the experiment and in the calculation as far as the PS mass inventory is concerned);
- difficulties were encountered in achieving a satisfactory steady state situation (see also below);
- valves are included in various zones of the nodalization to isolate PRZ and UH from PS during the test.

3.2 - Analyzed cases

Several attempts were made to achieve initial steady state situation in the code calculation.

Afterward, in agreement with discussions had with Lobi researchers /8/, the cases reported in Tab. VII have been analyzed.

The main purposes of the sensitivity calculations are as follows:

case A): to achieve steady state conditions adopting fluid temperature distribution measured in the experiment /3/ boundary and initial conditions defined in Tabs. I, II and II, and other conditions as in ISP 18 calculation /5/ including in particular heat losses to environment and localized pressure losses distribution;

case B): case A) led to inconsistencies between temperature distribution and flowrate in the various zones of PS, so the aim of case B) was to achieve the same flowrates as in the experiment by varying some localized pressure losses coefficients;

case C): to check the influence of pipes roughness on flowrate;

case D): to check the influence of incondensable gases in natural circulation;

case E): to check the influence of considering two different heights of U-tubes in the nodalization.

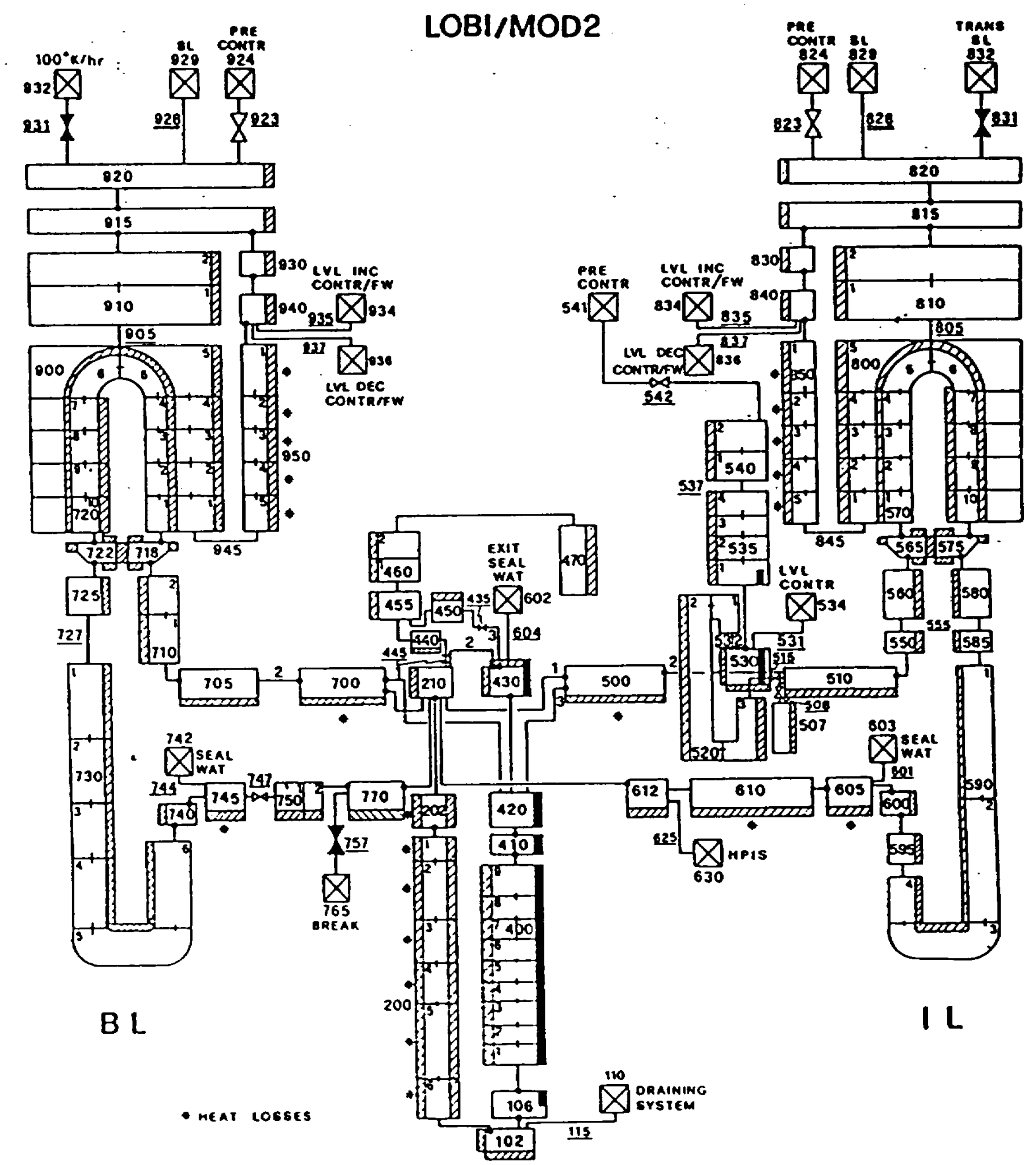

Fig. 4 - RELAP5/MOD2 nodalization for A2-77 test (1 U-tube, cases A to D)

	R5-A				R5-E			
QUANTITY	VESSEL	IL & BL PS	IL & BL SS	TOTAL	VESSEL	IL & BL PS	IL & BL SS	TOTAL
Nodes	28	66	32	126	28	86	32	146
Junctions	35	65	32	132	35	87	32	154
Time dependent hydr. components and connected valves	4	12	20	36	4	12	20	36
Heat structures	34	79	42	155	34	99	42	175
"Active" structures	13	2	--	15	13	2	--	15
Mesh points	441	567	294	1302	441	1001	294	1442
Trips (normal)	--	--	--	46	--	--	--	46
Trips (logical)	--	--	--	10	--	--	--	10
Control variables	--	--	--	92	--	--	--	98
Materials	--	--	--	5	--	--	--	5
General tables	--	--	--	13	--	--	--	13
Overall number of hydr components	--	--	--	294	--	--	--	336
Overall number of heat structures	--	--	--	170	--	--	--	190

Tab. V - Details of the nodalization used for RELAP5/MOD2 calculations (R5-A and R5-E models)

TIME (s)	DRAINED FLOWRATE (Kg/s)
0.	0.
0.01	0.95
10.	0.95
10.01	0.
500.	0.
500.01	0.65
510.	0.65
510.01	0.
1000.	0.
1000.01	0.613
1010.	0.613
1010.01	0.
1500.	0.
1500.01	1.333
1510.	1.333
1510.01	0.
2000.	0.
2000.01	1.264
2010.	1.264
2010.01	0.
2100.	0.
2100.01	1.293
2110.	1.293
2110.01	0.
2200.	0.
2200.01	1.253
2210.	1.253
2210.01	0.
2300.	0.
2300.01	1.133
2310.	1.133
2310.01	0.
2400.	0.
2400.01	1.148
2410.	1.148
2410.01	0.
2500.	0.
2500.01	1.134
2510.	1.134
2510.01	0.
2600.	0.
2600.01	1.094
2610.	1.094
2610.01	0.
2700.	0.
2700.01	1.092
2710.	1.092
2710.01	0.
2800.	0.
2800.01	1.096
2810.	1.096
2810.01	0.
2900.	0.
2900.01	1.093
2910.	1.093
2910.01	0.
3000.	0.
3000.01	1.095
3010.	1.095
3010.01	0.
3100.	0.
3100.01	1.090
3110.	1.090
3110.01	0.
3200.	0.
3500.	0.
3500.01	2.
3510.	2.
3510.01	0.
3600.	0.
3700.	0.
3700.01	3.
3710.	3.
3710.01	0.
3800.	0.
4000.	0.
4000.01	3.
4010.	3.
4010.01	0.
4100.	0.
4200.	0.
4200.01	3.
4210.	3.
4210.01	0.
4300.	0.
4300.01	5.
4310.	5.
4310.01	0.
4500.	0.
1.E6	0.

Tab. VI - Drainage steps used in code calculations

R5-M2 TEST IDENT.	PARAMETER								
	CORE INLET JUN KF/KR	ILSG UTs IN. JUN KF/KR	BLSG UTs IN. JUN KF/KR	IL RPV OU. JUN KF/KR	BL RPV OU. JUN KF/KR	PIPING RUGOSITY (m)	EQUIV. UTs NUMBER	NON CONDENSIBLE OPTION	NOTES
A	.7/.7	.35/.55	.7/.9	.9/.02	1.3/1.47	4.E-5	1	NOT USED	The calculated initial PS IL and PS BL mass flow rates are about 1.5 times the actual measured values.
B	35./35.	20./20.	50./50.	9./15.	13./14.7	4.E-5	1	NOT USED	Reference calculation localized loss coefficients increased to match initial mass flowrate valves in the loop.
C	.7/.7	.35/.55	.7/.9	.9/1.5	1.3/1.47	8.E-5	1	NOT USED	Piping rugosity increased.
D	35./35.	20./20.	50./50.	.9/1.5	1.3/1.47	4.E-5	1	USED	Not running
E	35./35.	20./20.	50./50.	.9/1.5	1.3/1.47	4.E-5	2	NOT USED	Effect of U-tubes separation.

Tab. VII - Significant characteristics of A2-77 calculations

4. COMPARISON BETWEEN MEASURED AND CALCULATED TRENDS

4.1 - Achievement of steady state

The initial part of the activity was devoted to the search of a steady state situation in the trends predicted by the code; in particular the effect was checked of:
1) fluid temperature distribution in SG SS;
2) heat losses in PS;
3) heat losses in SS;
4) initial temperature imbalance between fluid and structures in PS.

In all cases PRZ pressure and liquid level, SGs SS pressure and DC levels were maintained costant through proper time dependent volumes and junctions: the DC level in SS was maintained costant during the whole test by the AFW flowrate assumed at a temperature of 25 °C (same as in the experiment).

The coupling between natural circulation flowrate and fluid temperature distribution in PS including heat transfer from PS to SS was studied for each of the boundary conditions 1) to 4).

The consideration of subcooling in the DC of SGs (case 1)) leads to an heat exchange between PS and SS much greater than the core power, thus causing much larger natural circulation in the PS loops (the resulting power imbalance was partially compensated by the TMDPVOL connected with PRZ). The assumption of (roughly) initial saturation conditions in the DC of SGs led to the decrease of PS flowrate and to a better agreement with experimental data. In this case (case A in Tab. VII) the PS flowrate was roughly two times the measured value.

Doubling the values of heat losses in PS and SS (cases 2) and 3)) caused variations of the PS flowrate roughly around 10% of the experimental value (thus insufficient to match the measured values).

The influence of the initial temperature distribution in the structures was much stronger and proper tuning (± 1°C in almost all structures) could have had been used to match the measured values of flowrate in PS. This choice would have had unknown influence in the subsequent part of the transient, so the decision was taken to assume all the structures in equilibrium with the fluid in the steady state conditions (apart from the consideration of heat losses).

In the following paragraphs cases A, B, C, D and E of Tab. VII are discussed. It should be noted that no result is available for case D due to the failure of the code in evaluating non condensible gases. Still case B must be considered as the reference calculation.

4.2 - Case A (Initial calculation)

The analyses performed to achieve the initial conditions (sect. 4.1) led to the following decisions concerning unspecified or unclear boundary and initial conditions:
- heat losses in PS and SS as in ISP 18;
- initial fluid temperature in SS of SG assumed at saturation;
- HL fluid temperatures in both BL and IL equal to the measured values in IL;
- CL fluid temperatures in BL and IL as specified from the experiment;
- localized pressure loss coefficients and pipes roughness same as in ISP 18.

Significant results from steady state are shown in App. A. It can be noted that both IL and BL flowrate values are more than 50% higher than the experimental values. This result suggested to not continue the calculation without adjusting some input parameters.

4.3 - Case B (Reference calculation)

The results of case A demonstrated that some tuning in input data was necessary in order to make meaningfull the comparison between calculated and measured trends. Various possibilities can be used in this regard even remaining within the uncertainties limits of measured parameters (e.g. pressure drops, fluid temperatures, structures temperatures, DC level in SG SS, losses in the PRZ isolation valve, etc.)(*).

For the sake of simplicity it was decided to vary, with respect to case A, only the localized pressure loss coefficient at
- core inlet;
- HLs inlet in BL and IL;
- SGs PS U-tube inlet in BL and IL.

The achieved steady state situation is compared with experimental values in Figs. 5, 6, 7 and 8 and in Tab. VIII. Further information about steady state can be obtained from App. B where several variables trends are reported for the whole transients. Still in relation to steady state, a CNTRLVAR was set up as the (algebric) sum: CORE POWER - POWER EXCHANGE ACROSS U-TUBES OF SGs - HEAT LOSSES FROM PS (EXCLUDING PRZ).

It has been checked that the absolute value of this quantity was less than 10 Kw, in steady situation, at the beginning of the simulated test.

The resulting values of flowrate as a function of PS residual mass are compared with experimental data in Figs. 9 and 10 with reference to IL and BL, respectively. The PS pressure trends are compared in Fig. 11; a list of significant measured and calculated events or quantities during A2-77 is reported in Tab. IX (for brevity in this Table some results from case E have also been included). In particular some characteristics of the oscillations of fluid velocities and densities measured when PS mass inventory equals 285 Kg are also compared with calculated data.

The analysis of the reported trends allows one to conclude that the code predicts quantitatively well the important phenomena occurring during the test. With reference to the oscillations measured during the test, the reported figures (see also App. B) demonstrate that oscillatory behaviour also results from calculations: the related frequency has the same order of magnitude as the measured one. Nevertheless a more in depth analysis has been performed in relation to the nature of these oscillations also including the evaluation of the measurement error (sect. 5.1).

4.4 - Case C (Piping roughness changed)

The objective of calculation C is to assess whether tuning on roughness has the same effect on the results of variations in localized pressure losses coefficients /8/. To this aim taking as reference the case A, the pipe roughness already utilized in ISP 18 analysis was multiplied by two. Significant results are shown in App. C.

(*) Later analyses /9/,/10/ of the experimental data demostrated that the most plausible explanation for the discrepancies between measured and calculated trends in the single phase natural circulation, is the occurrence of reverse flow in some U-tubes (flow from outlet to inlet plenum of the SGs). This creates additional resistances in the loop that cannot be accounted for in a nodalization with only one U-tube. Nevertheless a two-dimensional model for the SG plena appears necessary to simulate this kind of phenomenon.

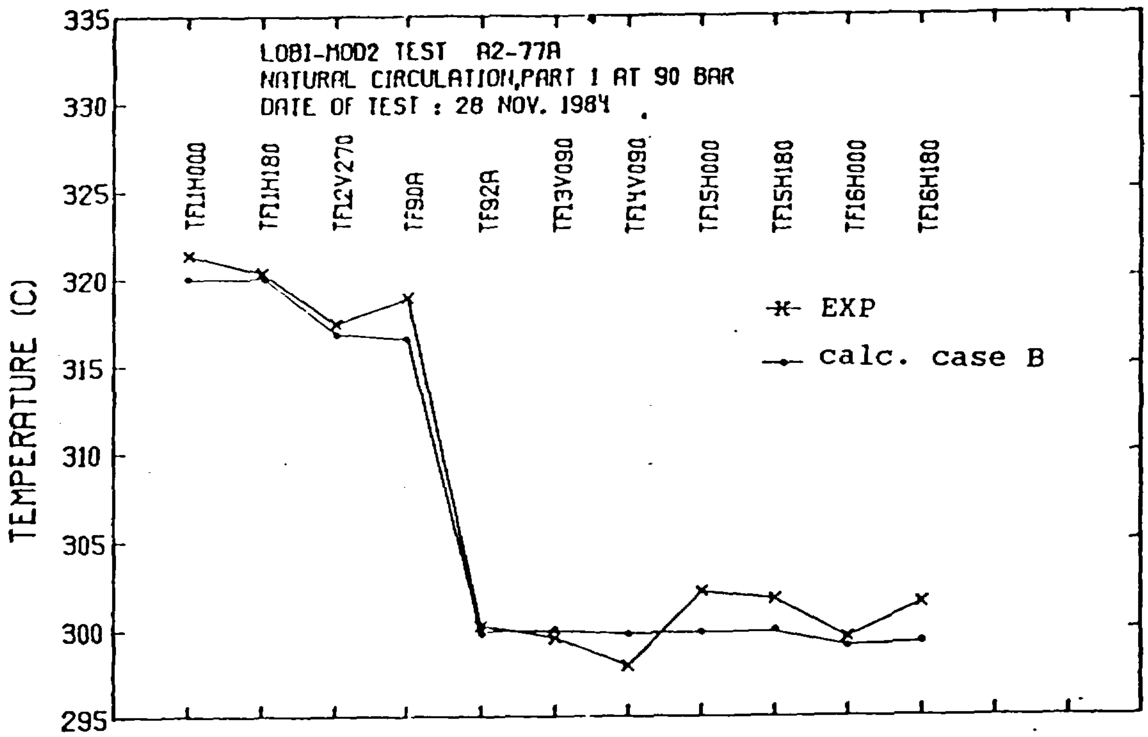

Fig. 5 - Primary Fluid Temperatures along Triple Loop at Steady State No.1. Comparison between measured and calculated trends

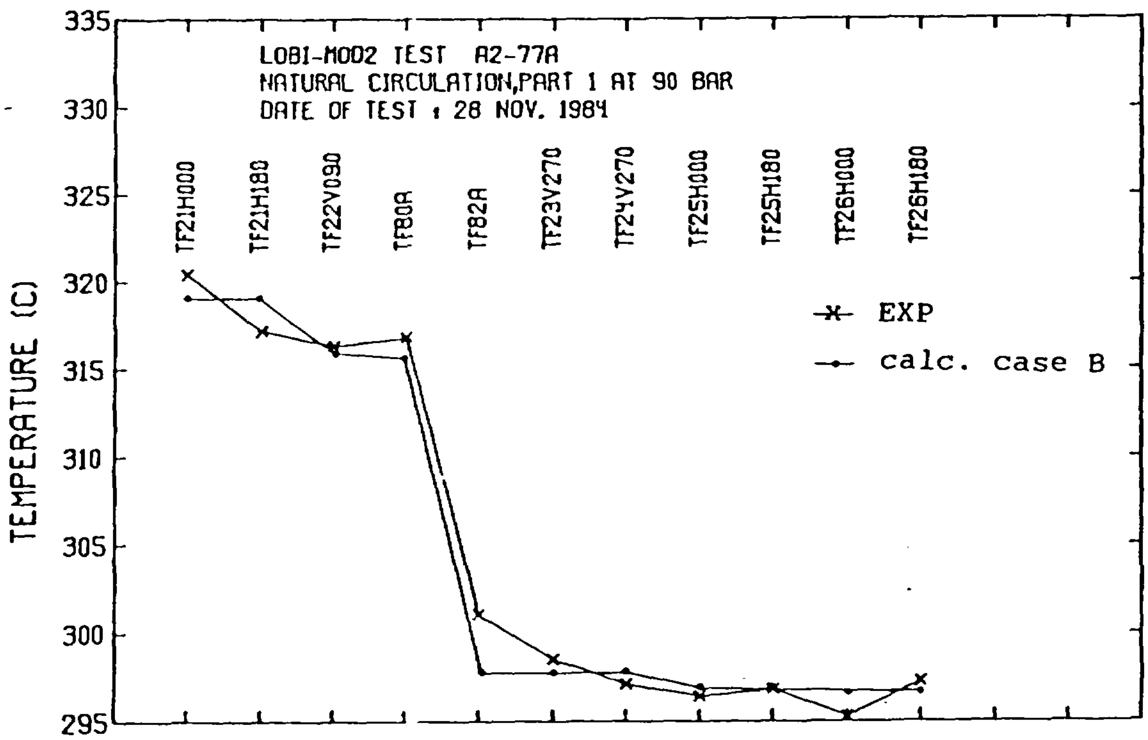

Fig. 6 - Primary Fluid Temperatures along Single Loop at Steady State No.1. Comparison between measured and calculated trends

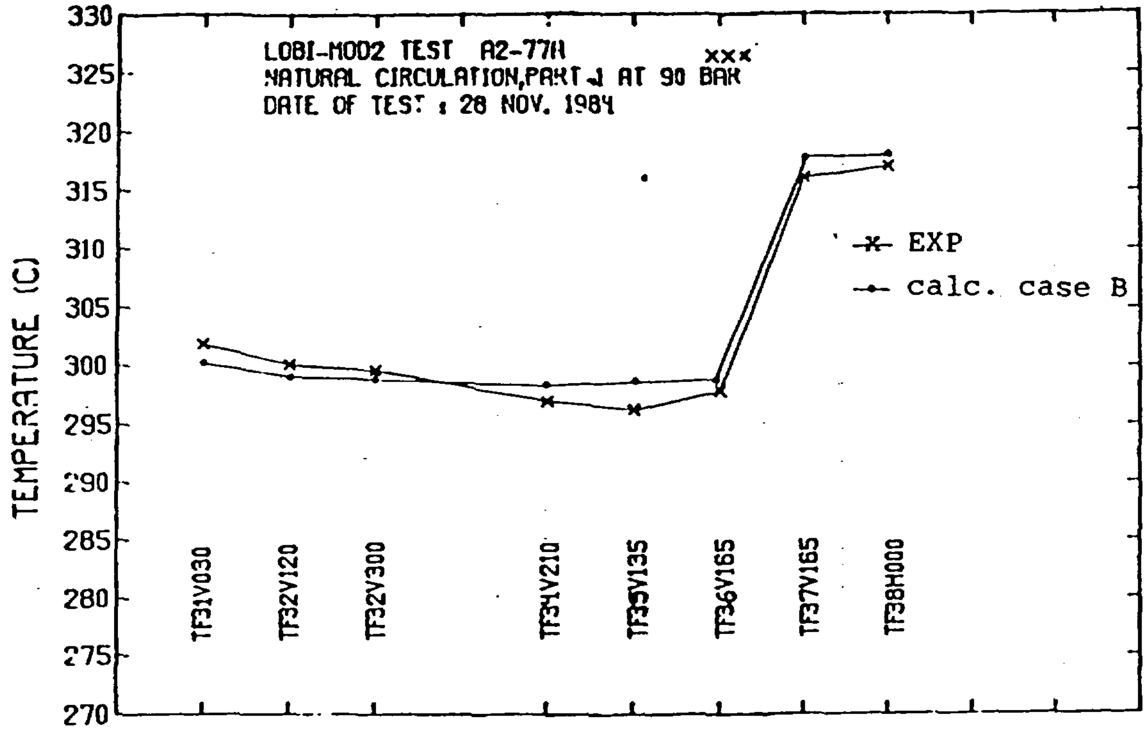

Fig. 7 - Primary Fluid Temperatures in Vessel at Steady State No. 1. Comparison between measured and calculated trends

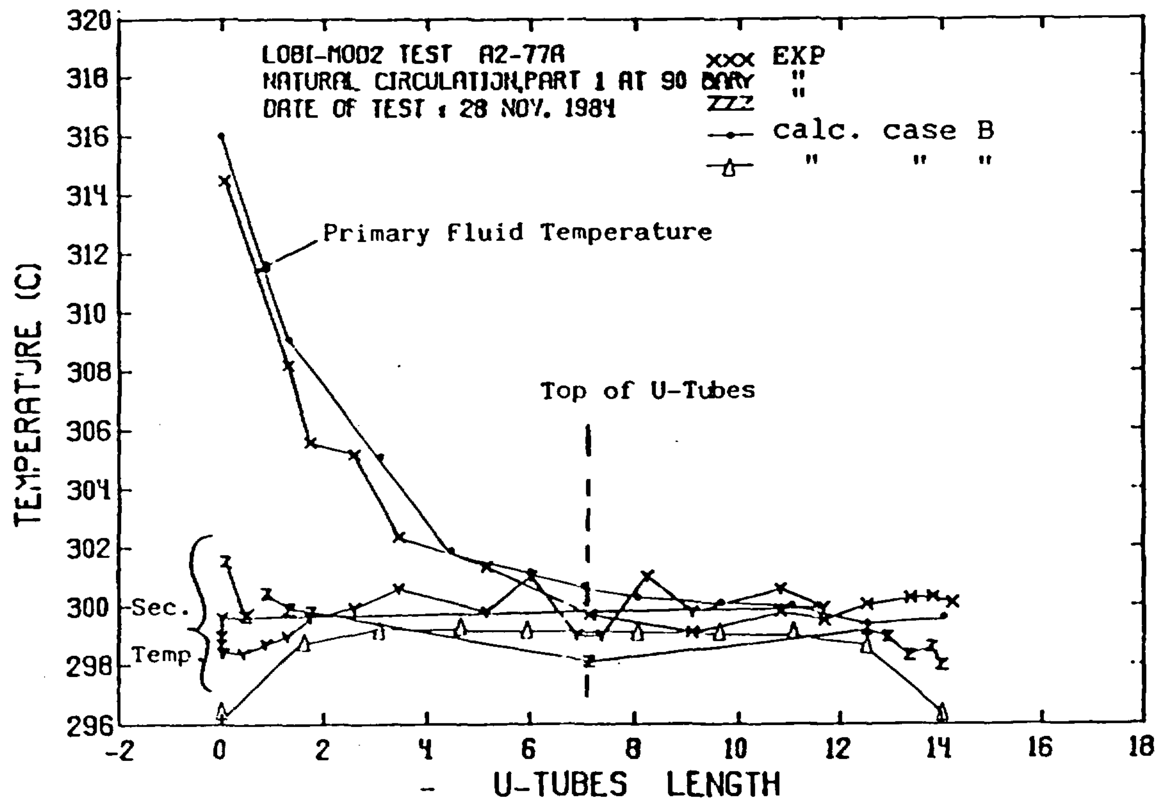

Fig. 8 - Primary and Secondary Fluid Temperatures in Triple Loop Steam Generator at Steady State No. 1.
Comparison between measured and calculated trends

		R5-B	EXP.	Units
Primary System				
Mass flow:	- Intact Loop	0.98	1.0	kg/s
	- Broken Loop	0.31	.3	kg/s
Pressure:	- Upper Plenum	14.0	14.0	MPa
Fluid temperatures:				
Vessel outlet	- Intact Loop	320	321	°C
	- Broken Loop	320	319	°C
Vessel inlet	- Intact Loop	300	300	°C
	- Broken Loop	296.	296	°C
Pressurizer:		336.	336	°C
Core Power:		0.183	0.183	MW
Liquid mass without pressurizer:		373.	c. 370	kg
Liquid volume without pressurizer:		0.524	0.522	m^3
Pressurizer water level:		2.52	c. 2.5	m
Secondary System				
Auxiliary Feedwater mass flow:				
	- Intact Loop	--	--	
	- Broken Loop	--	--	
Pressure:	- Steam Line	8.65	8.65	MPa
Temperatures:				
Steam Generator Inlet	- Intact Loop	25.	25	°C
	- Broken Loop	25.	25	°C
Steam Generator Outlet	- Intact Loop	300	300	°C
	- Broken Loop	300	300	°C
Downcomer Water Level:	- Intact Loop	8.58	c. 8.6	m
	- Broken Loop	8.9	c. 8.9	m

Tab. VIII - Test conditions at initiation test A2-77: comparison between measured and calculated data

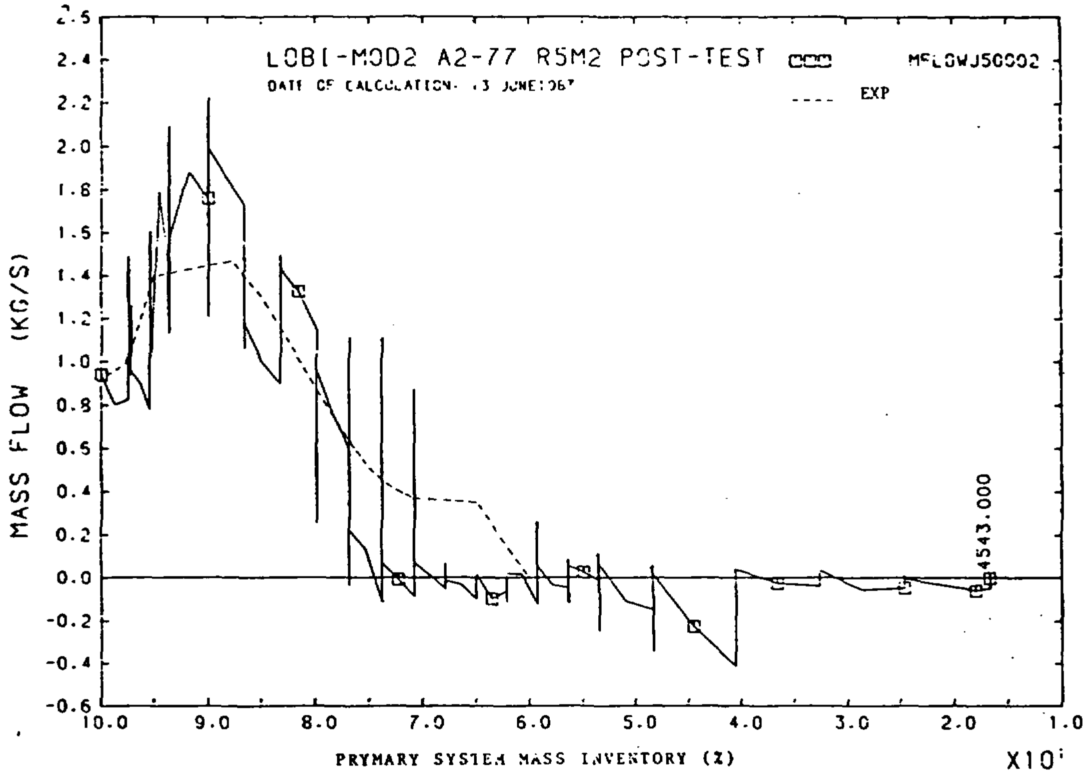

Fig. 9 - Mass Flow Rate in Triple Loop C.L.

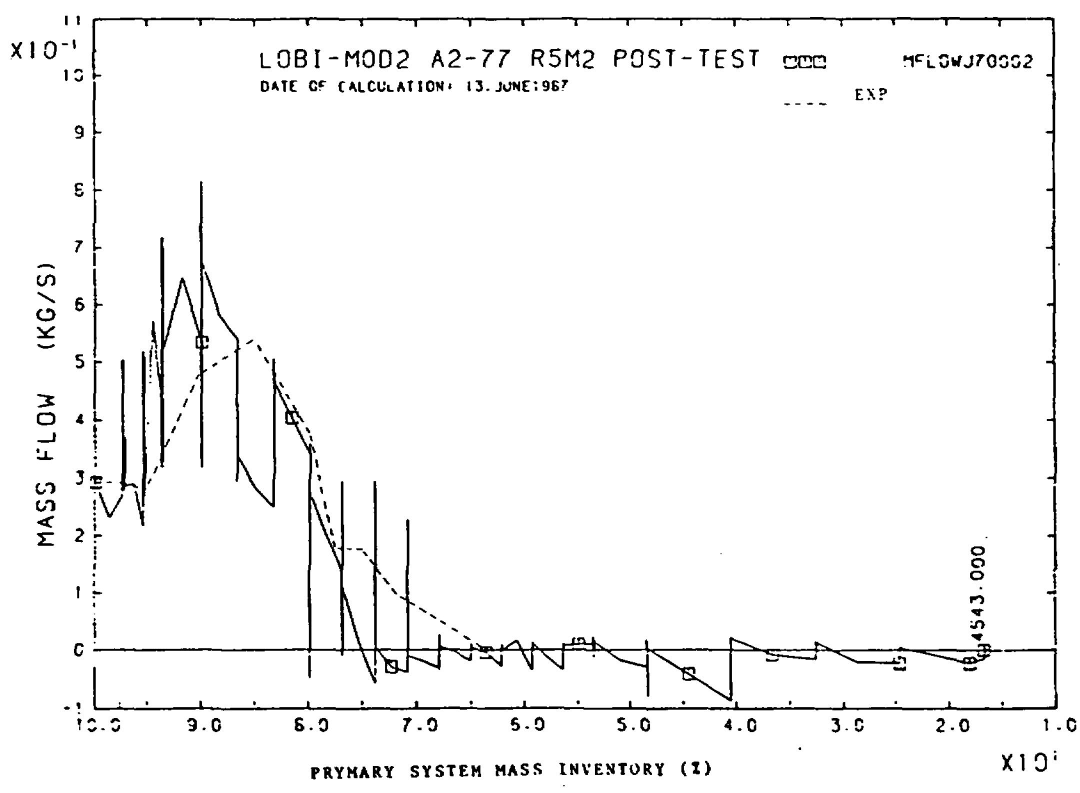

Fig. 10 - Mass Flow Rate in Single Loop C.L.

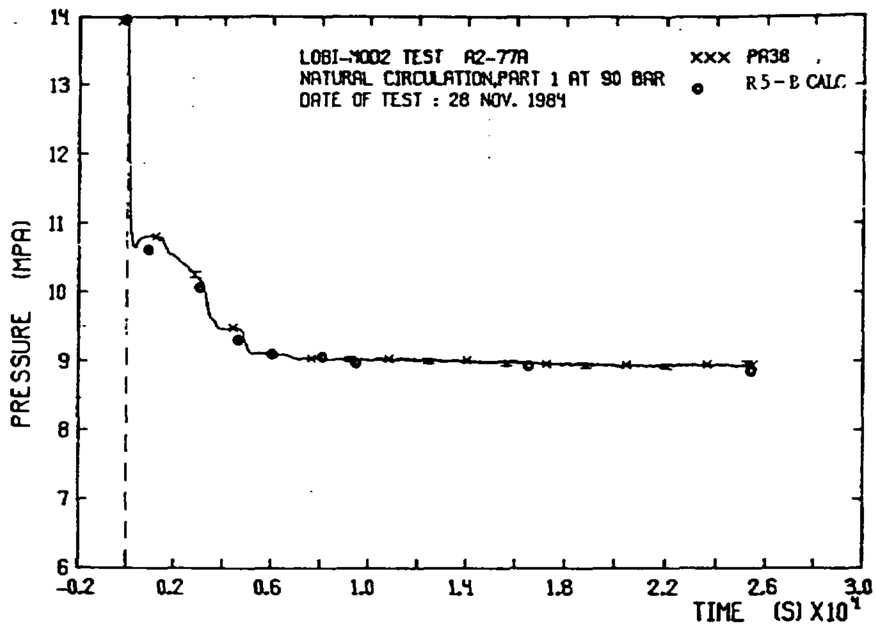

Fig. 11 - Comparison between calculated and measured trends for UP pressure (case B). Calculated points have been superimposed to the experimental ones considering the PS mass inventory

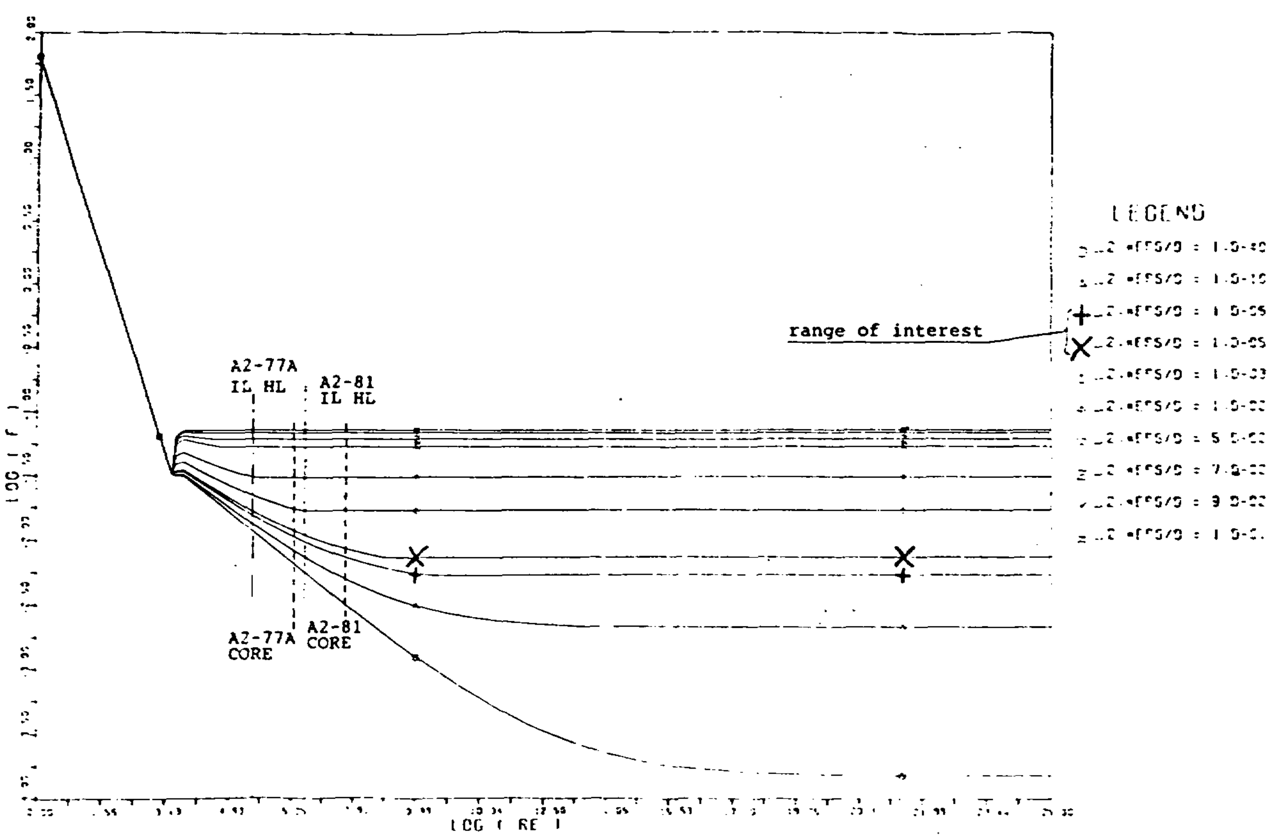

Fig. 12 - Friction coefficient in the core and in IL HL for tests A2-77 and A2-81 (initial/nominal conditions)

QUANTITY/EVENT	EXP.	CASE B	CASE E
IL/BL HL flowrate values at test beginning (kg/s)	1./0.3	0.98/0.31	0.98/0.31
Max. IL/BL HL flowrate values (kg/s)/PS mass inventory when this event occurs (kg)	1.5/326.;0.55/313.	2.2/332.;0.8/332.	2.2/332.;0.75/332.
Mass inventory in PS when PS pressure reaches 9.0 MPa (kg)	329.	338.	338.
Mass inventory in PS when fluid velocity in IL HL becomes negative (kg)	-(*)	277.	264.
Mass inventory in PS when dryout in UP occurs (kg)	240.	300.	351.
Mass inventory in PS when dryout in core active region occurs (kg)	207.	123.	121.
Mean frequency of IL HL velocity when PS mass inventory equals 285 kg	0.0083	0.011	0.015
Mean frequency of BL HL velocity when PS mass inventory equals 285 kg	-	0.011	0.015
Mean frequency of BL HL density when PS mass inventory equals 285 kg	-	0.012	0.013
Mean frequency of BL CL density when PS mass inventory equals 285 kg	-	0.012	0.013
Mean phase shift between BL HL and BL CL velocities/densities when PS mass inventory equals 285 kg	0./120.	0./117.	0./116.
Mean phase shift between IL HL and BL HL velocities when PS mass inventory equals 285 kg	155.	52.	51.
Mean phase shift between PS in the ascending leg of the two U-tubes in IL SG when PS mass inventory equals 285 Kg	80.	-	0.

(*) Unidirectional probes

Tab. IX - Comparison between significant parameters in the experiment and in code calculations

The observation of loop flowrates demonstrated that tuning on roughness has the same effect as tuning in localized pressure losses and appears to be more physically based owing to uncertainties in the value of roughness also caused by corrosion/erosion of pipes internal walls.

To better understand the results, in Fig. 12 the plotter of the wall friction coefficient (Colebrook formula) implemented in RELAP5/MOD2 code is reported as a function of Reynold number.

The working points in HL and inside core are also reported with reference to initial (measured) conditions in A2-81 and A2-77A. It should be noted that the working points when going from A2-81 to A2-77A move in a transition zone of the diagram where Reynold number is important in the evaluation of the friction coefficient. So a further explanation of the unsatisfactory results obtained in case A (e.g. apart from experimental uncertainties in evaluating roughness) could be the inadequancy of Colebrook model in the zone.

4.5 - Case D (Presence of incondensible)

The objective of case D was to study if incondensible gases possibly present in the loop at the beginning of the test /8/ could have the same effect as an increase of localized pressure losses. To this aim a mass of gas was given as input in the code equivalent to the volume occupied by the gas at ambient conditions in the U-tubes. The gas was assumed to be localized in the top of U-tubes. Unfortunatly the code did not work when the incondensible gas option was requested.

4.6 - Case E (Effect of parallel U-tubes)

The objectives of case E, that is the introduction in the nodalization of two parallel U-tubes characterized by different heights (difference in heights is 0.25 m) are essentially two:

- to observe if the lowest U-tubes allows larger natural circulation flowrates when steam appears in the top of the highest U-tubes;
- to observe possible links in the oscillations of velocities and densities inside the U-tubes.

The first problem which occurred in setting up the nodalization was the choice of the criteria by which separate the U-tubes. At least three possibilities did exist:

a) height, but almost each of the U-tubes has a different height;
b) position with respect to HL connection to SG PS (3D effect);
c) possible differences in inlet pressure losses (no data available).

As already mentioned the choice a) was made considering two U-tubes having equal characteristics apart from the height. The case B input was modified.

Significant results are shown in Tab. IX and in App. D. The main outcoming of the analysis is that natural circulation is slightly increased (as expected) with respect to the reference case (case B), when void formation occurs in the top of highest U-tubes. On the other side no interaction (parallel tube oscillations) appears to exit between the two U-tubes in both SGs.

Also in this case better conclusions can be achieved only if a 3D model is available for the inlet plenum of SG, and a more detailed characterization is available from the experiment (measurement of localized pressure losses of each tube, diameter etc.).

5. RELEVANT RESULTS ACHIEVED IN THE FRAME OF THE A2-77A TEST ANALYSIS

The LOBI A2-77A experiment constituted the basis of more in depth analysis at University of Pisa toward three main directions:

a) study of the instabilities during the two-phase natural circulation period /11/,/12/;
b) evaluation of the user influence on the setting up of the modalization and in the evaluation of the comparison between measured and calculated trends /13/;
c) evaluation of the possibility to extrapolate measured and calculated natural circulation scenarios to plant systems /14/.

The main outcomes of the studies at items a) and b) are reported in the sections 5.1 and 5.2, respectively.

5.1 - Characterization of instabilities

Oscillations in almost all measured signals were detected for several thousands seconds into the transient, starting roughly when Primary System (PS) mass inventory was equal to 64% of the initial nominal value (including pressurizer and upper head inventories). They lasted up to the time when "stable" reflux condensation occurred (primary loop-residual mass roughly equal to 55% of the initial value). The highest amplitude of the peaks was observed just at the beginning of the unstable period; 400 s in this phase are considered hereafter.

The trends of differential pressures, fluid densities, velocities and temperatures in few points of the loop are shown in Figs. 13-16.

It should be noted that measured values of fluid velocity cannot be related specifically to either of the two phases being the output of a full-flow turbine meter. So the local void faction values should be considered in interpreting the signals. Even the comparison of liquid and steam velocities with calculated terms should be made with caution.

Different interpretations of the roots of the observed oscillations are possible when one examines the experimental data:

1. Formation of relatively large steam slugs in the horizontal part of cold legs
2. Periodic clearing of loop seal
3. Formation of liquid level in the ascending legs of U-Tubes owing to entrainment of droplets and flooding at the inlet (Draining occurs when the liquid level reaches the top of the U-Tube)
4. Same scenario as in case 3, but with formation of liquid level due to condensation in U-Tubes
5. Combination of the above phenomena.

In cases 3 and 4, draining of tubes could be due to both a sort of syphon effect and the rise of the flooding and/or CCFL point from the bottom of U-Tubes toward the top.

The frequency and magnitude of differential pressure oscillation differed from tube to tube; they also took place out of phase. The interaction between the broken loop and intact loop, whose main variables oscillate out of phase, also can lead to energy exchange between the two steam generators. The relatively small pressure drop measured between the inlet and outlet of U-Tubes, with the possible presence of liquid in both rising and/or descending legs of U-Tubes, does not permit the identification of the flow direction.

Still, the relatively low temperature difference between primary and secondary sides (a few kelvins) leads to a quite large range of consistent values of the condensation heat transfer across the U-Tubes.

Finally, the eventual fill and dump of U-Tubes, or at least the fluid

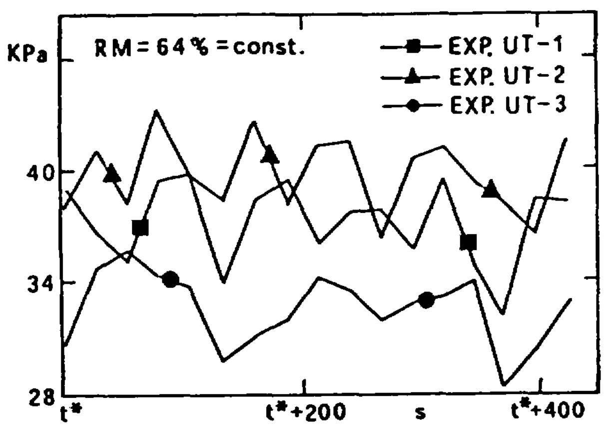

Fig. 13 - Differential pressure in intact-loop steam generator U-tube ascending leg (three U-tubes)

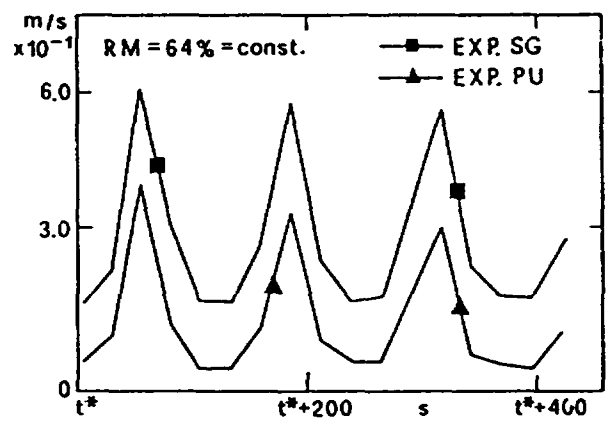

Fig. 15 - Fluid velocity at the inlet of intact-loop steam generator and pump

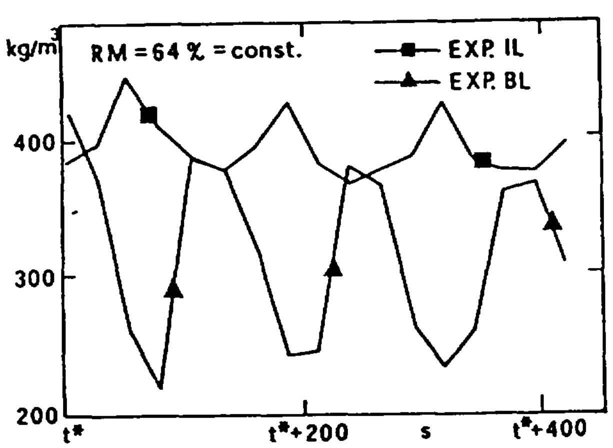

Fig. 14 - Fluid density (diametral) in intact-loop and broken-loop hot legs

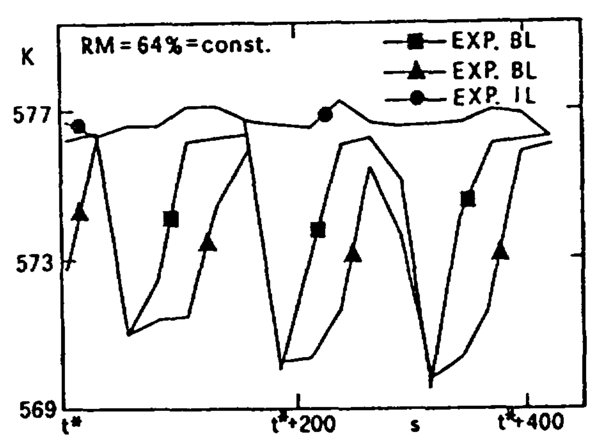

Fig. 16 - Fluid temperature in intact-loop and broken-loop cold legs

velocity oscillation in various zones of primary loop, creates variations in the heat transfer rate across steam generators, giving rise to temperature (and velocity) oscillations in the secondary side. This can cause feedback on the oscillations of primary side variables.

As far as the accuracy of the measurements is concerned, a very detailed procedure is adopted by the LOBI team to arrive at the definition of uncertainty bands for any measured signal /4/; these include consistency checks and calibrations before and after the test run. Reported values of accuracy should therefore be retained state-of-the-art values at least as far as integral facilities are concerned. Exemplary values are ± 0.07 m/s, ± 15 Kg/m^3, ± 10 KPa, and ± 1 K, with reference to velocity, densities, pressure drops and fluid temperatures, respectively.

5.1.1 - Code-predicted scenario

The application of the tuned nodalization (case B) as already mentioned produced a good agreement with the experimental data trends particularly with respect to the prediction of period and amplitude of oscillations. Comparison of measured and calculated data of differential pressure between the hot and cold legs of the intact loop and between the inlet and outlet of the U-Tubes in the broken-loop steam generator are presented in Figs. 17 and 18, respectively. Comparison of measured and calculated densities in the cold leg and velocities at the inlet of steam generator in broken loop are shown in Fig. 19 and 20, respectively.

The following main aspects can be outlined from the analysis of the corresponding couple of data:

- The mean values of the reported variables are essentially the same for both the experiment and the calculation.
- Liquid downflow appears in the calculation at U-Tube inlets (Fig. 20), whereas only steam flow can be detected from the experiment.
- The period of measured oscillations ranges around 130 s, while the calculated value is less than 100 s.
- Phase opposition occurs in the experiment (Fig. 14) between similar variables in the two loops, whereas essentially no phase shift is calculated by the code.
- Phase opposition still occurs in the experiment between hot and cold legs, whereas lower values of phase shift are calculated by the code /11/.

The analysis of predicted trends of void fractions inside the U-Tubes and of heat transfer between primary and secondary sides of steam generators permitted us to conclude that condensation in the ascending legs is the driving force of oscillations. In particular, the scenario depicted in Fig. 21 is the outcome of the calculation. At $t = t_1$ the steam-liquid mixture enters the ascending legs of U-tubes; condensation occurs on the walls owing to the lower temperature of the secondary system. This creates a rising mixture level in the ascending leg; in the descending leg the same phenomenon may occur owing to steam passing from the top of U-tubes and coming from the outlet plenum of the steam generator. Flooding, which occurs essentially at the inlet of the ascending leg, prevents the draining of the condensed liquid into the inlet plenum ($t = t_2$). At $t = t_3$ the mixture level reaches the top of U-tubes, and the liquid flow begins toward the descending leg, the loop seal, and again to the vessel (siphon effect). The draining of the ascending leg leads to a new cycle. It should be pointed out that the scenario in Fig. 21 represents only a rough estimation of the reality owing to the one-dimensional nodalization of the U-Tubes (only one equivalent U-Tube is nodalized).

Finally, it can be emphasized that the inception of oscillations in

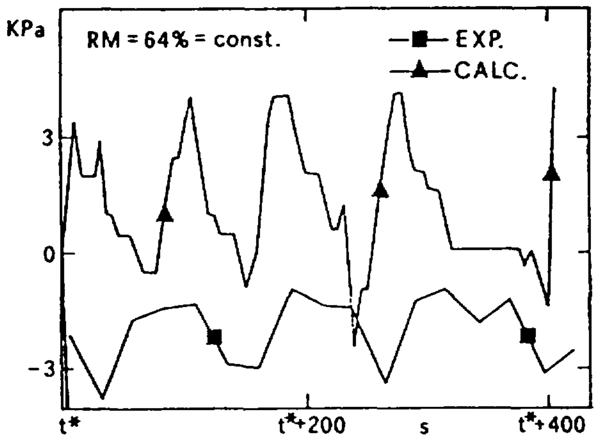

Fig. 17 - Comparison of measured and calculated differential pressures between hot and cold legs of intact loop

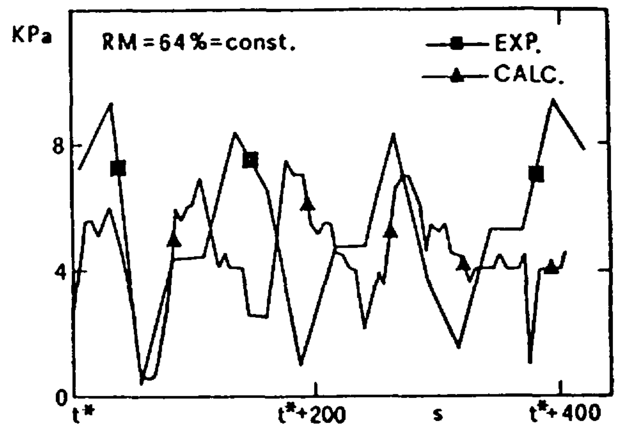

Fig. 18 - Comparison of measured and calculated differential pressures between inlet and outlet of steam generator broken loop

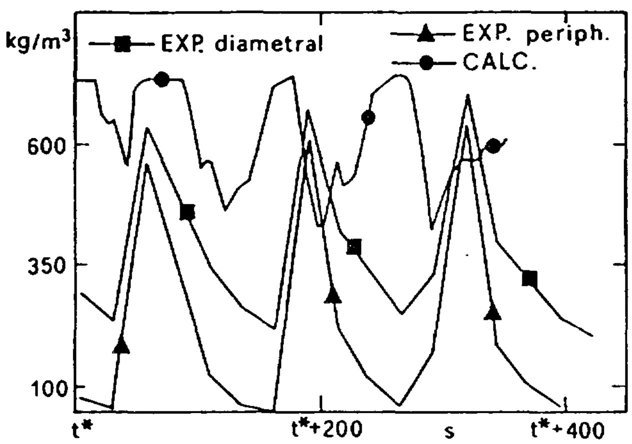

Fig. 19 - Comparison of measured and calculated densities in broken-loop cold leg

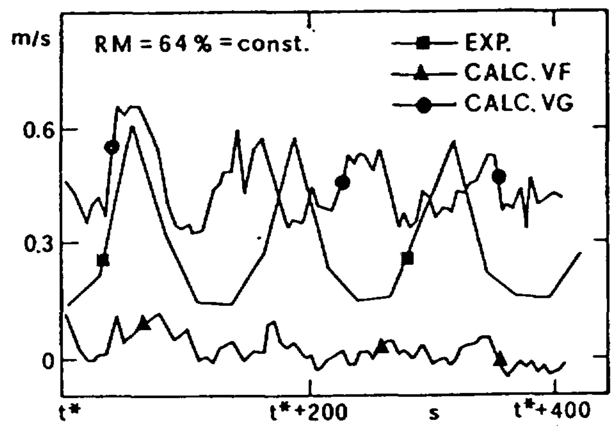

Fig. 20 - Comparison of measured and calculated velocities at the broken-loop steam generator inlet

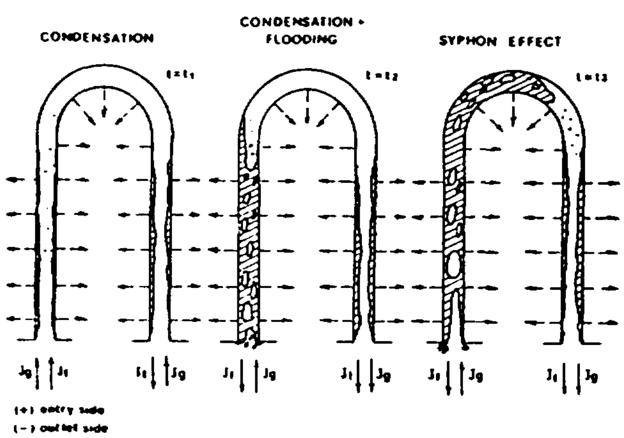

Fig. 21 - Scenario of siphon condensation foreseeable from code calculation

the code calculation coincides with void formation in the horizontal part of the cold legs between the pump and the main vessel. In particular, the periodic collapse of the slug in this zone further enhances the oscillatory behaviour of the loop.

5.1.2 - Results from the phenomenological study

Owing to limitations of the code model and of the experimental data base, two main problems arise from the above analysis. These copncern

- Identification of the roots or at least of the parameters affecting the oscillations and evaluation of the realism of the proposed scenario
- Evaluation of the possibility to extrapolate the above phenomena to real plant situations.

The two problems are dealt with hereafter by applying independent models and performing sensitivity calculations with the code.

Behaviour of Parallel Tubes in the Case of Flooding

The behaviour of parallel U-Tubes in case of flooding has generally been experimentally investigated by various authors in the past with air-water mixtures.

With reference to the typical curve, giving the channel pressure drop as a function of the steam superficial velocity, four configurations that can occur simultaneously were measured by Wallis et al. /15/ (Fig. 22). It should be noted that situation D corresponds to pure gas flow in the experiment performed by Wallis et al., while condensation can be considered in the present analysis. The experiment was carried out with straight tubes.

This simple experiment shows that different configurations may occur simultaneously for different parallel tubes having the same imposed pressure drop when countercurrent flows of liquid and steam are involved.

Furthermore it should be emphasized that parallel U-tubes have even a larger degree of freedom than straight tubes, thus allowing, potentially, a larger number of simultaneous configurations with an imposed pressure difference between inlet and outlet.

CCFL Occurrence in LOBI Steam Generator Broken-Loop U-Tubes

The Hawighorst et al. /16/ correlation was applied to evaluate the CCFL occurrence in the steam generator broken-loop U-Tubes of LOBI facility. The correlation is:

$$(J_{\ell,\mathrm{CR}}^{4}\rho_{\ell}^{2})^{0.125} = C[\sigma g(\rho_{f} - \rho_{\ell})]^{0.125} \qquad (1)$$

The coefficient C distinguishes this correlation from the Kutateladze-type correlations.

Assuming the measured velocity and pressure in the hot leg of intact loop and the geometry of the system as boundary conditions, Eq. (1) demonstrates that two to four tubes (out of eight) should be in stalled conditions (case A in Fig. 22) at a given time, depending upon the chosen value for the velocity in hot leg (0.2 to 0.6 m/s). In particular, the measured value of gas flow rate corresponds to a Jg value lower than the value at the CCFL point if one considers all the U-Tubes. In the remaining U-Tubes, situations B, C or D can occur, allowing a rise in level in the ascending part.

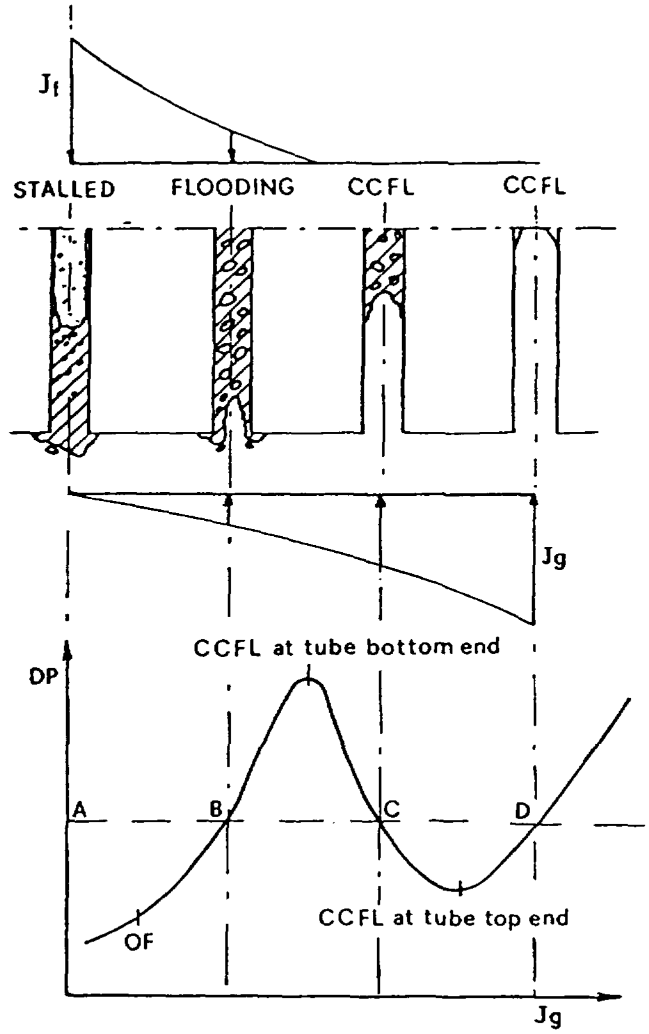

Fig. 22 - Behavior of parallel straight tubes

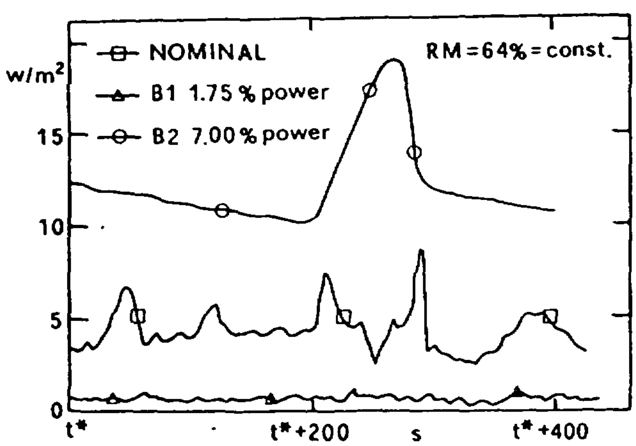

Fig. 23 - Sensitivity calculations related to LOBI: trends of heat transfer across U-tubes when core power is varied

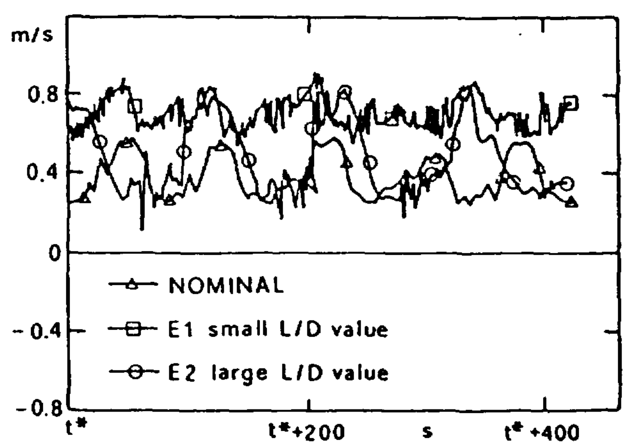

Fig. 24 - Sensitivity calculations related to LOBI: trends of velocities at the inlet of intact-loop steam generator U-tubes when the L/D ratio is varied

Condensation in U-Tubes of LOBI Steam Generator Broken Loop

The integral mass and energy balance of the fluid volume inside the ascending leg of U-Tubes, taking for simplicity the situation D in Fig. 22 as reference, yields for the time necessary to fill up a tube

$$\bar{t} = \frac{D h_{fg} \rho_f}{4 H_{cond} DT} \qquad (2)$$

In order to have a rough estimation, the Nusselt correlation for the condensation heat transfer coefficient and the measured values for the requested quantities have been assumed. In this situation, t varies between 100 and 250 s depending upon the value of DT (ranging between 8 and 3 K).

The range of variation of t is consistent with the period of oscillations, demonstrating that condensation is a possible mechanism of instability.

CCFL Breakdown in U-Tubes of LOBI Steam Generator Broken Loop

It appears worthwhile to investigate the possibility of steam entering the U-Tubes to sustain a liquid column in the ascending leg. Looking at the previously considered time into transient, a pressure difference across the ascending legs of the broken-loop U-Tubes of about 0.03 ± 0.01 MPa is obtained from the experimental data/4/. This means an equivalent collapsed level ranging between 6 m and 3 m.

As a consequence of the above result, in order to have liquid at the top of U-Tubes, presence of steam bubbles and/or movement of the location of CCFL from the U-Tube inlet must be assumed.

Specific Sensitivity Calculations

Sensitivity calculations were performed by RELAP5/MOD2 code. In principle, several parameters affect the characteristics of the oscillations. Some of these are inherent to the structure of the code (nodalization, time step, empirical models, etc.), others depend upon the manner in which boundary conditions are fixed (e.g., pressure control system in secondary side, draining modes), and others actually depend upon the system configuration (distribution of heat losses and of form loss coefficients, geometry, power, etc). Consideration of the entire set of parameters in sensitivity calculations requires a very extended work; attention is focused hereafter on the last class inherent to system configuration.

Sensitivity analyses were performed with reference to roughness, local loss coefficients, the length/diameter ratio (L/D) of both hot and cold legs, and core power. The last two parameters were found to be the most significant, and the related results are outlined here. The values assumed by the above quantities are reported in Table X and compared with typical values of PWR plants and of LSTF facility.

It should be noted that in sensitivity calculations E1 and E2 the length of horizontal parts of cold leg in the LOBI facility were varied by the same amount as those for the hot legs, maintaining the original diameter.

Significant results are shown in Figs. 23 and 24, where calculated system variables are plotted for the considered time span at constant value of primary-loop mass inventory. Comparison with the nominal case leads to the following observations:

Plant	Calculation Identification	Power (%)	Hot LcA L/D Ratio in IL/BL	SG Pressure (MPa)
LOBI	NOMINAL	3.5	74.3/119.5	8.6
LOBI	B1	1.75	74.3/119.5	8.6
LOBI	B2	7.	74.3/119.5	8.6
LOBI	E1	3.5	48.1/81.5	8.6
LOBI	E2	3.5	210./336.5	8.6
LSTF*	—	2.	17.9/17.9	7.4
DOEL†	DOE	3.5	10.6	5.9
1000 MWe PWR	—	—	9.5	6.5

*Test ST-NC-002
†See next section.

Tab. X - Values Assumed by Some Parameters in Sensitivity Calculations performed in order to characterize the oscillations

- The amplitude of oscillations decreases while the frequency increases when core power is reduced.
- The reduction of the L/D ratio creates new frequencies for the oscillations that are superimposed to the original ones, and an increase in L/D leads to an increase in amplitude.

The above analysis shows a close link between the characteristics of the siphon condensation phenomenon and the system geometry.

Consideration of U-Tube Height

As already mentioned (case E in sect. 4) the difference in heights has been considered in the literature as a possible reason for differences in the behaviour of U-Tubes that potentially contributes to the oscillations.

Taking this into account, parallel pipes were nodalized with RELAP5/MOD2, splitting into two egual parts (with reference to flow area) the original pipe simulating the U-Tubes. The new pipes are characterized by different heights and lengths.

The resulting void fractions at the top of the inverted U-bend of the intact-loop steam generator are compared in Fig. 25 with the mean trend of the nominal calculation. No appreciable differences can be seen from the above trends or from a more detailed comparison. On the contrary, arbitrary variations of inlet loss coefficient cause substantial differences in the behaviour of the two U-Tubes.

These results demonstrate that the splitting of U-Tubes into parallel pipes in a nodalization suitable for a one-dimensional code is meaningful only if a two-dimensional model is available for the inlet plenum. This would allow differences in behavior among the U-tubes caused by fluid dynamics inside the plenum itself. Without the availability of such a model, differences in the behaviour of U-Tubes can be caused by different heights (this has been shown to be irrelevant), by different values of the inlet/outlet form loss coefficient (to be fixed almost arbitrarily), or by different number of U-Tubes in each group (to be fixed arbitrarily).

Presumed Scenario

The above results and considerations made it possible to define a more complex scenario for the ensemble of U-Tubes than that reported in Fig. 21. In particular, the following additional items are taken into account:
- Groups of tubes may exhibit substantially different behaviour with fixed boundary conditions: some tubes must be in stalled conditions in order to have CCFL in others.
- The height of tubes has little influence on the global evolution of the phenomenon; the two-dimentional fluid dynamics inside inlet plenum mainly differentiate the U-Tubes behaviour;
- The CCFL front is likely to advance.

The scenario in Fig. 26 was contrived with these considerations in mind.

5.2 - Influence of the code user on the results

The post-test analysis of the A2-77A experiment has been carried out independently, in the frame of an European Community research Program, by six different users utilizing five advanced codes. An outline of codes and users is given in Tab. XI /13/. A detailed descriptions of the codes can be found in ref. /17/.

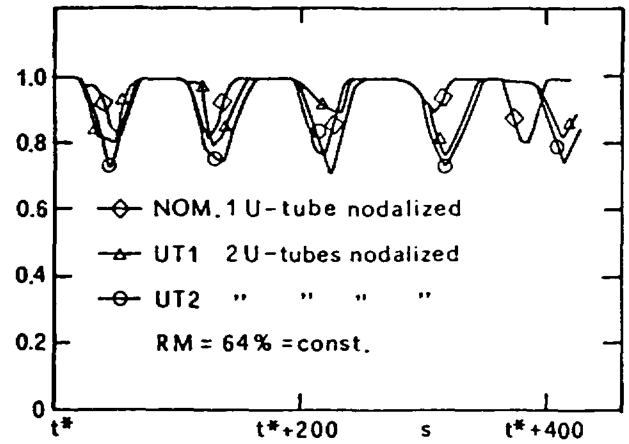

Fig. 25 - Calculated trends of void fraction at the top of U-tubes using a single pipe (nominal case) and two parallel pipes to nodalize the U-tubes

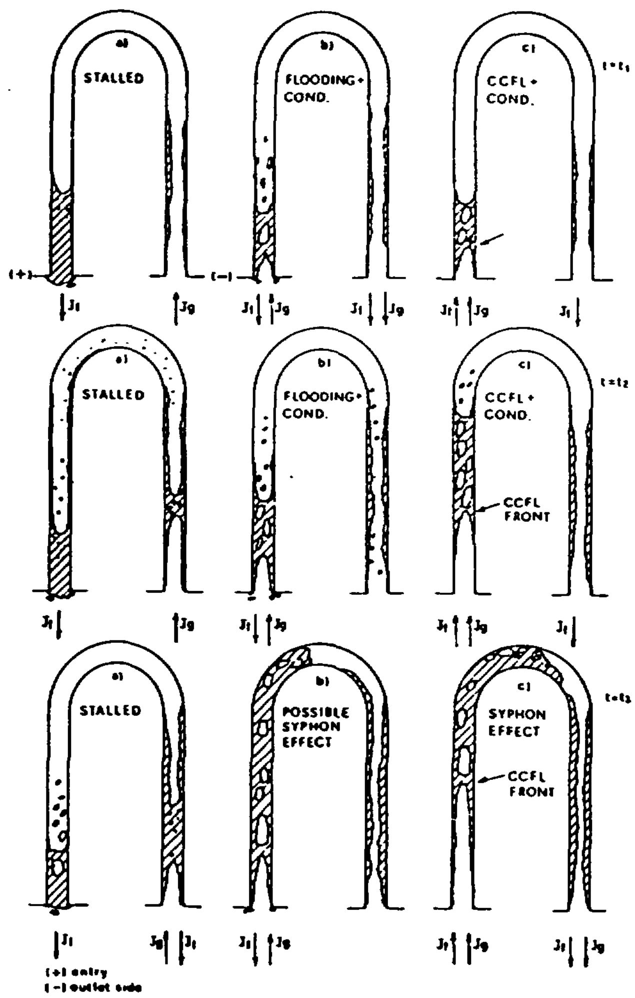

Fig. 26 - Presumed scenario for explaining siphon condensation. At each time t_1, t_2, and t_3, U-tubes are in configurations (a), (b), and (c), respectively.

USER	CODE
CEA - Paris	TRAC/PF1- MOD1
CENG - Grenoble	CATHARE 1 V1.3
DCMN - Pisa	RELAP5/MOD2
GRS - Garching	ATHLET
JRC - Ispra	RELAP5/MOD1- EUR
UKAEA - Winfrith	RELAP5/MOD2

Tab. XI - Involved users and codes

5.2.1 - Comparison among input parameters

The lack of reflection on the input parameters may result as the most significant limitation of a current code analysis: the first specific objective pursued hereafter is to consider this gap, for a specific thermalhydraulic problem, by means of the comparison of the input decks developed by several users. The existence of different approaches pursued by the involved users, dealing with a wide variety of choices requiring subjective judgements, will be demostrated.

The starting point in setting up the nodalization is the knowledge of the following subjects:

1) engineering of the facility and its instrumentation;
2) test specifications;
3) experiment scenario when dealing with post-test calculation as in the case here considered.

The final product is a "code model", that is a compromise between the user knowledge of the code performance, of the facility hardware and of the simulated transient scenario; the code cabilities and the required CPU time also play a role in defining the specifications of the input model.

Taking into account of the above, in order to realize a critical comparison of the nodalizations, twenty items related to the input decks (Tab. XII, Figs. 27 to 30) are compared among each other. These have been split into three groups:

- the elements characterizing the degree of detail of the code model (e.g. number of nodes etc.; items 1 to 5);
- the elements characterizing the "nodalization fidelity" to the geometrical data of the facility (e.g. value of the overall volume of the facility; items 6 to 11);
- the elements characterizing the interface between hydraulics and geometry (essentially pressure drop coefficients; items 12 to 20).

From the comparison of the above data, the following considerations can be made:

1) <u>elements characterizing the nodalization detail</u>.

In relation to the number of nodes, on one hand RELAP and ATHLET codes, with roughly 150 nodes, on the other hand the CATHARE code, with more than 300 nodes, and the TRAC code, with 250 nodes, can be distinguished.

This choice is only partially due to the user; instead the code numerical structure plays an important role for establishing the degree of detail of the code model. As an example, RELAP code, owing to the Courant limit, needs nodes having length greater than few tens of centimeters for making possible the simulation of typical LOCA transients, while CATHARE code has not such a constraint, allowing a greater freedom. Still, a geometrical discontinuity cannot be modelled as it is by the CATHARE code, but needs several components (nodes) of small dimension in the flow direction which are characterized by different areas.

In principle, the best results for a physical simulation should be given by a nodalization with a number of nodes ad large as possible, but this idea is abruptly nullified by the majority of the current system codes. Otherwise, an optimal number of nodes can be recognized for each code for a given simulation problem. Directions for the attainment of this number are not available in any code manual: only the user experience can achieve this parameter, considering the phenomena to be analyzed, in line with the available resources (CPU, computers, etc.) and the goals of the study, e.g. sensitivity analyses aiming at the interpretation of physical phenomena, licensing calculations, etc. It should be noted that a large

ITEM	TRAC/PF1 CEA	CATHARE V1.3 CENG	R5/M2 DCMN	ATHLET GRS	R5/M1-EUR JRC	R5/M2 UKAEA	EXP	notes
1. number of nodes	249	331	126	145	177	160	-	
2. number of junctions	40	-	132	163	185	165	-	
3. number of heat structures	151/64°	212	155	167	216	201	-	° pipe walls, SG U tubes
4. number of core structures	17	42	15	10	12	6	-	
5. overall number of structures mesh points	1355	848	1302	510	1036	1062	-	
6. free total volume of the facility without PRZ (m^3)	0.527	0.522	0.524	0.522	0.522	0.523	0.522	
7. free total volume of IL SG SS (m^3)	0.869	0.750	0.770	0.770	0.770	0.797	0.771	
8. free total volume of BL SG SS (m^3)	0.285	0.260	0.259	0.258	0.257	0.270	0.260	
9. fluid mass in PS (kg)	375	370	373	373	373	370.05	370	without PRZ and UH
10. fluid mass in IL SG SS (kg)	353	310	392	359	228	360	359.5	
11. fluid mass in BL SG SS (kg)	118	110	144	132	77	144.2	133.4	
12. K_f/K_r at free core area	28/28	1.9/0.9	35/35	27/27	2.0/2.0	2.32/2.3	-	
13. K_f/K_r at SG IL inlet of the U-tubes	9/9	0.26/0.26	20/20	12/12	0.36/0.36	1/0.3	-	
14. K_f/K_r at SG BL inlet of the U-tubes	24/24	0.38/0.38	50/50	58/58	0.37/0.37	2.05/0.55	-	
15. K_f/K_r at PU IL inlet	0.25/0.25	3.6/2.6	0.6/0.2	48/49	0.06/0.02	0.291/0.251	-	
16. K_f/K_r at PU BL inlet	0.25/0.25	3.6/2.6	0.3/0.7	7.6/7.5	0.03/0.08	0.16/0.21	-	including HL and CL connections to RPV
17. $\Sigma K_f(\Sigma K_r)$ in IL	37	7	32.2(32.2)	-	68	1.85(1.85)	-	as above
18. $\Sigma K_f(\Sigma K_r)$ in BL	73	64	173.1(173.1)	-	-	3.95(3.76)	-	
19. friction factor in IL HL	NFF=2°	-	0.018	0.02	-	-	NA	° TRAC option
20. friction factor in core region	-	-	0.012	0.02	-	-	NA	

Tab. XII - Items related to the input decks

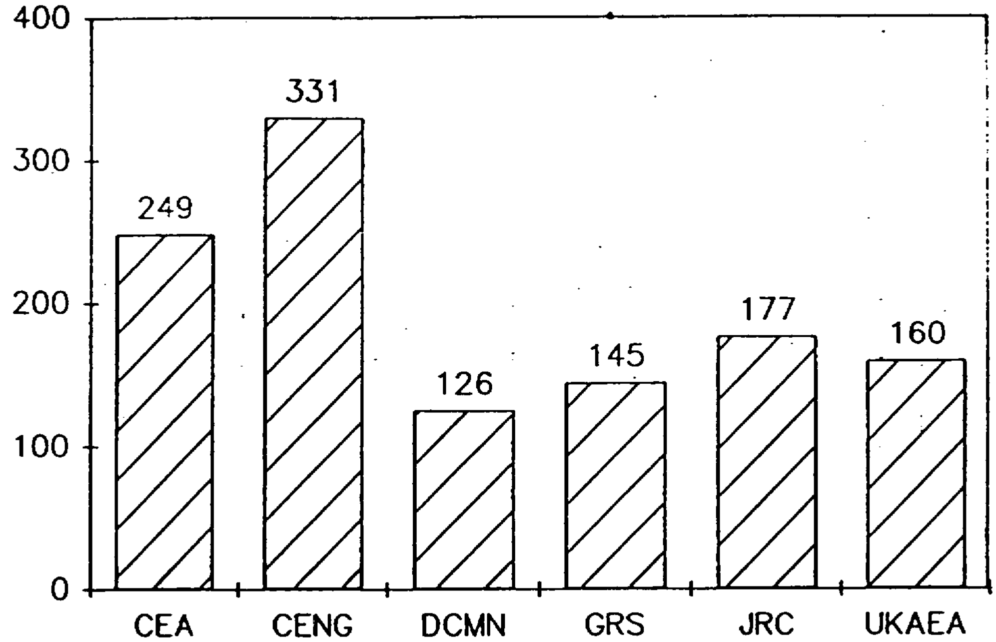

Fig. 27 - Number of nodes chosen by various users for nodalizing the LOBI facility

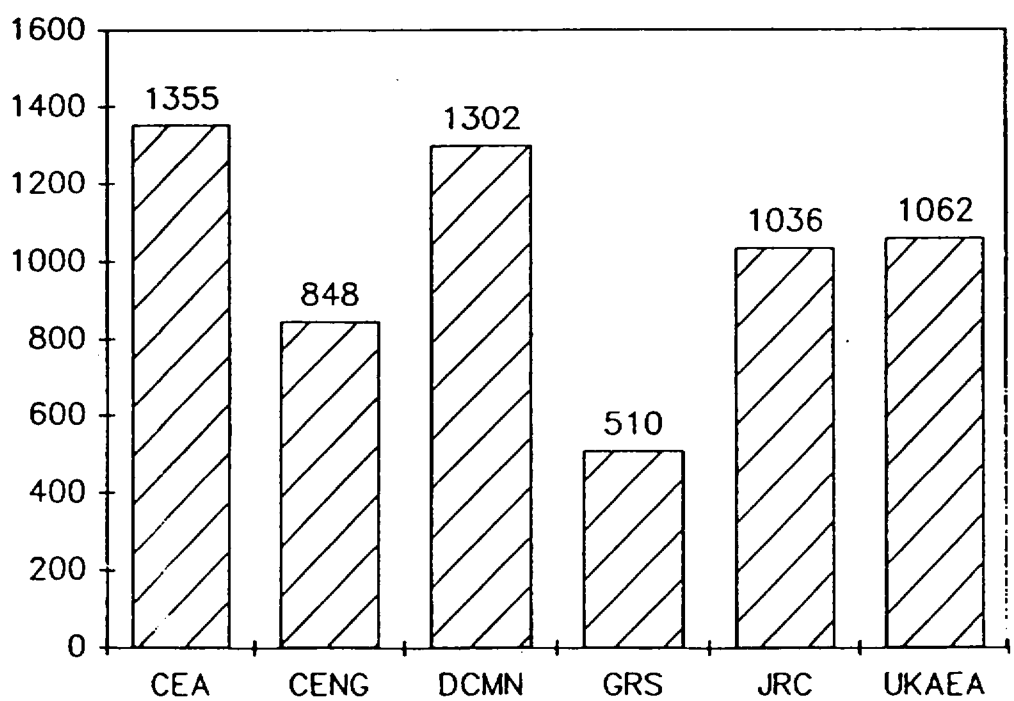

Fig. 28 - Overall number of structures mesh points chosen by various users for nodalizing the LOBI facility

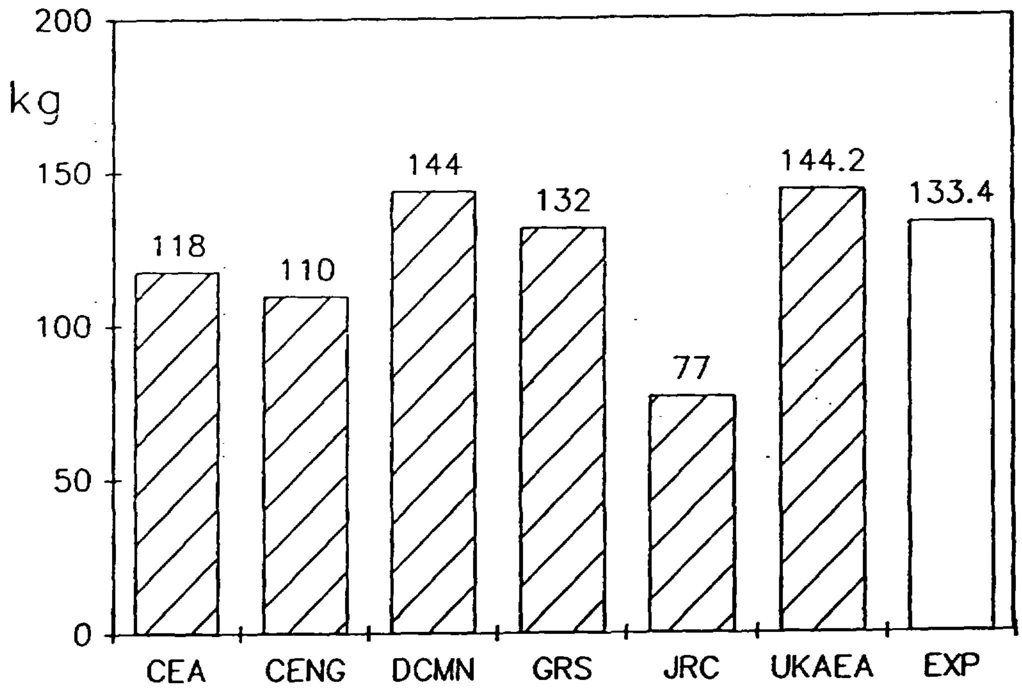

Fig. 29 - Mass inventory in broken loop steam generator secondary side resulting from steady-state calculation by various users and comparison with experimental data

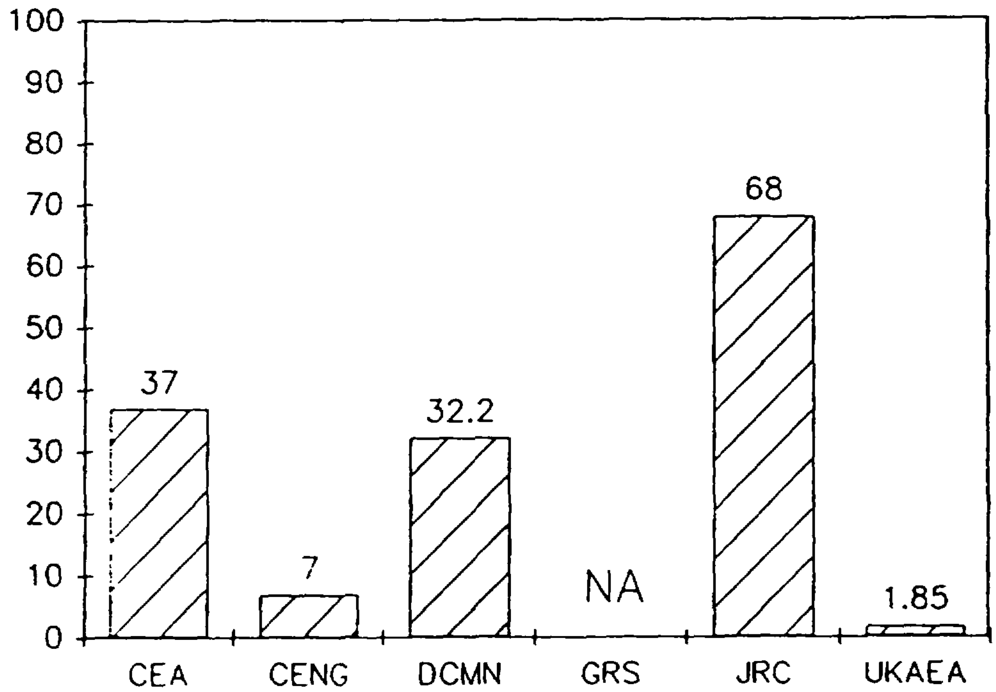

Fig. 30 - Forward pressure drop coefficient at intact loop connection with pressure vessel as selected by various users

amount of sensitivity analyses can bring substantial improvements of nodalization parameters; in this way coarse nodalization, with few elements, can produce better results than fine nodalization with much larger number of elements. This is valid for items 1 to 5.

Concerning the overall number of structures mesh points (item 5), the capital influence of this parameter on the heat transfer mechanism must be stressed. In particular, the heat release from structures is strongly affected by the number of meshes. The experience on system code assessment demonstrate that mesh thickness of few millimeters for piping and flanges, few tenths of millimeters for fuel rods, should be used for a suitable schematization.

2) "nodalization fidelity" to the geometrical data

The geometrical fidelity of the nodalization to the system hardware is a code model peculiarity that should be considered very carefully. As a difference from the nodalization detail, that is essentially an user choice, the agreement betwen input and actual system related parameters is an objective goal to be pursued. With reference to the overall volume of the facility, that can be considered the most important parameter in this group, the following approximations or inadequacies affect the agreement between actual system value and code input value:

- imperfect knowledge of the plant data (drawings inadequacies, consideration of thermal dilatation of structures, etc.);
- presence of dead ends (nozzle, instrumentations lines, etc.);
- need to simulate a three dimensional configuration with a one-dimensional one.

The experience demonstrates, for example, the acceptability of few percent error on the nominal value of the overall facility volume.

Another aspect of the nodalization fidelity is related to the active heat transfer areas, i.e. sources and sinks. In relation to this, the most important characteristics to be preserved are the total core area and the overall steam generator heat transfer surface. Usually, these parameters are respected with an error less than 1%.

Two further problems, typically encountered by system code user, arise during the development of a nodalization:

a) with reference to a PWR typical plant, the choice of the hydraulic channels number in the steam generator and in the core (for a BWR plant the same problem may occur in relation to the number of jet pumps and still to the number of core channels /8/). A schematization with only few "pipes" can preserve the overall thermal energy balance, but is blind towards a nonuniform behaviour of the various channels (e.g. nonuniform flow distribution in the steam generator U-tubes, or in the lower plenum of reactor vessel or in the steam generator plena, channel oscillations, etc.);
b) passive structures of the plant. The consideration of all the structures constituting vessel, piping and internal wall, as well as flanges, valves and pump casing is almost impossible owing to limitations of computer memory. Approximations are needed and are usually done. Errors of the order of few percent and less than 20% of the nominal values of passive heat transfer areas and volumes, respectively, appear to be acceptable.

3) interface between hydraulics and geometry of the code model

This topic refers, essentially, to local and distributed pressure drops coefficients. With reference to the friction factor, a substantial difference among the various basic models implemented in the codes can be observed, e.g. the dependency of friction factor upon the Reynolds number is not considered in the same way in all codes: for example Colebrook correlation is used in RELAP5/MOD2 and peculiar correlations are adopted by TRAC and CATHARE. Still roughness is only accounted by the RELAP input deck, while it has no influence on calculated pressure drops in CATHARE and TRAC.

Finally, with regard to the form loss coefficients, items 12 to 18 in Tab. XII the following remarks can be made:

a) there is no theoretical model siutable to calculate this parameter in the wide variety of configurations encountered in modelling a typical nuclear plant or simulator; still no relaptionship gives the dependency of these factors upon Reynolds number and local void fraction;
b) experimental uncertainties are often connected to this parameter, usually derived from pressure drop measurements;
c) loss coefficients values have to account for the three-dimensional effects that cannot be modelled by a one-dimensional code;
d) in definitive, these factors are a sort of "magic numbers", that, in order to have a good code prediction, must counterfeit many of the thermalhydraulic model deficiencies.

The data reported in Tab. XII and in Fig. 31 to 34 give an idea of typical dispersion range associated with assumed values of these parameters. It should be noted that "all" the above values lead to "reasonable agreement" with experimental data at least as far as the initial steady state in concerned (next section).

5.2.2 - Significant results from the calculations

The first natural circulation steady state of the test is executed at nominal mass inventory (100% of Residual Mass excluding upper head). During this period, a subcooled single-phase natural circulation flow takes place between core and steam generator.

This presents a particular interest because:

a) it constitutes the first way to test the computer codes as well as the nodalizations during natural circulation flow;
b) this is the situation that comes out in the primary side of a PWR after scram and main circulating pumps trip, without loss of coolant.

Relevant results from steady state calculations by the various codes are summarized in Tab. XIII and in Figs. 35 to 38. At least two inherent limitations of the available experimental data base should be pointed out:

a) core power is 183 kW, while heat losses to environment from primary loop are of the order of 60 kW, with at least 10 kW uncertainty;
b) the operation of feedwater and steam line in the secondary side is not entirely specified: involved flowrates are sufficient to maintain constant the pressure in the secondary side and to remove the residual power coming from primary loop, but the recirculation flowrates and the temperature distribution in the riser of the secondary side steam generator are not fully specificed.

The above two facts, together with the different possibilities of assigning the initial temperature distribution inside the wall structures in the zones where heat losses are concentrated, lead to indetermination in the calculation of loop energy balance. As an example, 1 K of uncertainty in secondary side mean temperature in the subcooled riser region may correspond to about 10 kW of indetermination in the power exchange between primary and secondary side.

Still, a variation of about 10% around the nominal experimental value of loop flowrate also corresponds to variation of few tens kW in the heat transfer across steam generators.

Finally, the pressure differences over the steam generators (less than

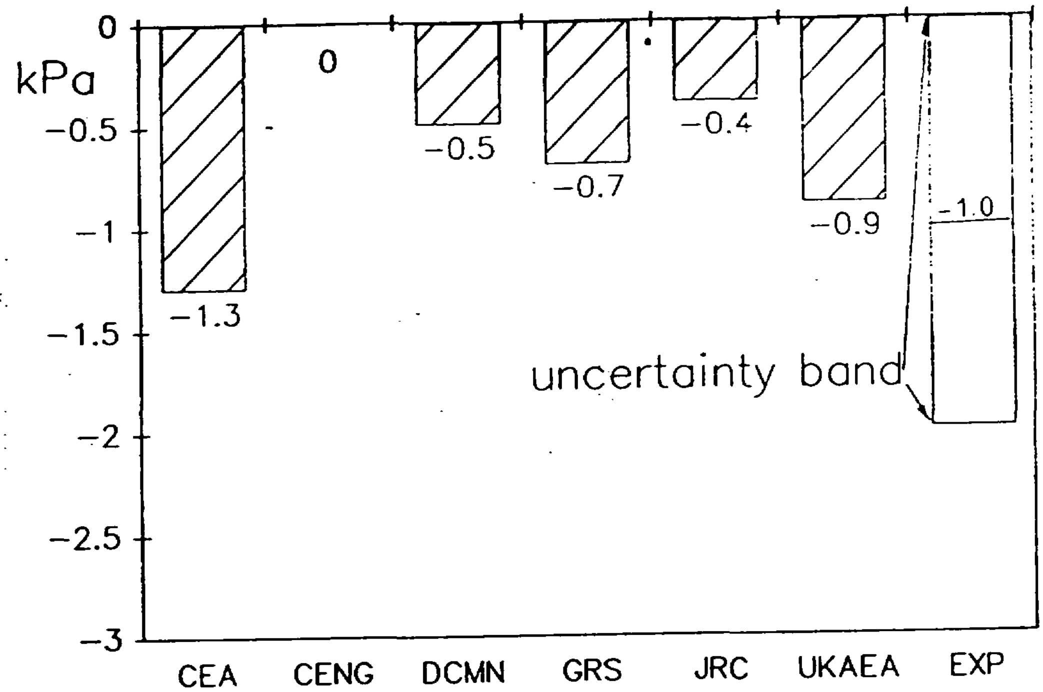

Fig. 31 - Pressure drop over steam generator intact loop primary side resulting from steady-state calculation by various users and comparison with experimental data

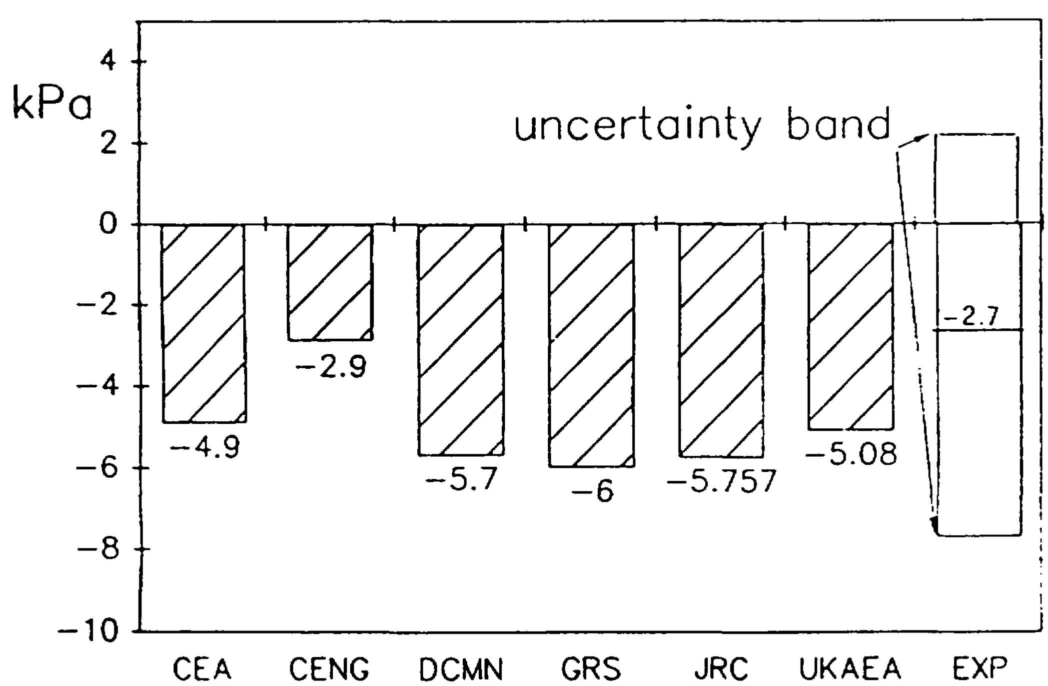

Fig. 32 - Pressure drop over steam generator broken loop primary side resulting from steady-state calculation by various users and comparison with experimental data

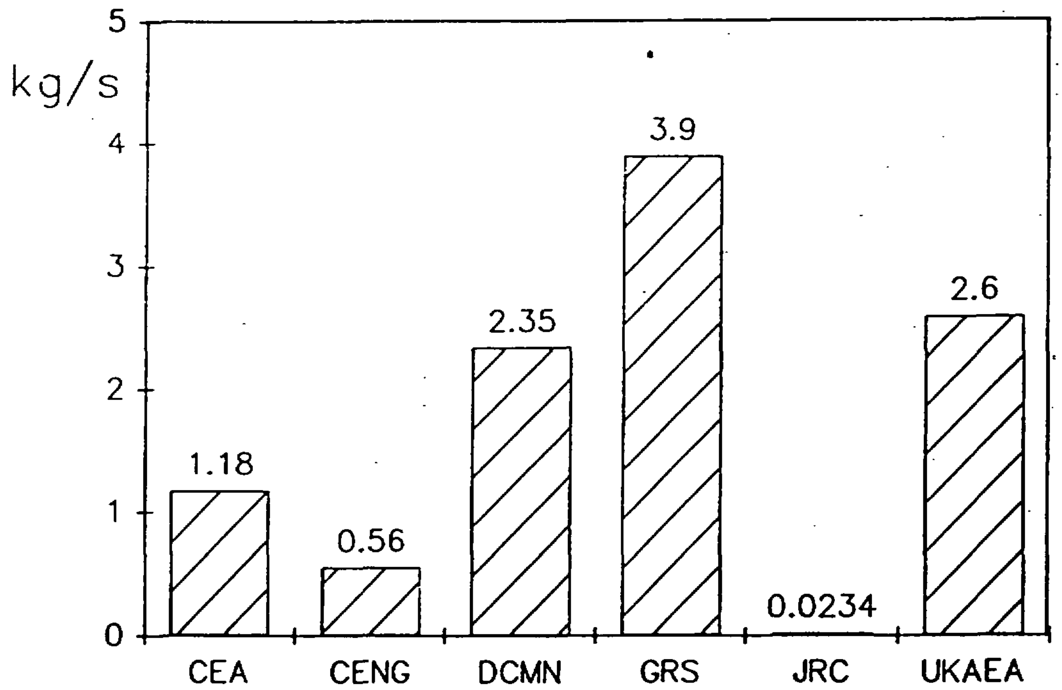

Fig. 33 - Mass flowrates in downcomer of steam generator intact loop resulting from steady-state calculation by various users

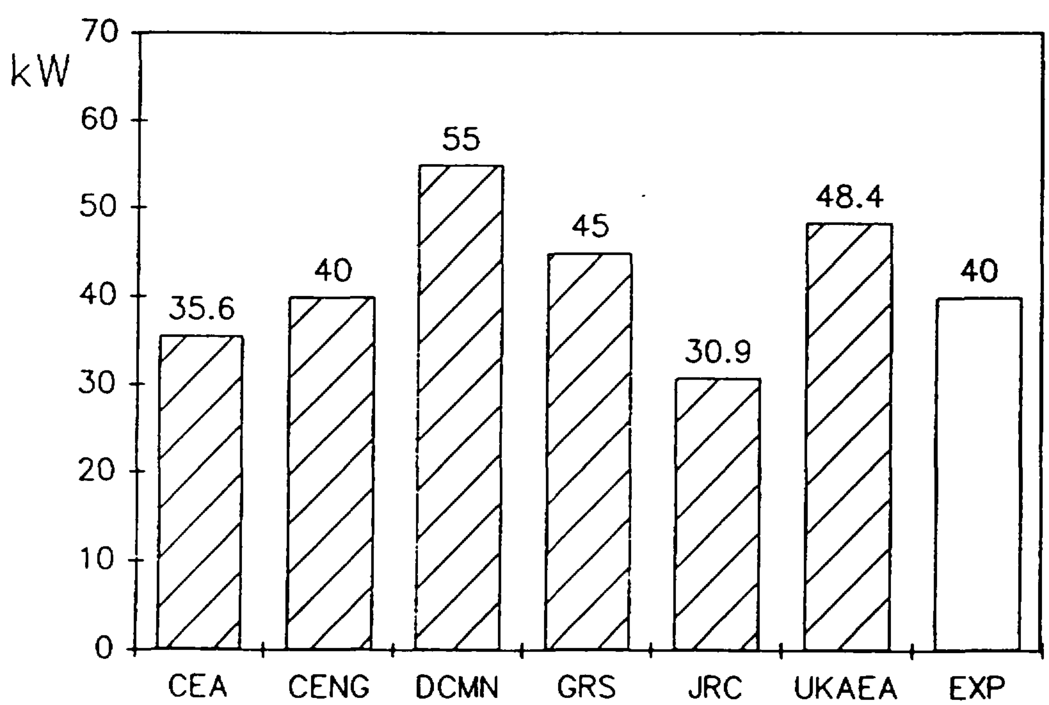

Fig. 34 - Power losses to environment considered by various users and comparison with experimental data

ITEM	TRAC/PF1 CEA	CATHARE V1.3 CENG	R5/M2 DCMN	ATHLET GRS	R5/M1-EUR JRC	R5/M2 UKAEA	EXP	notes
21 distribution of fluid temperature in IL	Fig. 12	Fig. 12	Fig. 12	Fig. 12	Fig. 12	Fig. 12	Fig. 12	enclosed
22 distribution of fluid temperature in RPV	Fig. 13	Fig. 13	Fig. 13	Fig. 13	Fig. 13	Fig. 13	Fig. 13	enclosed
23 distribution of fluid temperature in IL SG UT	Fig. 14	Fig. 14	Fig. 14	Fig.14	Fig. 14	Fig. 14	Fig. 14	enclosed
24 distribution of fluid temperature IL SG SS RI	Fig. 15	Fig. 15	Fig. 15	Fig. 15	Fig. 15	Fig. 15	Fig. 15	enclosed
25 Dp over IL (kPa)	-0.45	0	-0.70	-0.7	-0.928	-1	0. ±2	
26 Dp over BL (kPa)	-0.40	0	-0.70	-0.6	-0.988	-1.05	-0.8 ±0.8	
27 Dp over SG IL (kPa)	-1.3	0	-0.50	-0.7	-0.400	-0.9	-1.0 ±1.0	
28 Dp over SG BL (kPa)	-1.3	0	-0.40	-0.6	-0.400	-0.8	-0.75 ±1.0	
29 Dp over IL PU (kPa)	-5.9	-6.7	-5.8	-8.0	-6.204	-8.02	-8.0 ±2.0	
30 Dp over BL PU (kPa)	-4.9	-2.9	-5.7	-6.0	-5.757/-1.80	-5.08	-2.7 ±5.0	
31 mass flowrate in IL CL (kg/s)	1	1.03	0.98	1.1	1.02	1.1	1.0	
32 mass flowrate in BL (kg/s)	0.3	0.33	0.31	0.38	0.32	0.36	0.3	
33 pressure in UP (MPa)	14.0	14.3	14.0	14.0	14.03	14.0	14.0	
34 temperature in PRZ (K)	-	609	609	609	609.8	609	609	
35 level (collapsed) in PRZ (m)	-	2.7	2.52	2.5	4.9	1.9	2.5	
36 pressure in SGs SS (MPa)	8.66/8.62 °	8.65	8.65	8.65	8.66	8.65	8.65	° IL/BL
37 FW temperature at IL & BL (K)	298	298	298	298	298	303.15	298	
38 temperature at IL & BL SG outlet (K)	574	563/571 °	573	573	573.75	573.62	573	° IL/BL
39 DC collapsed level in SG IL (m)	8.19	8.6	8.58	8.6	6.44	8.7	8.6	
40 DC collapsed level in SG BL (m)	8.25	8.9	8.90	8.9	6.56	8.9	8.9	
41 mass flowrate in DC of SG IL (kg/s)	1.18	0.56	2.35	3.9	0.0234	2.6	NA	
42 mass flowrate in DC of SG BL (kg/s)	0.27	0.52	0.52	1.0	-0.11	0.8	NA	
43 power losses PS environment (kW)	35.6	40	55	45	30.9	48.4	40	excl. PU and water
44 power losses SG IL environment (kW)	8.9	22	14	12.4	16.83	24	29 ±5	
45 power losses SG BL environment (kW)	10.4	20	12	14.3	12.1	18	21 ±5	
46 power exchange across SG IL (kW)	117.8	96	105	105	72.9	NA	NA	
47 power exchange across SG BL (kW)	32	47	31	32	22.3	NA	NA	
48 core power (kW)	183	183	183	183	178.5	183	183	
49 UP DC bypass flow (kg/s)	-	0.013	0.023	0.039	0.018	0.064	-	
50 HL - DC bypass flow (kg/s)	-	0.025	0.013	0.039	0.037	0.032	-	
51 core bypass (kg/s)	-	0	-	0.052	0	-	-	

Tab. XIII - Items related to the initial steady state

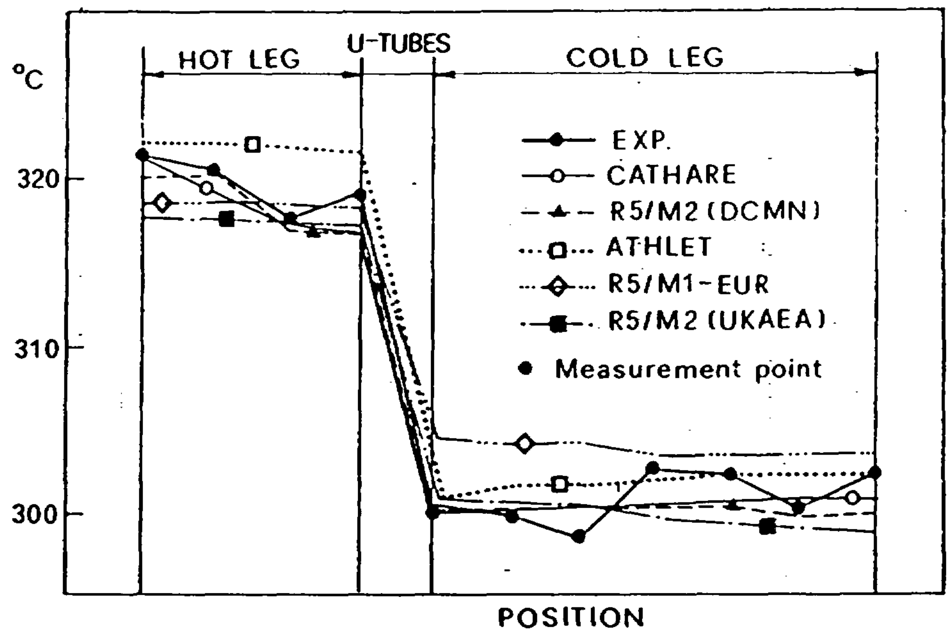

Fig. 35 - Distribution of fluid temperature along intact loop resulting from steady-state calculation by various users and comparison with experimental data

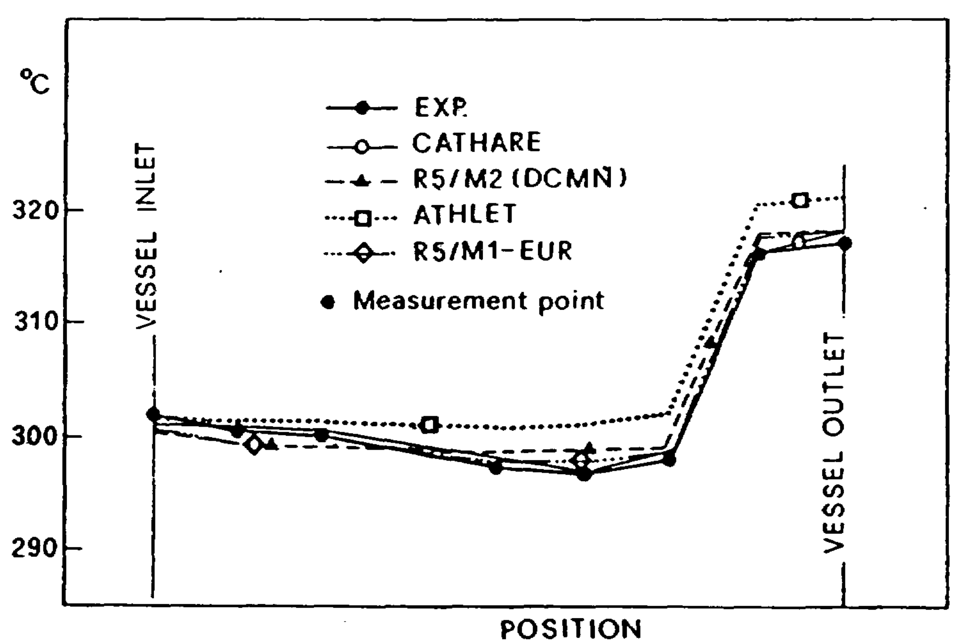

Fig. 36 - Distribution of fluid temperature inside reactor pressure vessel resulting from steady-state calculation by various users and comparison with experimental data

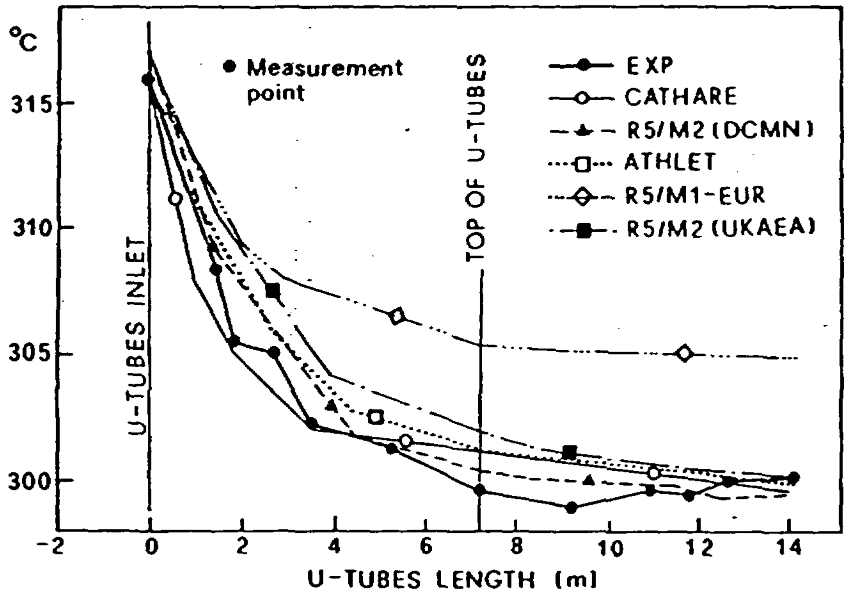

Fig. 37 - Distribution of fluid temperature along U-tubes of steam generator intact loop resulting from steady-state calculation by various users and comparison with experimental data

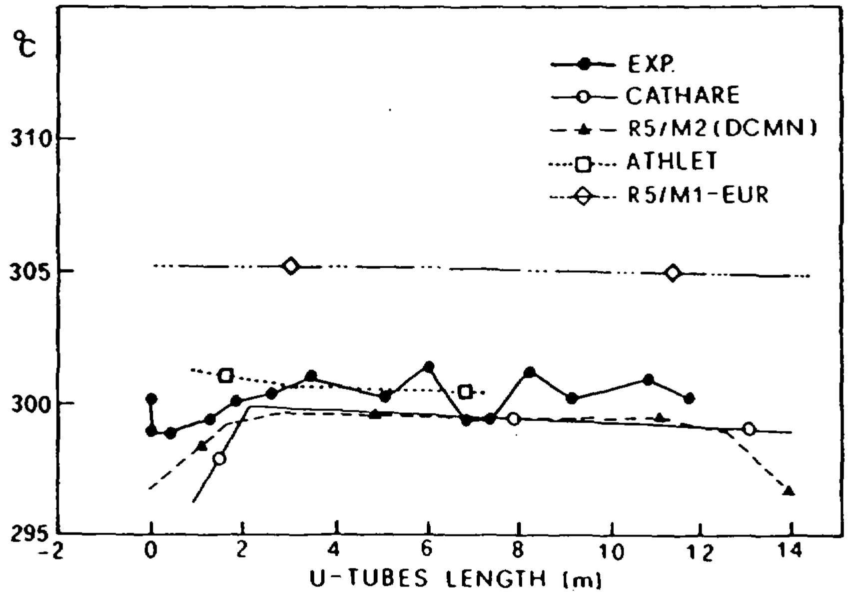

Fig. 38 - Distribution of fluid temperature in intact loop steam generator secondary side riser resulting from steady-state calculation by various users and comparison with experimental data

zero, that is with a pressure gain, in this case; items 27 and 28 and Fig. 31) have an error band of the order of 200% of the measured value. This uncertainty is very critical because inherent to a quantity strongly affecting the U-tubes behaviour.

The above considerations partially explain the differences between initial values of parameters shown in Tab. XIII and in Fig. 27 to 38. In definitive, each user interprets in a subjective way the uncertainties characterizing the experimental data; then the importance of the user quantification is once again highlighted.

An exaustive report of the comparison between measured and predicted results of each calculation is not the objective of the present document. In the attempt to be more complete and, partly, to give an idea of the consequences of the choices discussed in the previous section, the calculated flowrates during the whole transient are compared with the nmeasured values in Fig. 39 and 40 as a function of the overall residual mass of the primary side. Reference is made to the intact and the broken loop, respectively.

The qualitative evaluation of the transient is well predicted by each code, that is the various codes capture the basic physics of the involved phenomena, but the quantitative values of the physical variables are nor satisfactory. The codes limitations already discussed before also apply in this case.

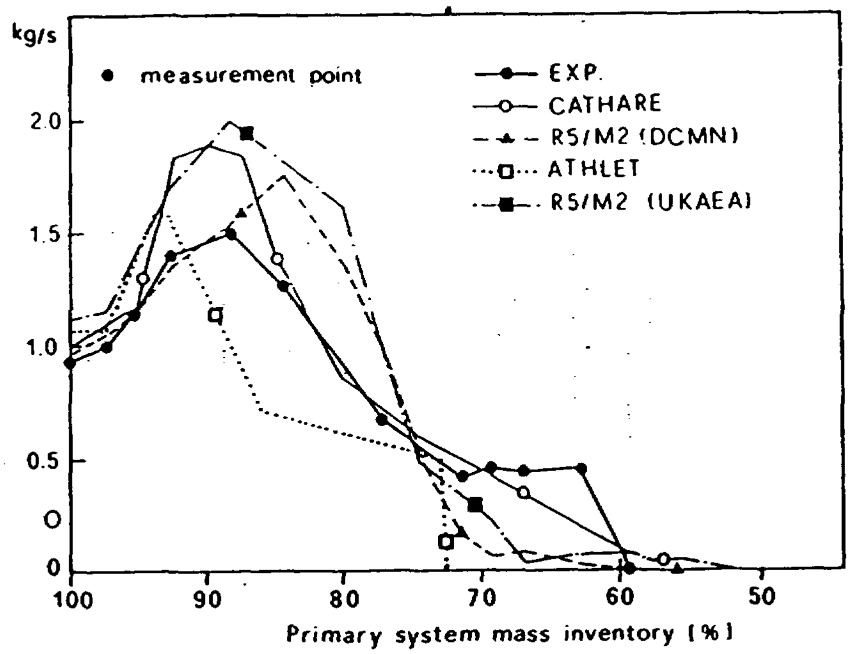

Fig. 39 - Comparison between measured and calculated trends of steady-state mass flowrate in intact loop during the whole transient as a function of primary side mass inventory

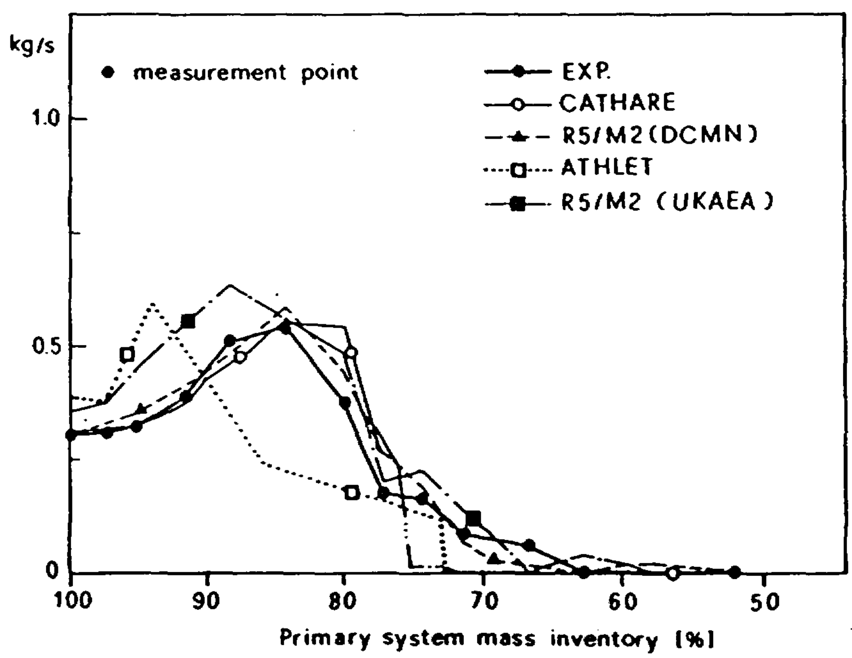

Fig. 40 - Comparison between measured and calculated trends of steady-state mass flowrate in broken loop during the whole transient as a function of primary side mass inventory

6. CONCLUSIONS

The appplication of RELAP5/MOD2 to post-test analysis, of the natural circulation test A2-77A performed in LOBI/MOD2 facility, showed the good quantitative capability of the code in predicting a transient characterized by low fluid velocities. The "tuning" of some input conditions also allowed the achievement of good quantitative agreement.

The analysis led to the identification of deep differences in the interpretation of an assigned experimental data base, from various users.

The evaluation of the relationship between user choice and code predicted test scenario was not the main purpose of the present paper; nevertheless, the study allowed to emphasize the role of user and raised some concern in relation to the validity of large system code assessment activities performed all over the world.

The discrepancies between experimental data and code predictions are due both to the intrinsec code limit and to the user behaviour. There is a worthful need to quantify the percentage of disagreement due to the poor utilization of the code and that due to the code itself.

The quality of the input data base (nodalization) should be consistent with the quality of the prediction: i.e. a good prediction obtained by the use of a unrealistic input deck should be seen as unphysical. A check in this connection is always necessary from the code user; in particular, exhaustive and objective information related to the approach pursued in setting up the nodalization and possibly in its "tuning" should be supplied in any calculation report.

Unfortunately the emphasized uncertainties in the boundary conditions prevent the possibility to definetely evidence code limitations. An example of this is given by the influence of roughness on the results (sect. 4.4).

Taking into account of the above, the following thermalhydraulic models are presumed to be mostly responsible of the disagreement between measured and calculated trends:

- one-dimensional approach in modelling some components (e.g. steam generator plena);
- flooding (especially during the "reflux condensation" period);
- stratification in horizontal pipes: the inadequacy of this model, with main reference to the prediction of piping related phenomena, is the possible cause of the flowrates overestimation shown during the transient by most codes;
- dependence of local pressure drop upon Reynolds number and void fraction.

As an additional result of the study, an explanation of the phenomenology at the basis of the oscillations measured in the LOBI PWR simulator during natural circulation has been proposed. The origin of the instabilities is a sort of siphon condensation controlled by flooding that occurs in the ascending legs of U-tubes. The energy transfer between core and steam generators constitutes the driving force for the instability mechanism.

The application of basis thermalhydraulic models demonstrated that different configurations presumably occur at the same time for the different U-tubes. Some of these are in stalled conditions as far as inlet steam flow is concerned, others are in the flooding process, the CCFL occurs in a third group ot U-tubes (Fig. 26).

The application of RELAP5/MOD2 code made it possible to evaluate the influence on the phenomena of boundary and initial conditions. In particular, it was found that different parameters affect the frequency and amplitude of oscillations; the length/diameter ratios of the hot legs and core power are significant ones. The occurrence of voiding in the horizontal parts of cold legs at the onset of instability also resulted from calculations and is in agreement with the experimental observation. This conclusion should be obvious if one considers the limitations of the current generation codes not discussed in the present paper.

The phenomenon is typical of U-tube geometry, so oscillations are foreseeable for nuclear plant situations. A code calculation performed with reference to the DOEL PWR supported this conclusion. Interaction between neutronics and thermal hydraulics should be evaluated in different plant configurations.

Finally the consideration of two parallel U-tubes in SG PS does not appear convenient due to the basic 1-D model implemented in the code (case E) and owing to uncertainties in fixing the boundaries, which overshadow the differences between calculations utilizing one or two U-tubes.

REFERENCES

/1/ F. D'Auria: "Experimental Facilities and System codes in Nuclear Reactor Safety". Int. Seminar State of the Art on Safety and Licensing of Nuclear Power Plants, Varna (BG), Nov. 2-6 1987.

/2/ F. D'Auria, G.M. Galassi: "Code assesment methodology and results" IAEA Tech. Committee on Computer Aided Safety Analysis, Moscow (USSR), May 14-17 1990.

/3/ G. De Santi, G. Leva: "Quick Look report on LOBI-MOD2 Test A2-77A" - LQC 85-32, JRC Ispra (I), Dec. 1985.

/4/ J. Sanders, E. Ohlmer: "Experimental data Report on LOBI-MOD2 test A2-77A" - LEC 85-33, JRC Ispra (I), April 1985.

/5/ F. D'Auria, G.M. Galassi, F. Oriolo: "Advancements in the assessment of system codes used for Safety Analyses of Nuclear Power Plant" - Workshop on the IAEA Programme on Computer Aided Safety Analysis, Warsaw (Pl), May 1985.

/6/ G. De Santi, L. Piplies, W.L. Riebold: "Analysis of natural circulation phenomena in the LOBI/MOD2 facility" - ANS/ENS Top. Meet. on Thermal Reactor Safety - San Diego (CA), Feb. 1986.

/7/ G. De Santi, L. Piplies, J. Sanders: "Mass flow Instabilities in LOBI Steam Generator U-tubes array under natural circulation conditions" - 2nd Int. Top. Meet. on NPP Thermalhydraulics and Operation, Tokio, (J) Apr. 1986.

/8/ H. Stadke, B. Worth: "Personal communication to F. D'Auria" - June 1987.

/9/ J. Sanders: "Stability of single phase natural circulation with inverted U-tube steam generator", J. Heat Transfer, Vol. 110, 635-742, 1988.

/10/ A. Annunziato: "Influence of Secondary System Conditions on SG U-tubes Flow Distribution during Single Phase Natural Circulation", JRC NT 1.90.39, Ispra (I), May 1990.

/11/ F. D'Auria, G.M. Galassi: "Flowrate and density oscillations during two-phase natural circulation in PWR typical conditions", Third Int. Topical Meeting on Nuclear Power Plant Thermalhydraulics and Operations, Seoul (K), Nov. 4-7 1988; also J. of Nuclear Engineering and Design (1990).

/12/ F. D'Auria, G.M. Galassi: "Characterization of Instabilities during two-phase natural circulation in PWR typical conditions", Fourth Int. Top. Meet. on Nuclear Reactor Thermalhydraulics, Karlsruhe (FRG) Oct 10-13 1989; also J. Experimental Thermal and Fluid Science (1990).

/13/ F. D'Auria, G.M. Galassi, P. Lombardi: "Interaction of User and Models in system Codes Predictions", CNS-ANS Int. Conf. on Simulation Methods in Nuclear Engineering, Montreal (C), Apr. 18-20 1990.

/14/ A. Calastri, F. D'Auria, G.M. Galassi, P. Vigni: "Scaling of natural circulation in PWR Systems", Eurotherm Seminar Nr. 16: Natural Circulation in Industrial Applications, Pisa (I), Oct. 11-12, 1990.

/15/ G.B. Wallis, A.S. Karlin, C.R. Clark, D. Barathan, Y. Hagi, H.J. Richter: "Countercurrent gas liquid flow in parallel vertical tubes", Int. J. Multiphase Flow, vol. 7, 1981.

/16/ A. Hawighorst, H. Kroning, D. Mewes, R. Spatz, F. Mayinger: "Fluiddynamic effects in the fuel element top nozzle area during refilling and reflooding", Report EUR 10165 EN, Bruxelles (B), 1985.

/17/ A. Calastri, F. D'Auria, P. Lombardi: "Parametric Analysis of Parallel Channel behaviour in BWR Conditions performed by RELAP5/MOD2 code" (in Italian) University of Pisa Report DCMN NT 147 (89), Pisa (I) 1989.

ABBREVIATIONS

ACC : Accumulator
AFW : Auxiliary FeedWater
AL : Ascending Leg
BL : Broken Loop
BWR : Boiling Water reactor
CAT1 V1.3 : CATHARE 1 V1.3
CCFL : CounterCurrent Flow Limitation
CEA : Commissariat à l'Energie Atomique
CEC : Commission of European Communities
CENG : Centre d'Etudes Nucleaires de Grenoble
CL : Cold Leg
CSNI : Committee on the Safety of Nuclear Installations
CPU : Central Processing Unit
DC : Downcomer
DCMN : Dipartimento di Costruzioni Meccaniche e Nucleari
DL : Descending Leg
EXP : Experiment
F : France
FRG : Federal Republic of Germany
FW : Feedwater
GRS : Gesellschaft für Reaktorsicherheit
HL : Hot Leg
HPIS : High Pressure Injection System
I : Italy
IAEA : International Atomic Energy Agency
IL : Intact Loop
IN : Inlet
ISP : International Standard Problem
JRC : Joint Research Centre
LP : Lower Plenum
MCP : Main Coolant Pump
NC : Natural Circulation
OECD : Organization for Economic and Commercial Development
OF : Onset of Flooding
OU : Outlet
PRV : Reactor Pressure Vessel
PRZ : Pressurizer
PS : Primary System
PU : Pump
PWR : Pressurized Water Reactor
R5/M1-EUR : RELAP5/MOD1-EUR
R5/M2 : RELAP5/MOD2
RHO : Density
RI : Riser
RM : Residual Mass
RPV : Reactor Pressure Vessel
SCA : Shared Cost Action
SG : Steam Generator
SS : Secondary Side
T : Temperature
UH : Upper Head
UK : United Kingdom
UKAEA : United Kingdom Atomic Energy Authority
UP : Upper Plenum
UT : U-Tubes

V : Velocity
VF : Liquid Velocity
VG : Steam Velocity
VOIDG : Void Fraction

SYMBOLS

C : constant in the Hawighorst formula [= $1+\tanh(P/80)(\sigma/g\rho_{gf})^{0.5}$], dimensionless
D : hydraulic diameter, m
DP : differential pressure, N/m^2
DT : mean temperature difference between primary and secondary sides of U-Tubes, °C
g : gravity constant, m/s^2
h : enthalpy, J/Kg
H : heat transfer coefficient, W/(m^2·°C)
J : superficial velocity, m/s
K_f : forward localized pressure loss coefficient
K_r : reverse localized pressure loss coefficient
P : wetted perimeter, m
s : time into the transient, s
t* : time at which residual mass in the primary loop equals 64% of the initial value, s
t : time necessary to fill the ascending leg of one U-Tube,s

Greek Symbols

ρ : density, kg/m^3
σ : surface tension N/mn

Subscripts

cond : Condensation
CR : Critical value
f : Related to liquid
fg : Such that $Y_{fg} = Y_g - Y_f$
g : Related to gas
gf : Such that $Y_{gf} = Y_f - Y_g$
in : Inlet

APPENDIX A

Measured and calculated trend for case A (Initial calculation)

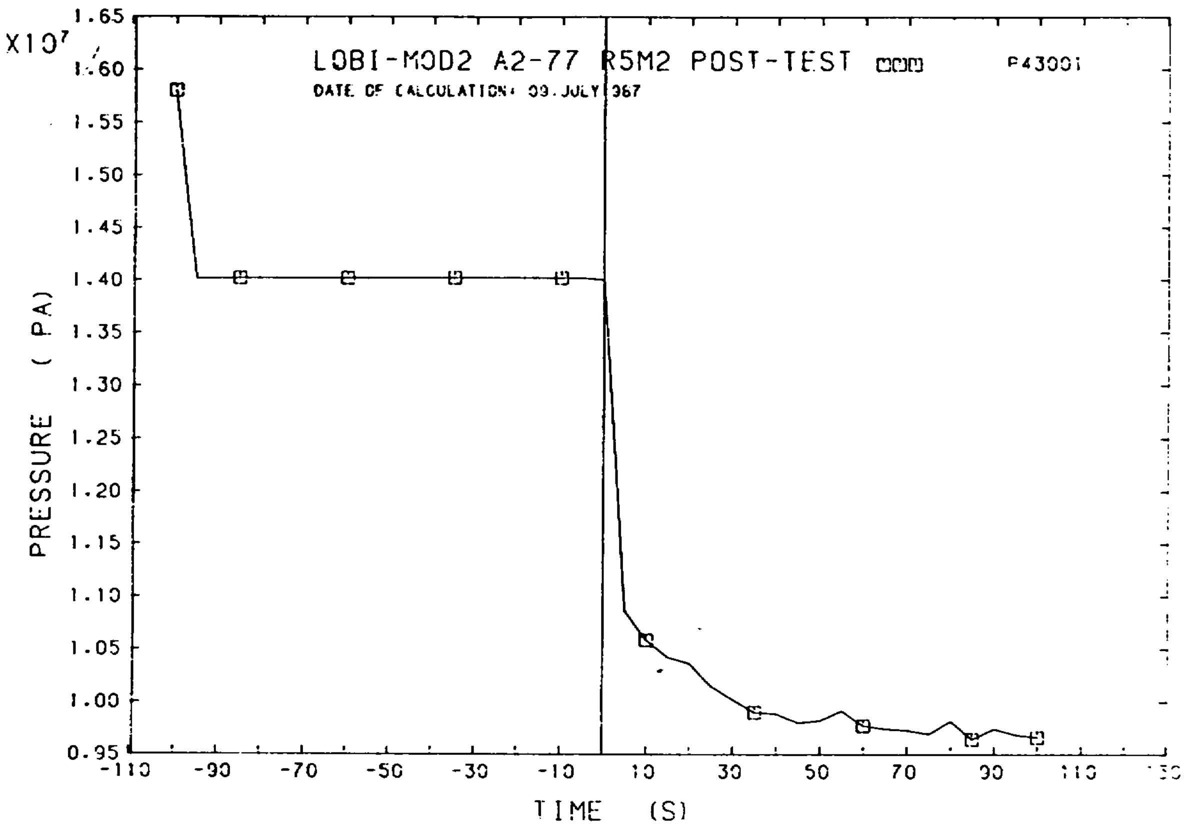

FIGURE A1 UPPER PLENUM PRESSURE

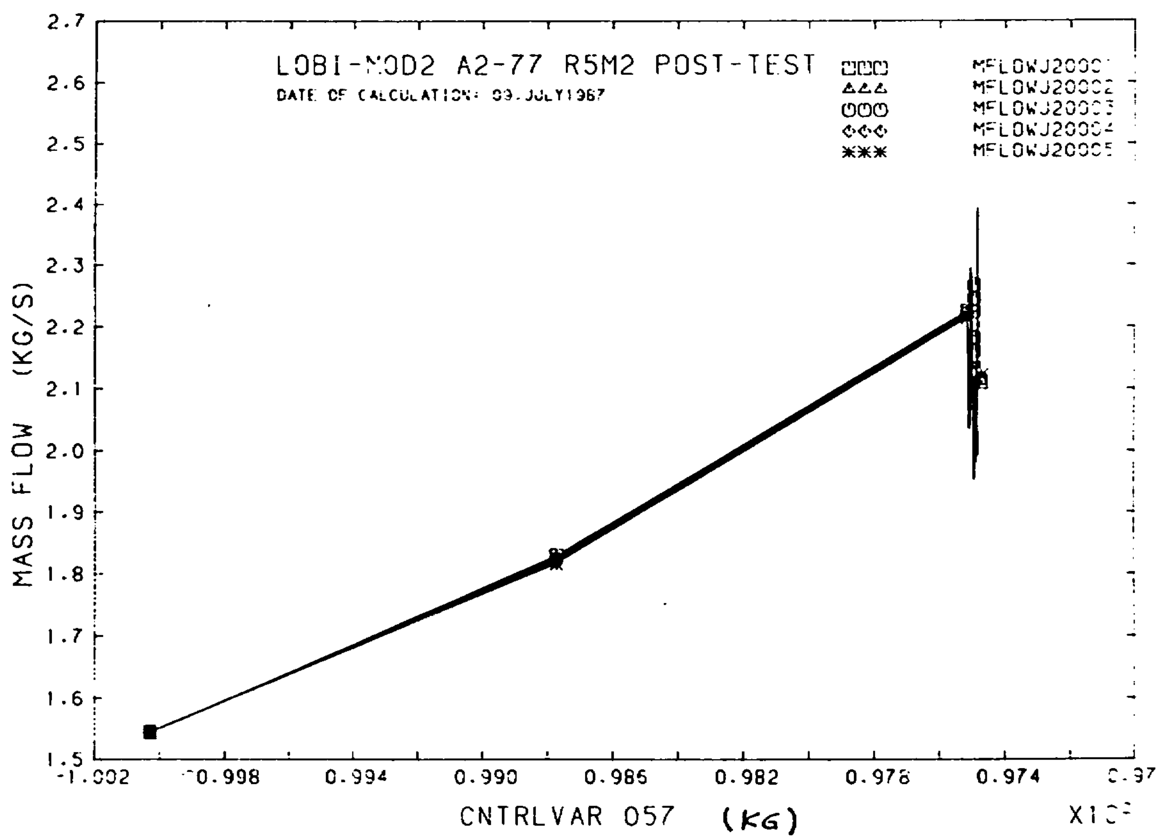

FIGURE A2 MASS FLOW RATE IN DOWNCOMER VS PS MASS INVENTORY

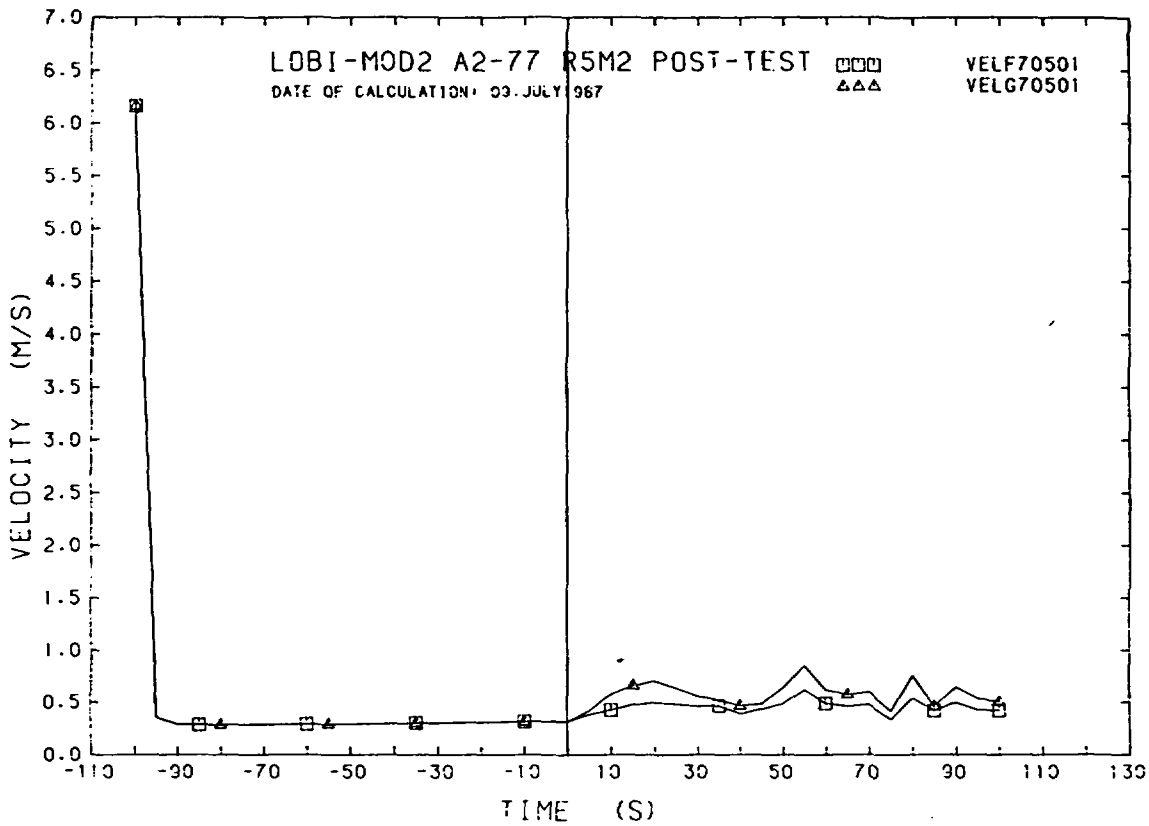

FIGURE A3 FLUID VELOCITIES IN B.L.S.G. INLET

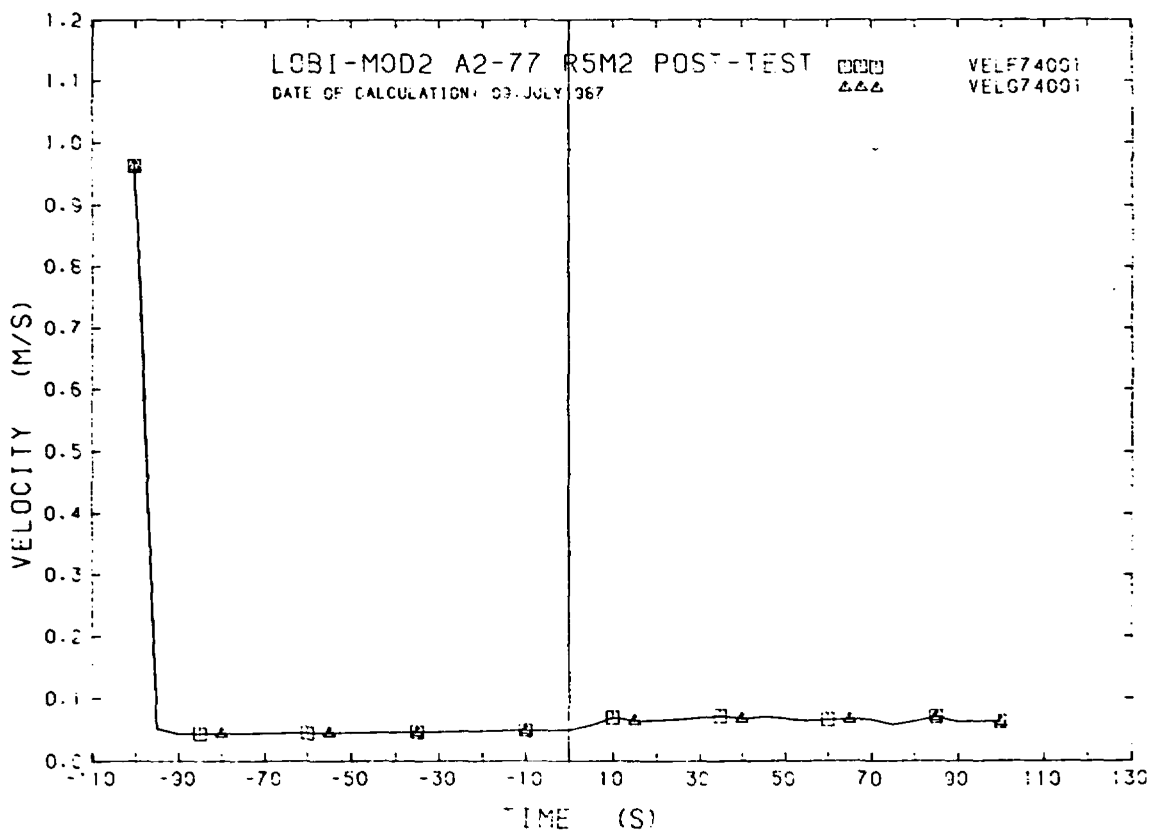

FIGURE A4 FLUID VELOCITIES IN B.L. PUMP INLET

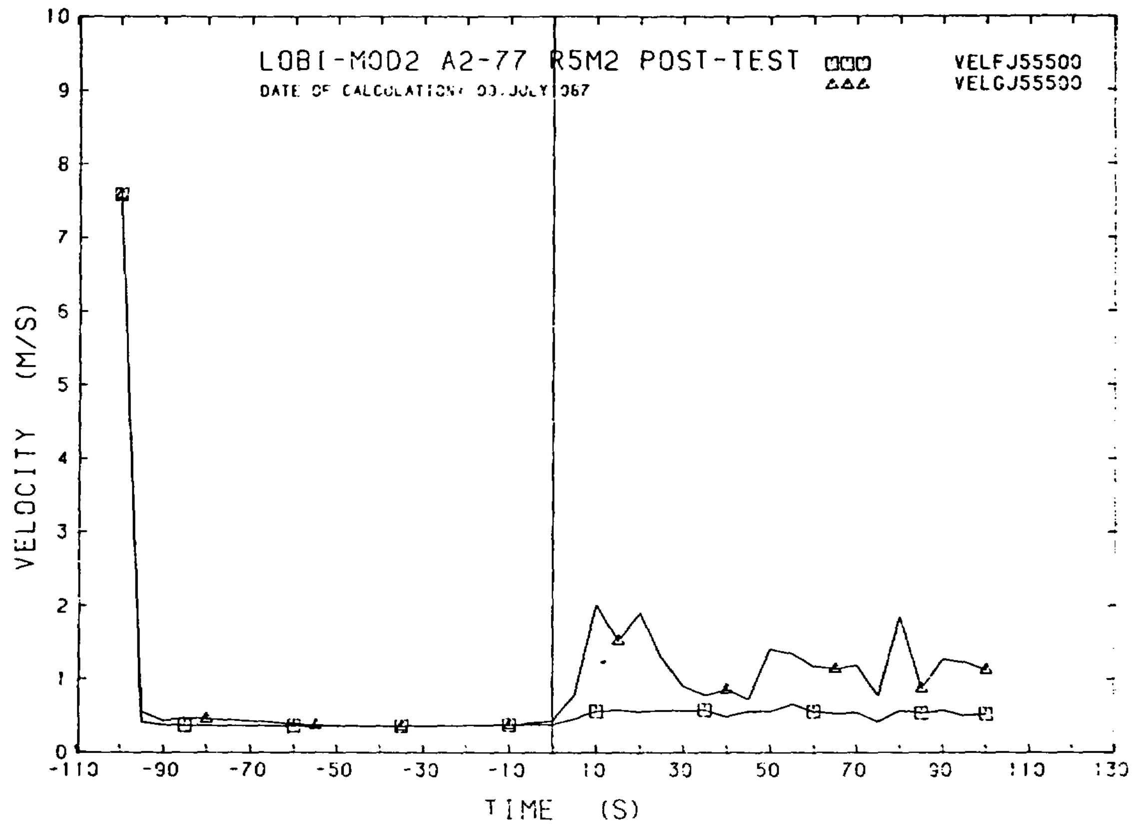

FIGURE A5 FLUID VELOCITIES IN I.L.S.G. INLET

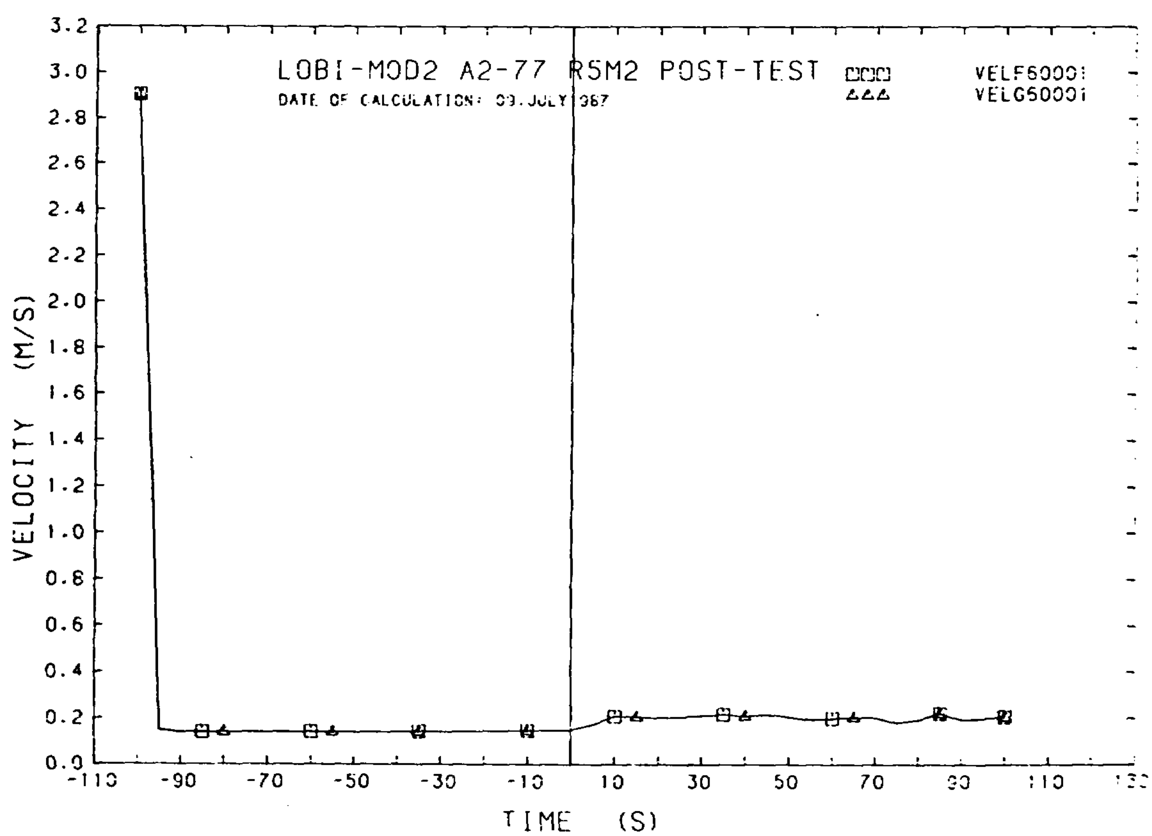

FIGURE A6 FLUID VELOCITIES IN I.L. PUMP INLET

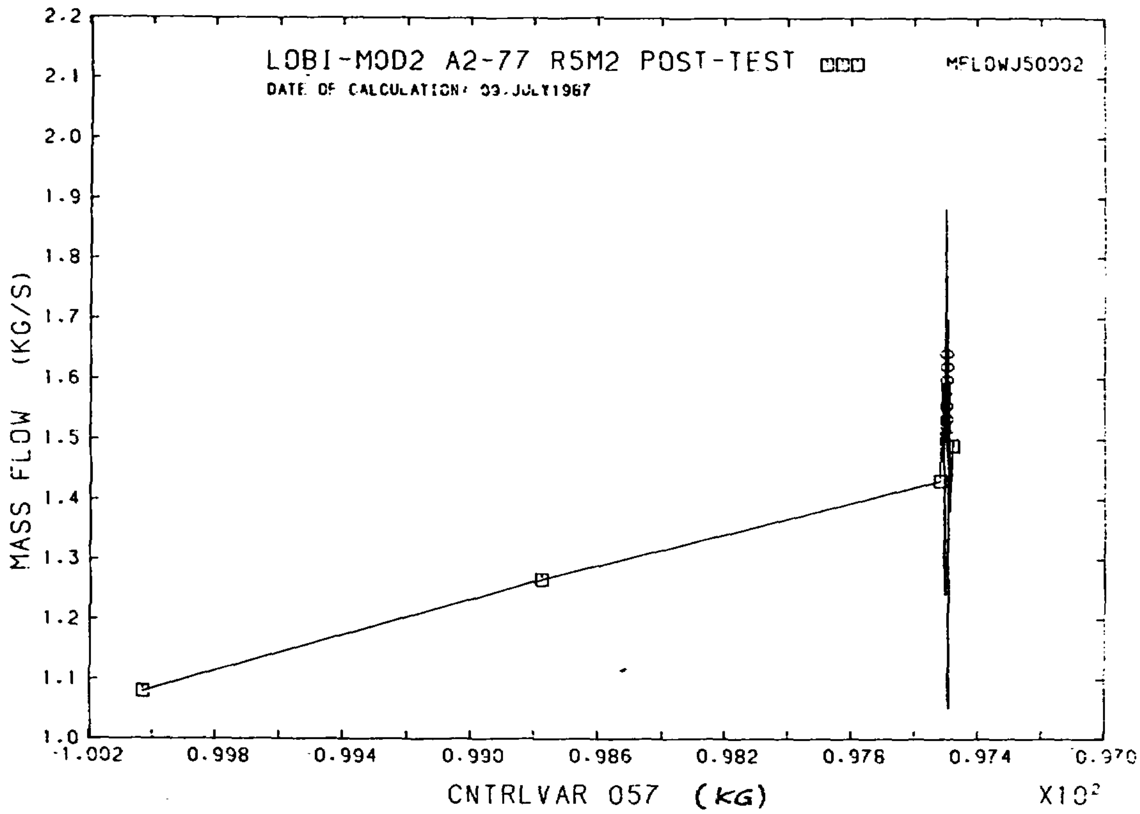

FIGURE A7 MASS FLOW RATE IN TRIPLE LOOP C.L. VS PS MASS INVENTORY

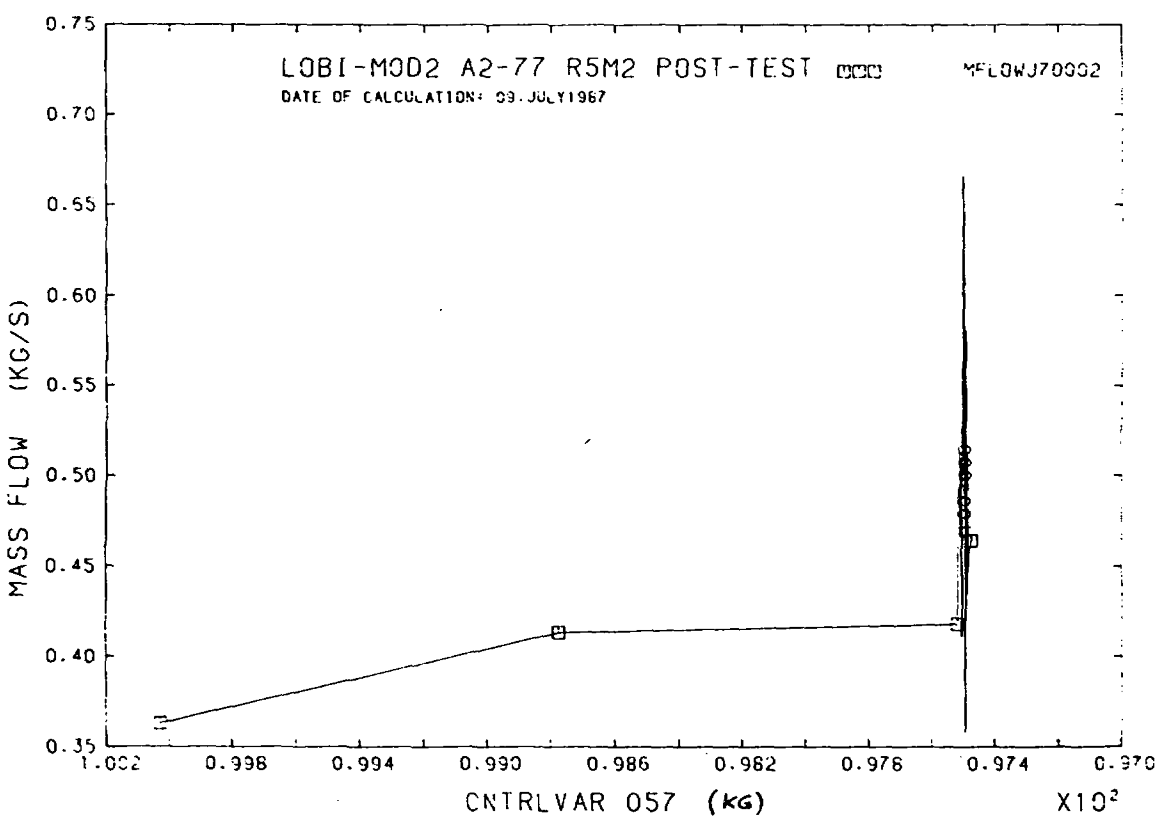

FIGURE A8 MASS FLOW RATE IN SINGLE LOOP C.L. VS PS MASS INVENTORY

APPENDIX B

Measured and calculated trends for case B (Reference calculation)

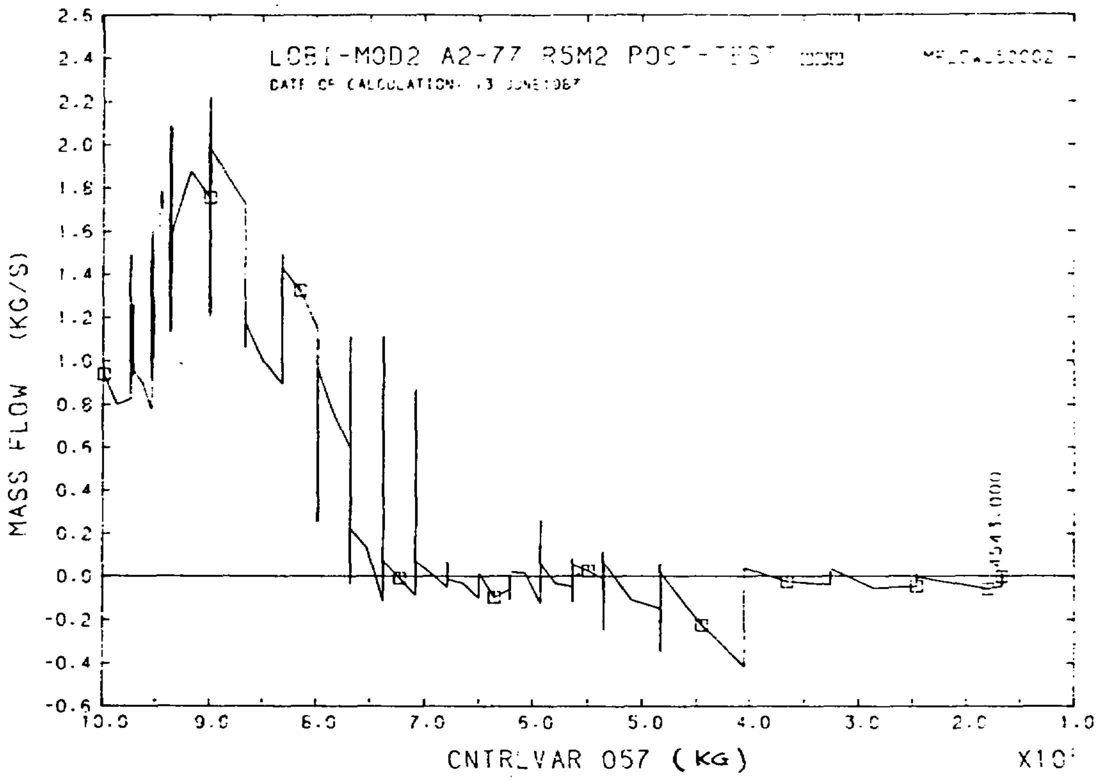

FIGURE B1 MASS FLOW RATE IN TRIPLE LOOP C.L. VS PS MASS INVENTORY

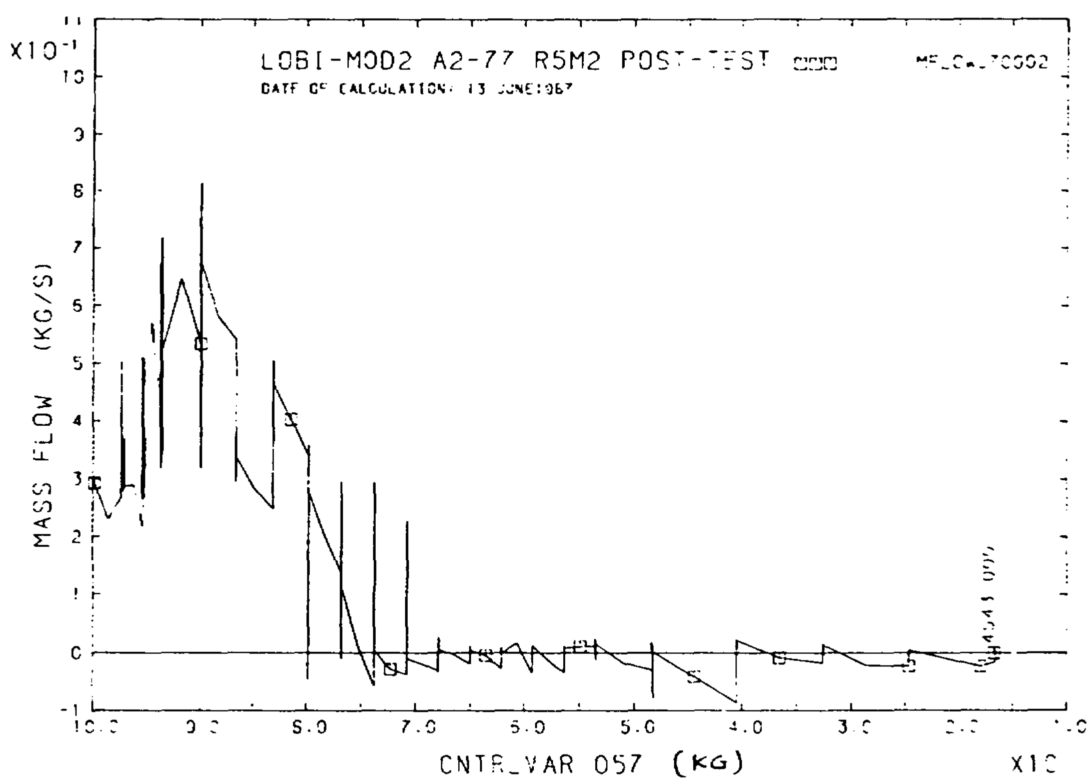

FIGURE B2 MASS FLOW RATE IN SINGLE LOOP C.L. VS PS MASS INVENTORY

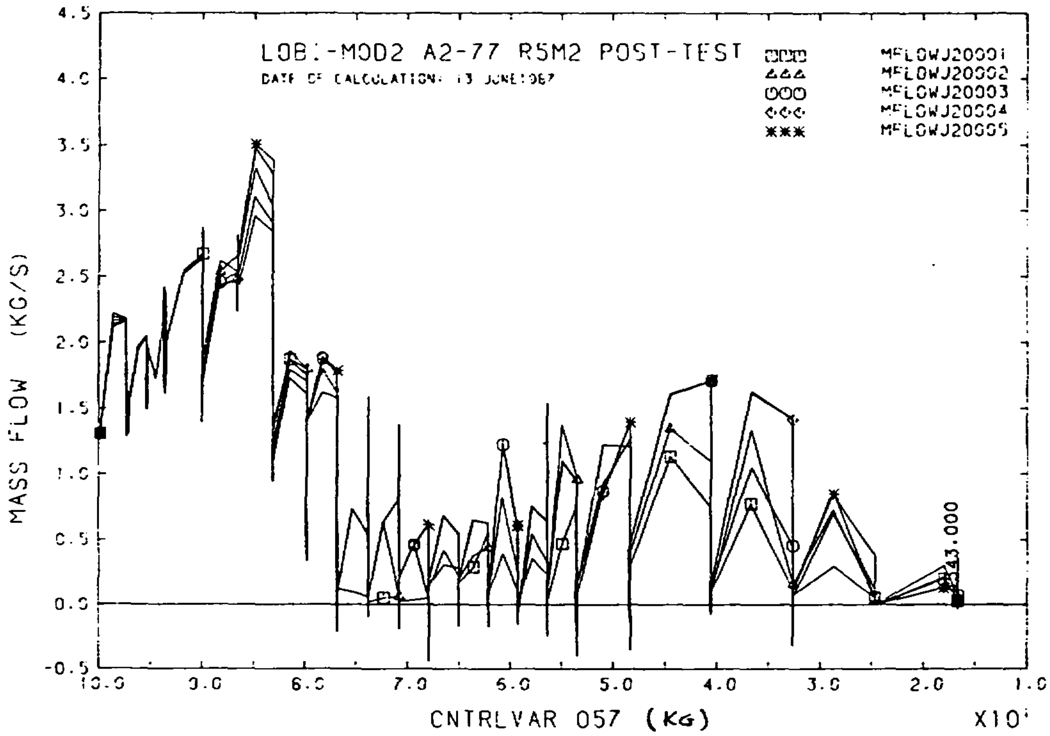

FIGURE B3 MASS FLOW RATE IN DOWNCOMER VS PS MASS INVENTORY

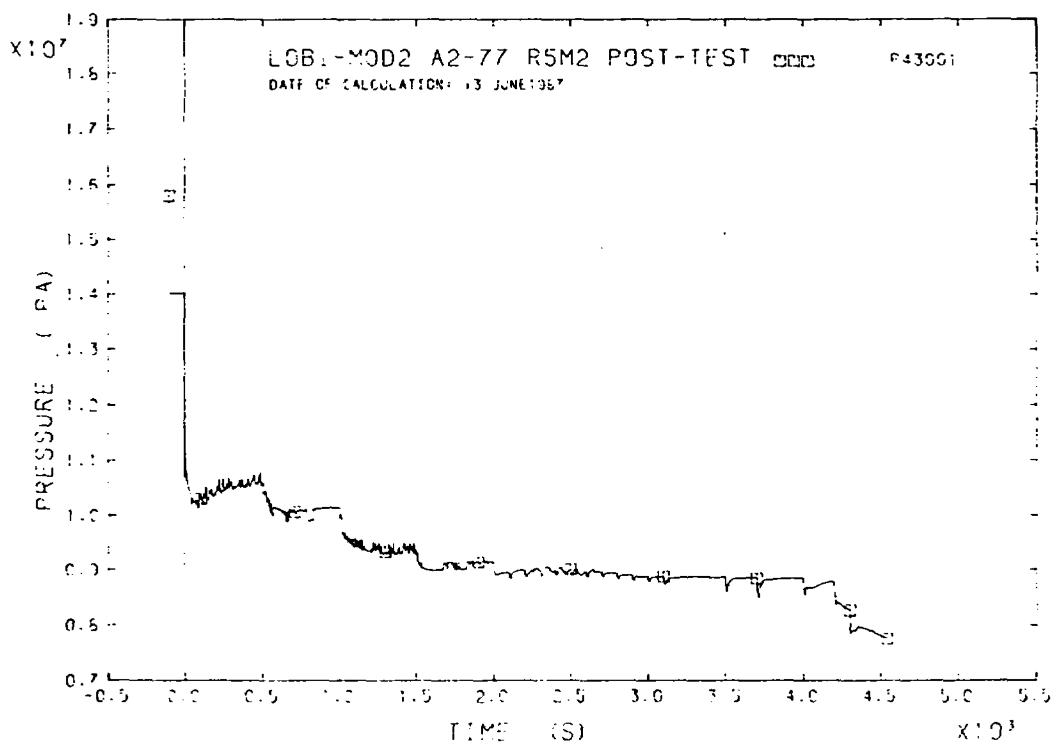

FIGURE B4 UPPER PLENUM PRESSURE

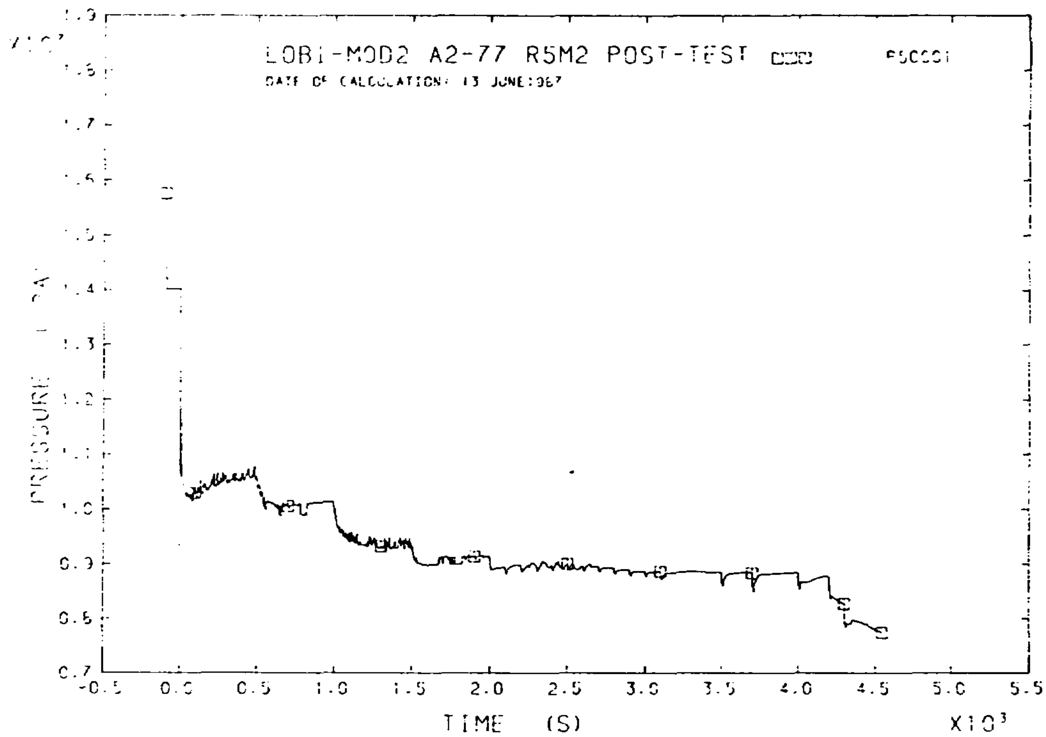

FIGURE B5 I.L. HOT LEG PRESSURE

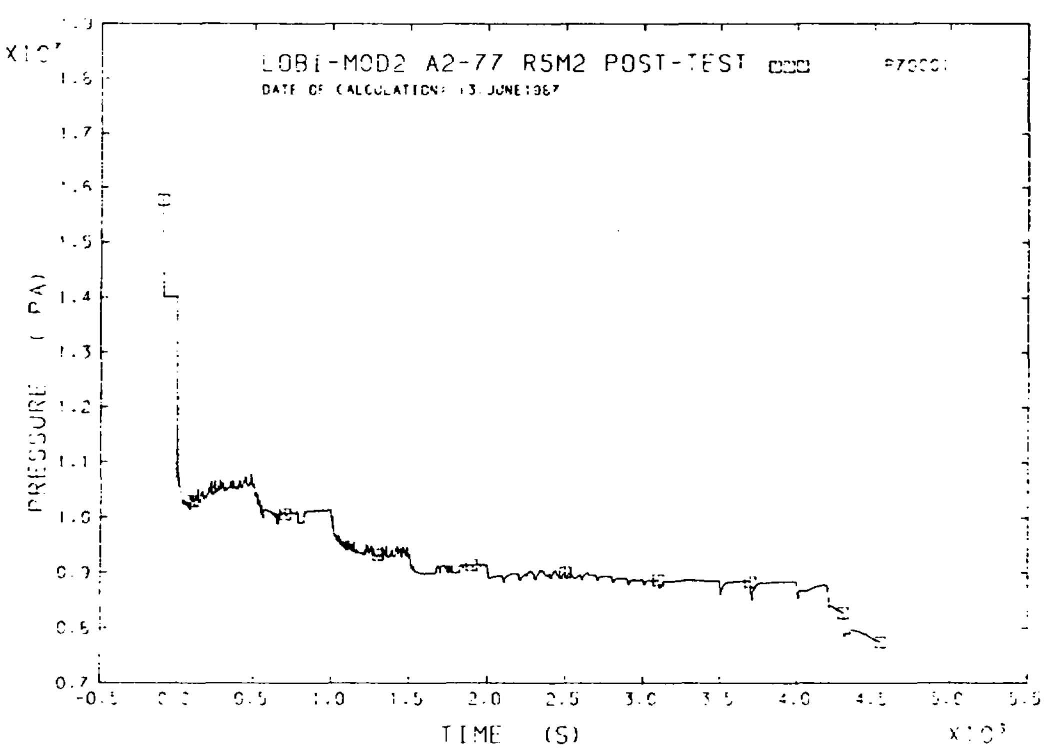

FIGURE B6 B.L. HOT LEG PRESSURE

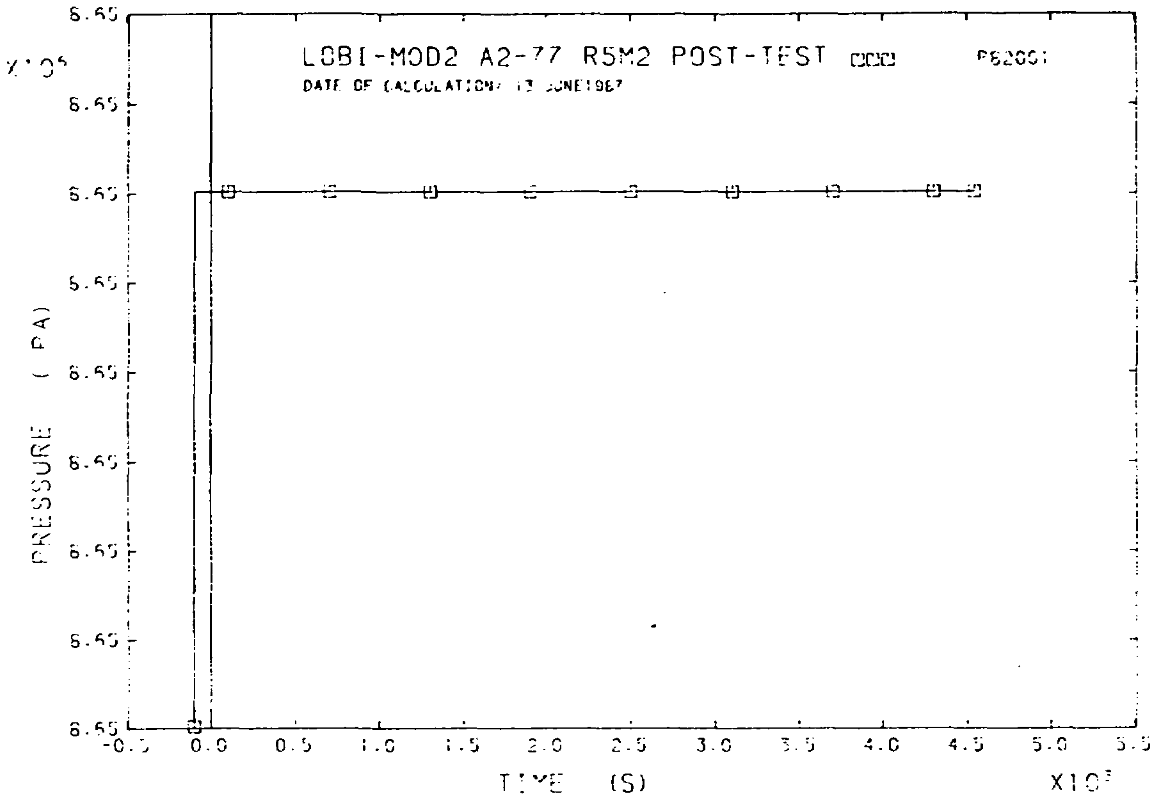

FIGURE B7 SG SECONDARY PRESSURE

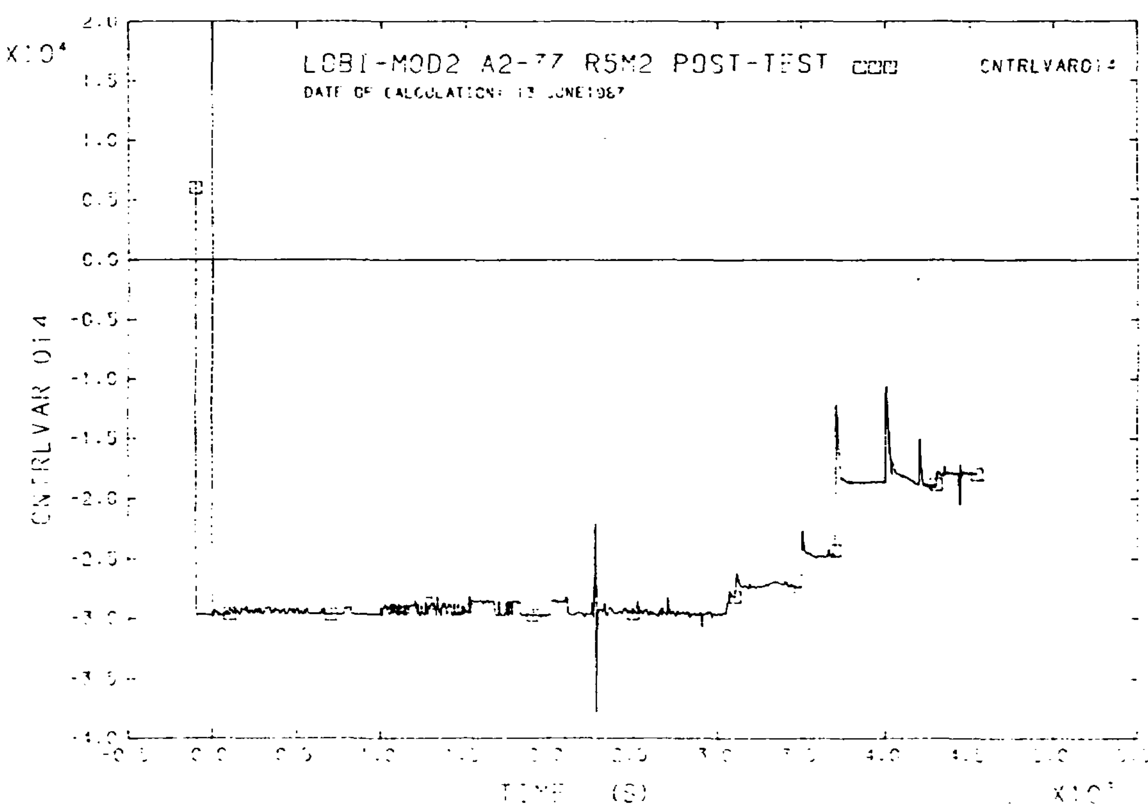

FIGURE B8 DIFFERENTIAL PRESSURE PD3017

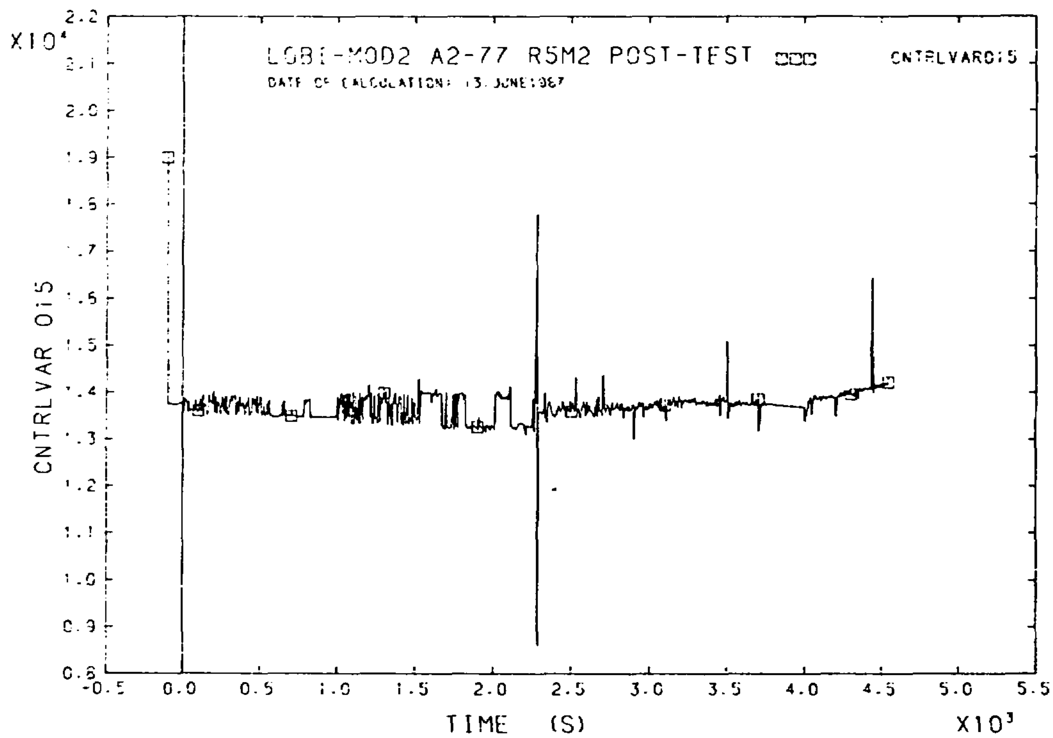

FIGURE B9 DIFFERENTIAL PRESSURE PD1714

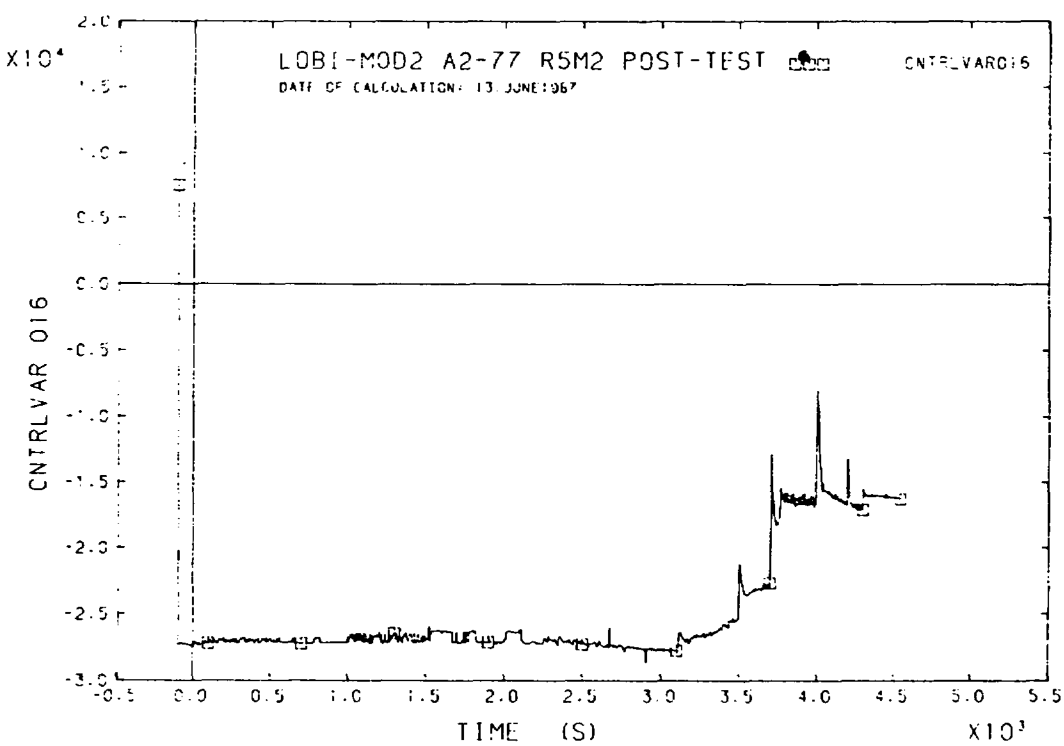

FIGURE B10 DIFFERENTIAL PRESSURE PD6227

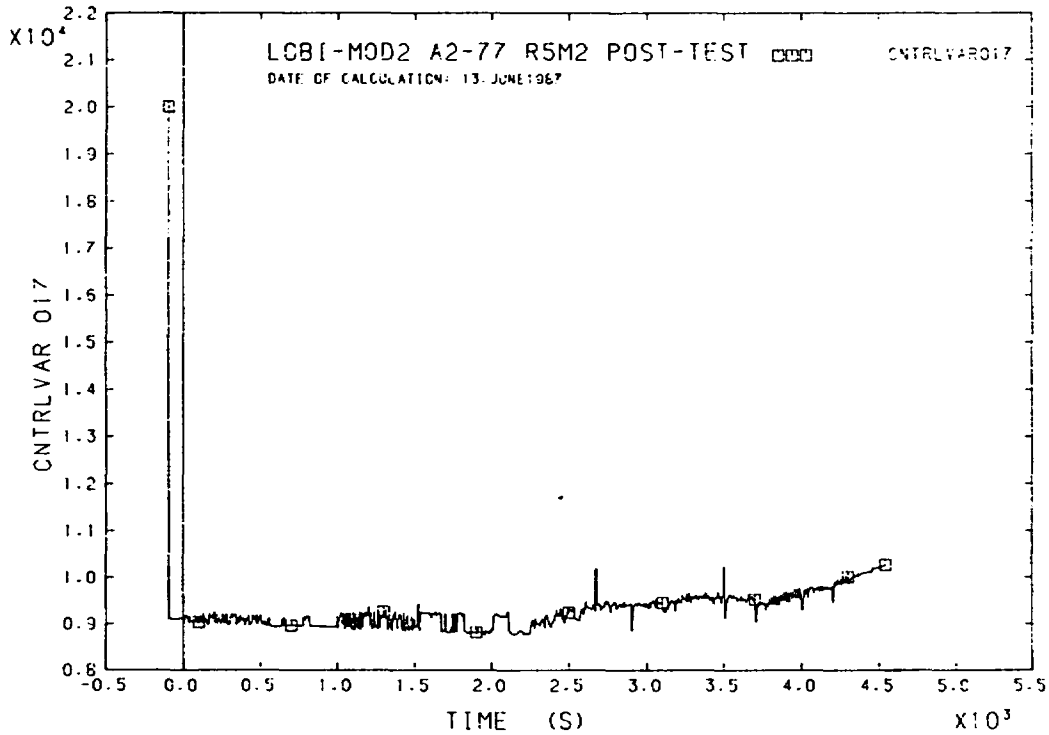

FIGURE B11 DIFFERENTIAL PRESSURE PD2724

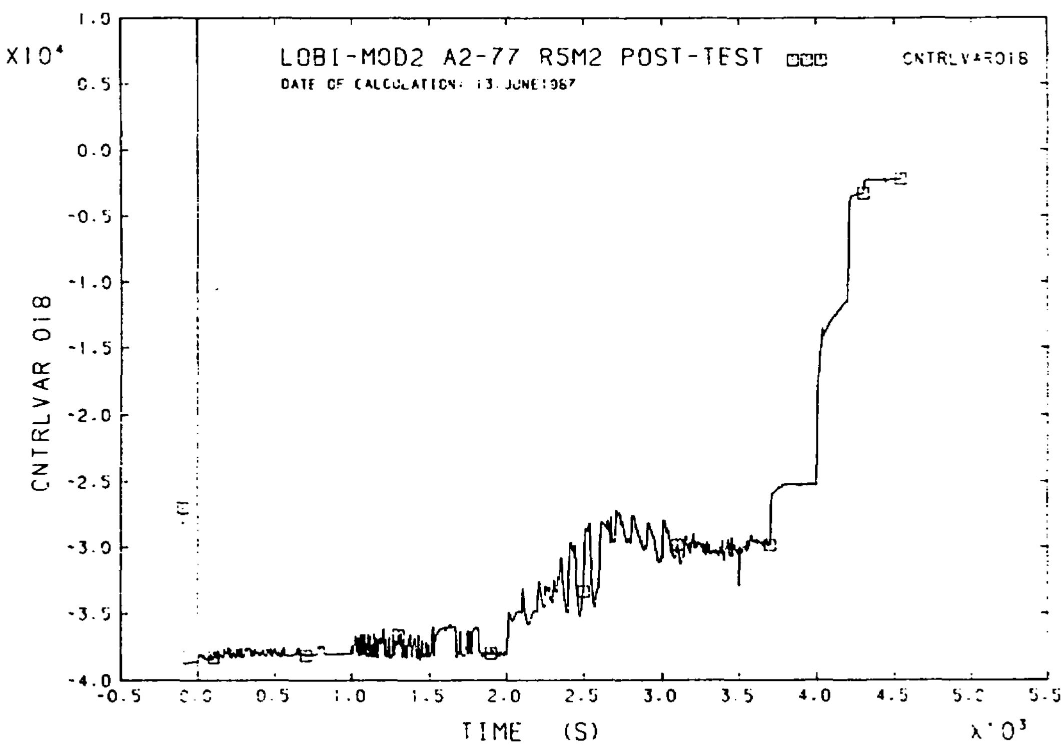

FIGURE B12 DIFFERENTIAL PRESSURE PD3DBT

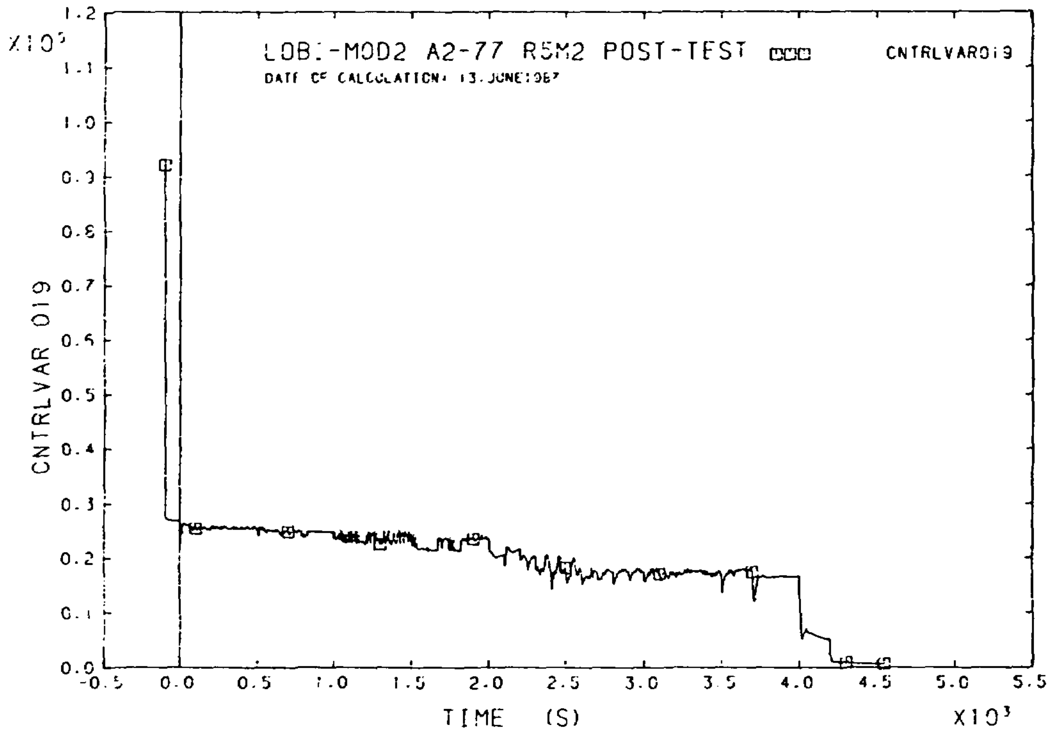

FIGURE B13 DIFFERENTIAL PRESSURE PD3RTK

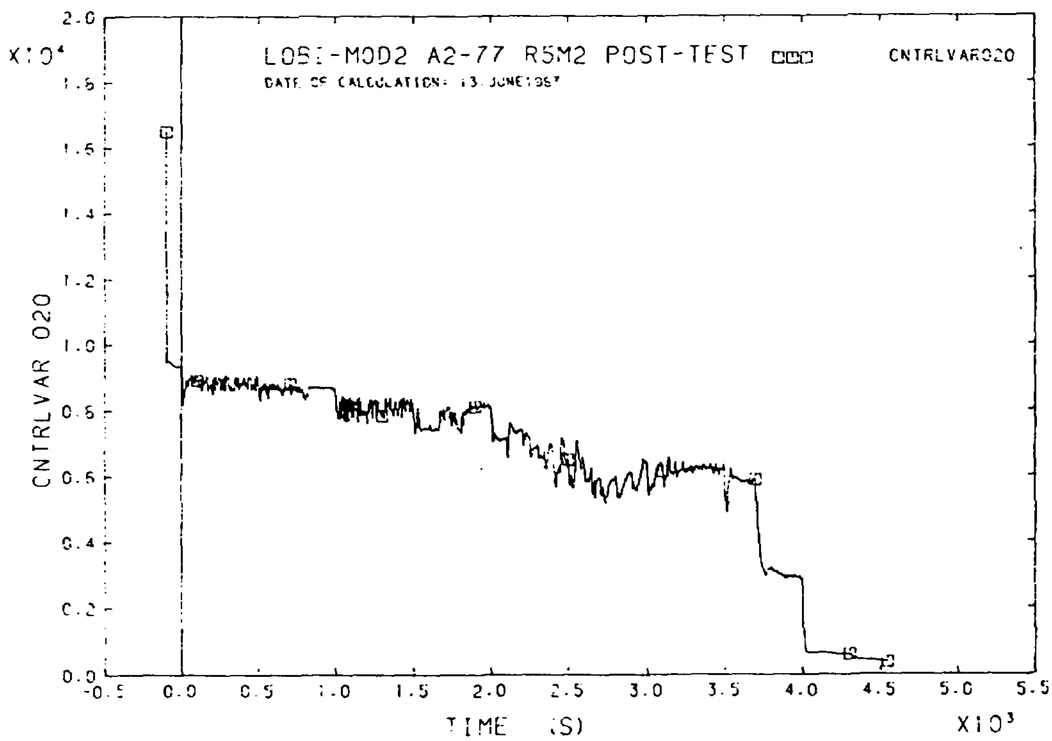

FIGURE B14 DIFFERENTIAL PRESSURE PD3RKA

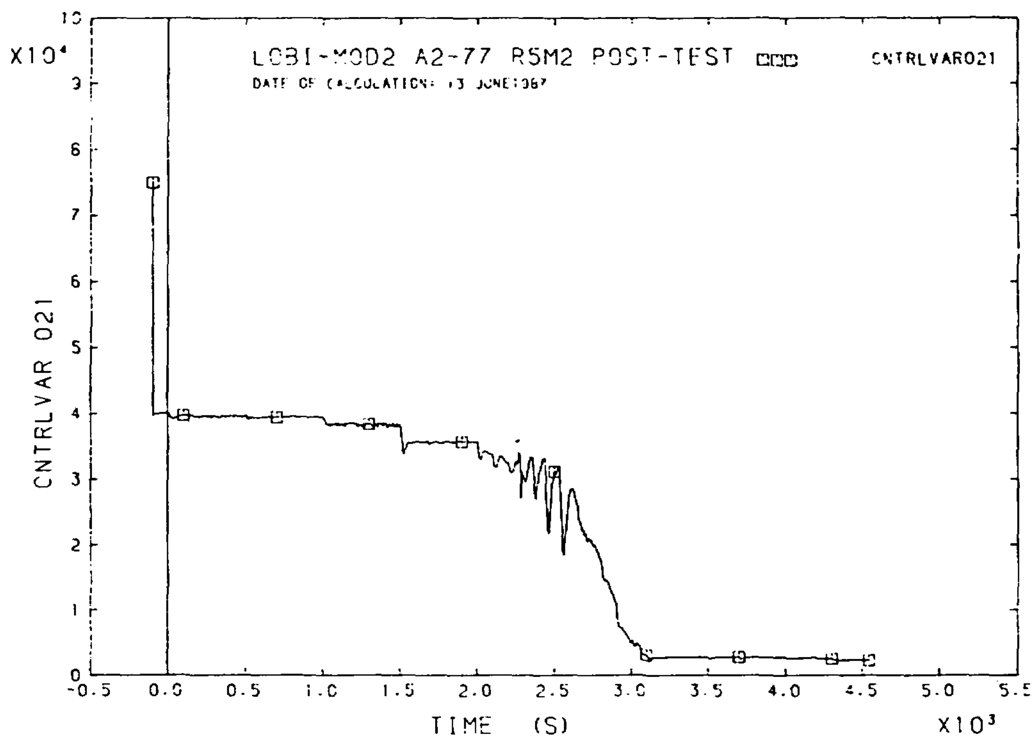

FIGURE B15 DIFFERENTIAL PRESSURE PD9C3N

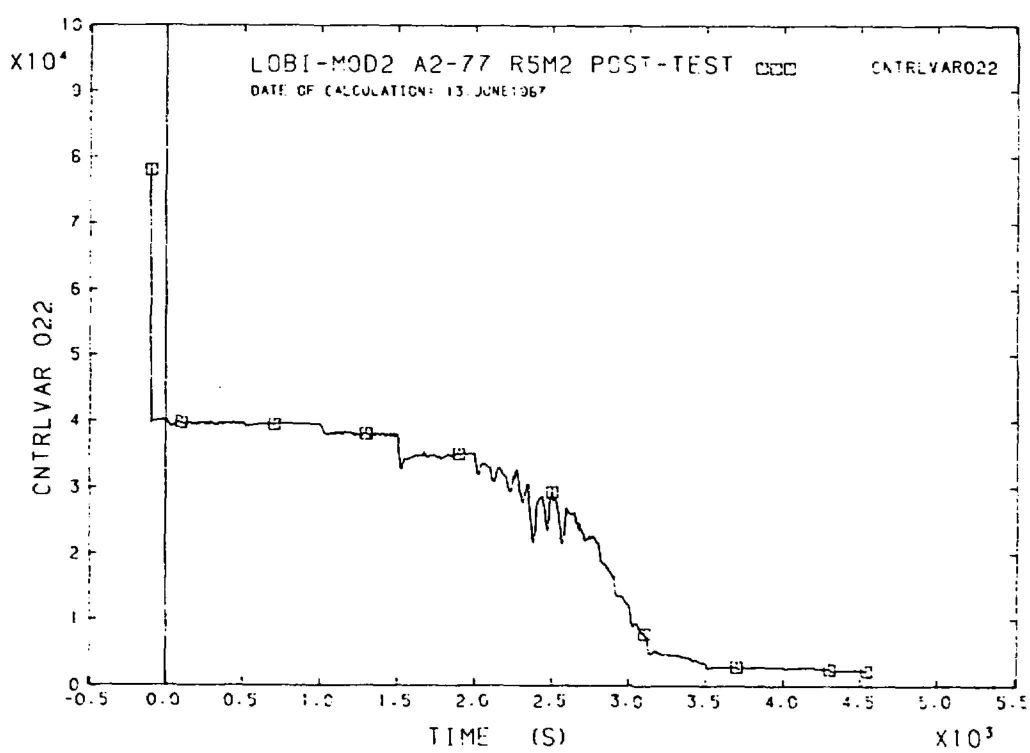

FIGURE B16 DIFFERENTIAL PRESSURE PD8C3N

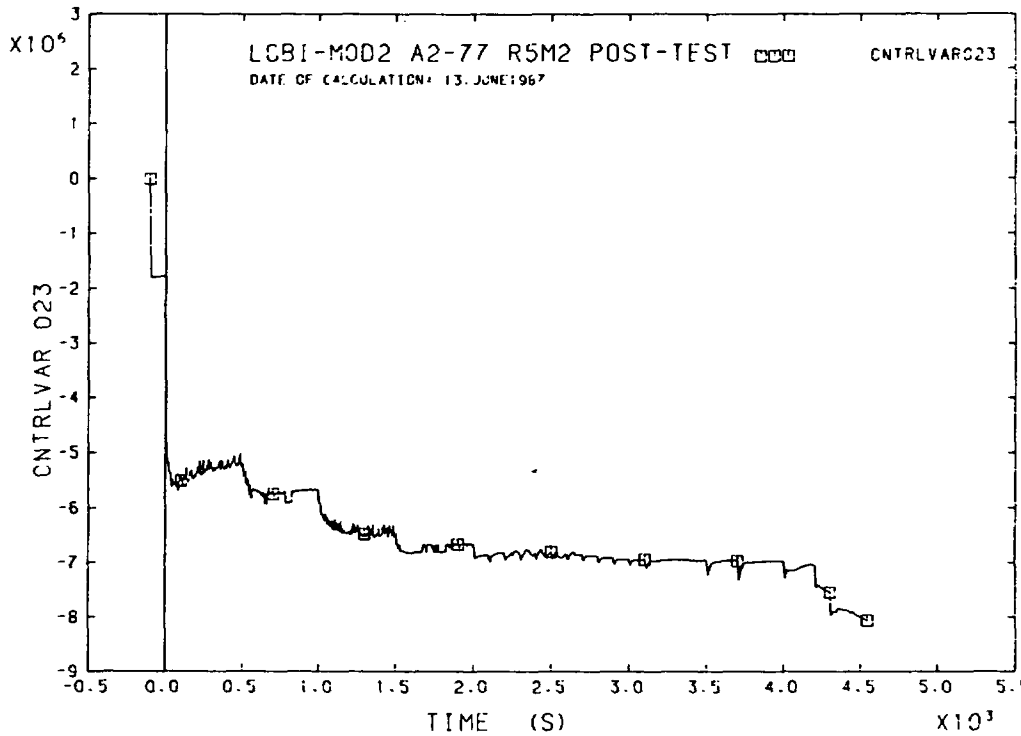

FIGURE B17 PD3R39

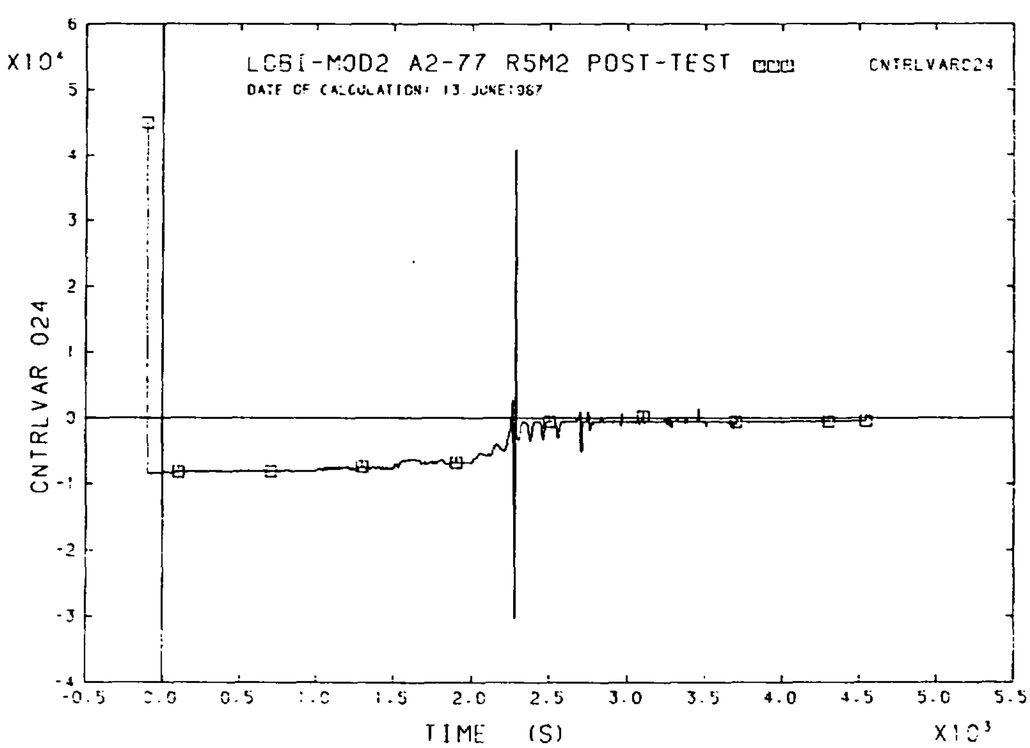

FIGURE B18 DIFFERENTIAL PRESSURE PD163DB3

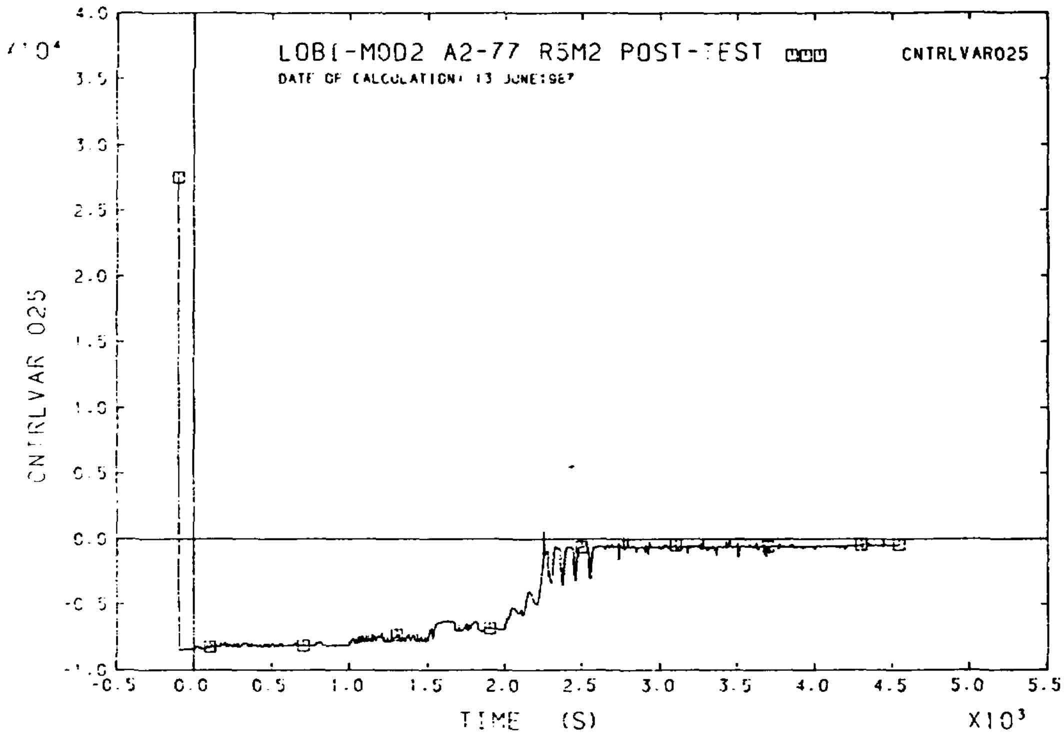

FIGURE B19 DIFFERENTIAL PRESSURE PD263DB7

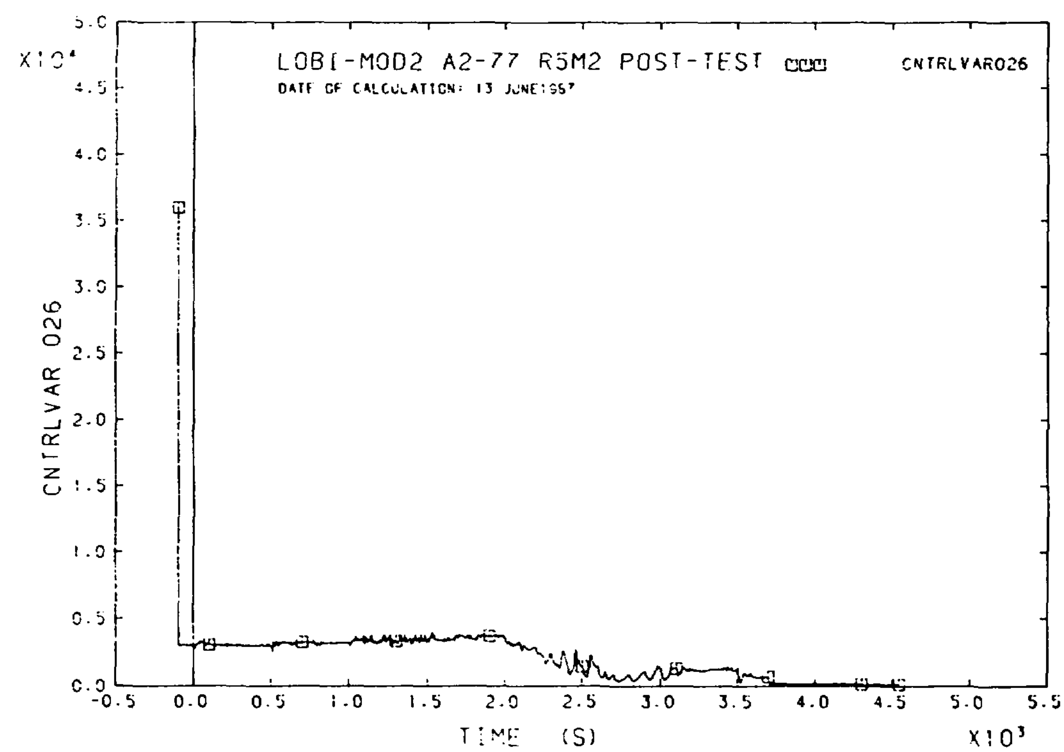

FIGURE B20 DIFFERENTIAL PRESSURE PD3R''A4

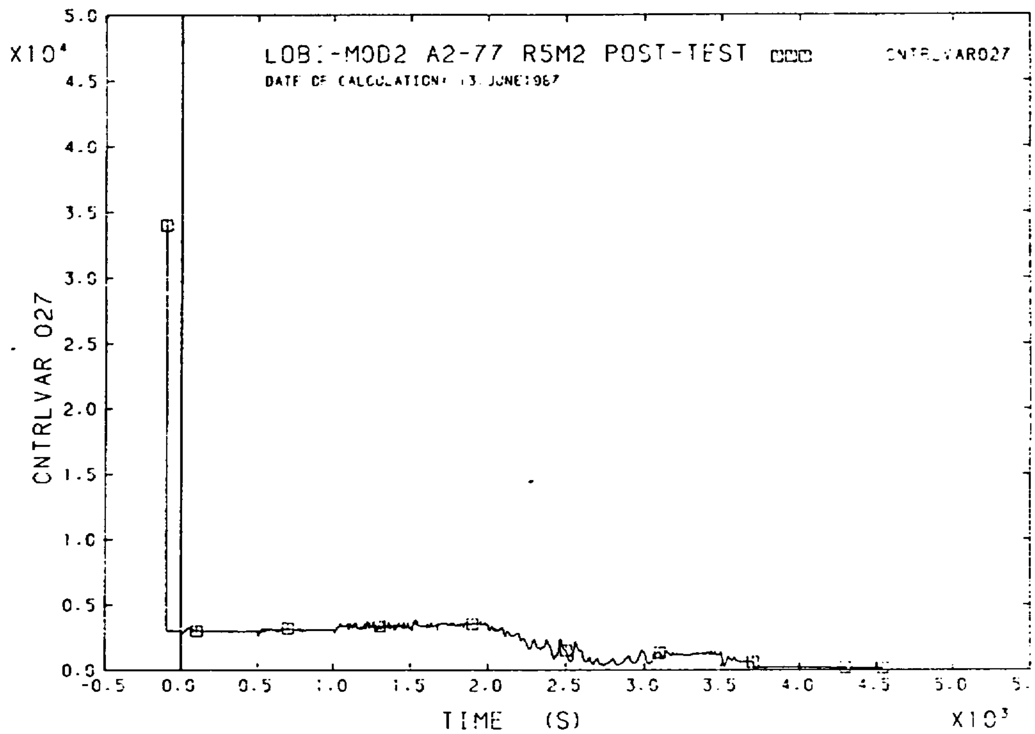

FIGURE **B21** DIFFERENTIAL PRESSURE PD3R21A3

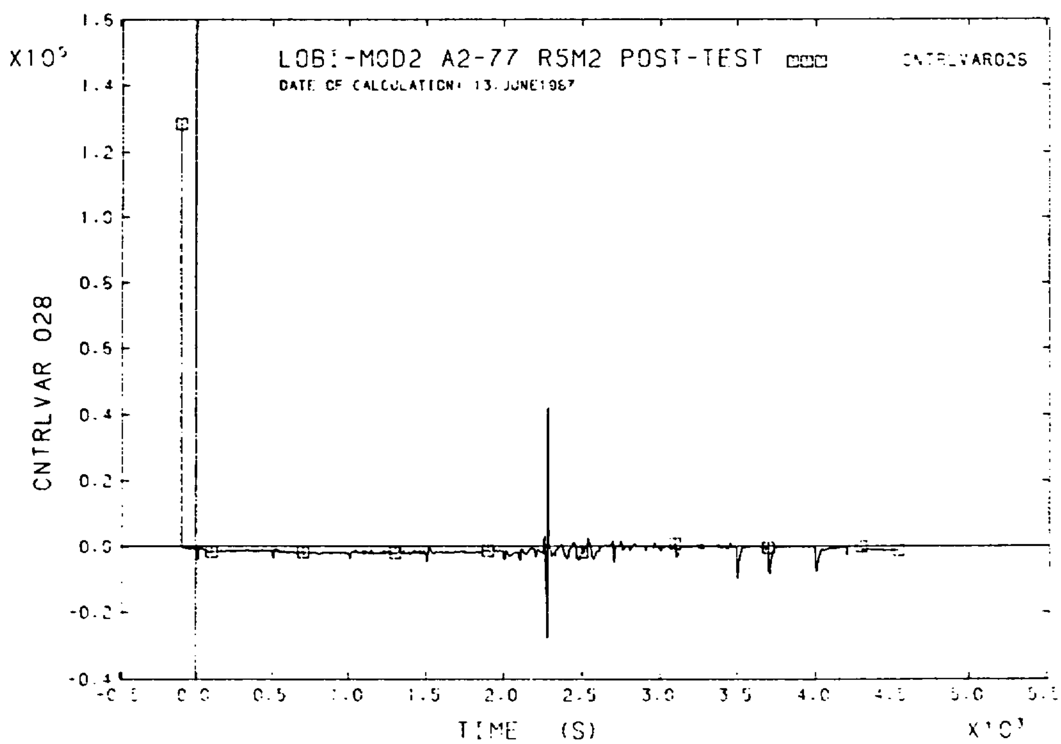

FIGURE **B22** DIFFERENTIAL PRESSURE RPV TOTAL IL SIDE

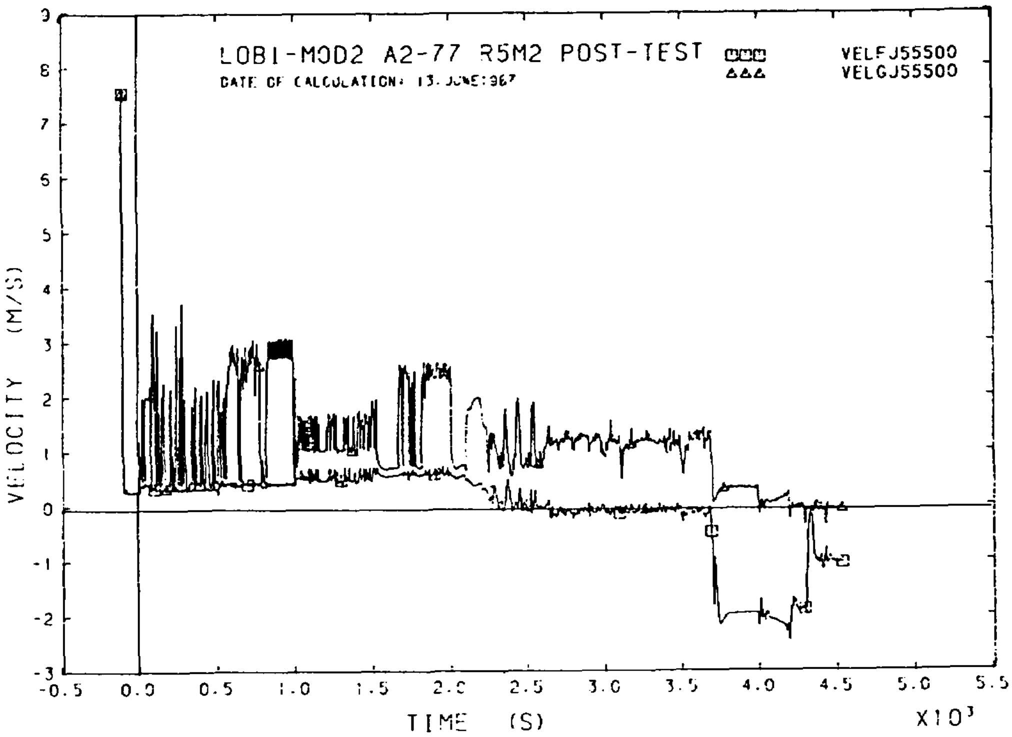

FIGURE B23 FLUID VELOCITIES IN I.L.S.G. INLET

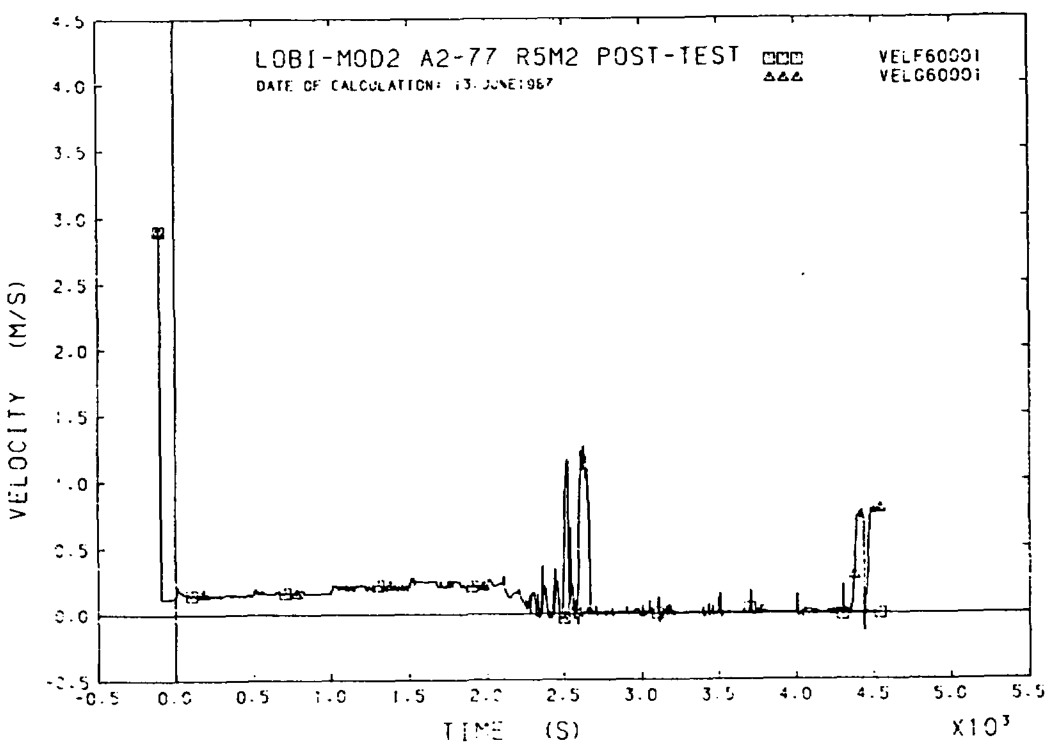

FIGURE B24 FLUID VELOCITIES IN I.L. PUMP INLET

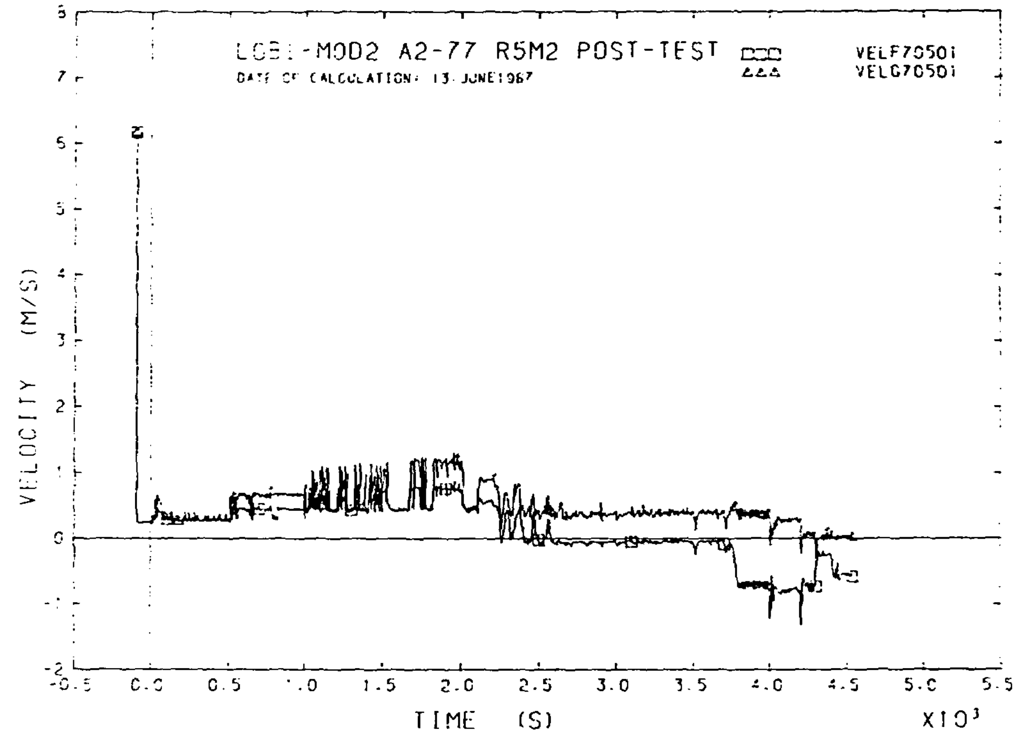

FIGURE B25 FLUID VELOCITIES IN B.L.S.G. INLET

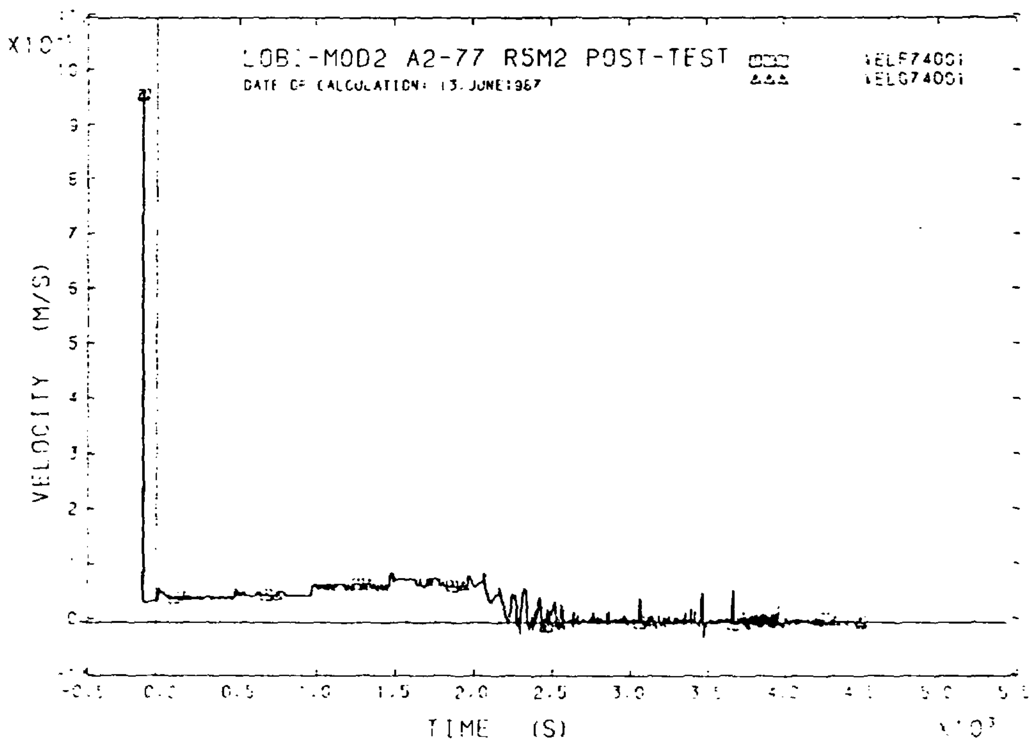

FIGURE B26 FLUID VELOCITIES IN B.L. PUMP INLET

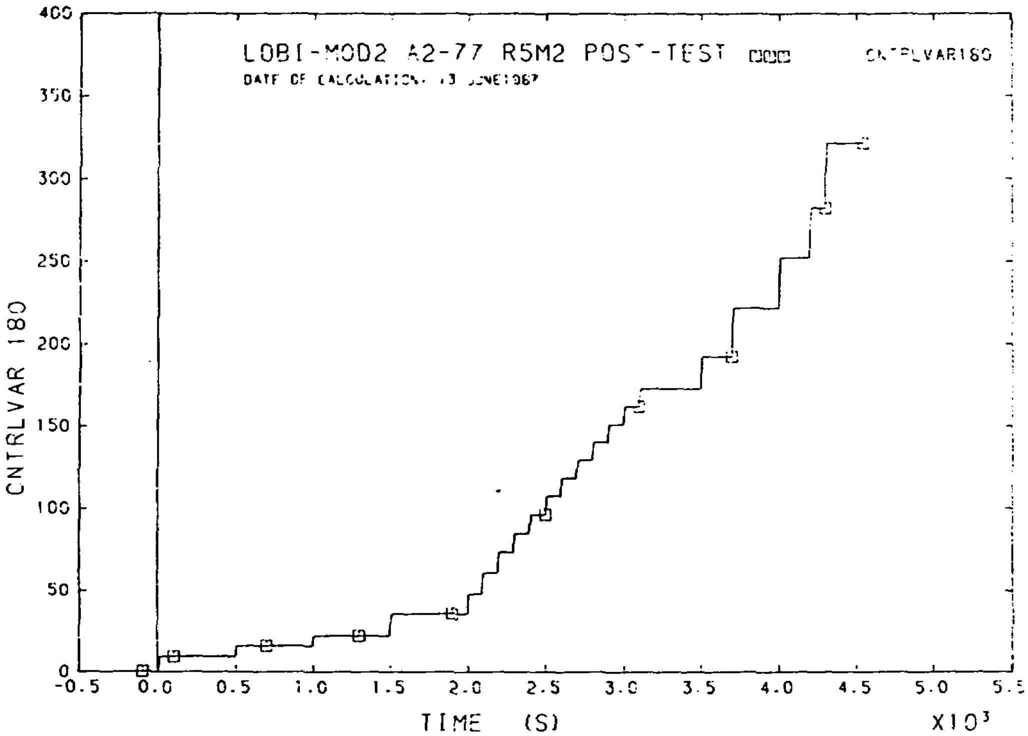

FIGURE B27 DRAINED MASS INTEGRAL

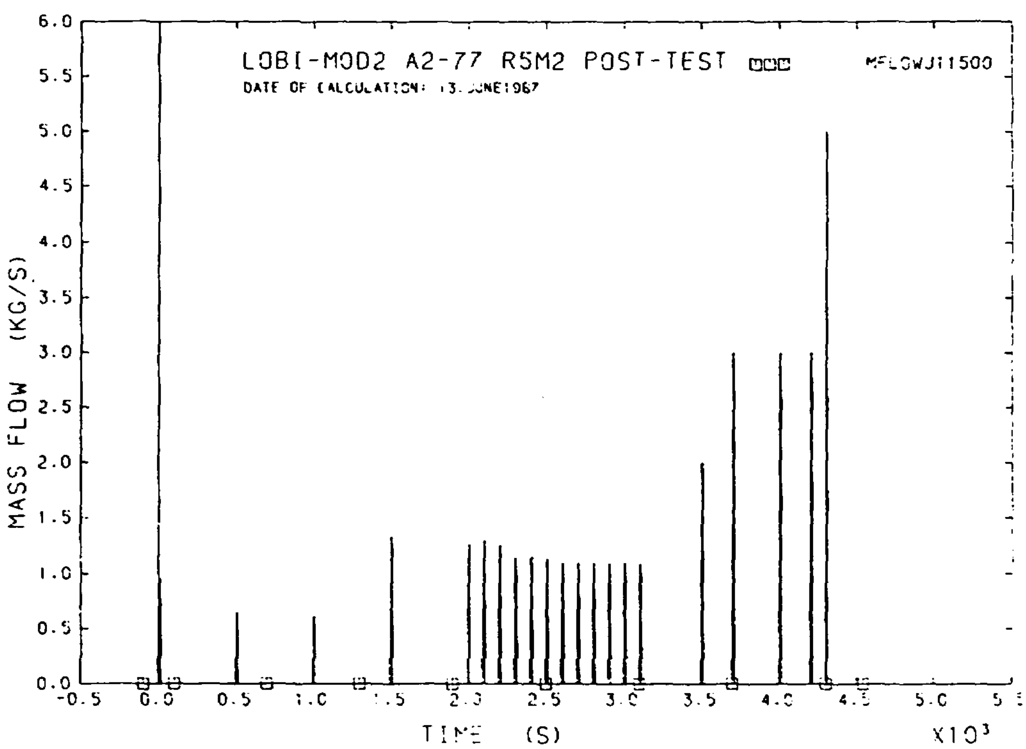

FIGURE B28 FLOWRATE DRAINED FROM LP

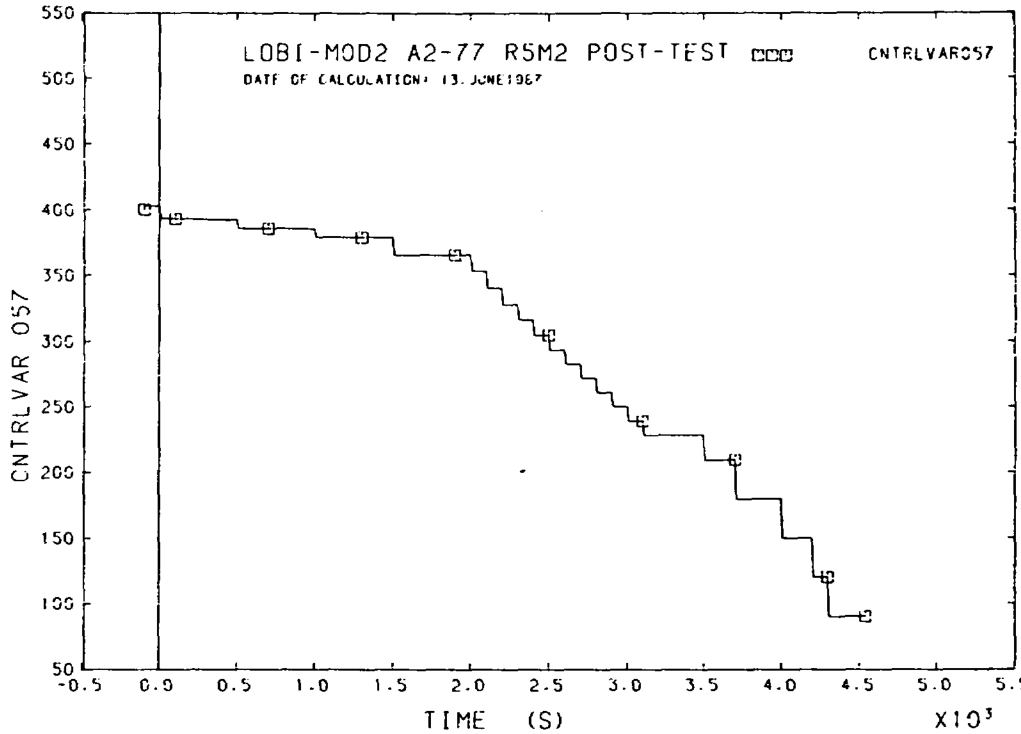

FIGURE B29 PRIMARY LOOP RESIDUAL MASS

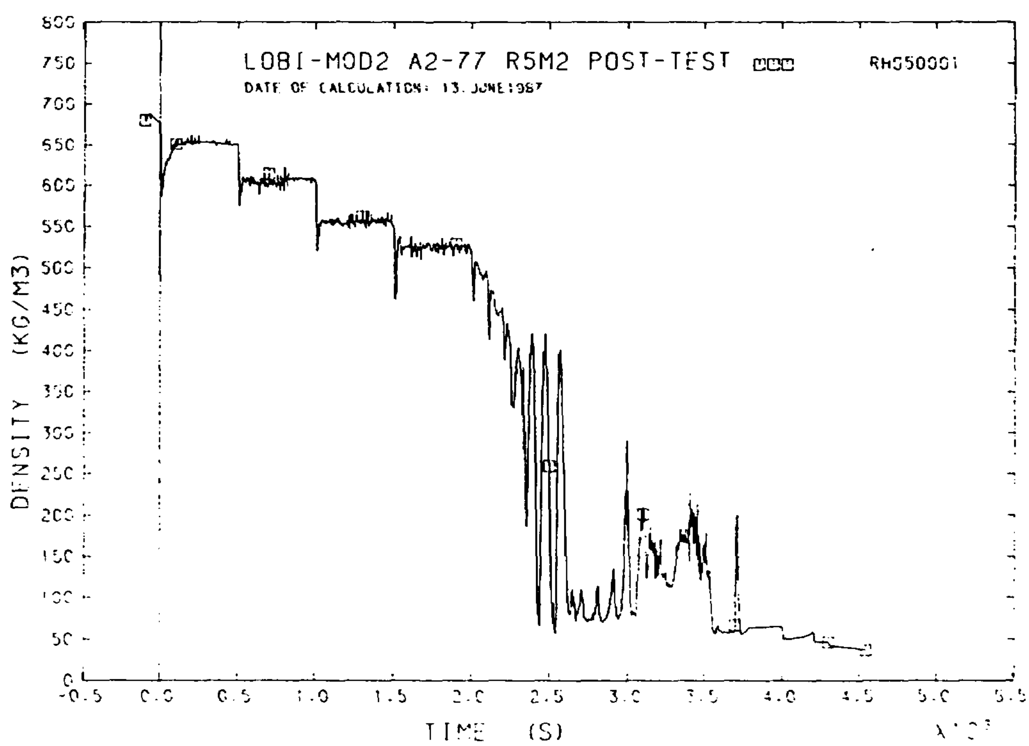

FIGURE B30 FLUID DENSITY IN I.L.-H.L. VESSEL OUTLET

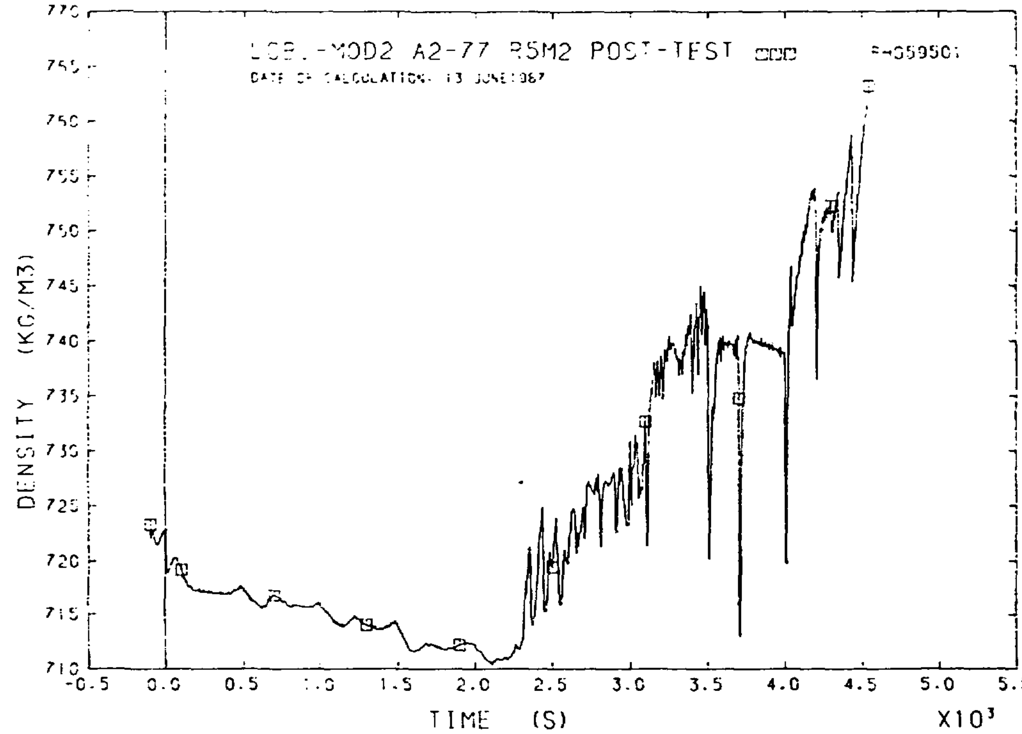

FIGURE B31 FLUID DENSITY IN I.L.-PUMP INLET

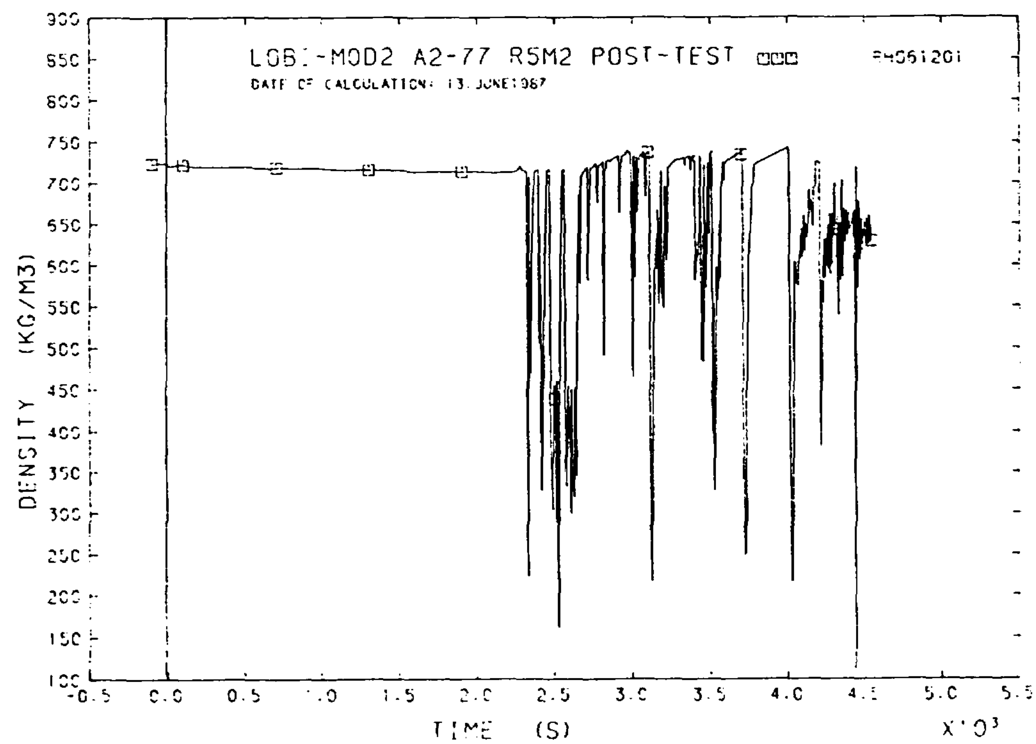

FIGURE B32 FLUID DENSITY IN I.L.-C.L. VESSEL INLET

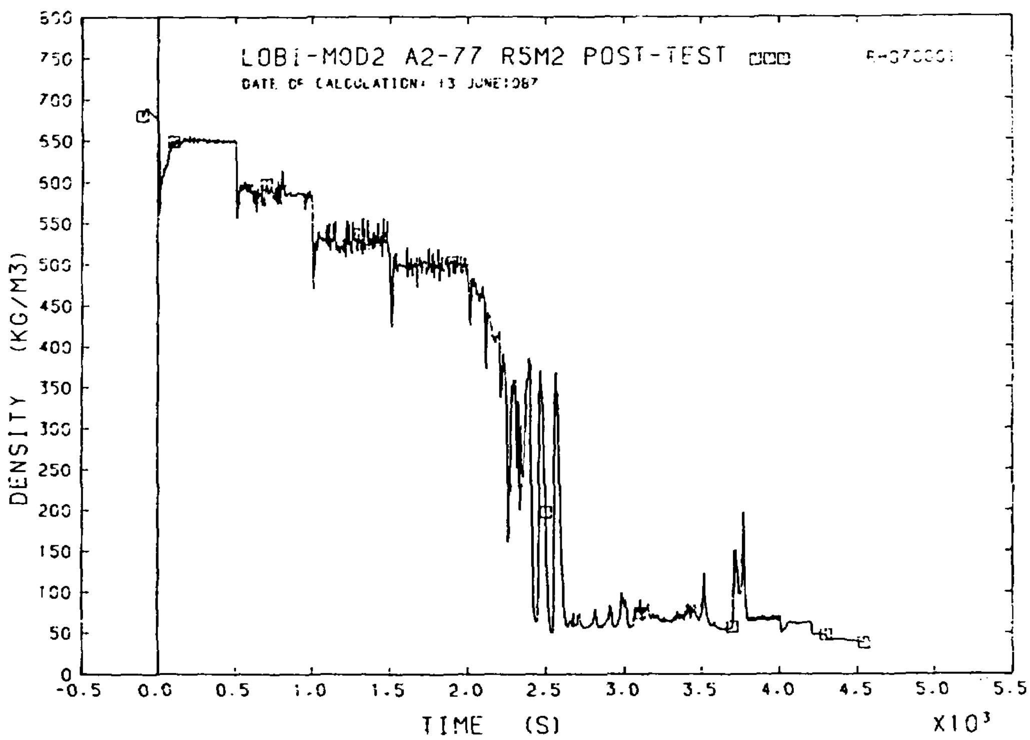

FIGURE B33 FLUID DENSITY IN B.L.-H.L. VESSEL OUTLET

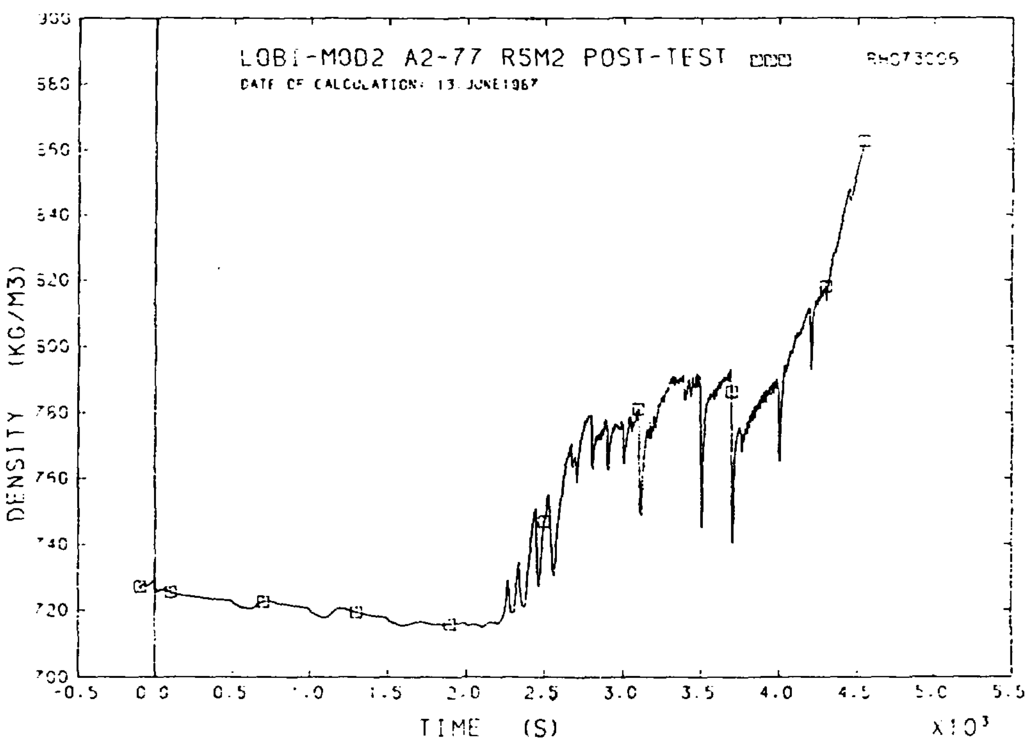

FIGURE B34 FLUID DENSITY IN B.L.-PUMP INLET

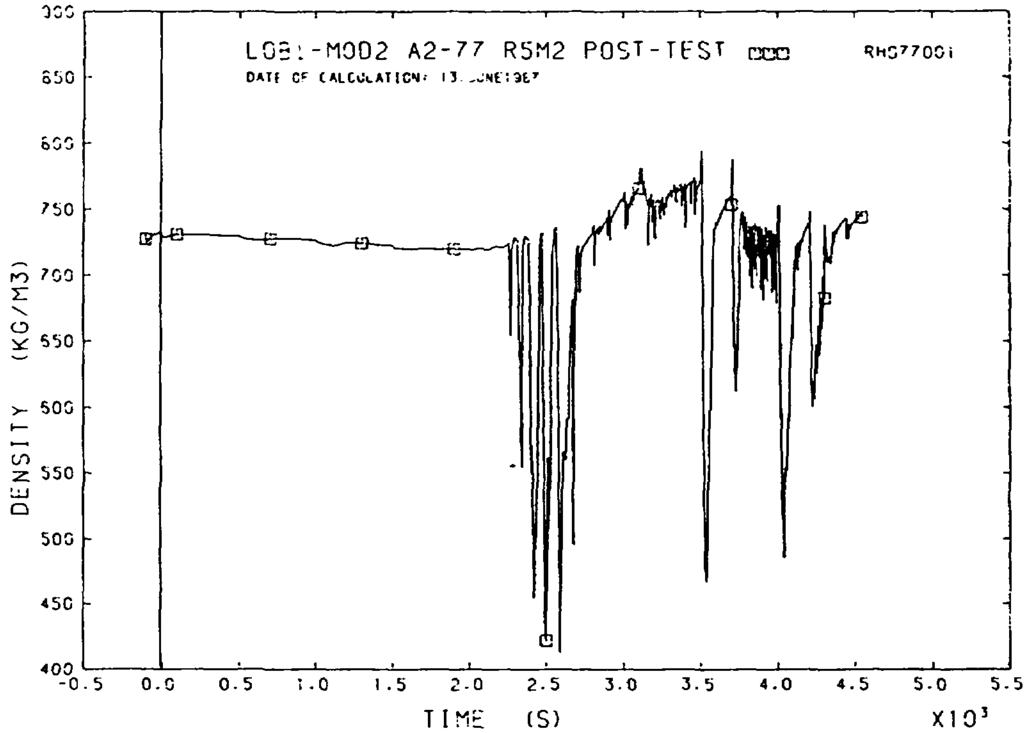

FIGURE B35 FLUID DENSITY IN B.L.-C.L. VESSEL INLET

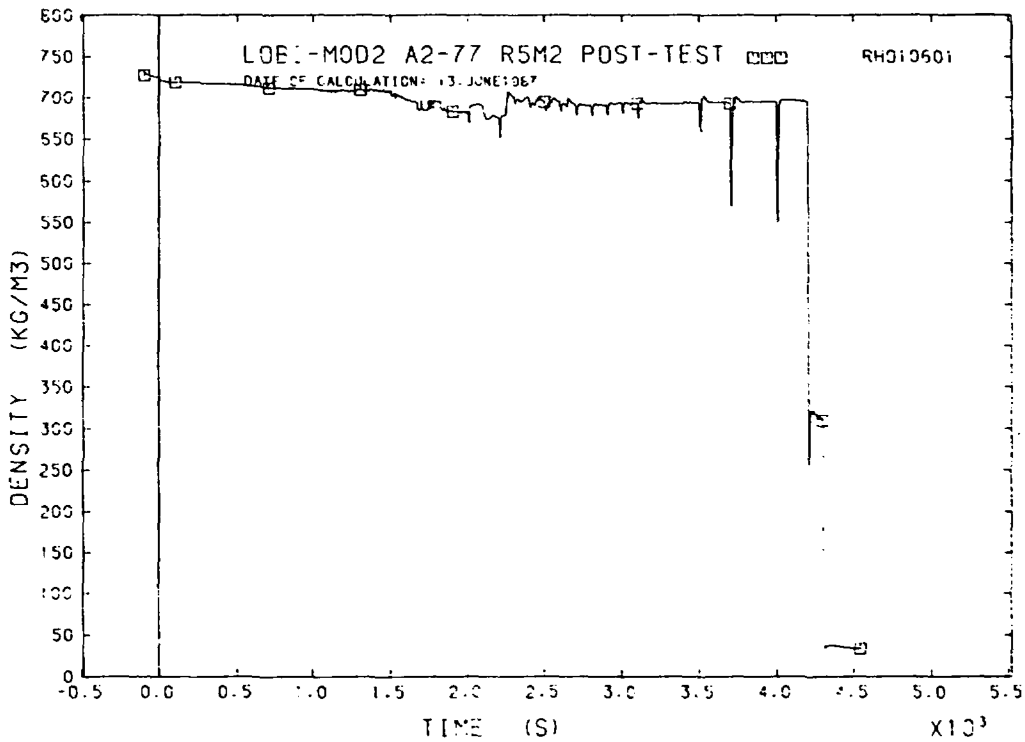

FIGURE B36 FLUID DENSITY IN PRESSURE VESSEL

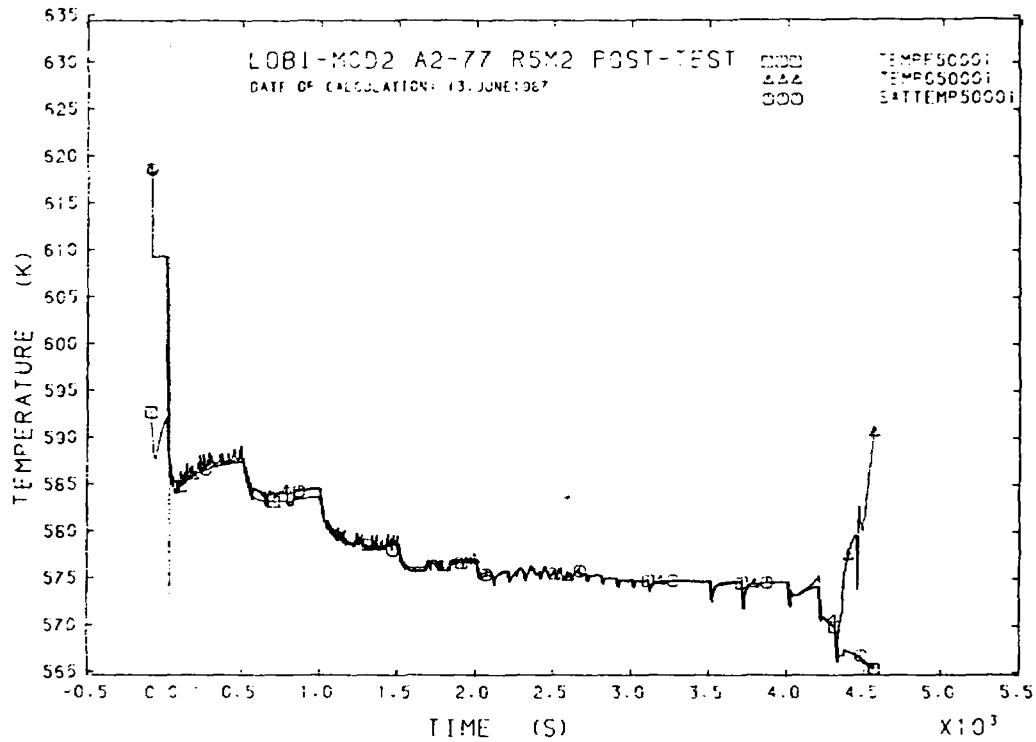

FIGURE B37 FLUID TEMPERATURE IN I.L.-H.L. VESSEL OUTLET

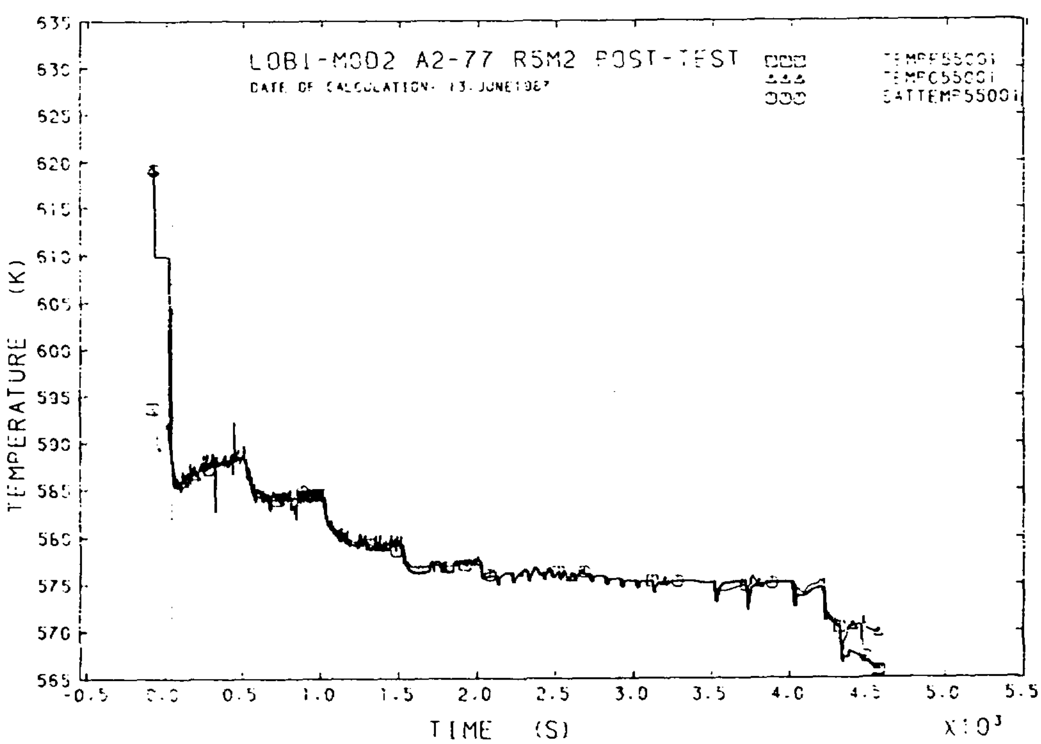

FIGURE B38 FLUID TEMPERATURE IN I.L.-S.G. INLET

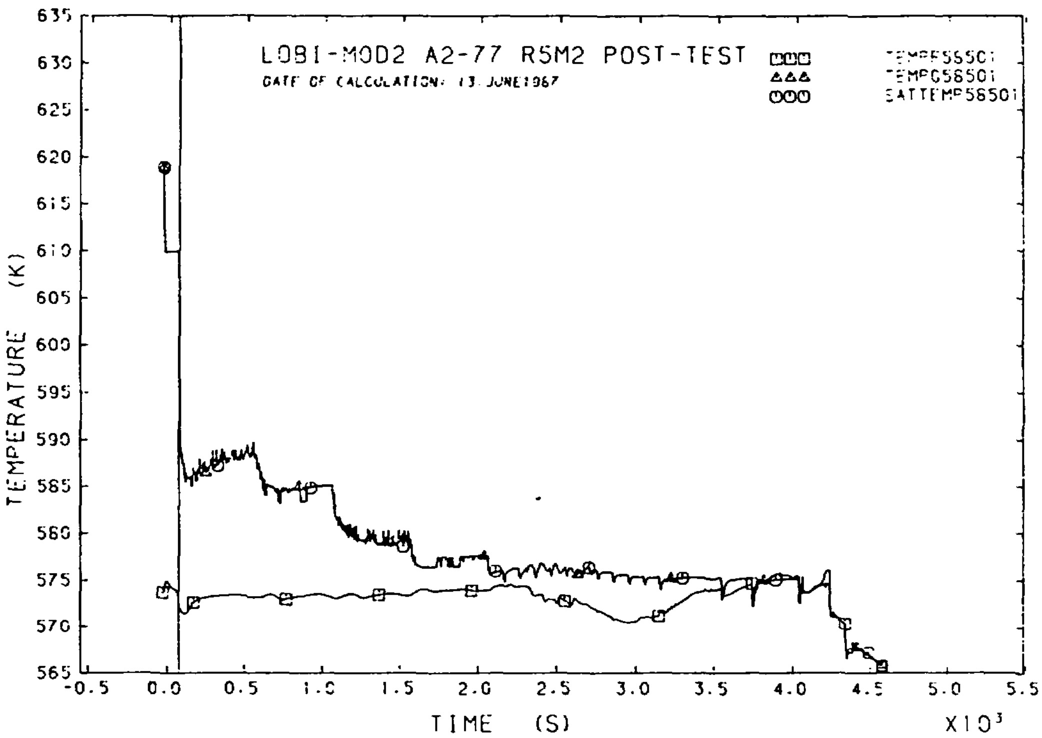

FIGURE B39 FLUID TEMPERATURE IN I.L.-S.G. OUTLET

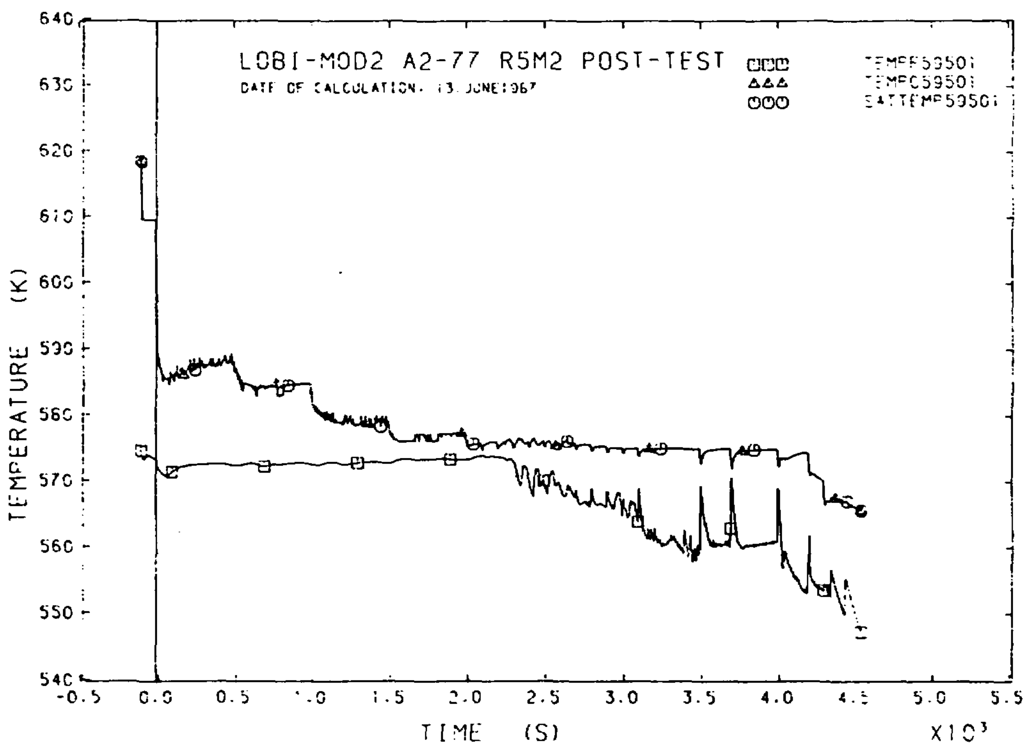

FIGURE B40 FLUID TEMPERATURE IN I.L.-PUMP INLET

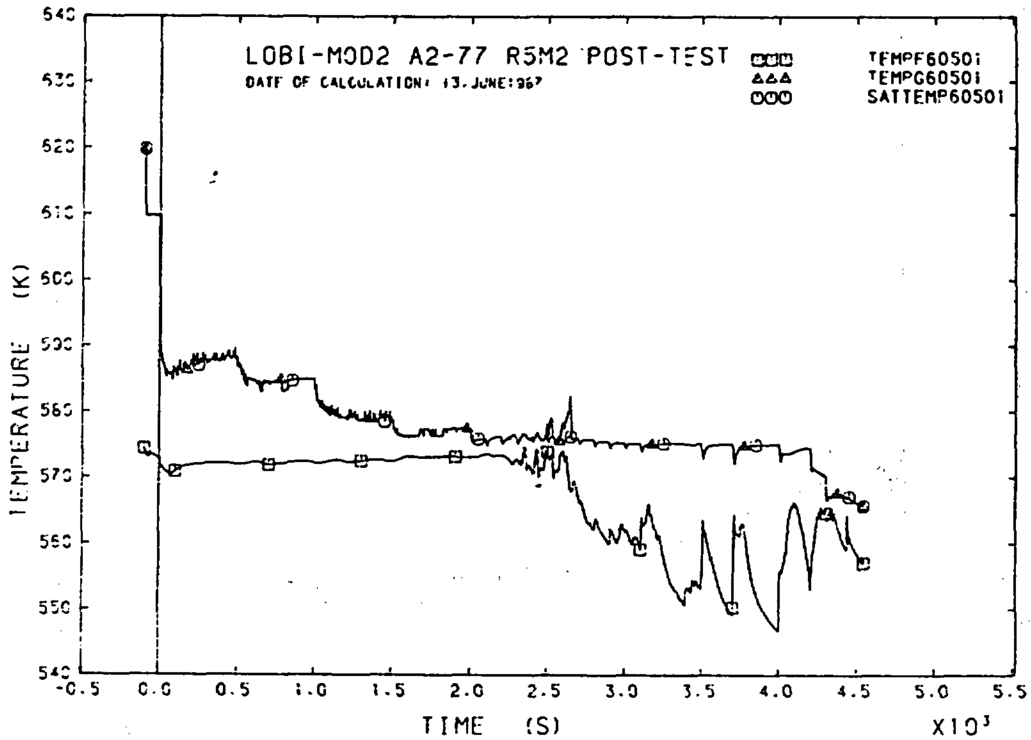

FIGURE B41 FLUID TEMPERATURE IN I.L.-PUMP OUTLET

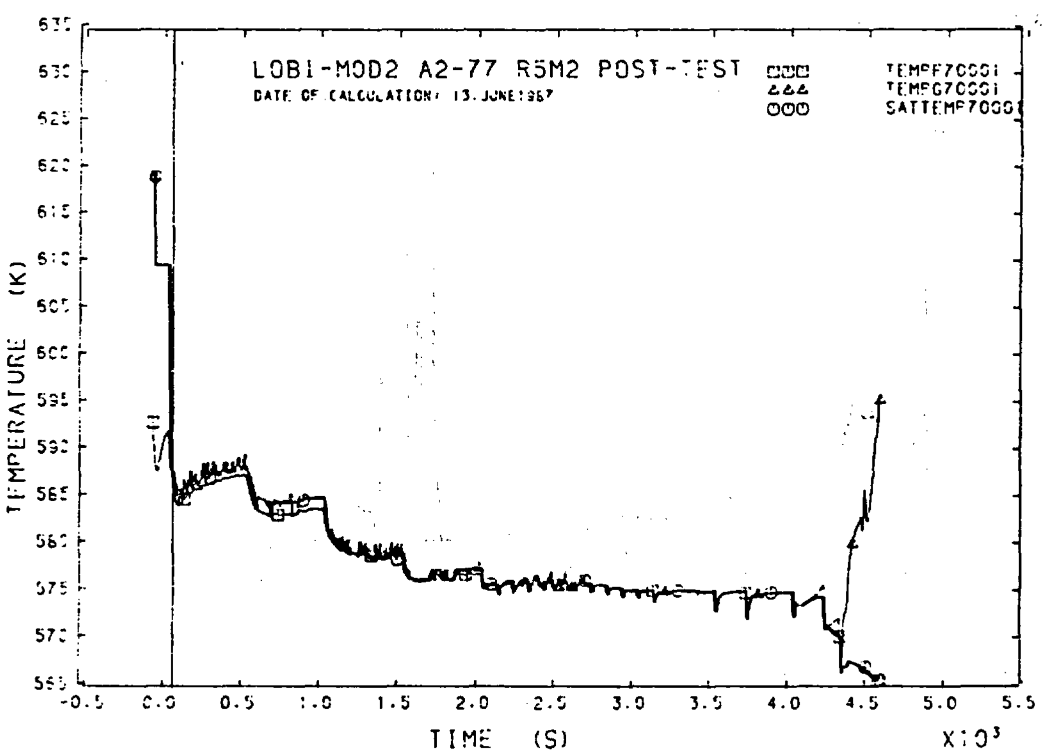

FIGURE B42 FLUID TEMPERATURE IN B.L.-H.L. VESSEL OUTLET

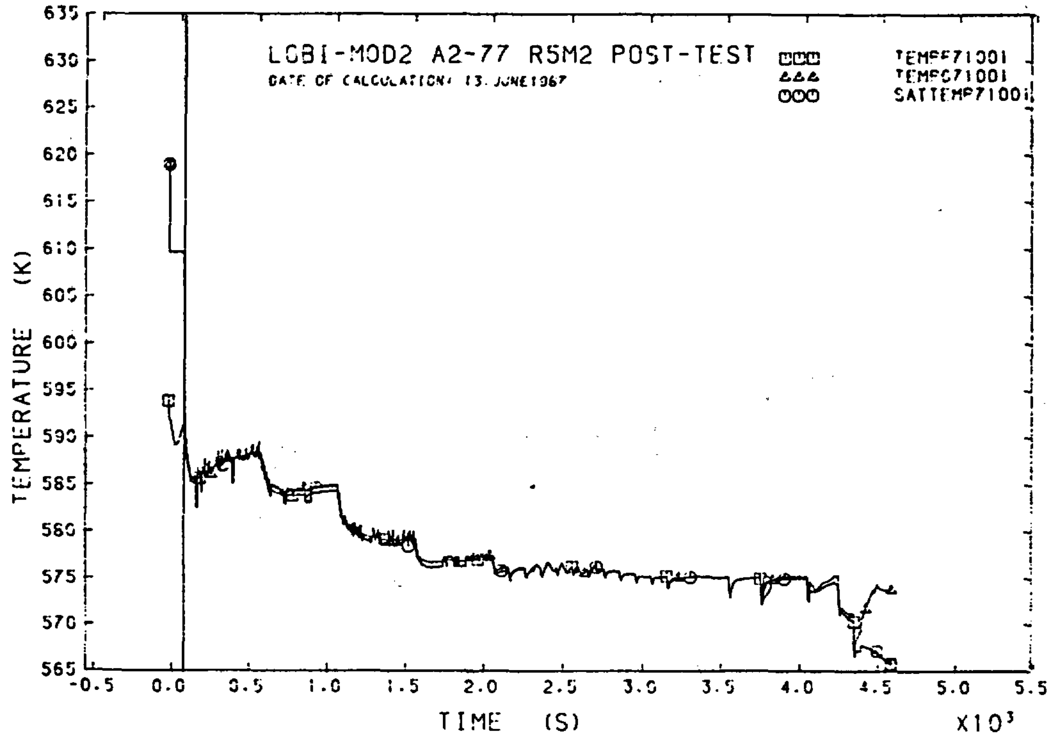

FIGURE B43 FLUID TEMPERATURE IN B.L.-S.G. INLET

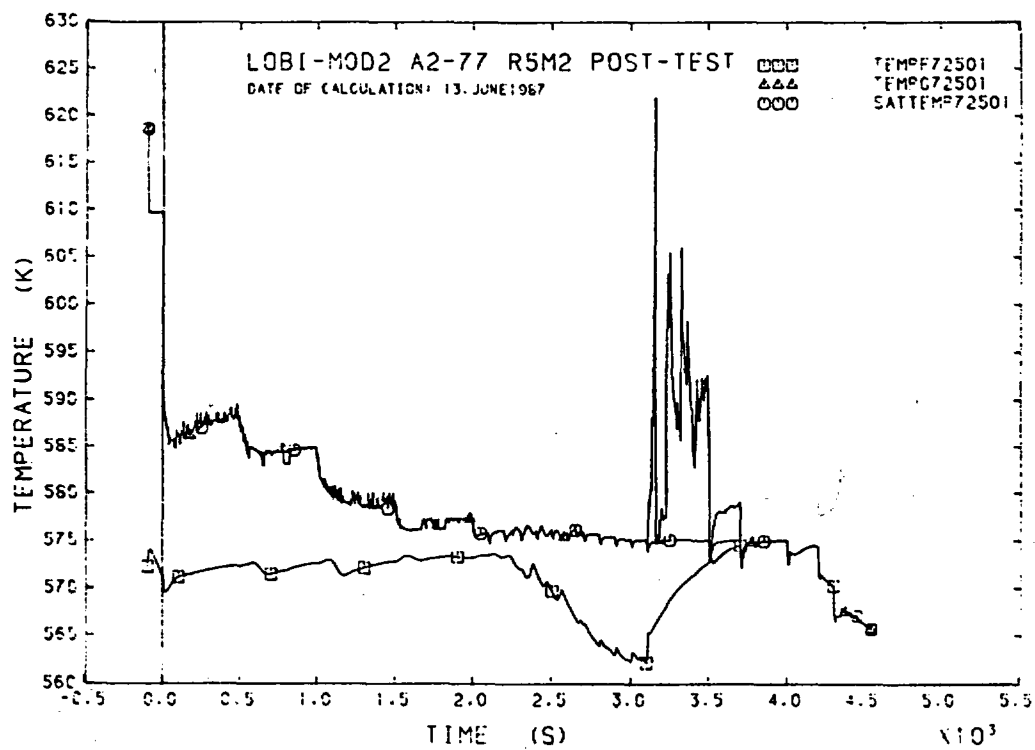

FIGURE B44 FLUID TEMPERATURE IN B.L.-S.G. OUTLET

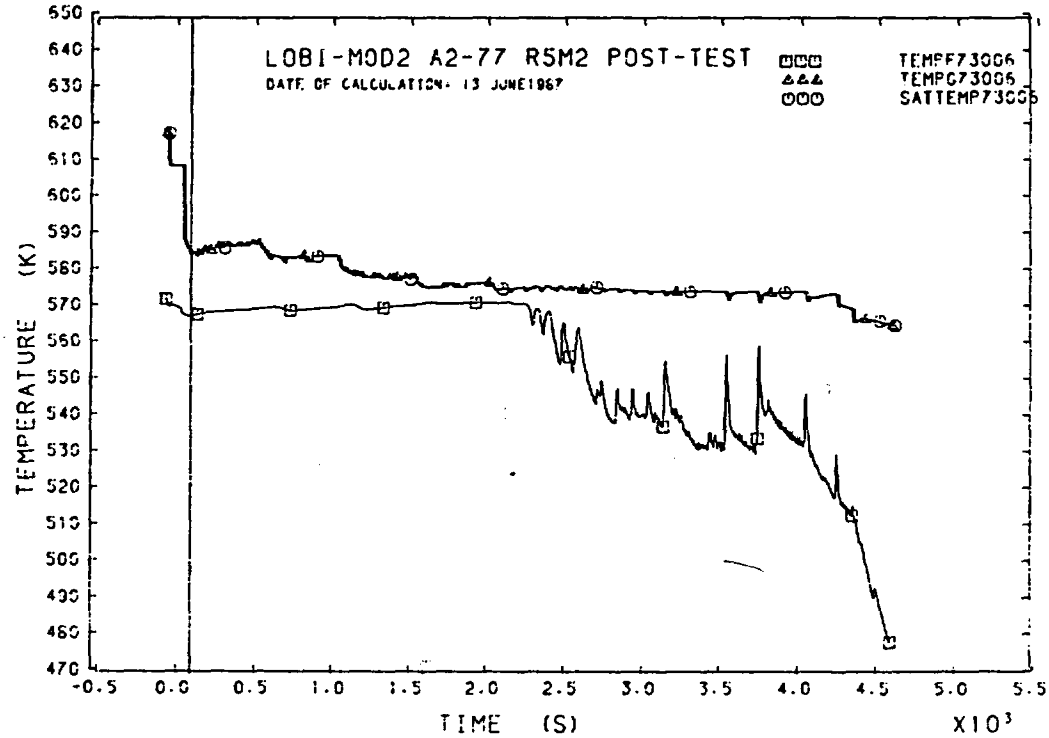

FIGURE B45 FLUID TEMPERATURE IN B.L.-PUMP INLET

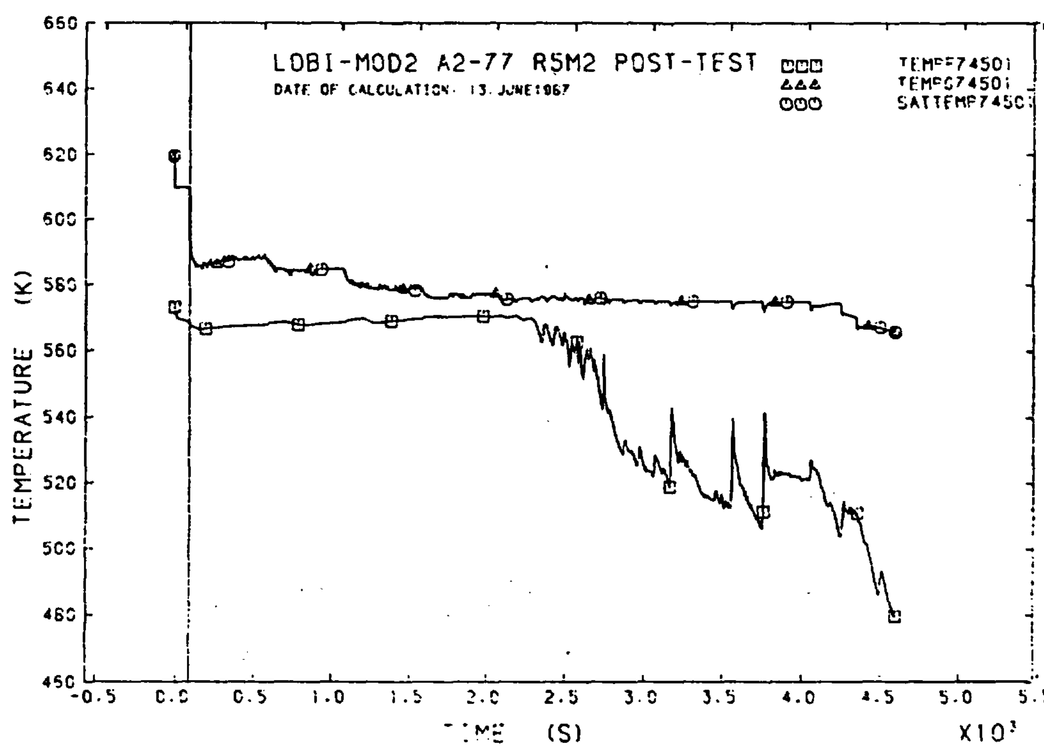

FIGURE B46 FLUID TEMPERATURE IN B.L.-PUMP OUTLET

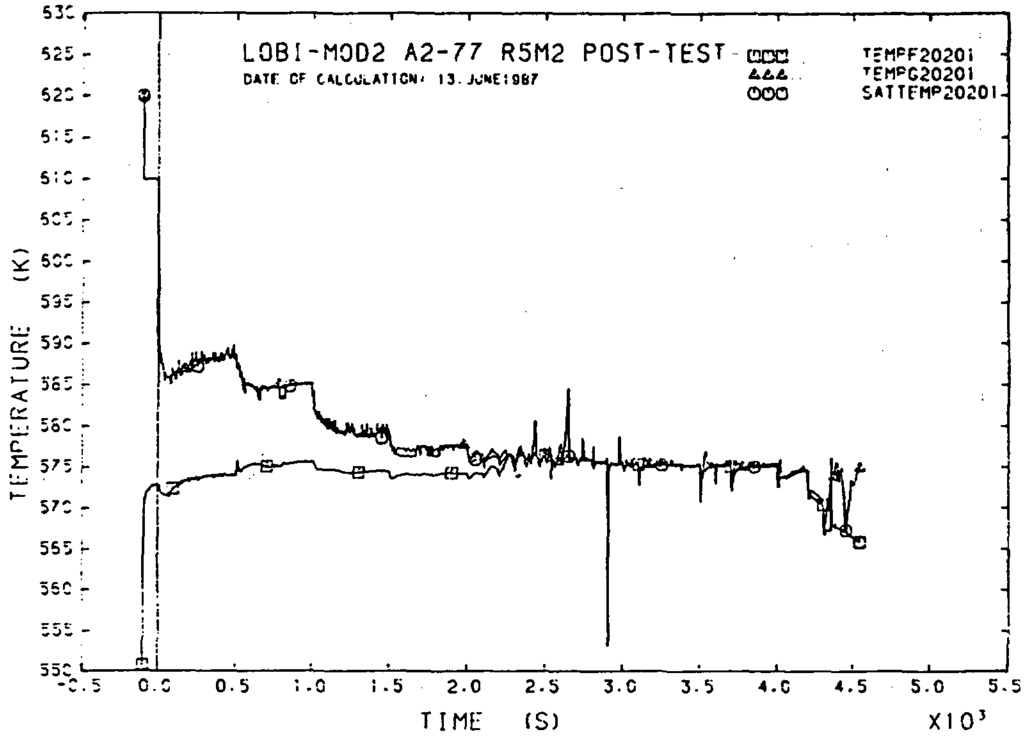

FIGURE B47 FLUID TEMPERATURE IN D.C. ANNULUS LOWER PART

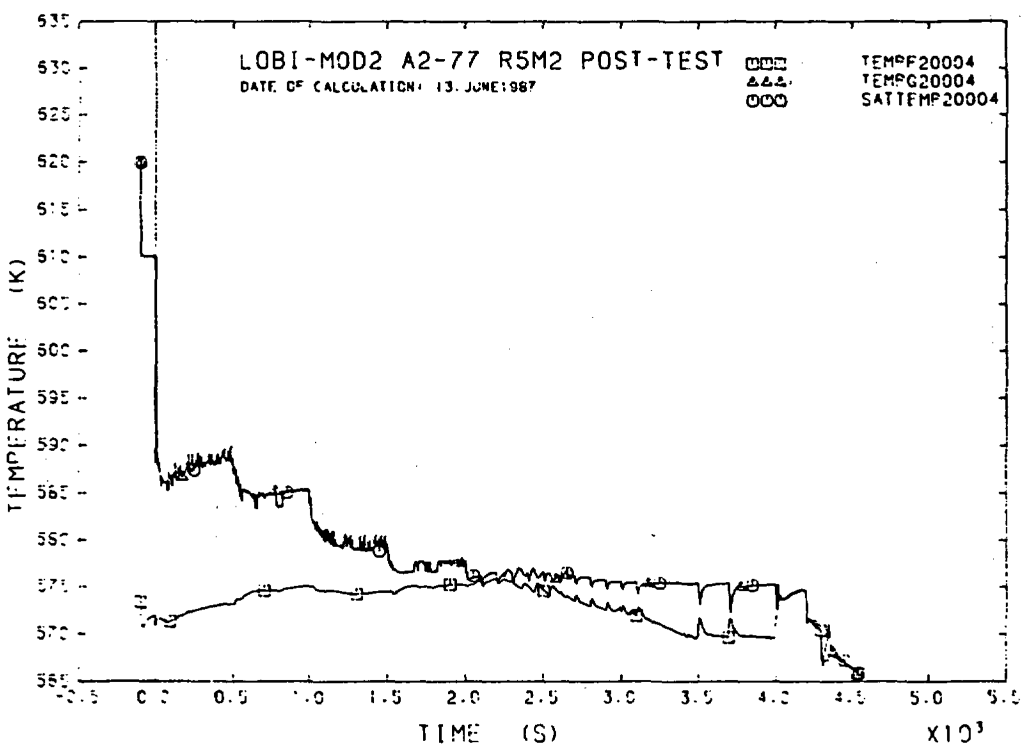

FIGURE B48 FLUID TEMPERATURE IN D.C. MIDDLE SECTION

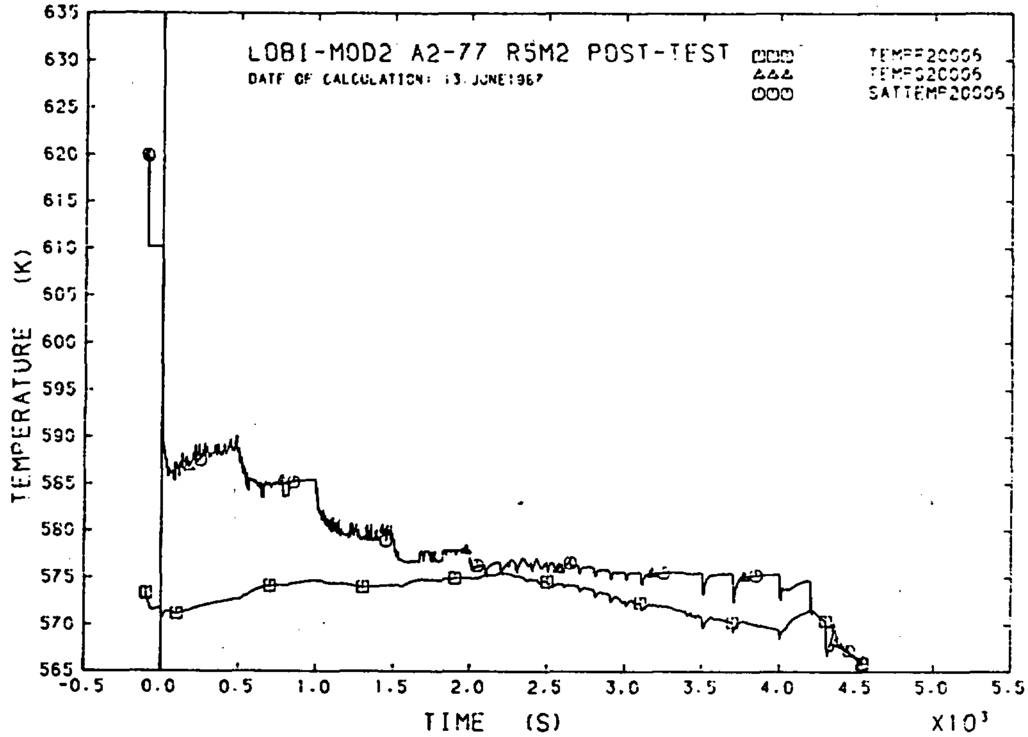

FIGURE B49 FLUID TEMPERATURE IN D.C. BOTTON

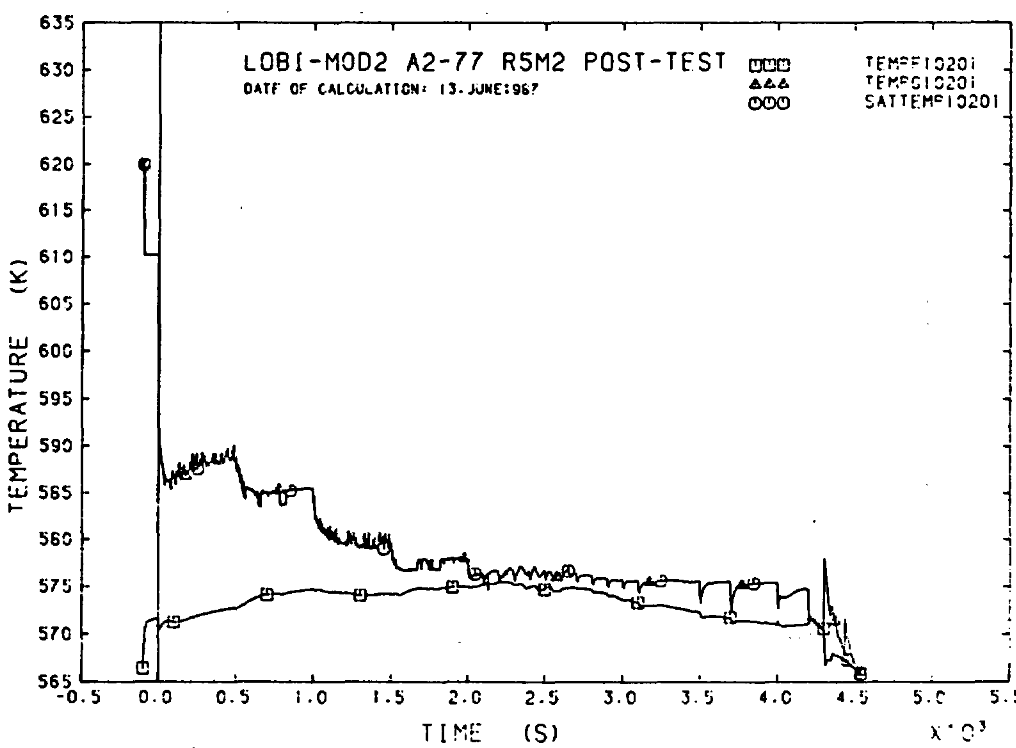

FIGURE B50 FLUID TEMPERATURE IN L.P.

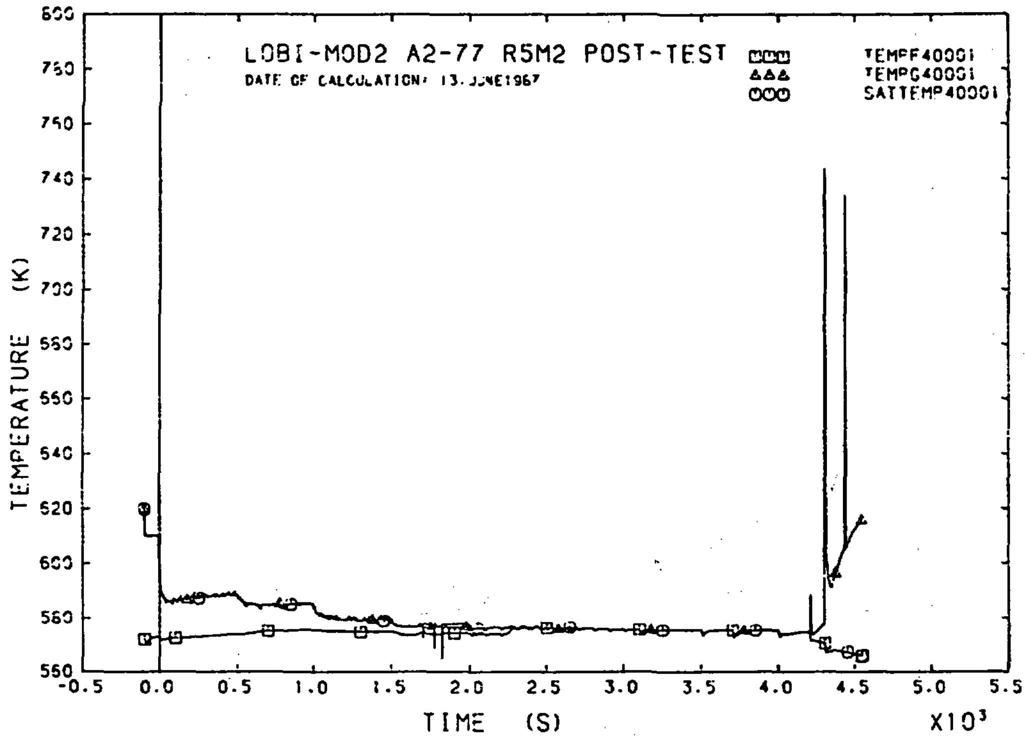

FIGURE B51 FLUID TEMPERATURE IN U.P.

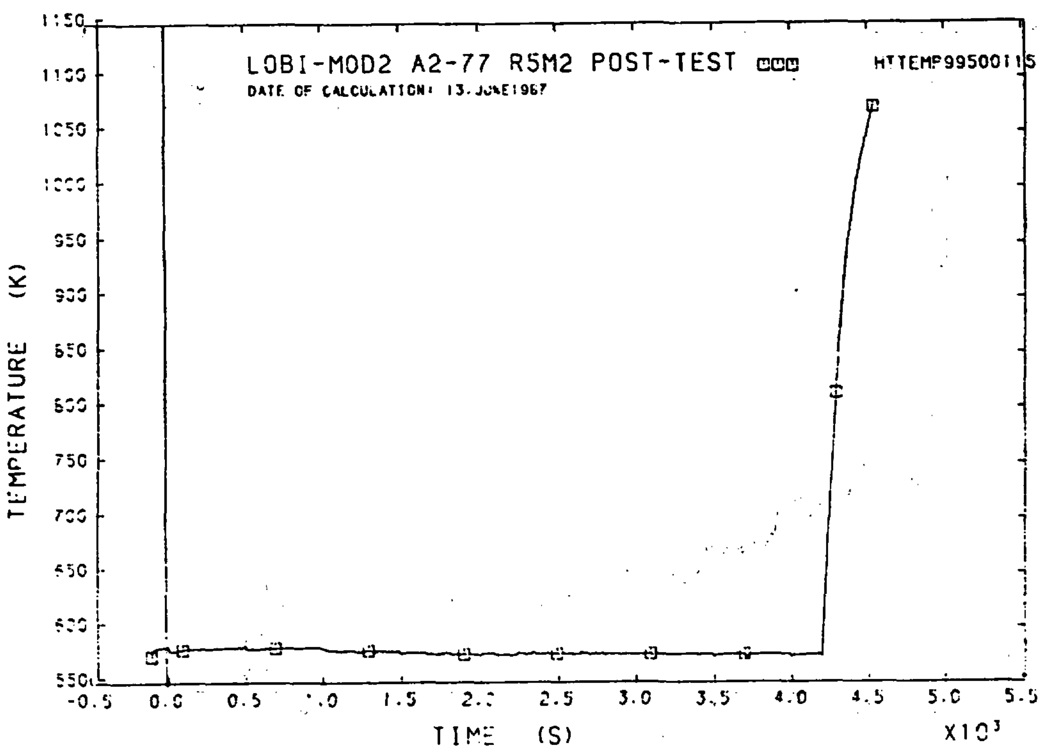

FIGURE B52 SURFACE ROD TEMPERATURE

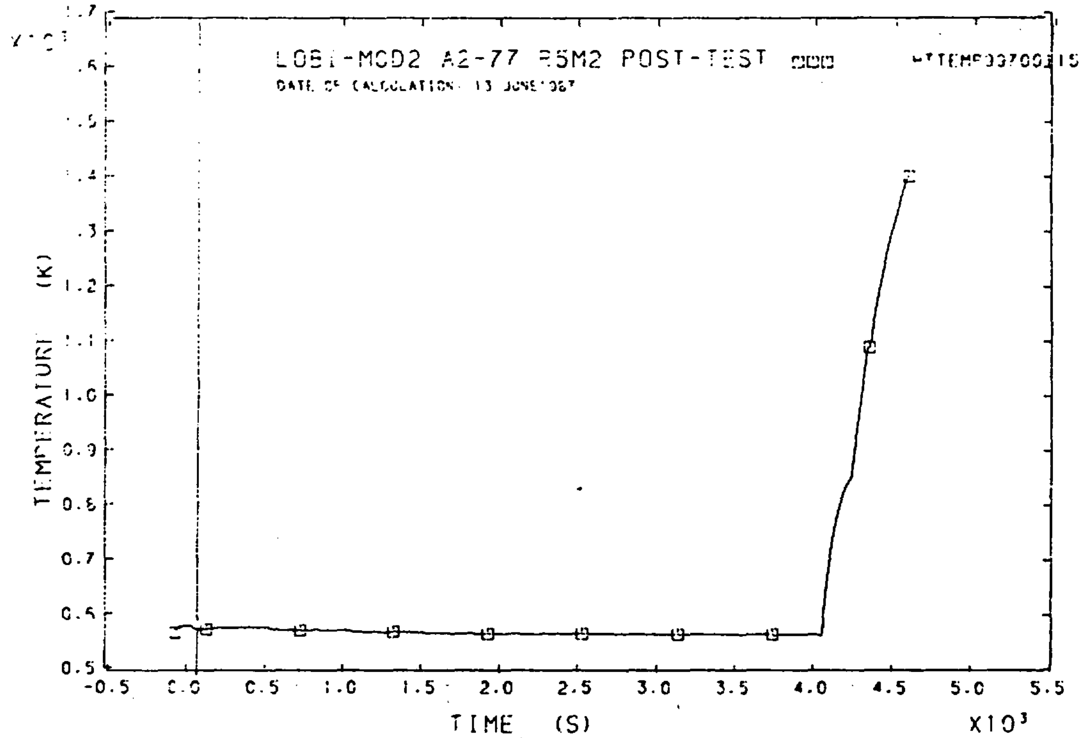

FIGURE B53 SURFACE ROD TEMPERATURE

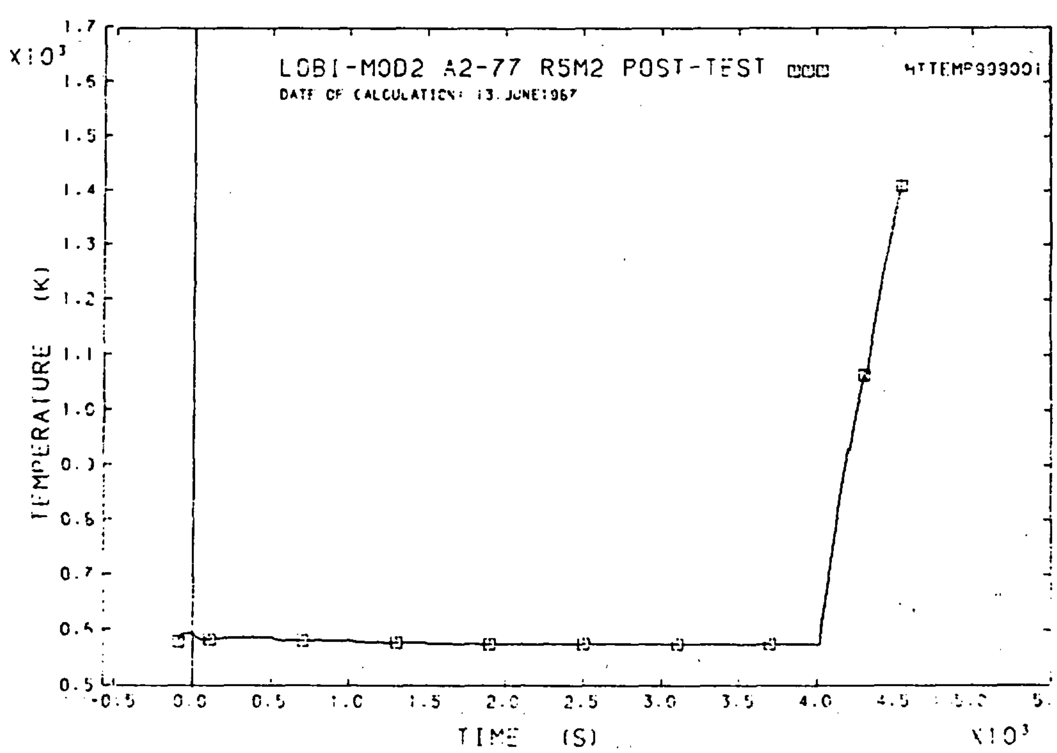

FIGURE B54 SURFACE ROD TEMPERATURE

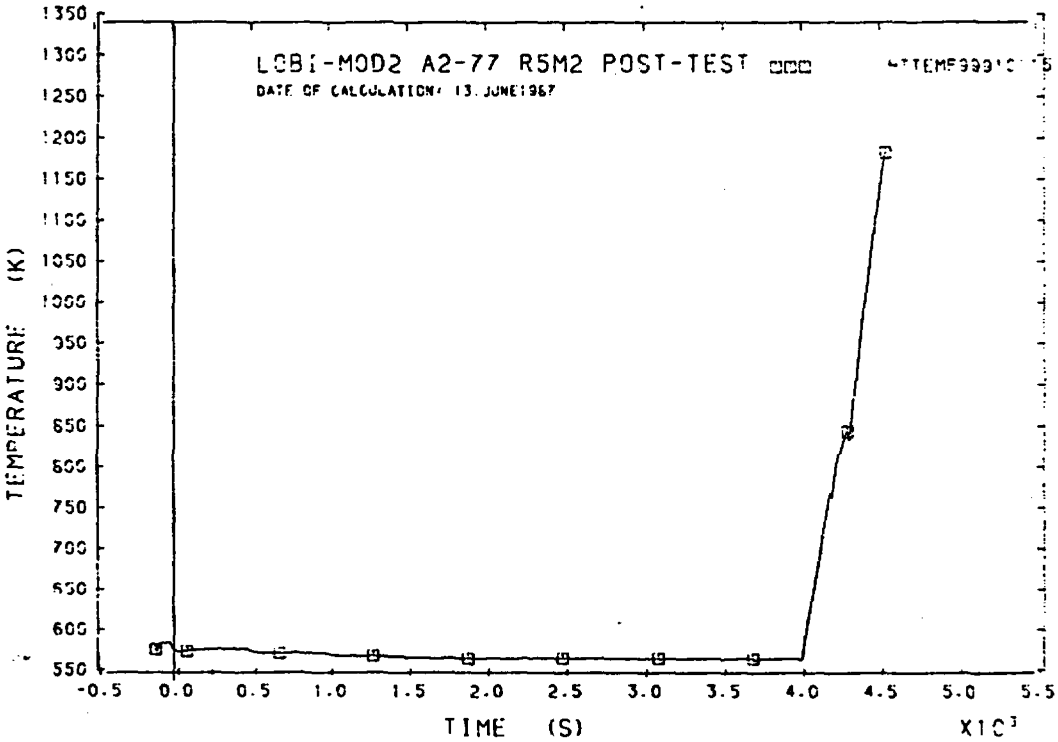

FIGURE B55 SURFACE ROD TEMPERATURE

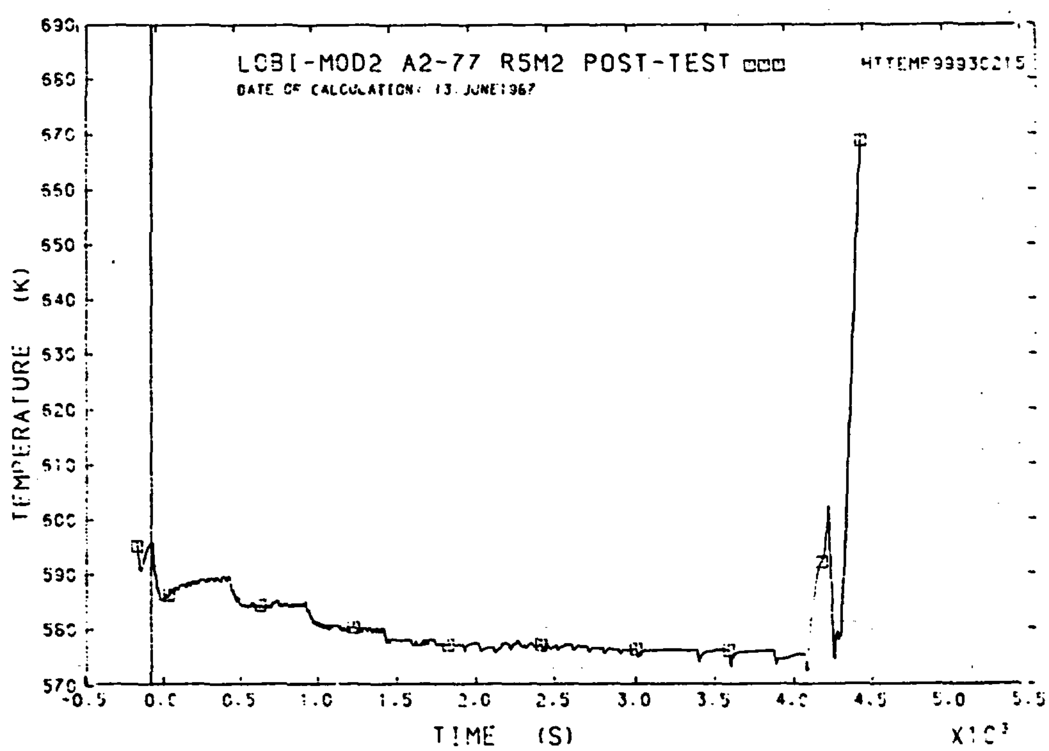

FIGURE B56 SURFACE ROD TEMPERATURE

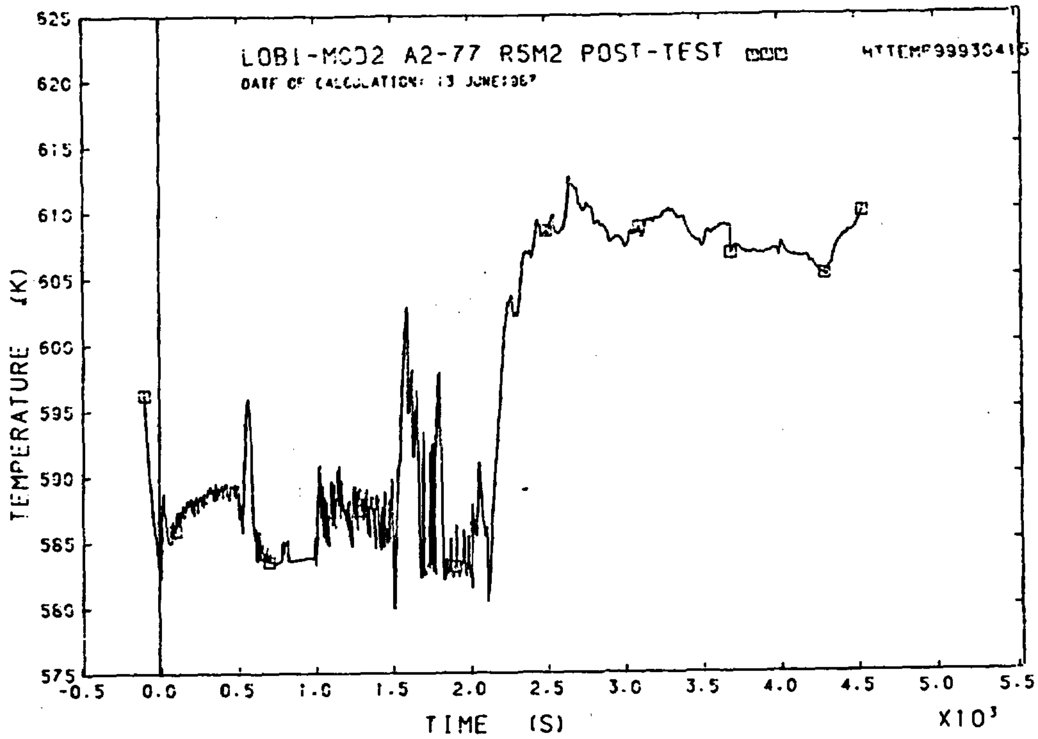

FIGURE **B57** SURFACE ROD TEMPERATURE

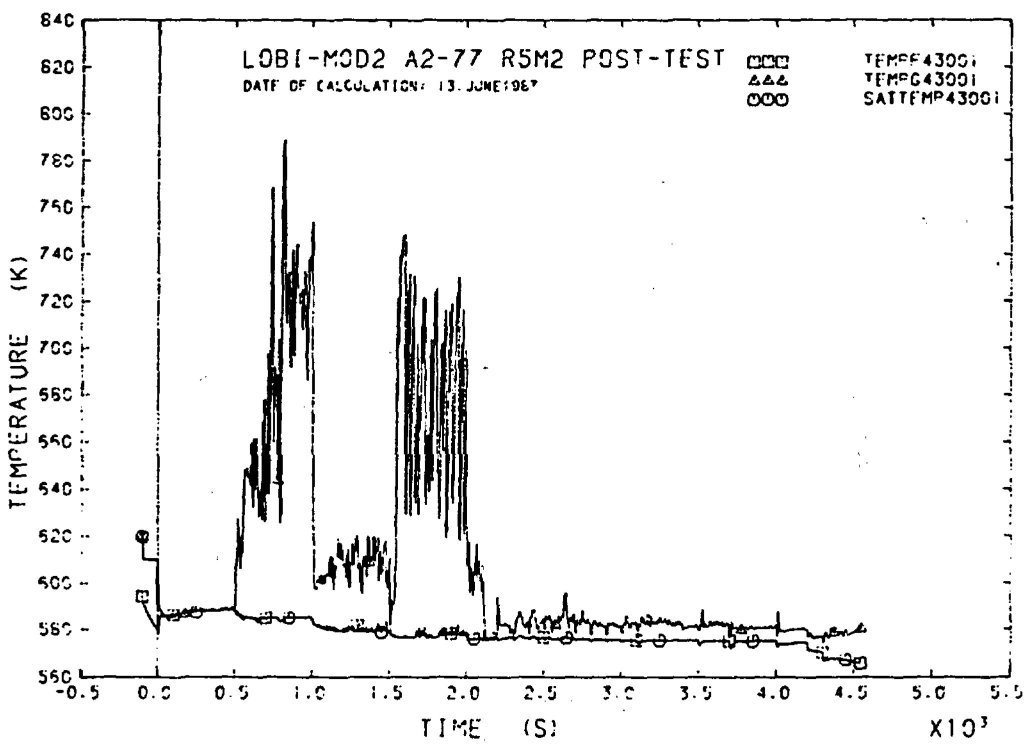

FIGURE **B58** FLUID TEMPERATURES IN UPPER PLENUM

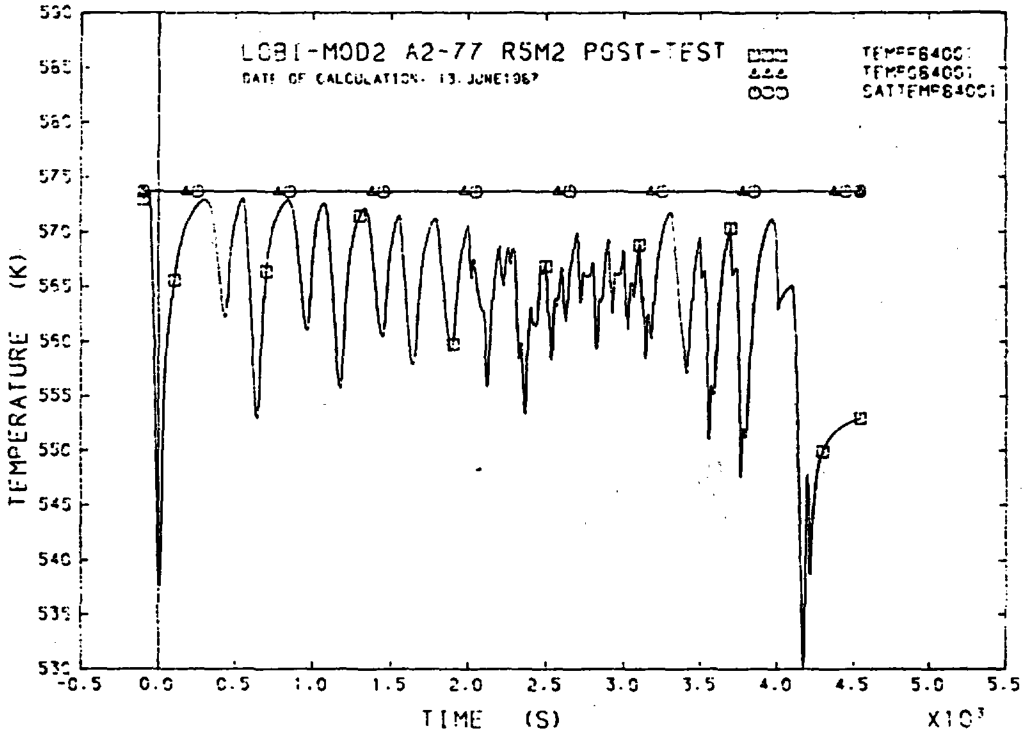

FIGURE B59 FLUID TEMPERATURES IN I.L. S.G. SECONDARY SIDE TOP

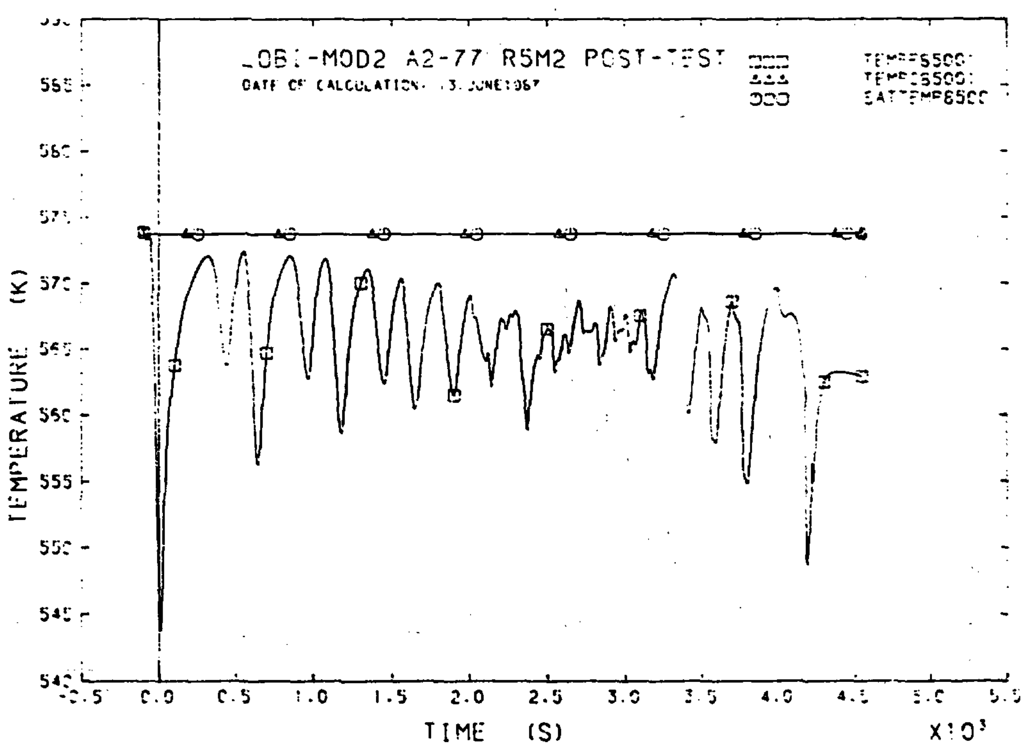

FIGURE B60 FLUID TEMPERATURES IN I.L. S.G. SECONDARY SIDE DOWNCOMER

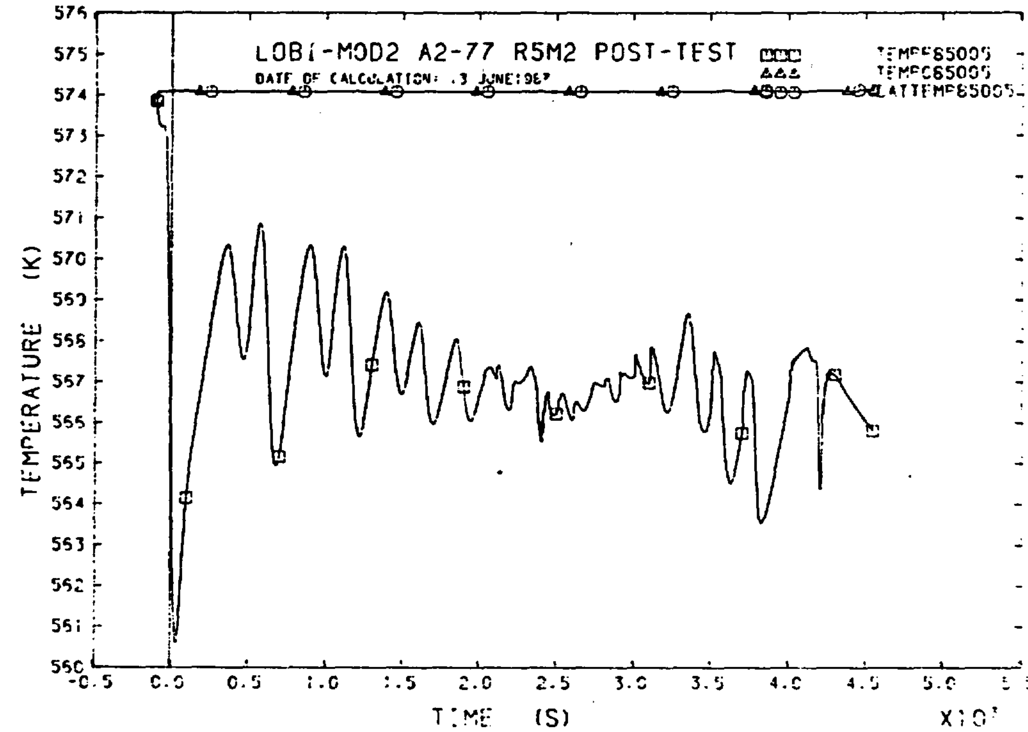

FIGURE **B61** FLUID TEMPERATURES IN I.L. S.G. SECONDARY SIDE DOWNCOMER

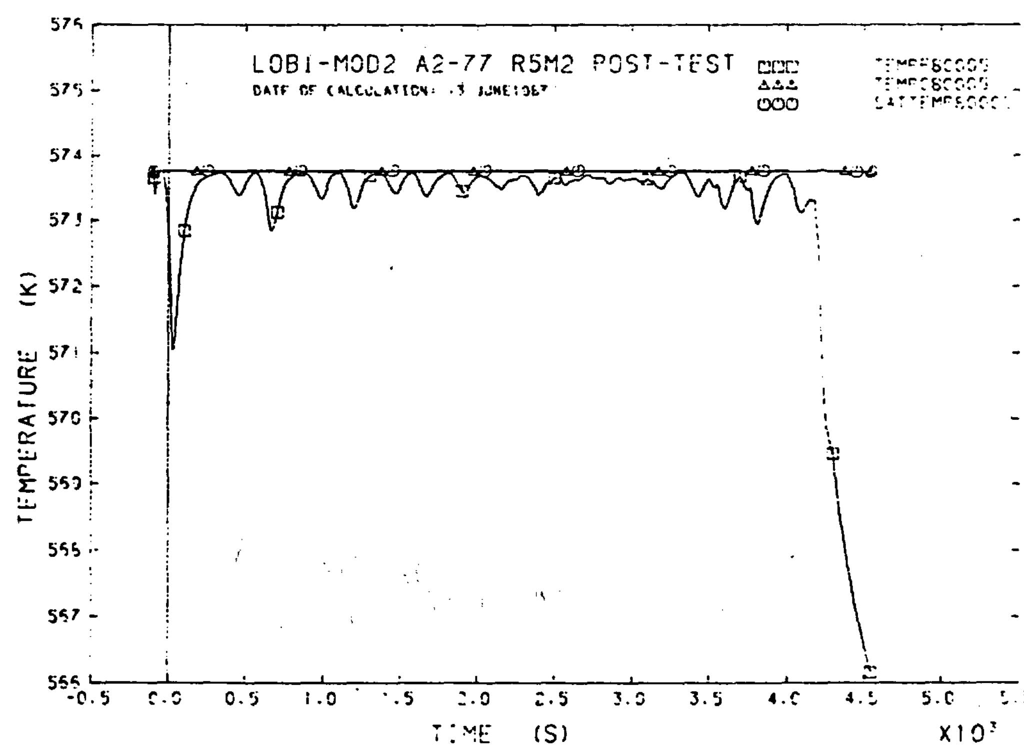

FIGURE **B62** FLUID TEMPERATURES IN I.L. S.G. SECONDARY SIDE RISER

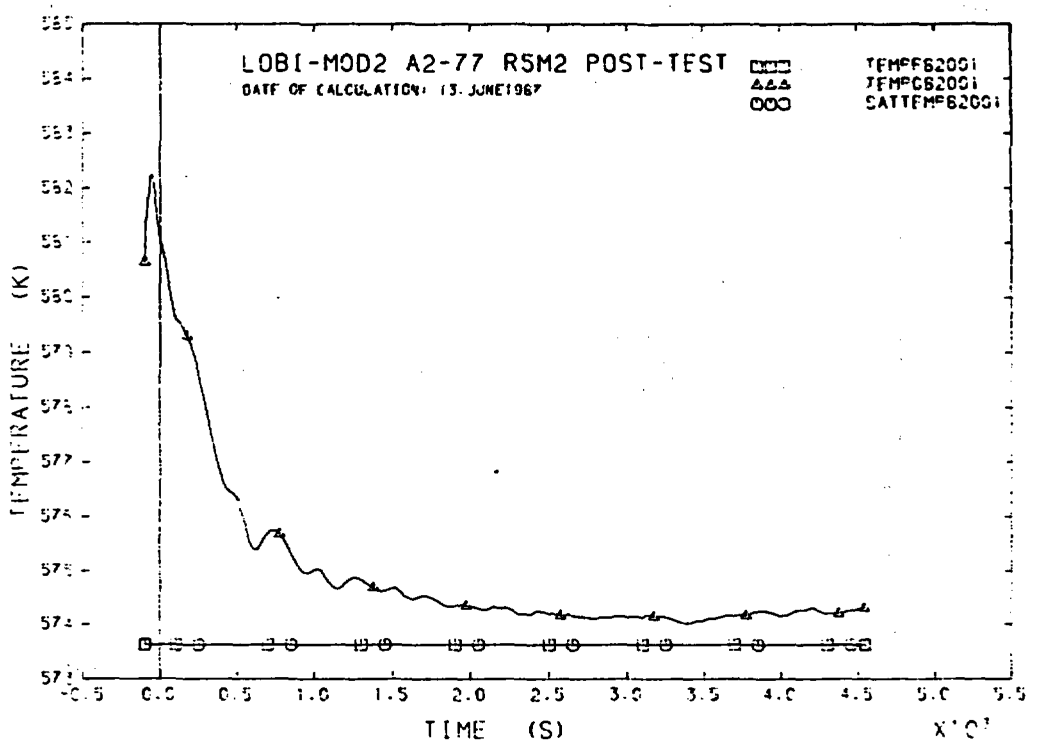

FIGURE B63 FLUID TEMPERATURES IN I.L. S.G. SECONDARY SIDE U-TUBES OUTLE

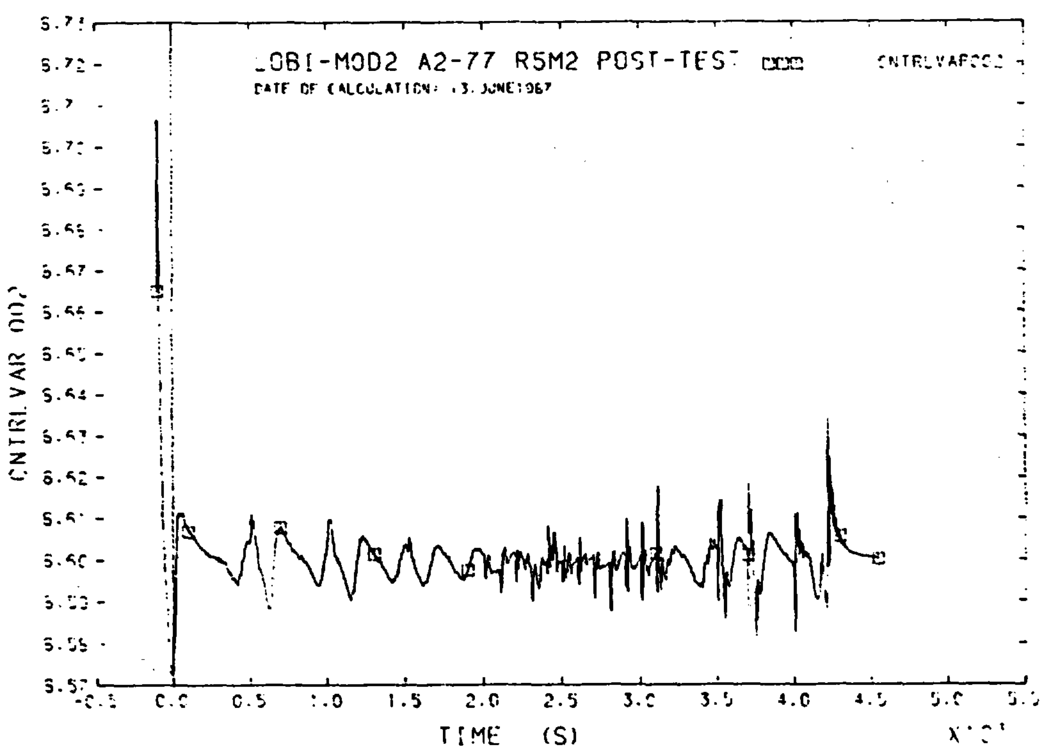

FIGURE B64 FLUID DOWNCOMER LEVEL IN I.L.S.G.

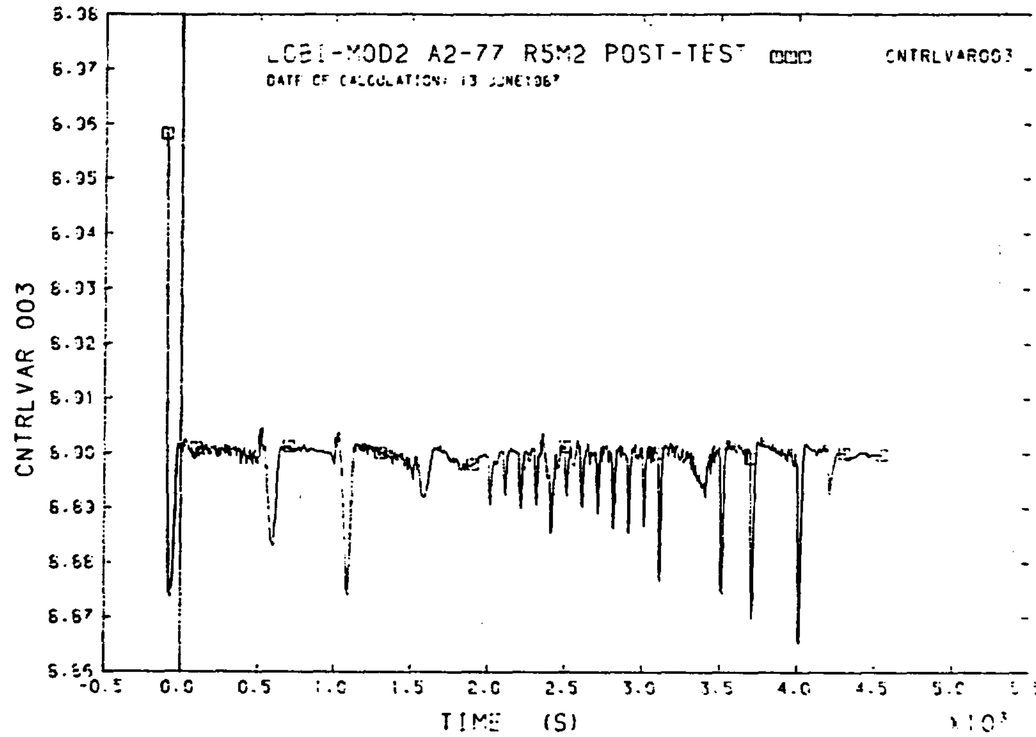

FIGURE B65 FLUID DOWNCOMER LEVEL IN B.L.S.G.

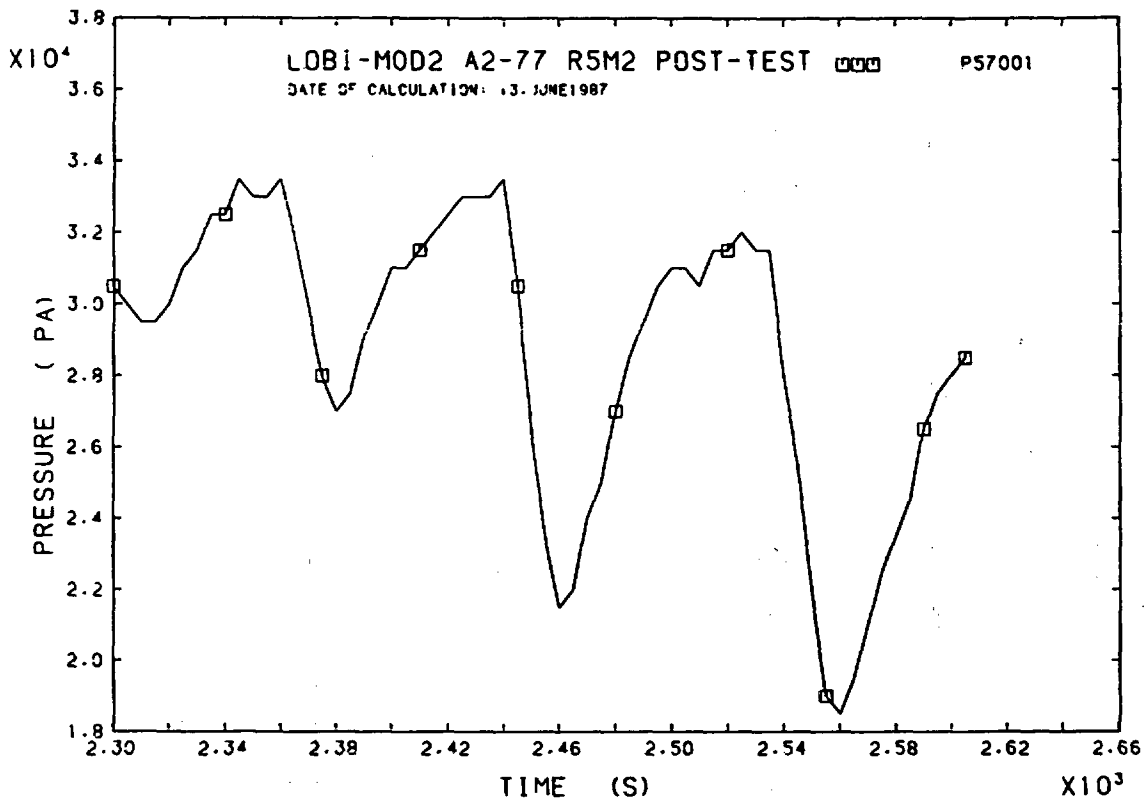

FIGURE B66 DIFFERENTIAL PRESSURE IN I.L. UT ASCENDING LEG

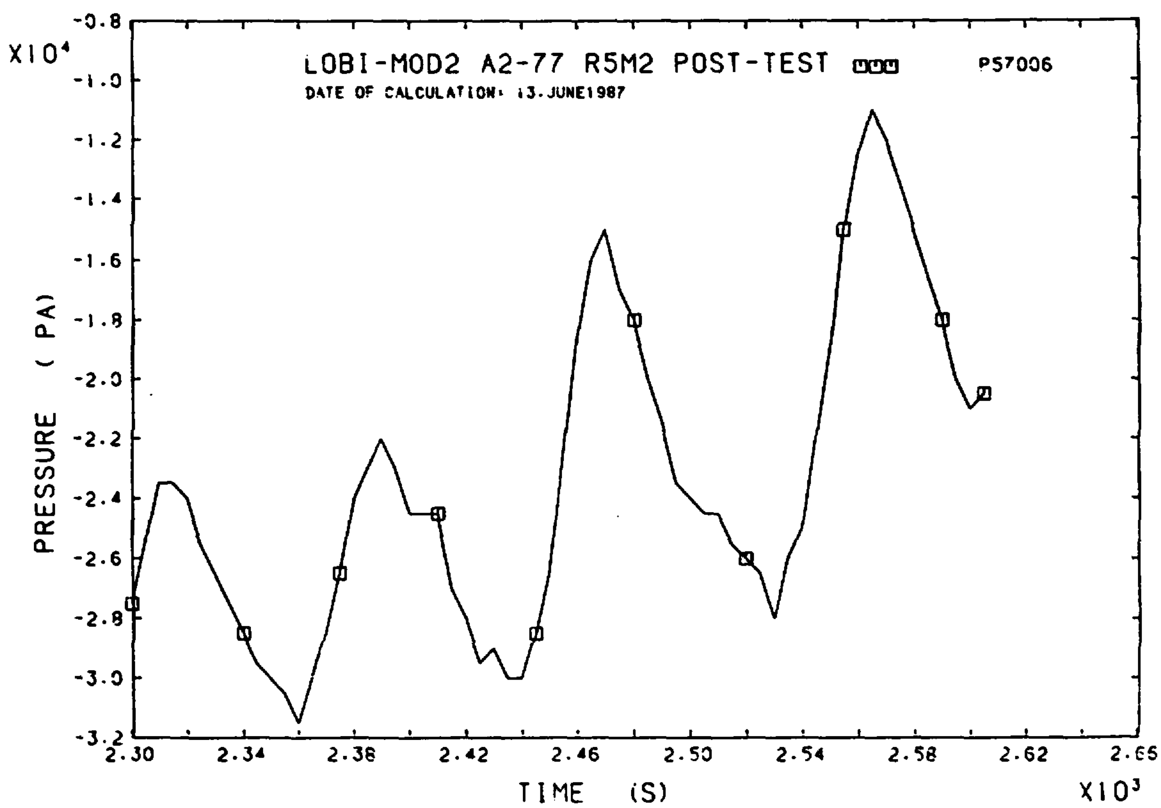

FIGURE B67 DIFFERENTIAL PRESSURE IN I.L. UT DESCENDING LEG

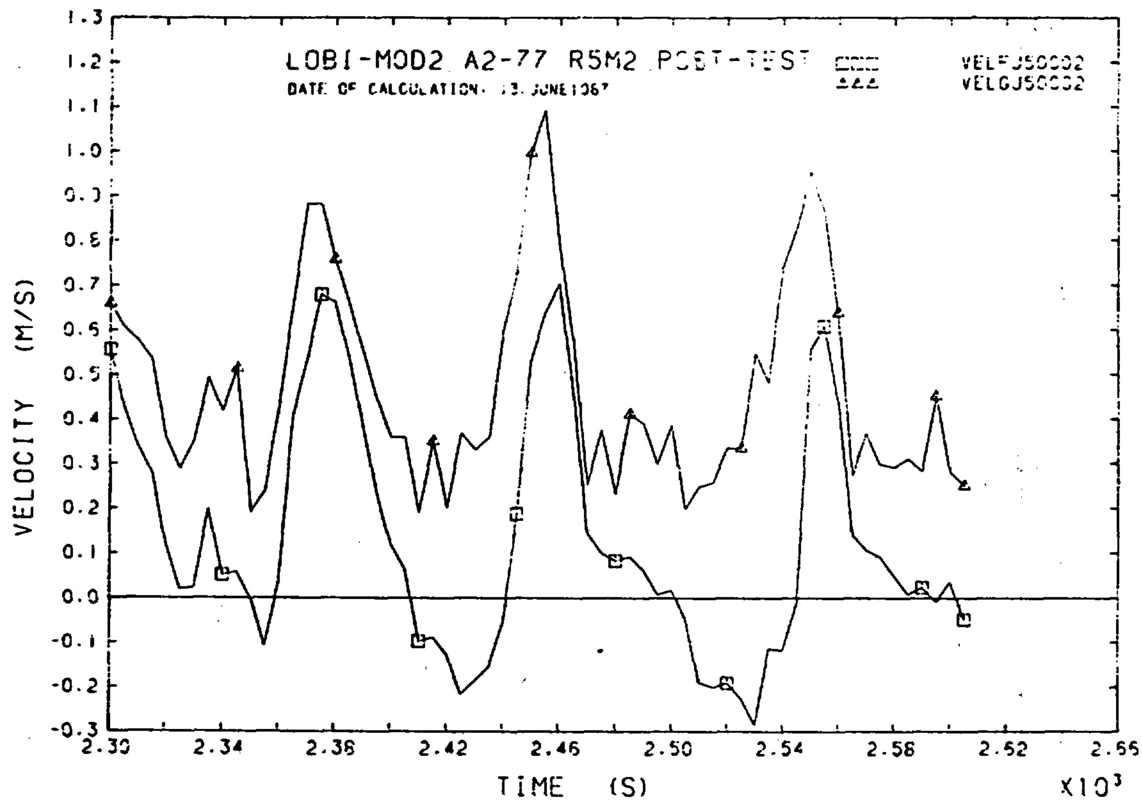

FIGURE B68 FLUID VELOCITIES IN TRIPLE LOOP H.L.

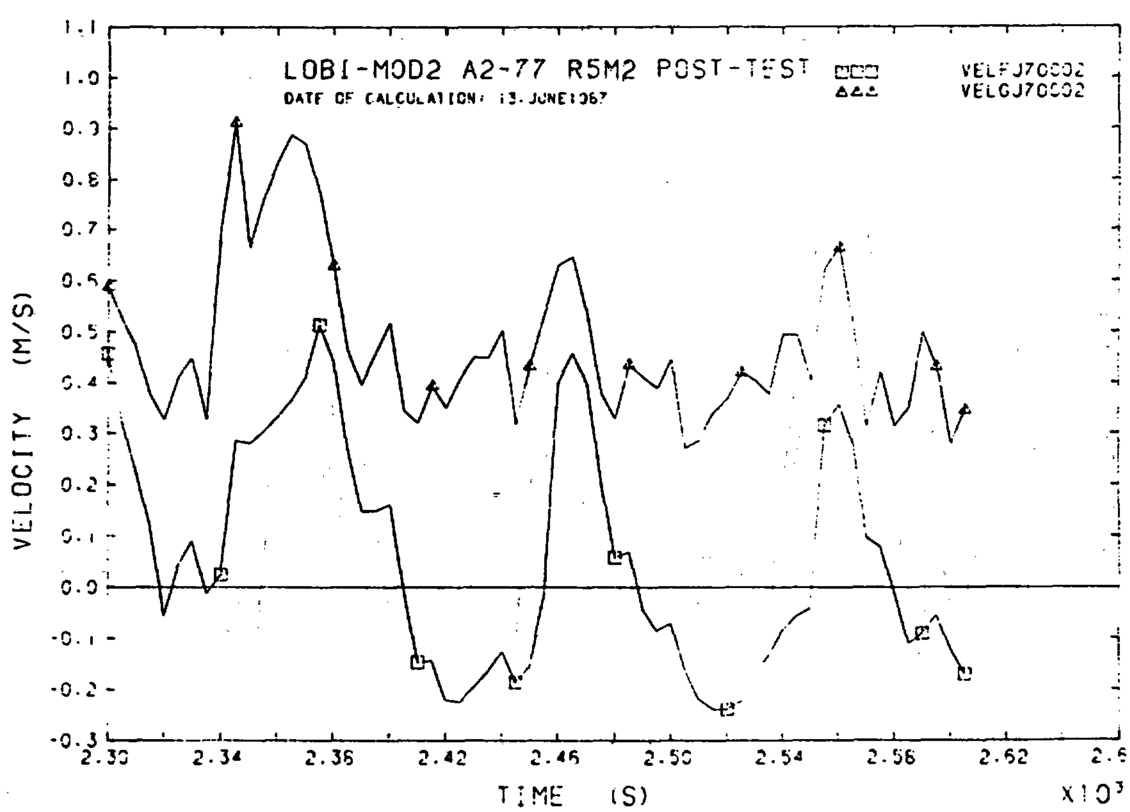

FIGURE B69 FLUID VELOCITIES IN SINGLE LOOP H.L.

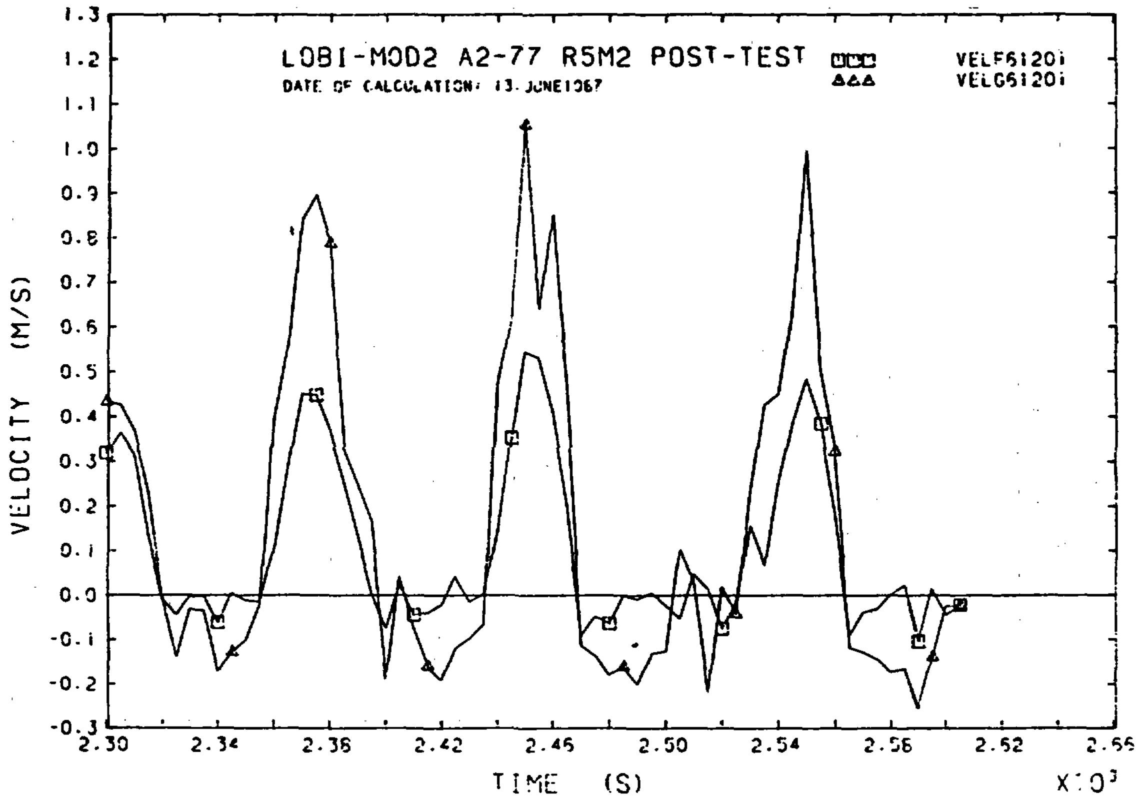

FIGURE B70 FLUID VELOCITIES IN TRIPLE LOOP C.L.

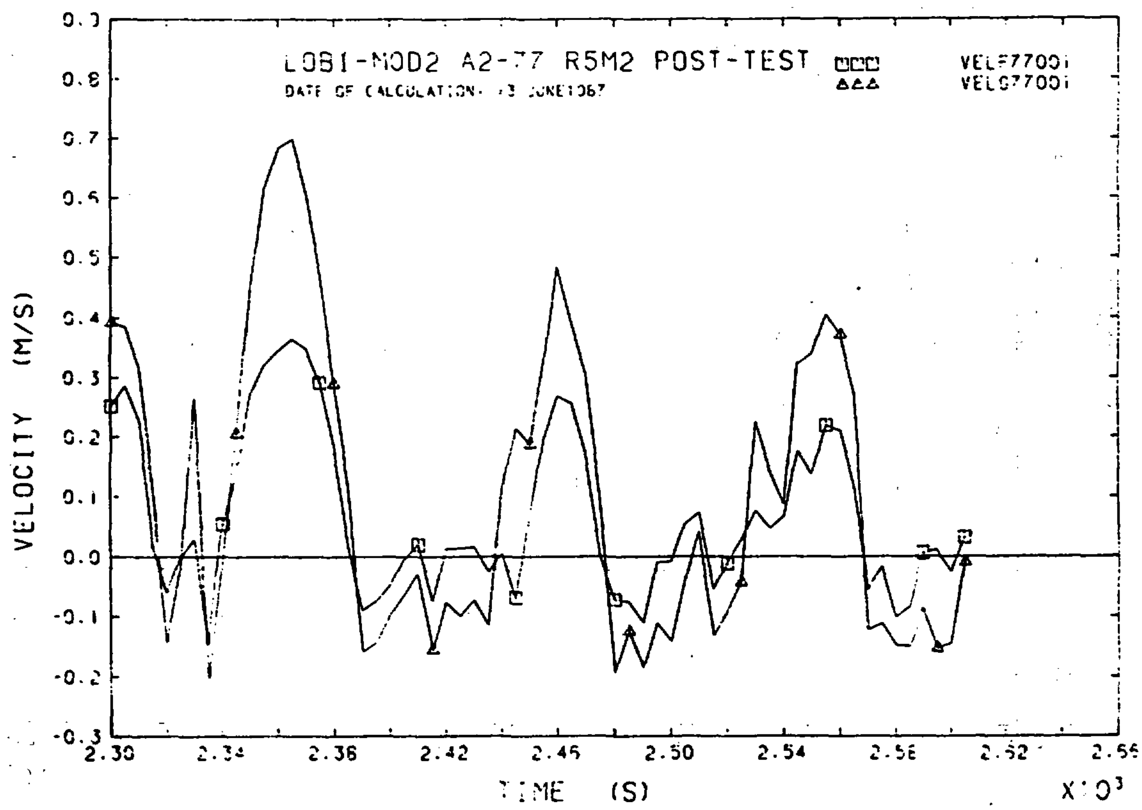

FIGURE B71 FLUID VELOCITIES IN SINGLE LOOP C.L.

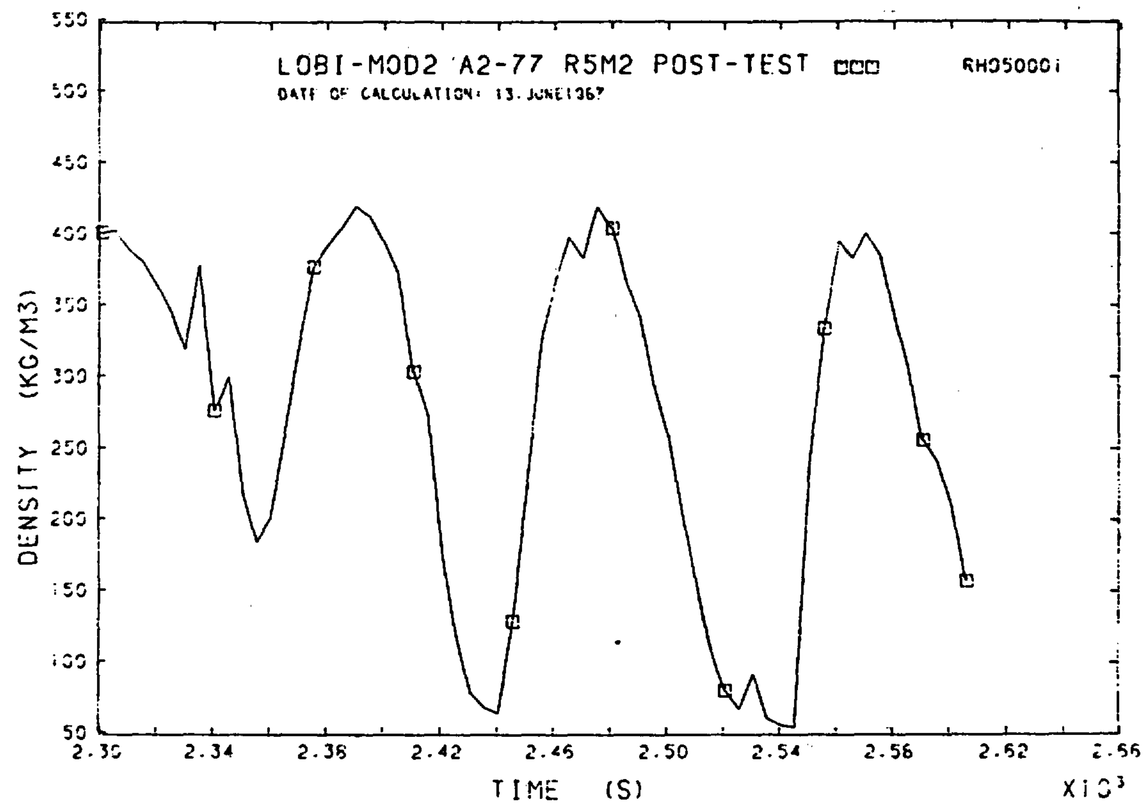

FIGURE B72 FLUID DENSITY IN I.L.-H.L.

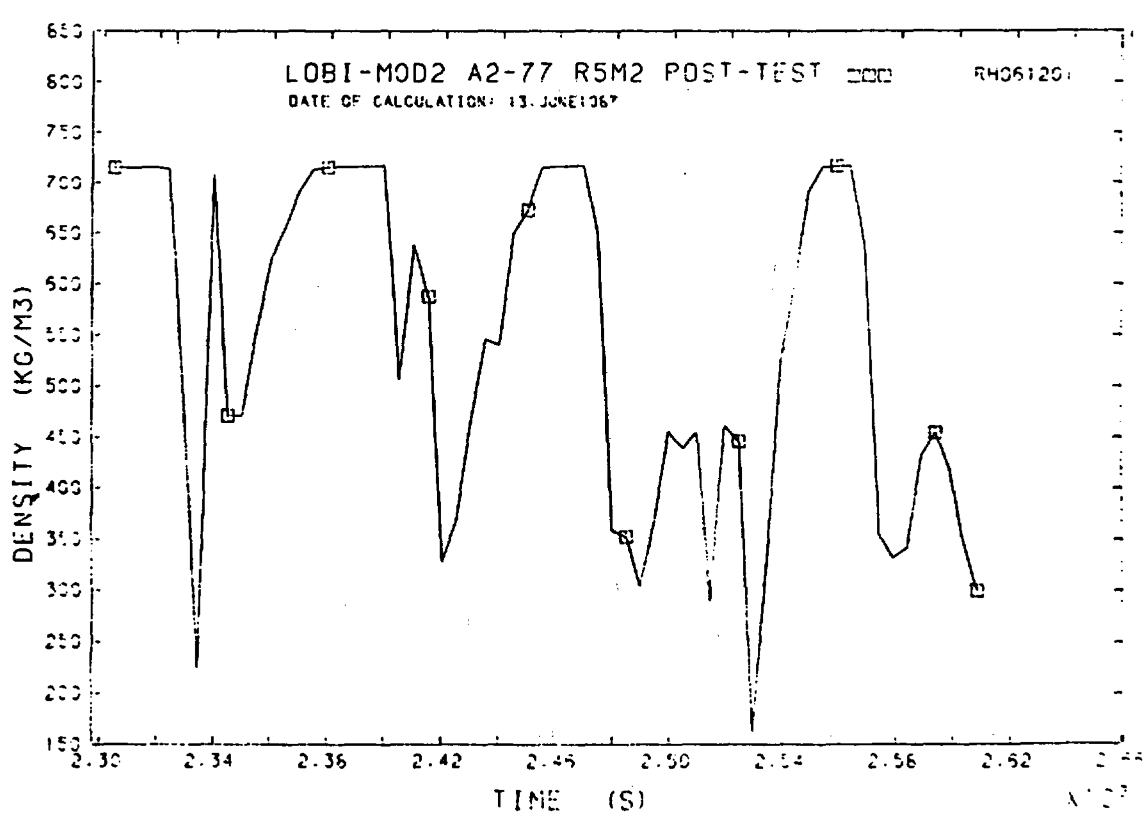

FIGURE B73 FLUID DENSITY IN I.L.-C.L.

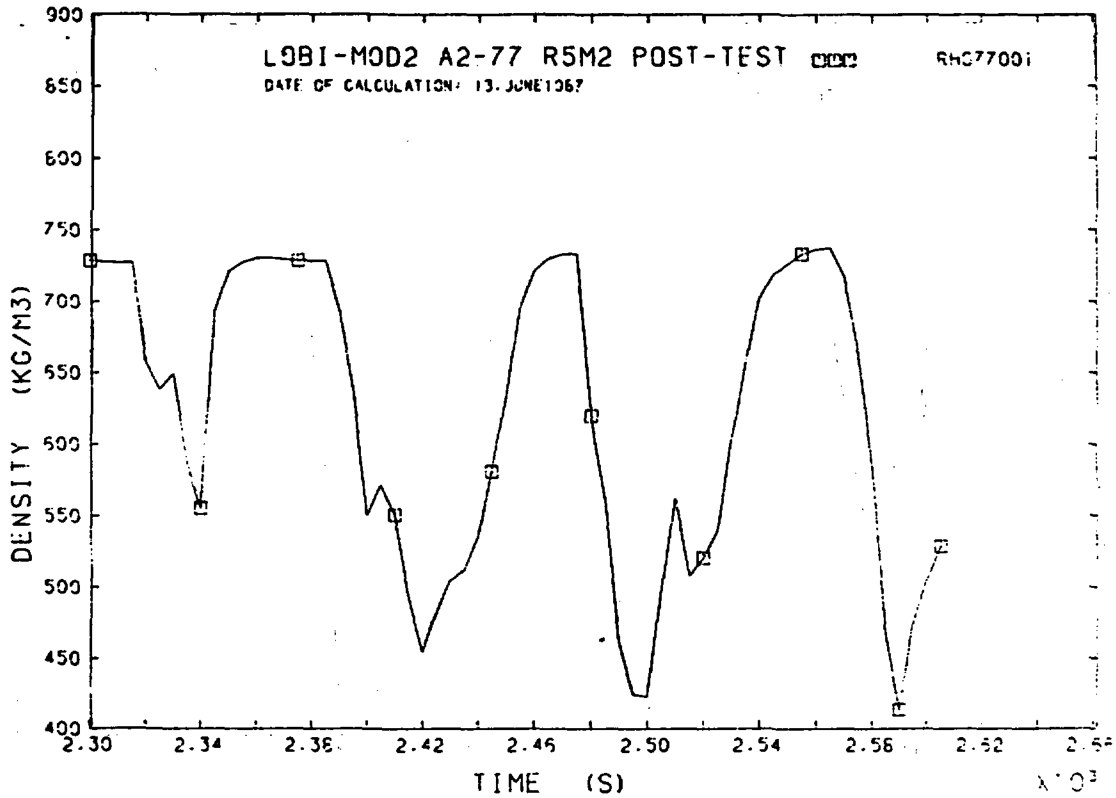

FIGURE B74 FLUID DENSITY IN B.L. C.L.

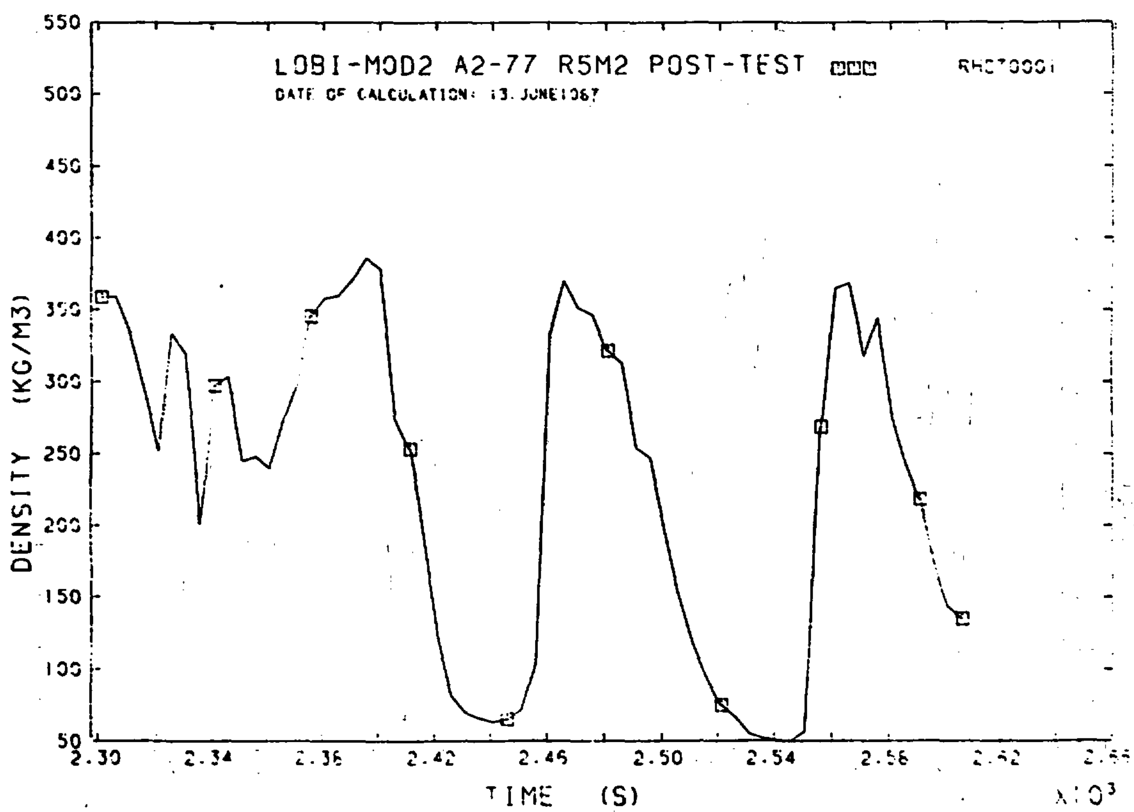

FIGURE B75 FLUID DENSITY IN B.L-H.L.

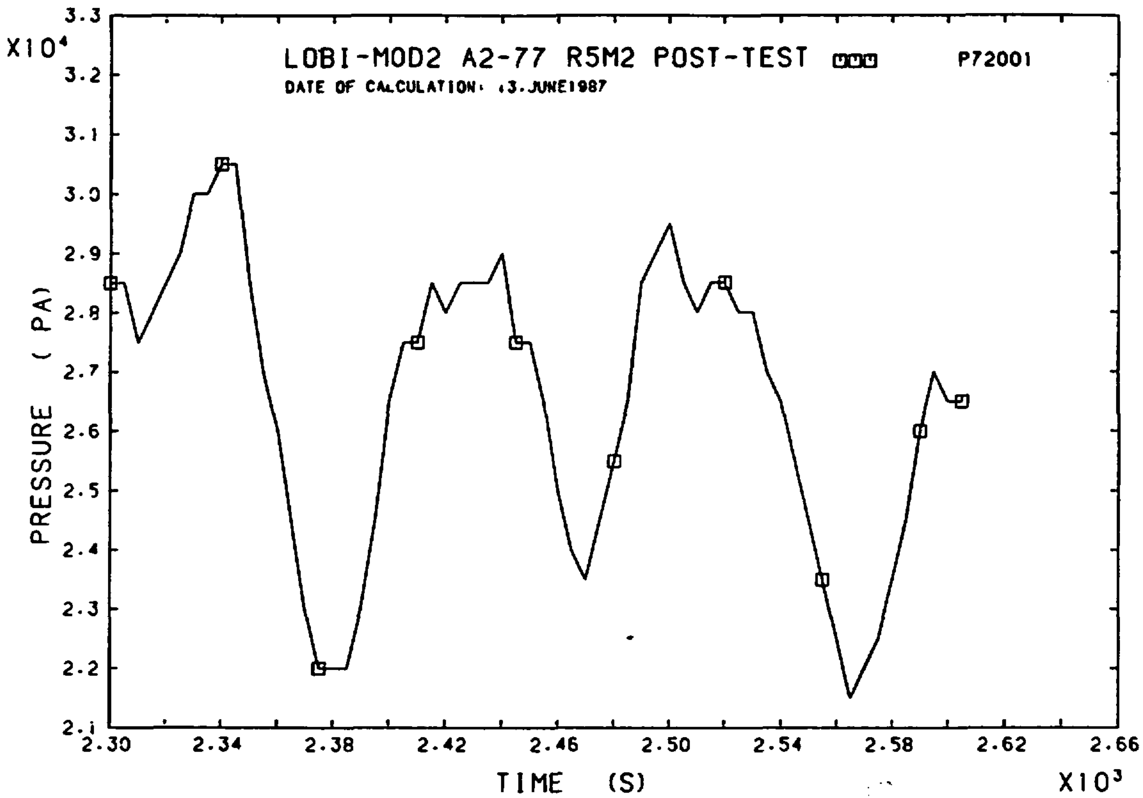

FIGURE B76 DIFFERENTIAL PRESSURE IN B.L. UT ASCENDING LEG

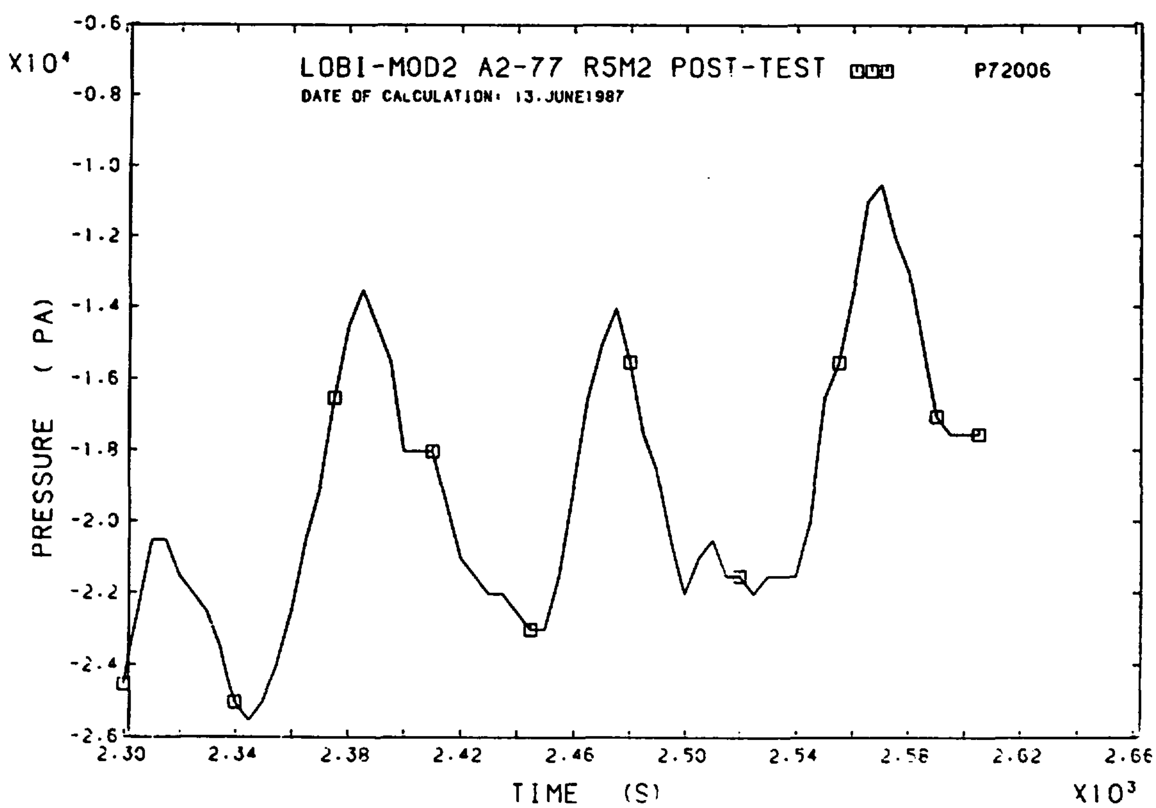

FIGURE B77 DIFFERENTIAL PRESSURE IN B.L. UT DESCENDING LEG

APPENDIX C

Measured and calculated trends for case C (Piping roughness changed)

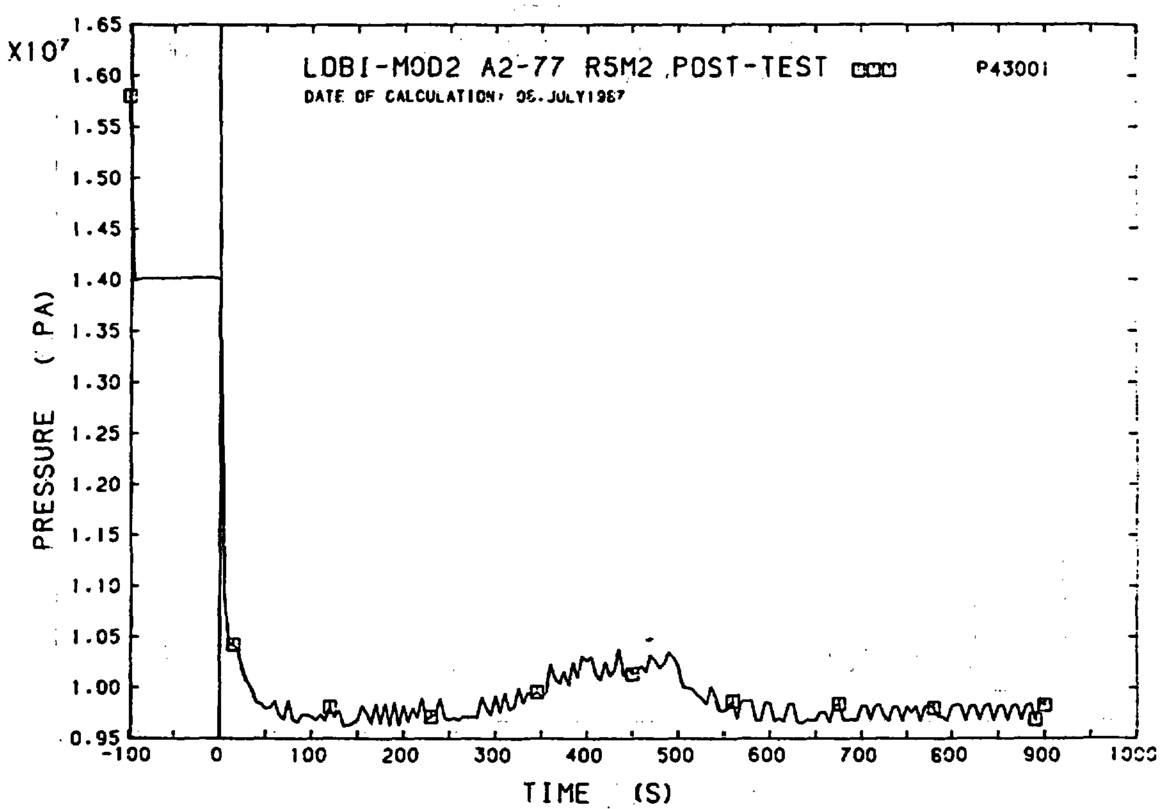

FIGURE C1 UPPER PLENUM PRESSURE

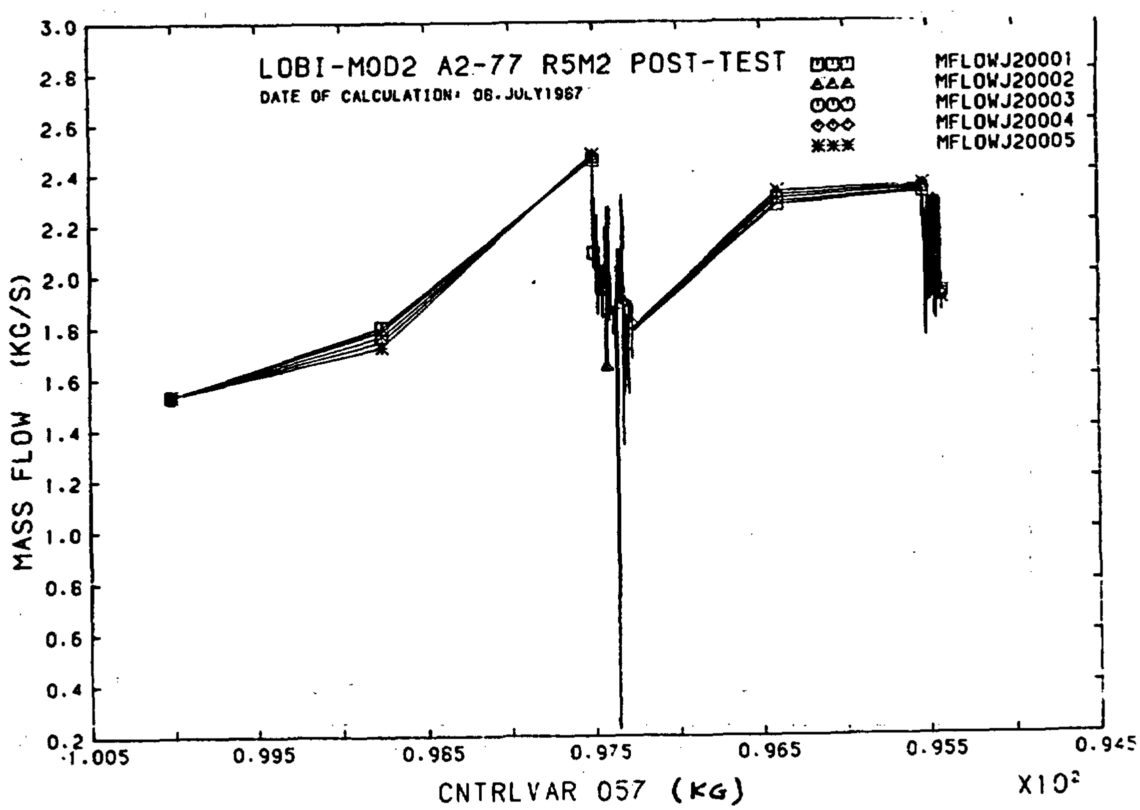

FIGURE C2 MASS FLOW RATE IN DOWNCOMER VS PS MASS INVENTORY

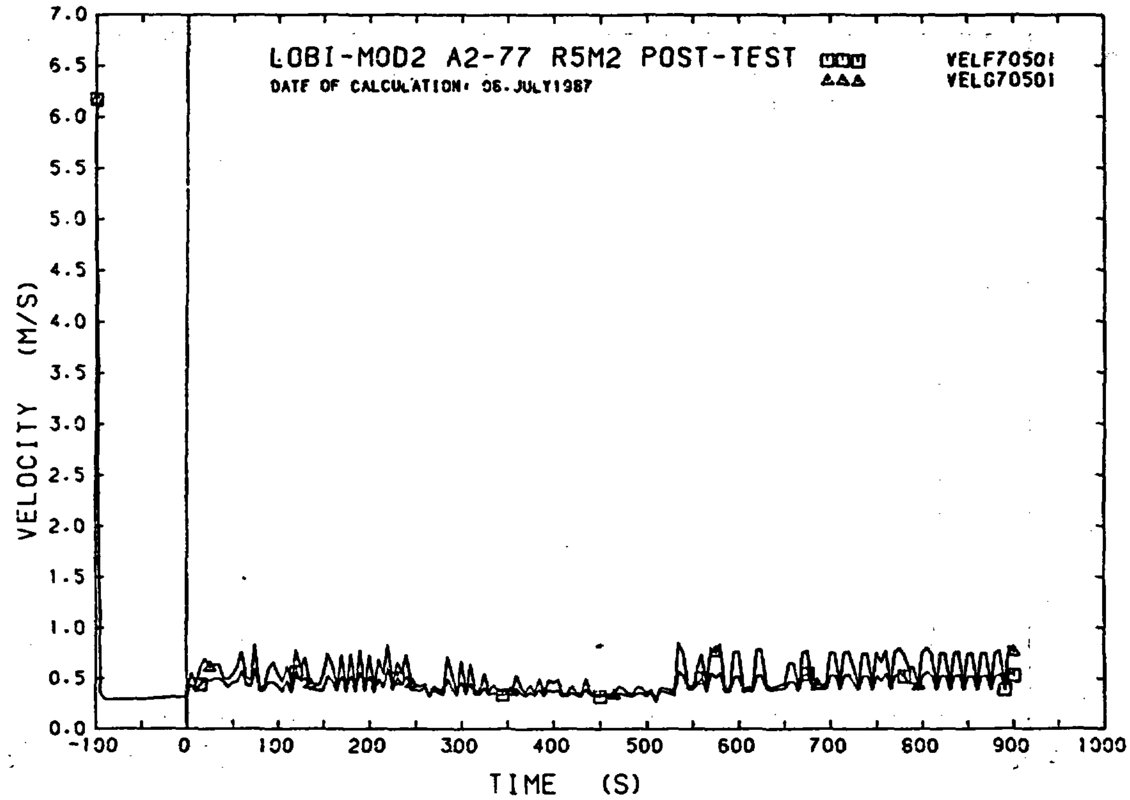

FIGURE C3 FLUID VELOCITIES IN B.L.S.G. INLET

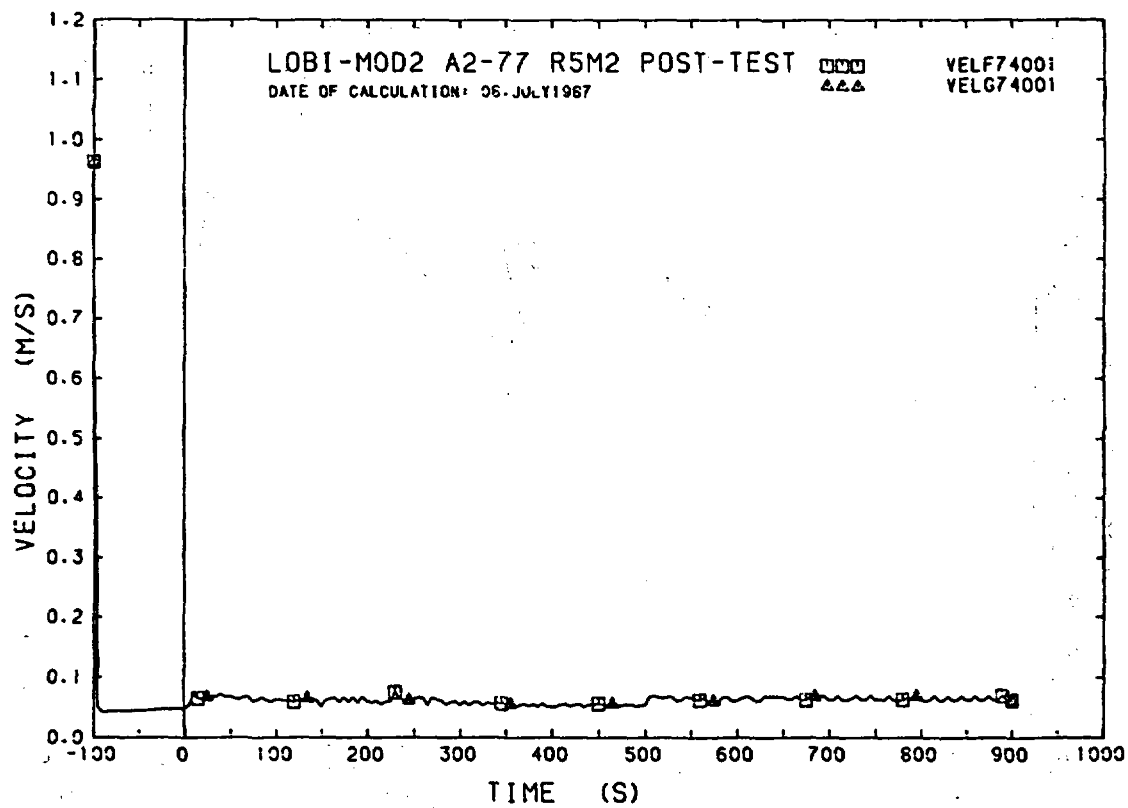

FIGURE C4 FLUID VELOCITIES IN B.L. PUMP INLET

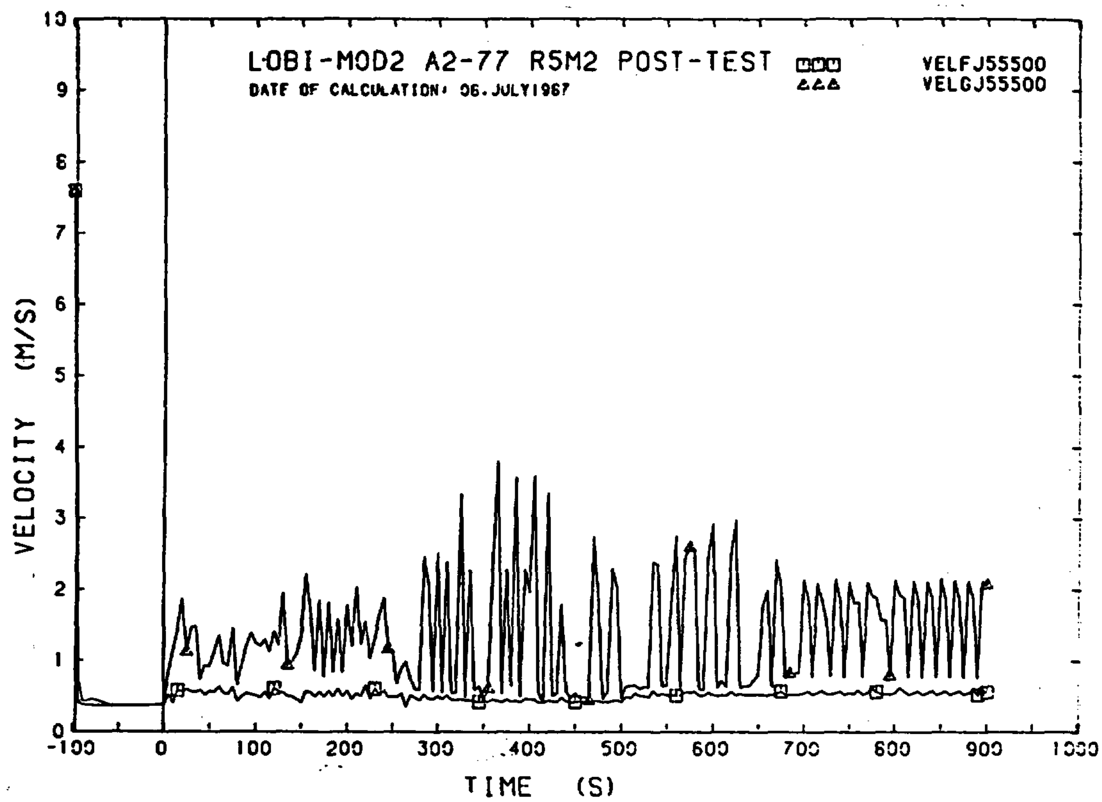

FIGURE C5 FLUID VELOCITIES IN I.L.S.G. INLET

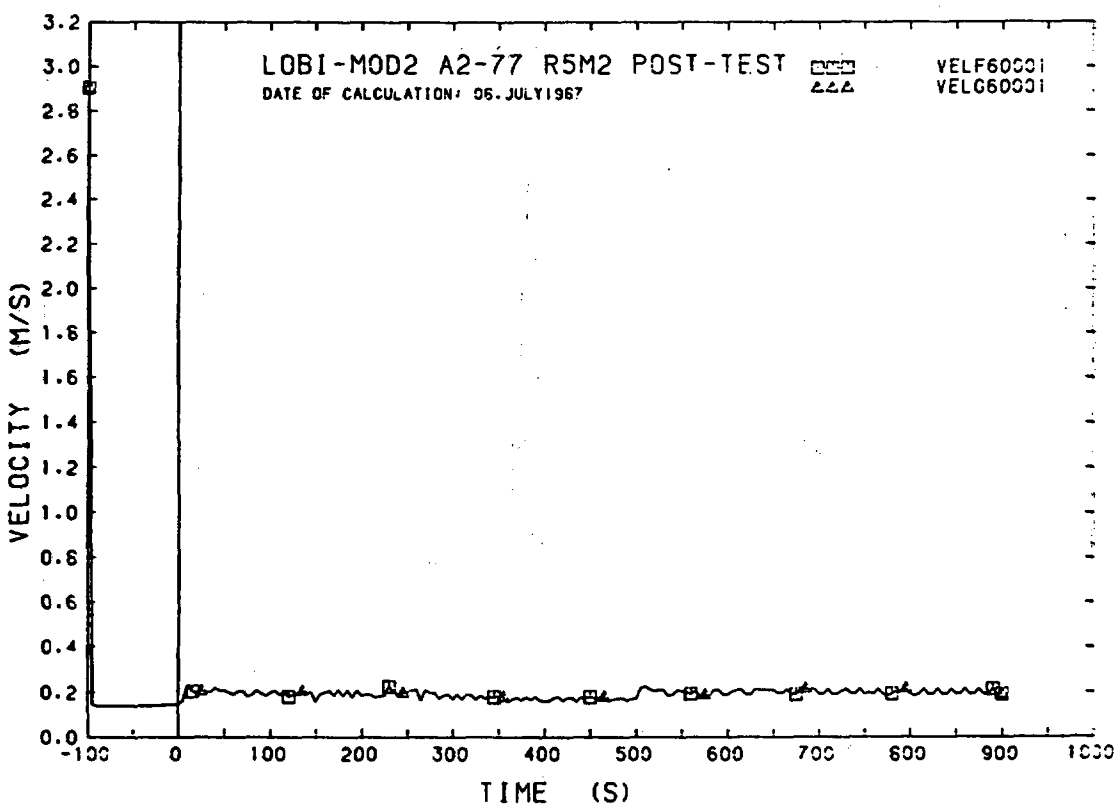

FIGURE C6 FLUID VELOCITIES IN I.L. PUMP INLET

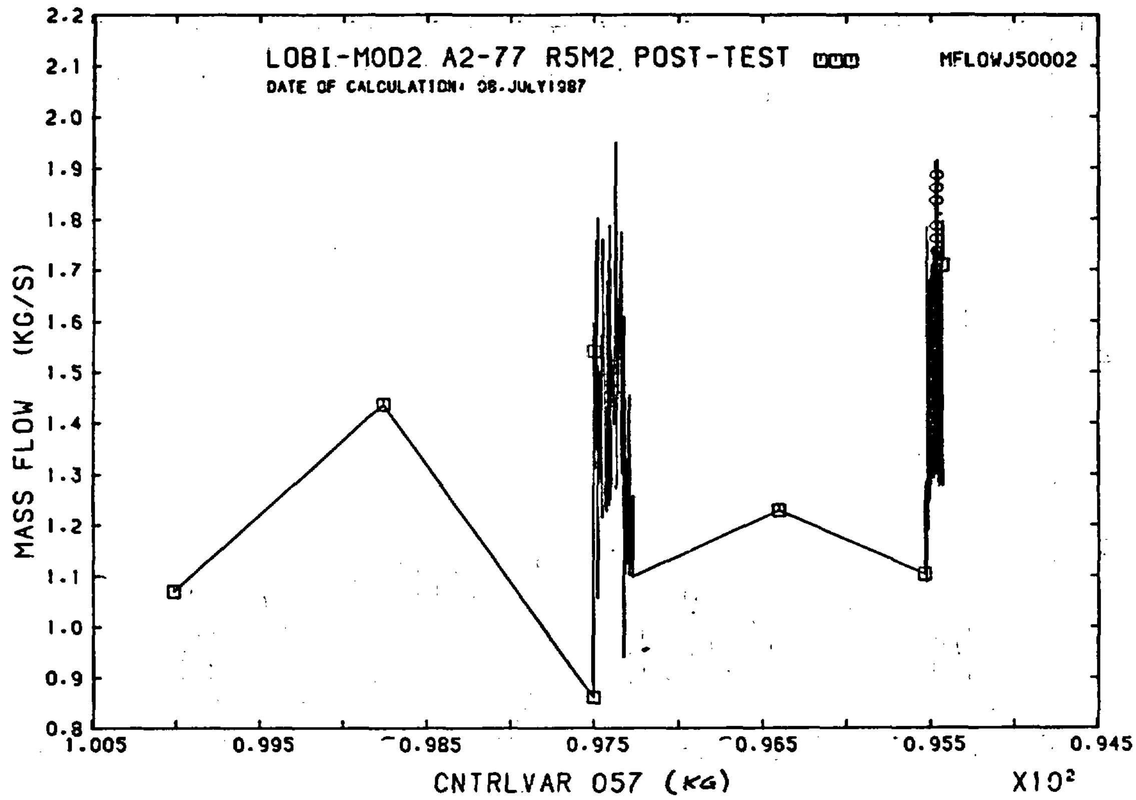

FIGURE C7 MASS FLOW RATE IN TRIPLE LOOP C.L. VS PS MASS INVENTORY

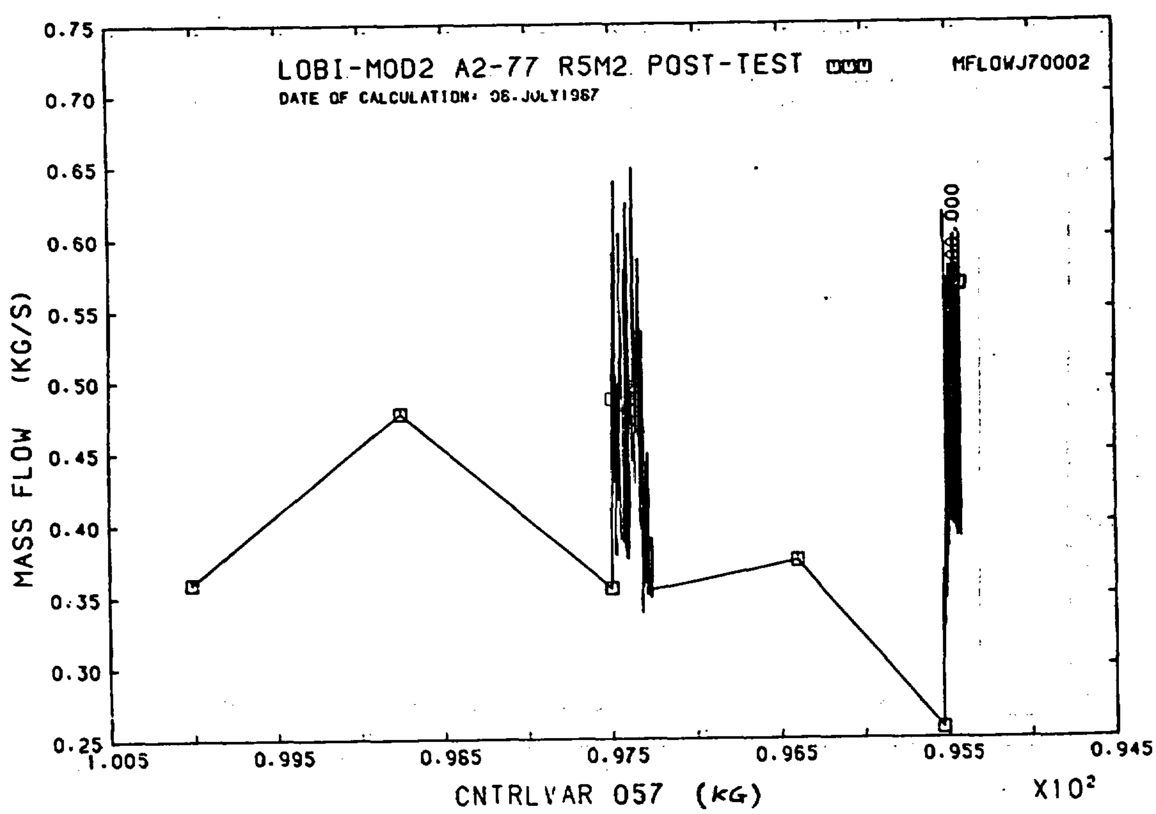

FIGURE C8 MASS FLOW RATE IN SINGLE LOOP C.L. VS PS MASS INVENTORY

APPENDIX D

Measured and calculated trends for case E (Effect of parallel U-Tubes)

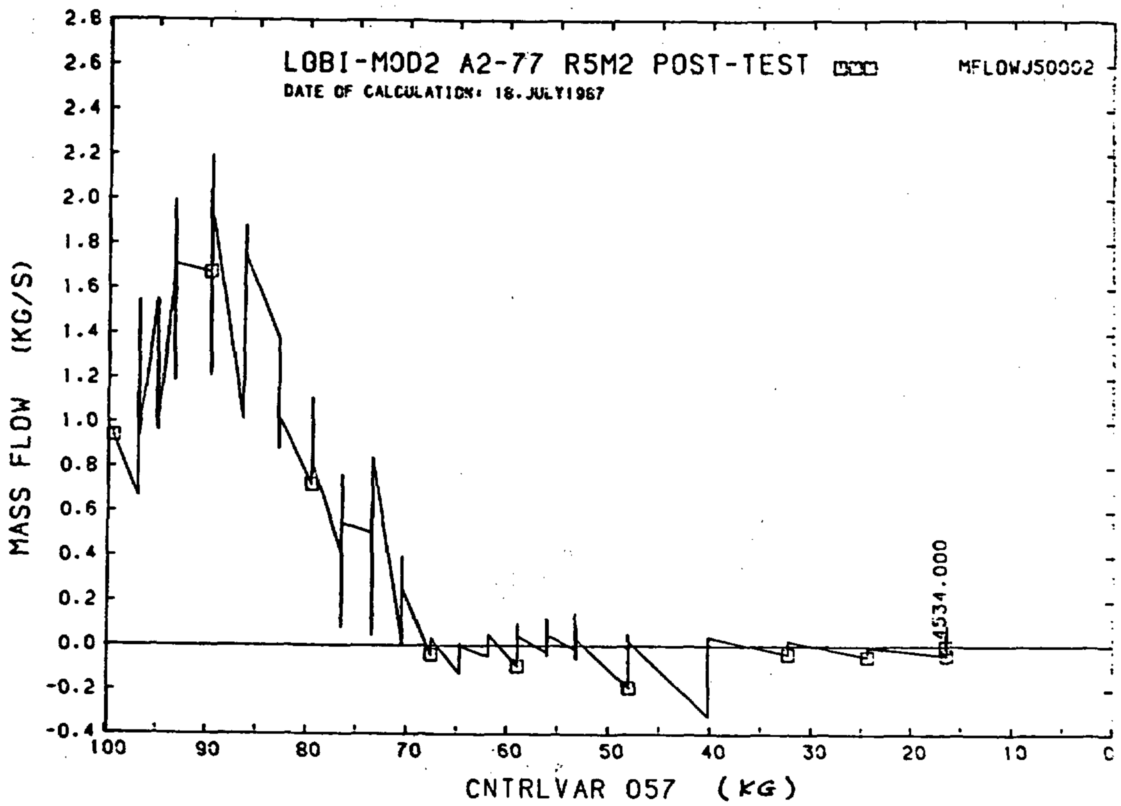

FIGURE D1 MASS FLOW RATE IN TRIPLE LOOP C.L. VS PS MASS INVENTORY

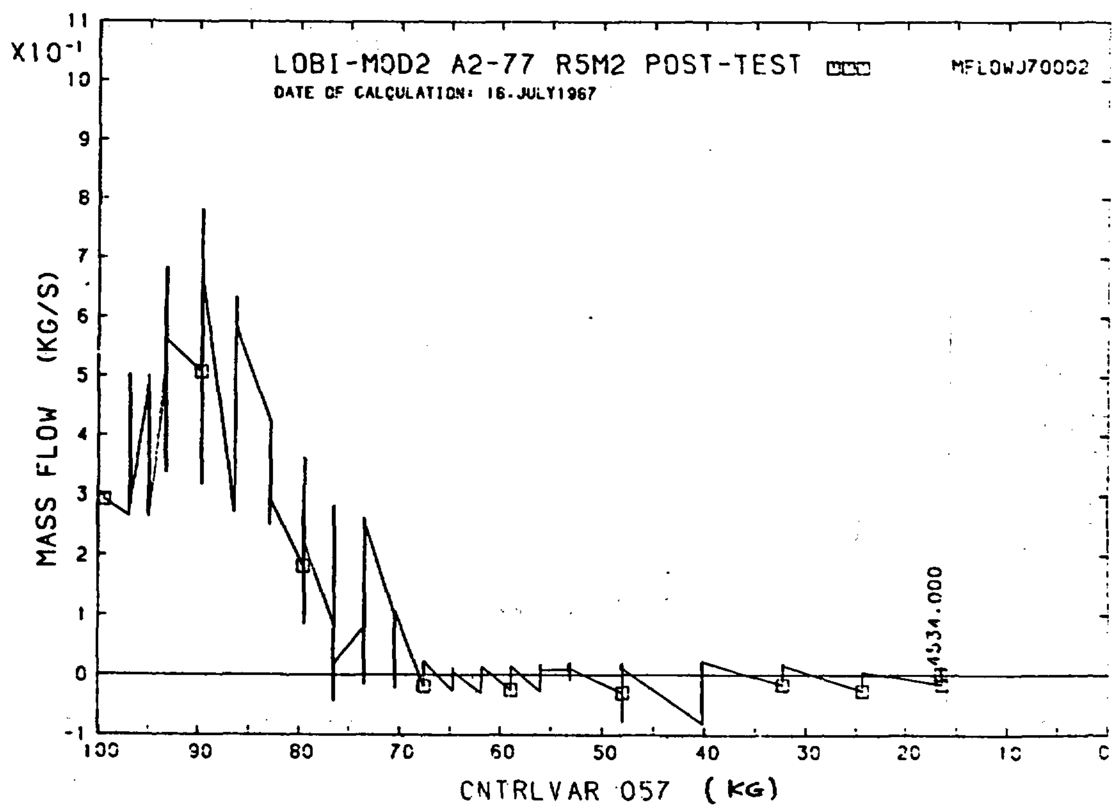

FIGURE D2 MASS FLOW RATE IN SINGLE LOOP C.L. VS PS MASS INVENTORY

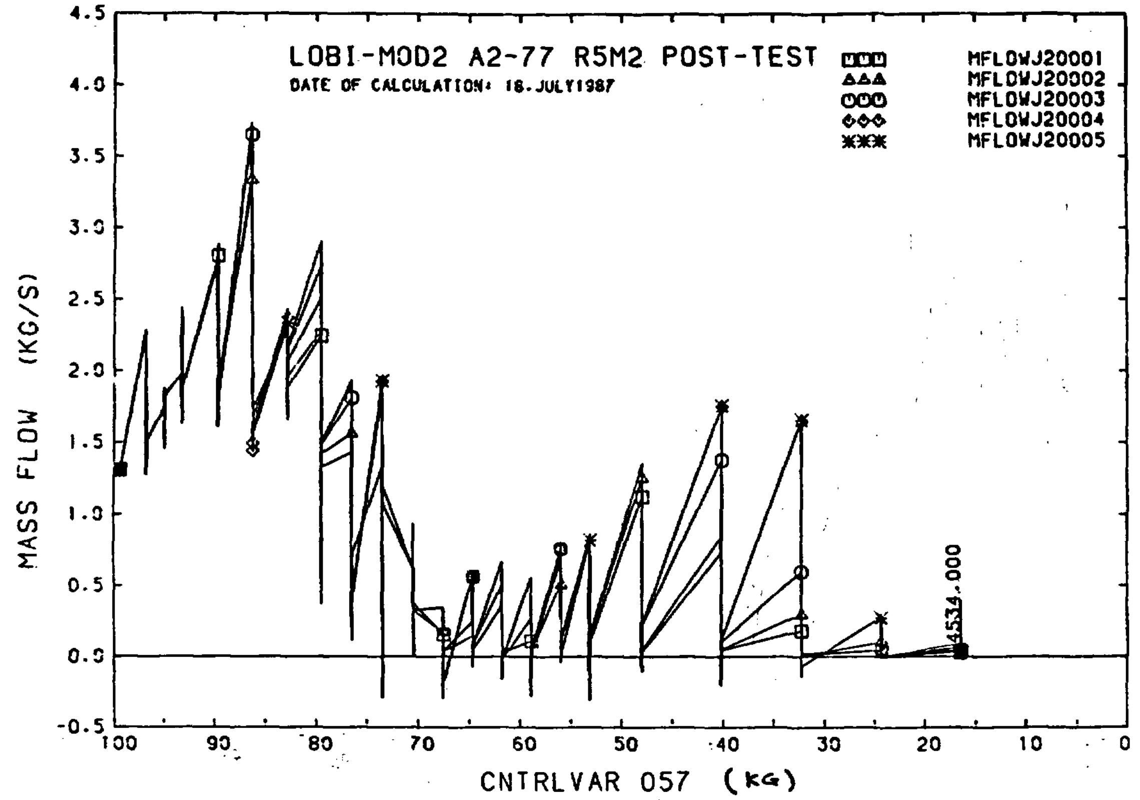

FIGURE D3 MASS FLOW RATE IN DOWNCOMER VS PS MASS INVENTORY

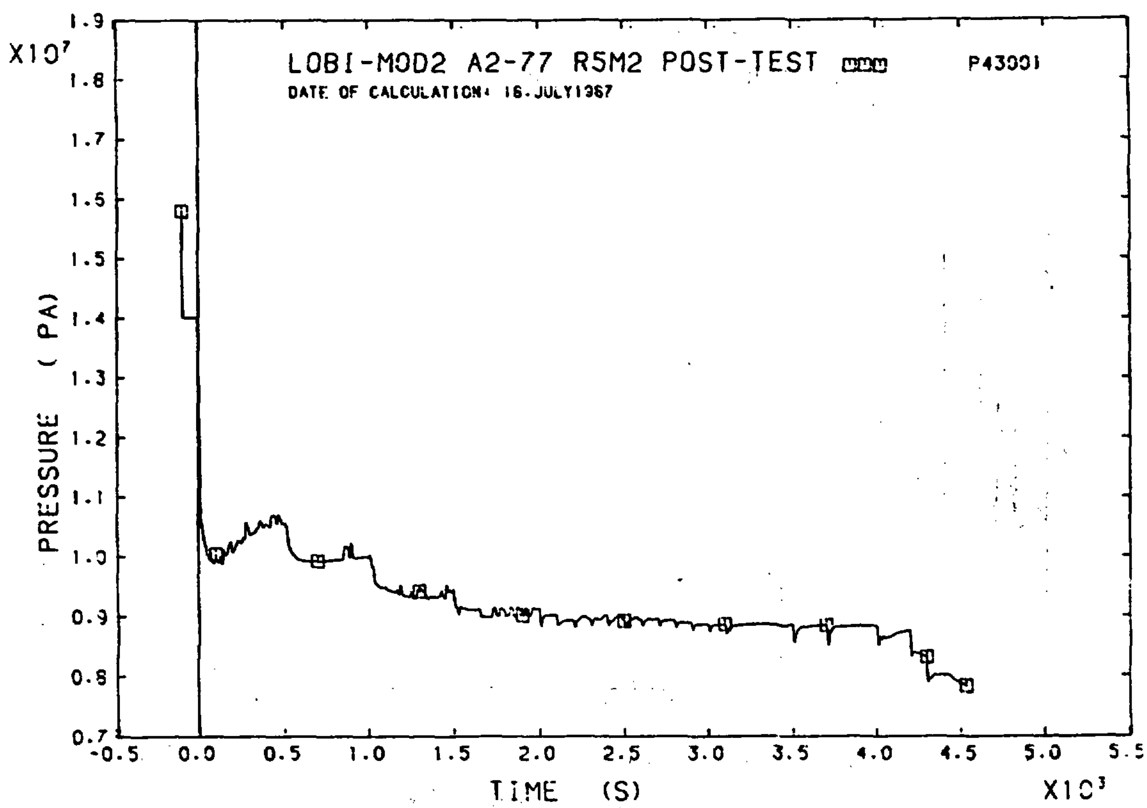

FIGURE D4 UPPER PLENUM PRESSURE

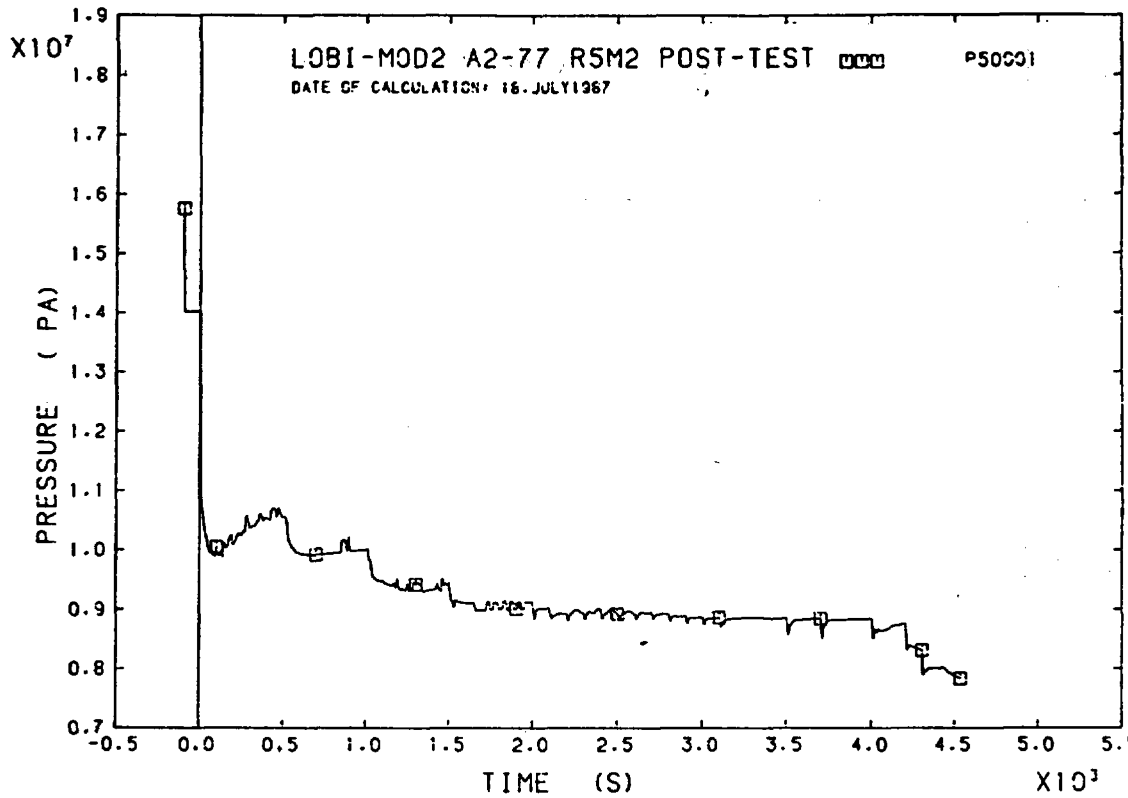

FIGURE D5 I.L. HOT LEG PRESSURE

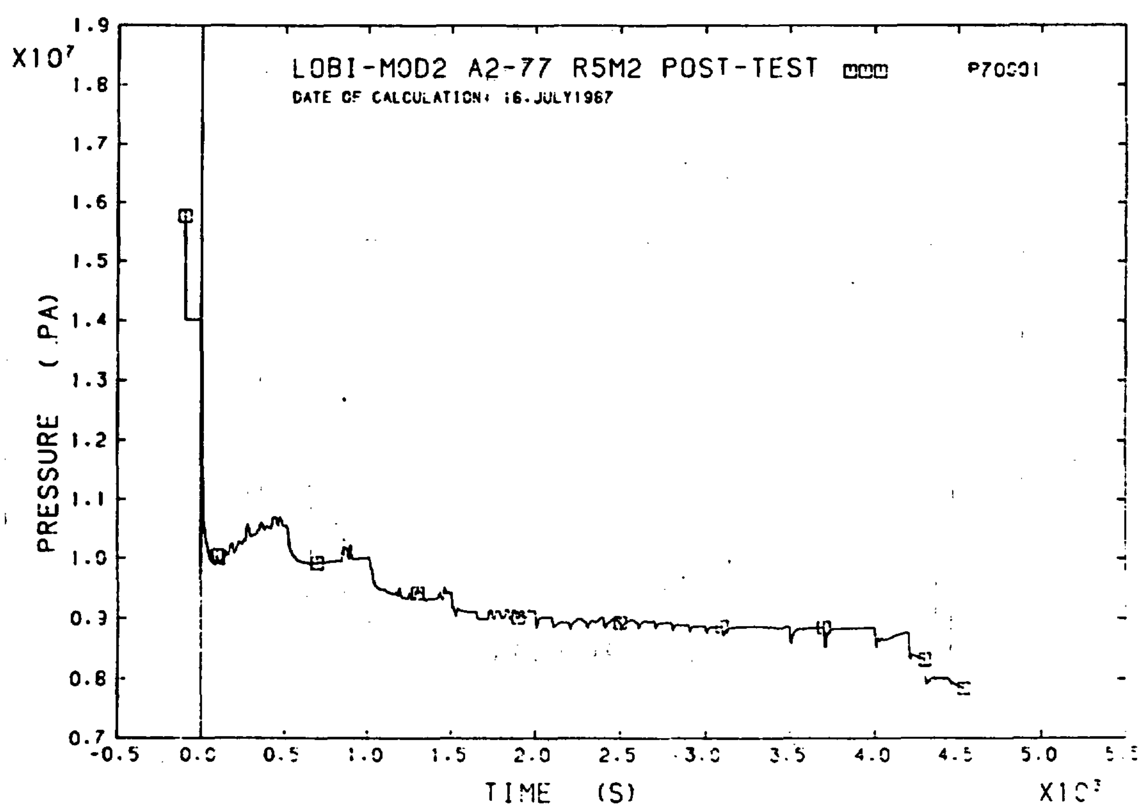

FIGURE D6 B.L. HOT LEG PRESSURE

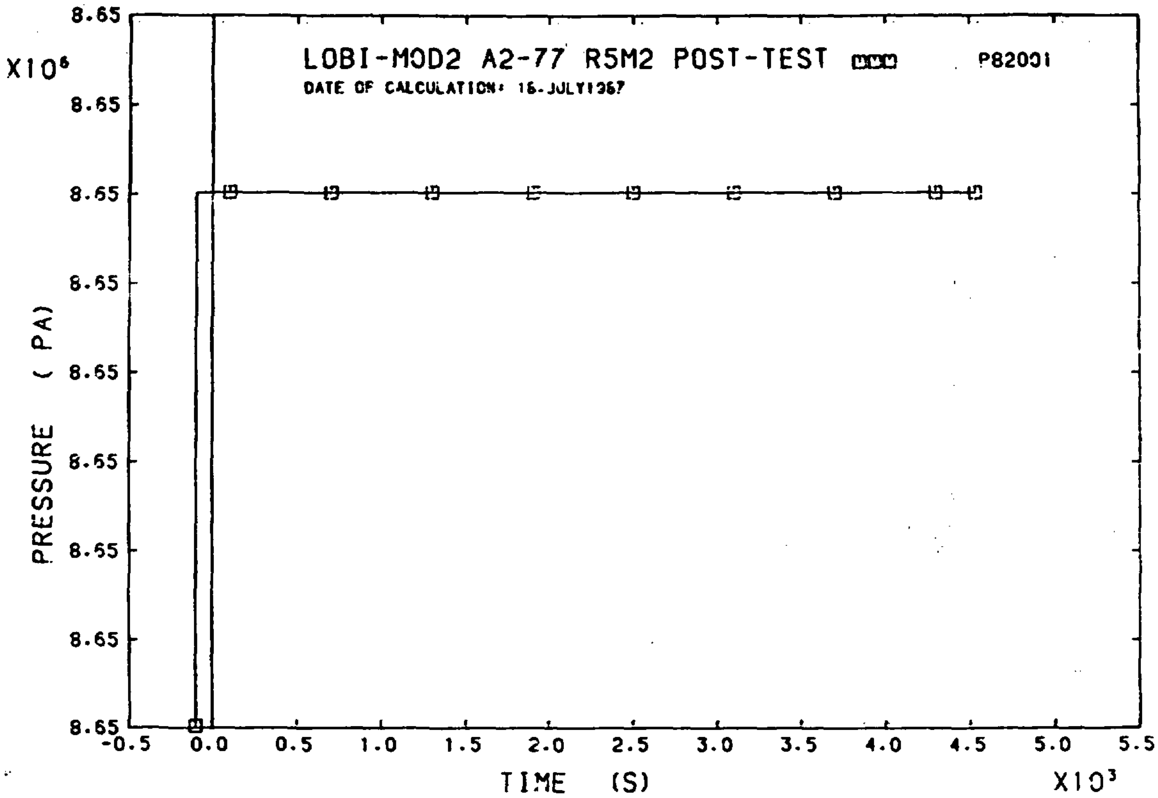

FIGURE D7 . SG SECONDARY PRESSURE

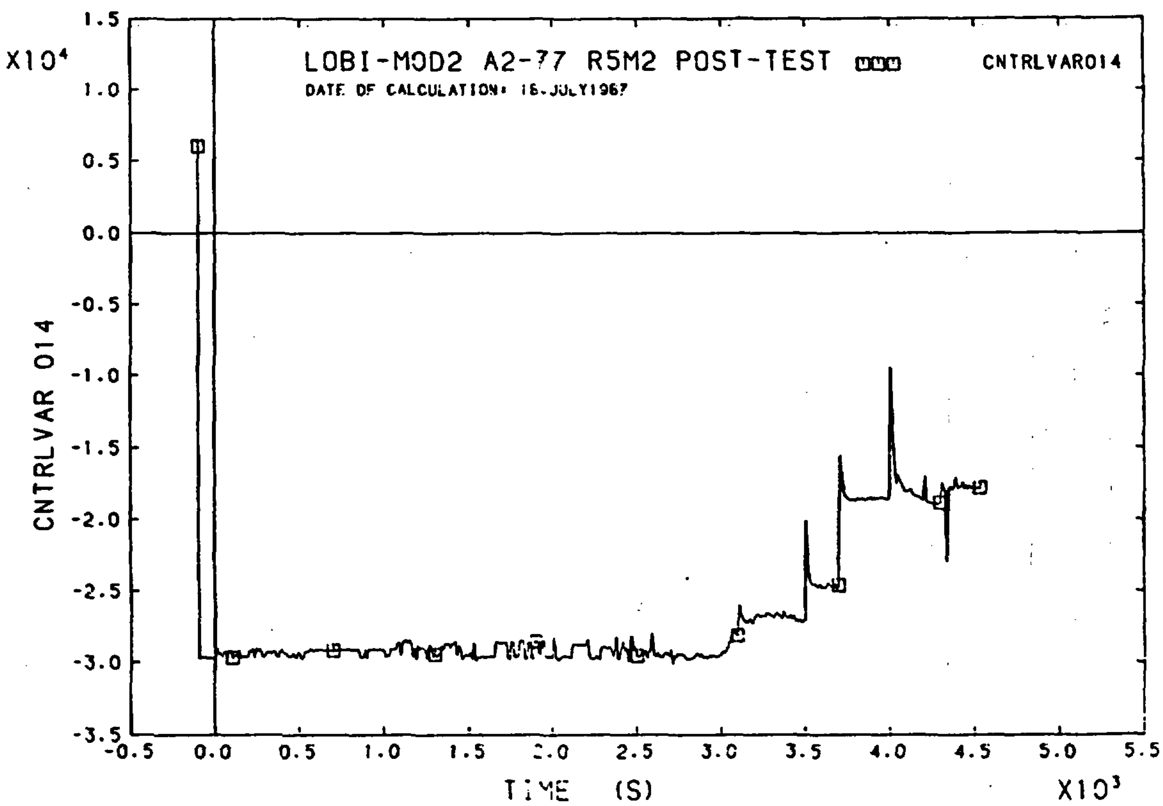

FIGURE D8 DIFFERENTIAL PRESSURE PD9217

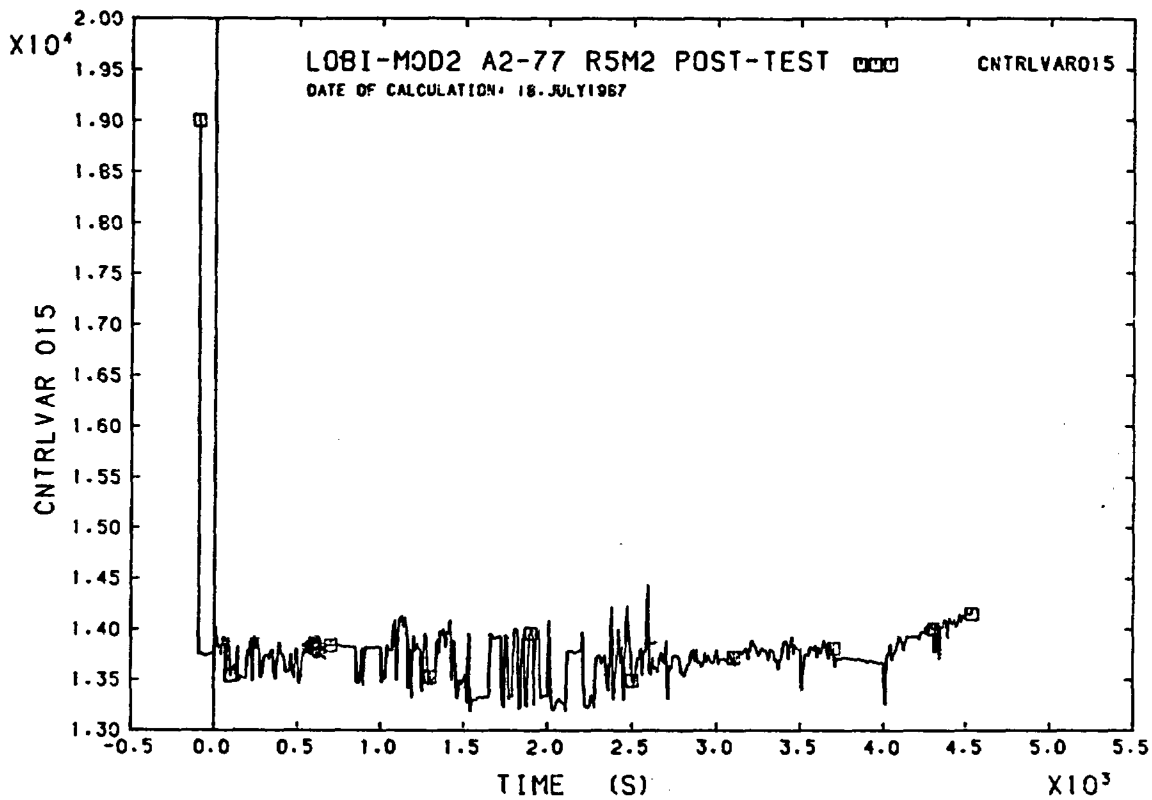

FIGURE D9 DIFFERENTIAL PRESSURE PD1714

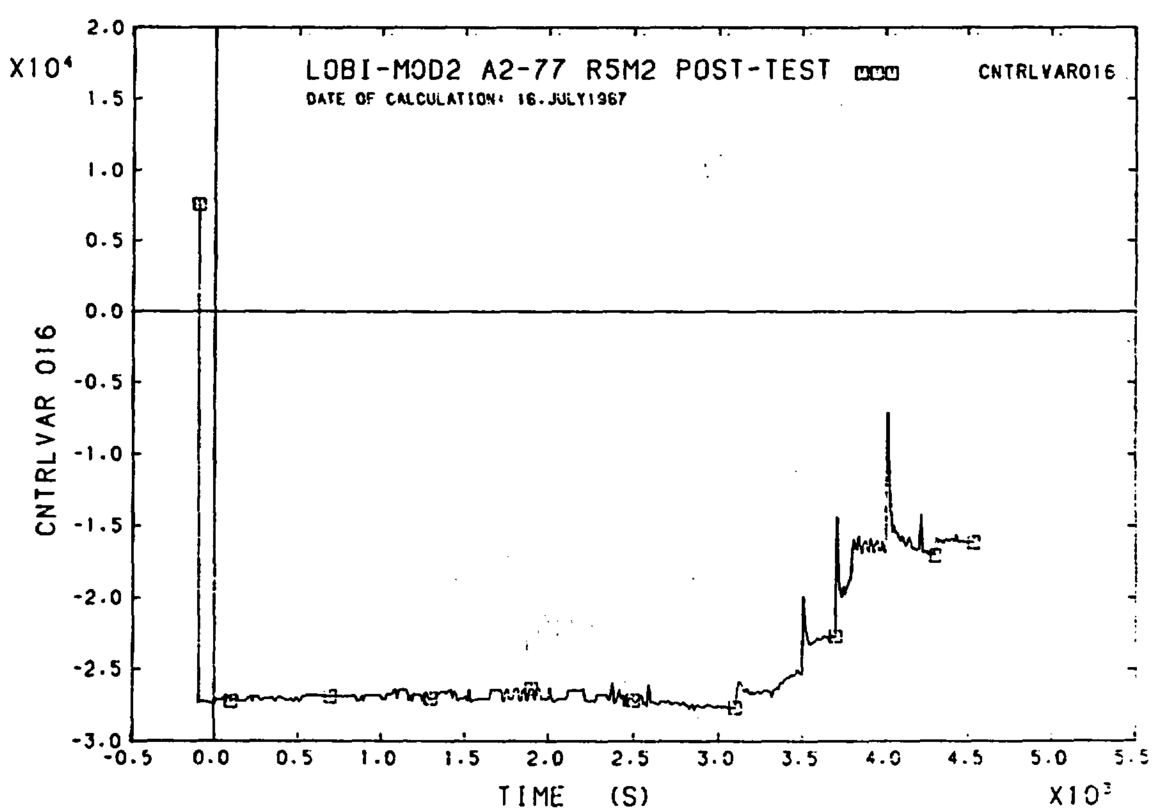

FIGURE D10 DIFFERENTIAL PRESSURE PD8227

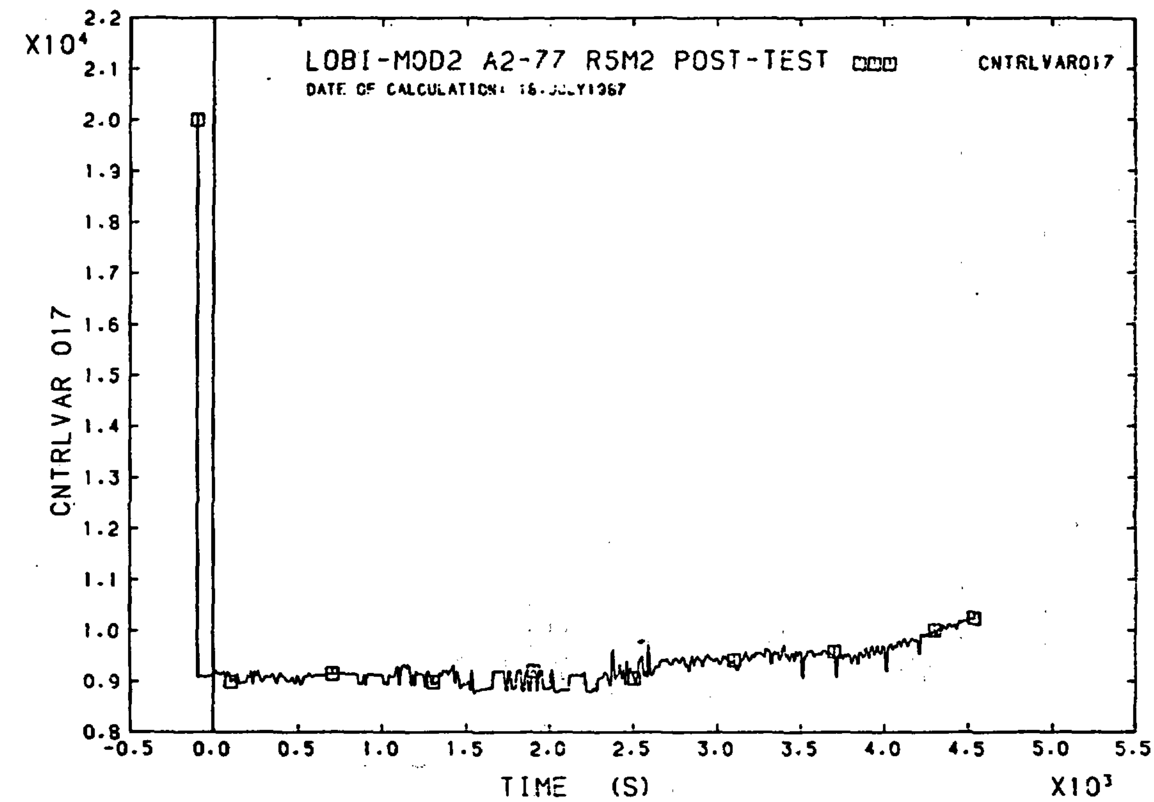

FIGURE D11 DIFFERENTIAL PRESSURE PD2724

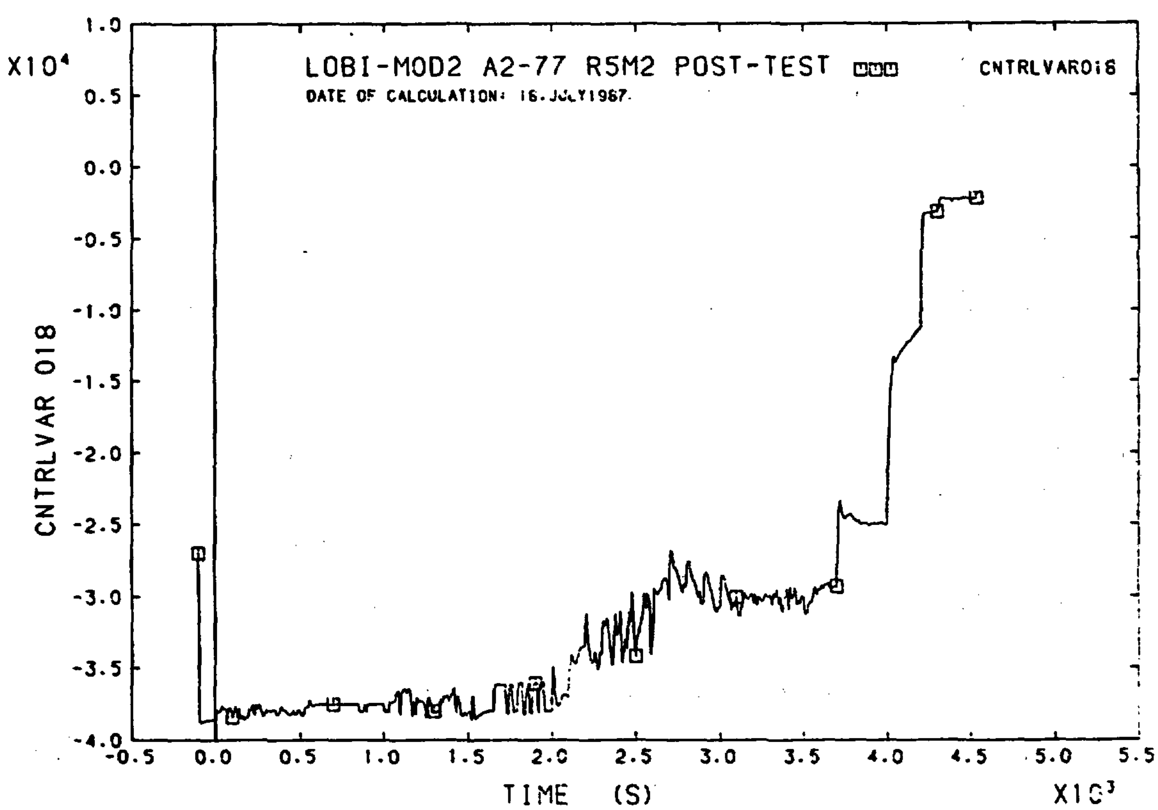

FIGURE D12 DIFFERENTIAL PRESSURE PD3DBT

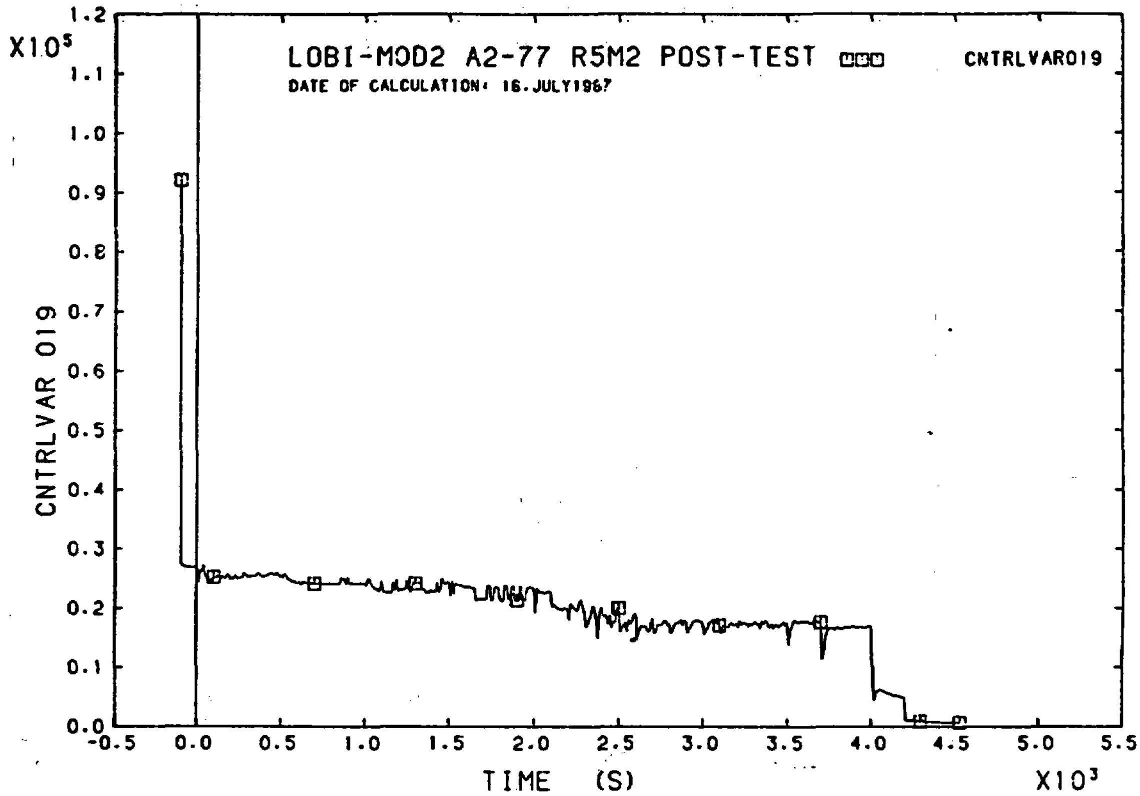

FIGURE D13 DIFFERENTIAL PRESSURE PD3RTK

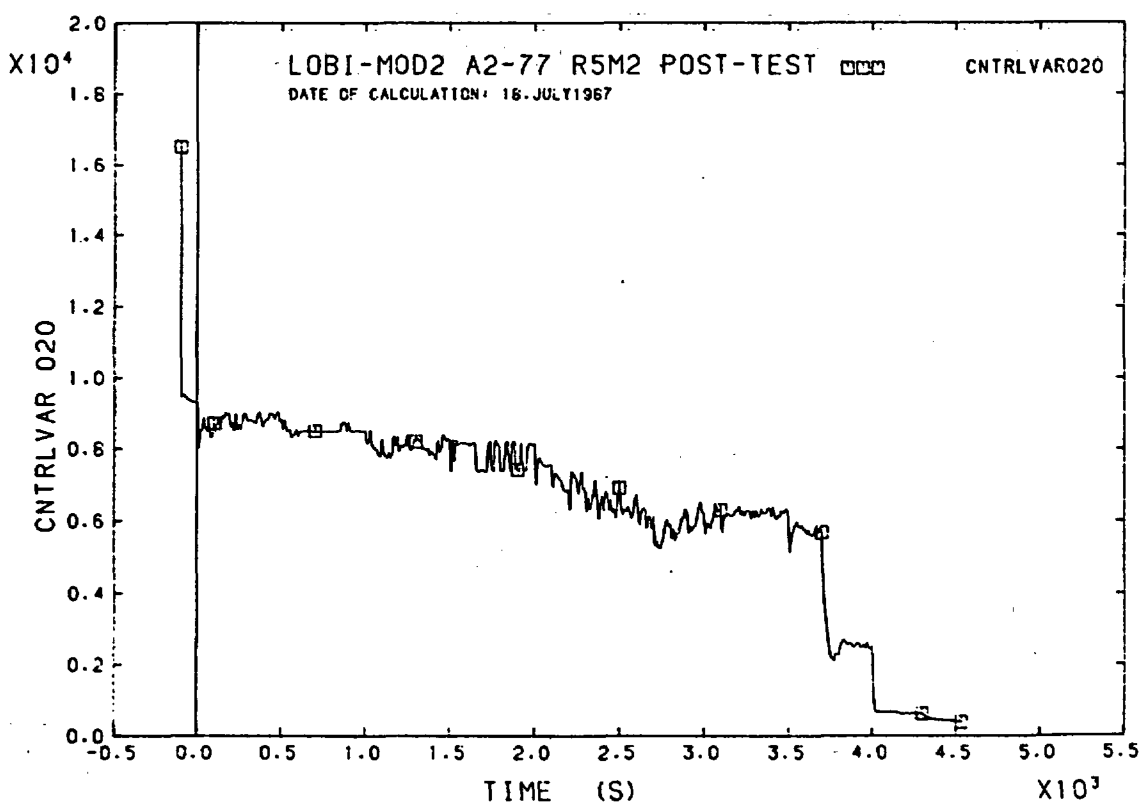

FIGURE D14 DIFFERENTIAL PRESSURE PD3RKA

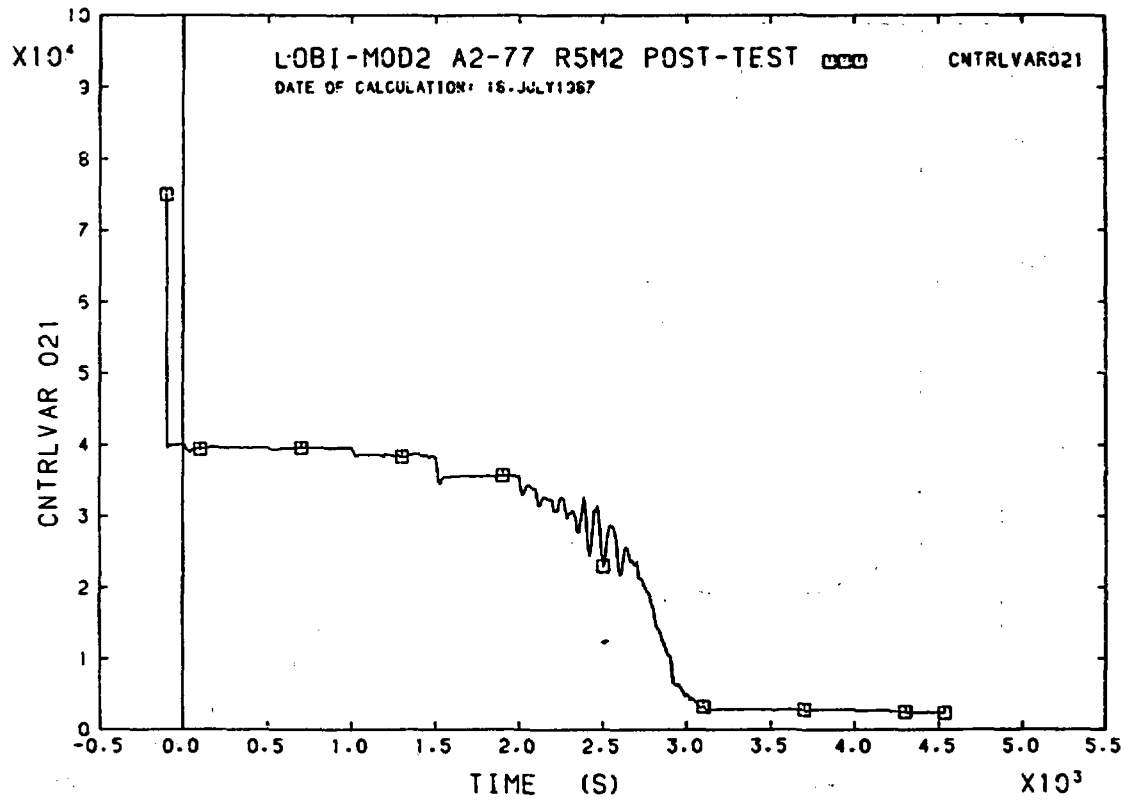

FIGURE D15 DIFFERENTIAL PRESSURE PD90BN

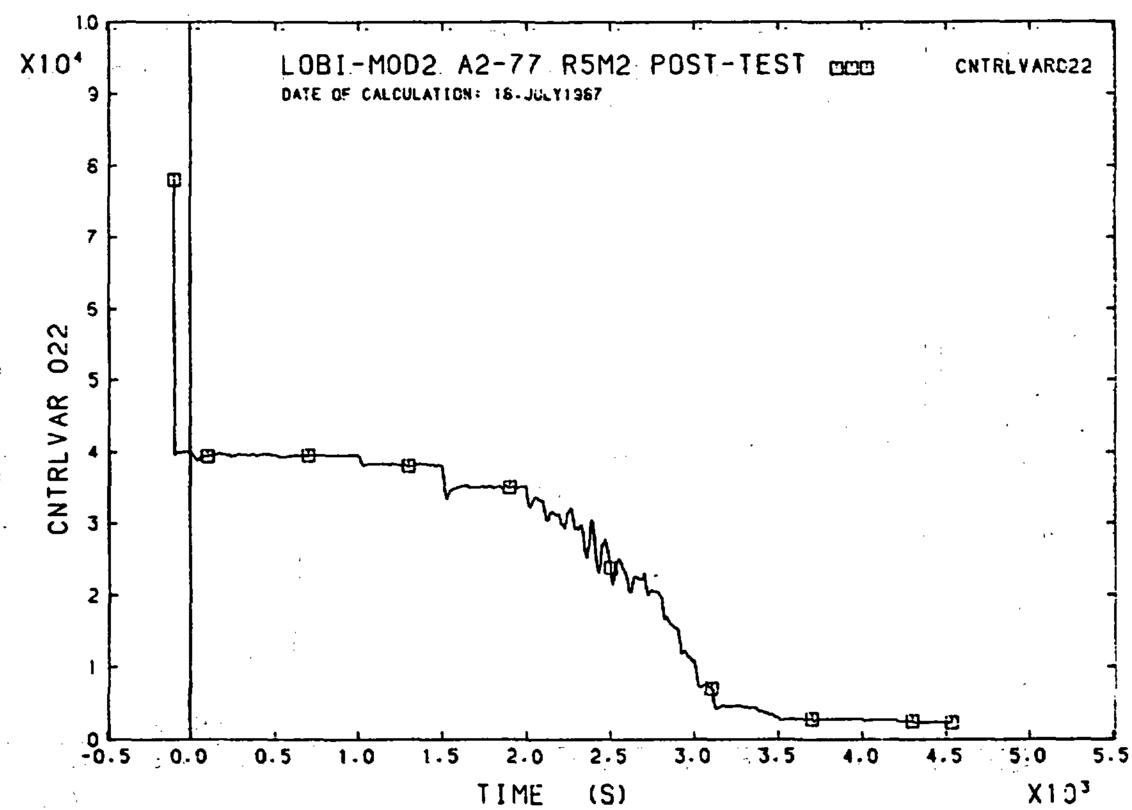

FIGURE D16 DIFFERENTIAL PRESSURE PD80BN

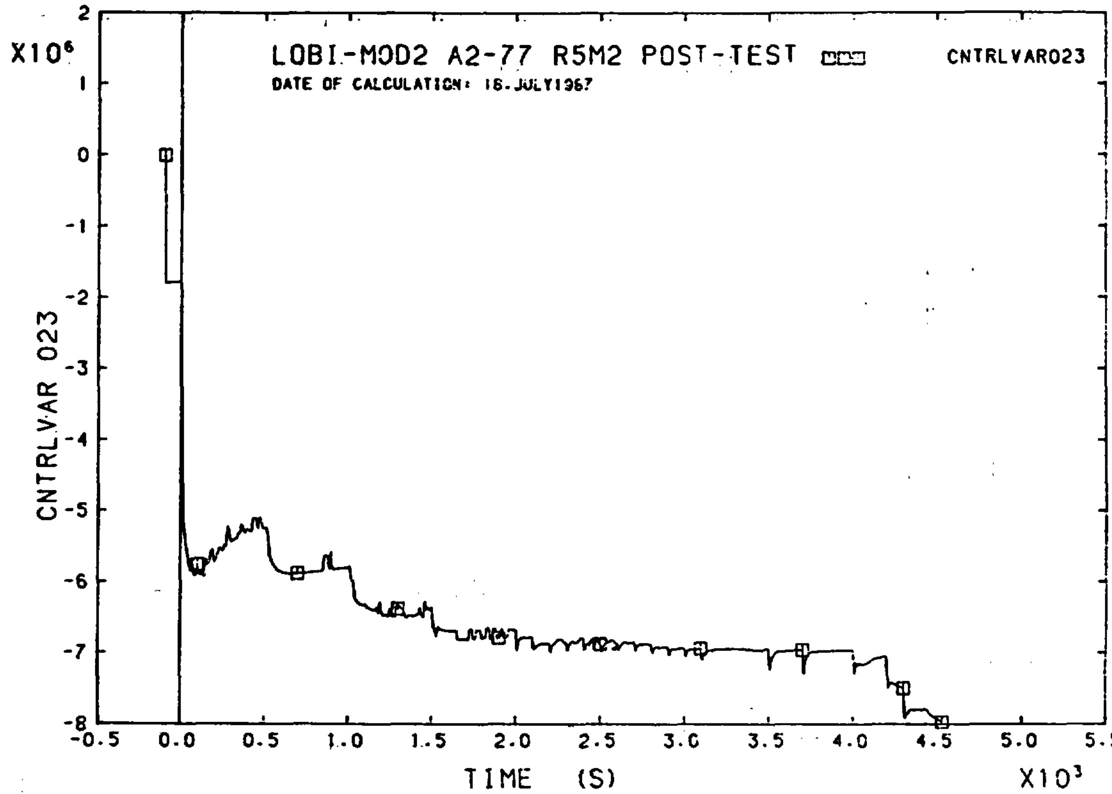

FIGURE D17 PD3R39

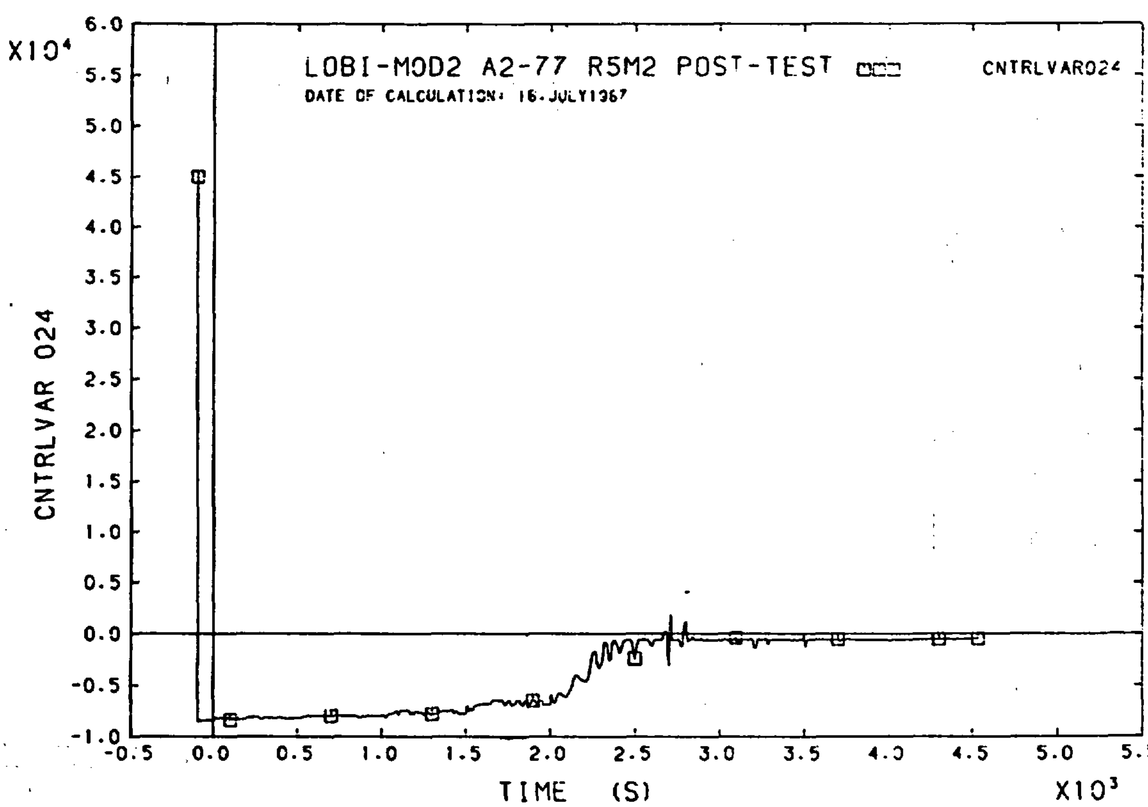

FIGURE D18 DIFFERENTIAL PRESSURE PD163DB3

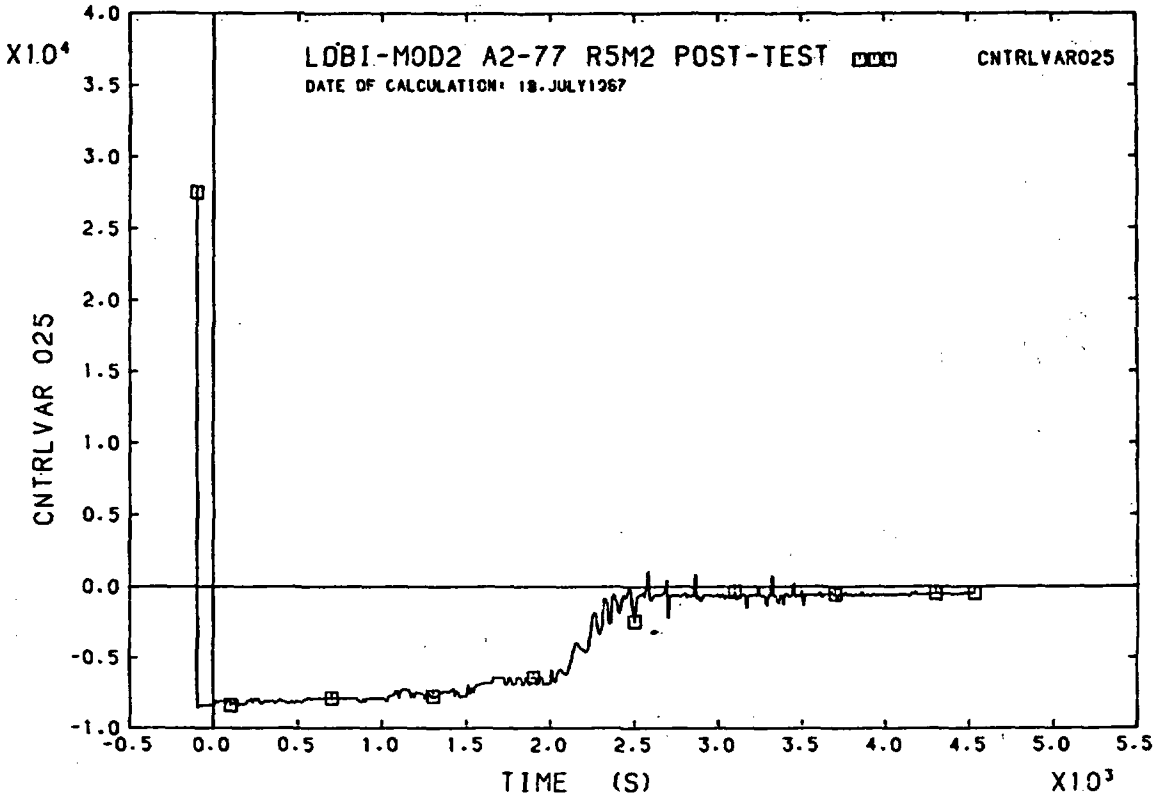

FIGURE D19 DIFFERENTIAL PRESSURE PD263DB7

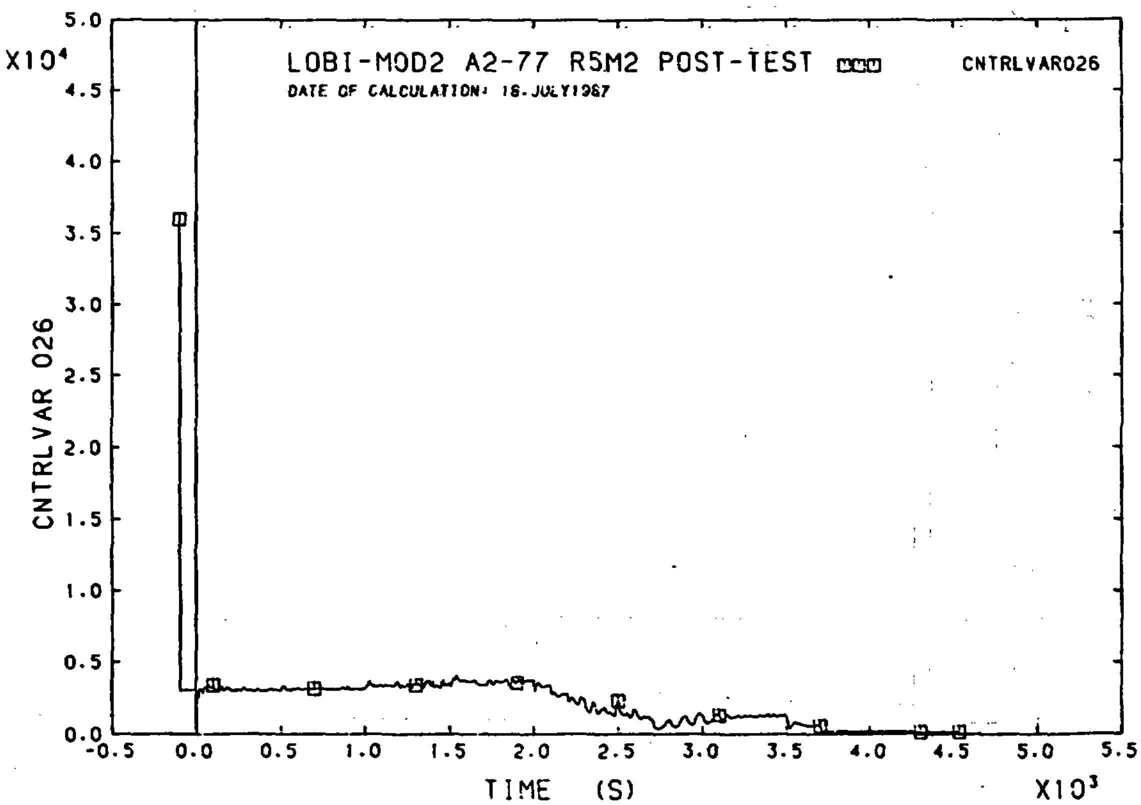

FIGURE D20 DIFFERENTIAL PRESSURE PD3R11A4

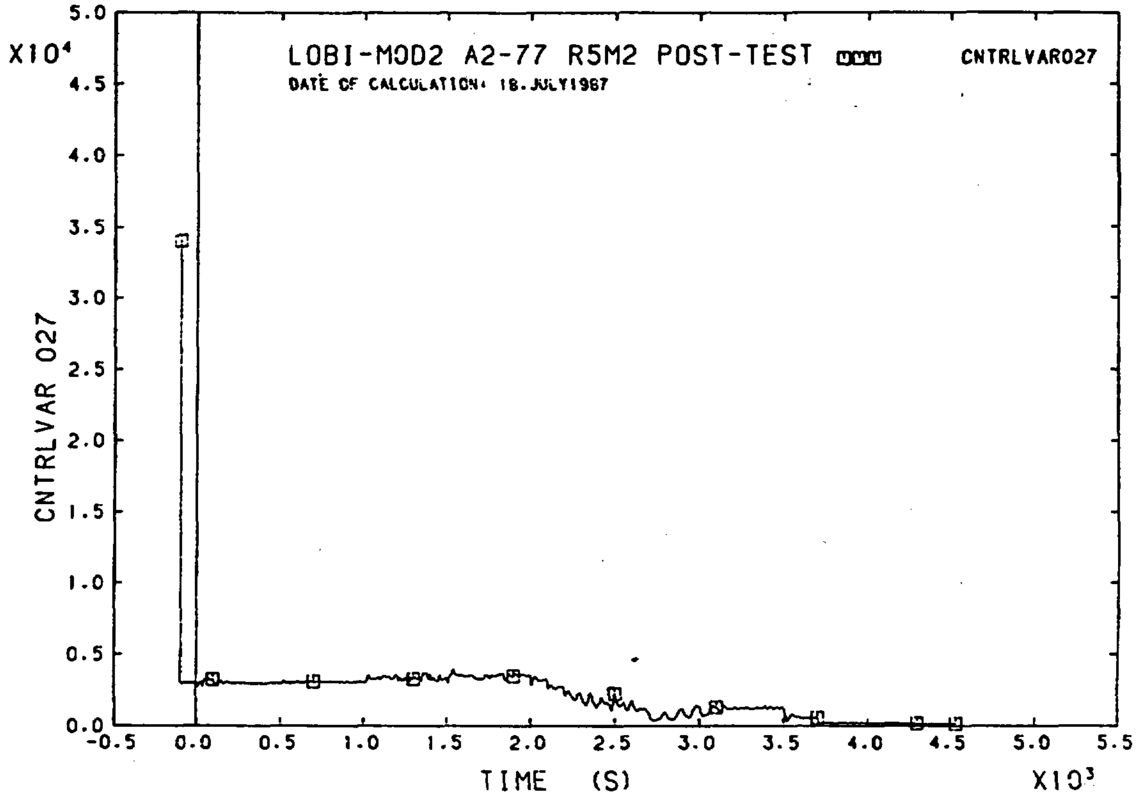

FIGURE D21 DIFFERENTIAL PRESSURE PD3R21A3

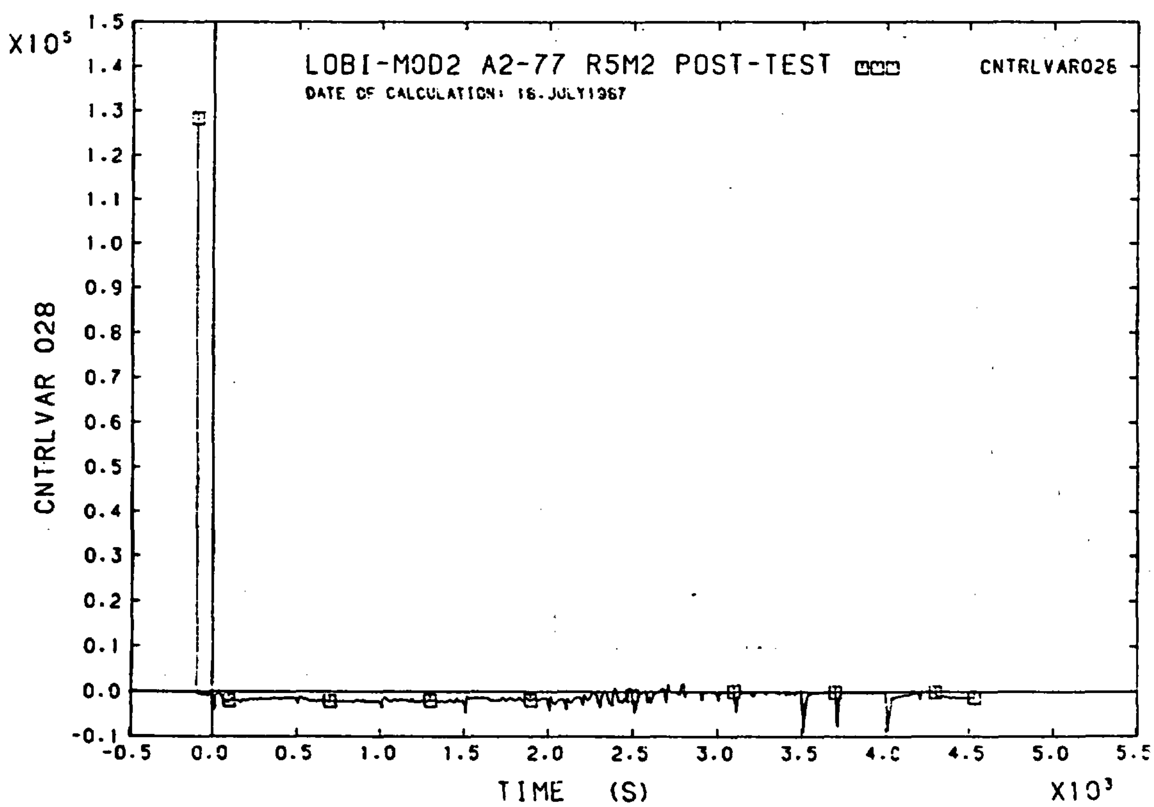

FIGURE D22 DIFFERENTIAL PRESSURE RPV TOTAL IL SIDE

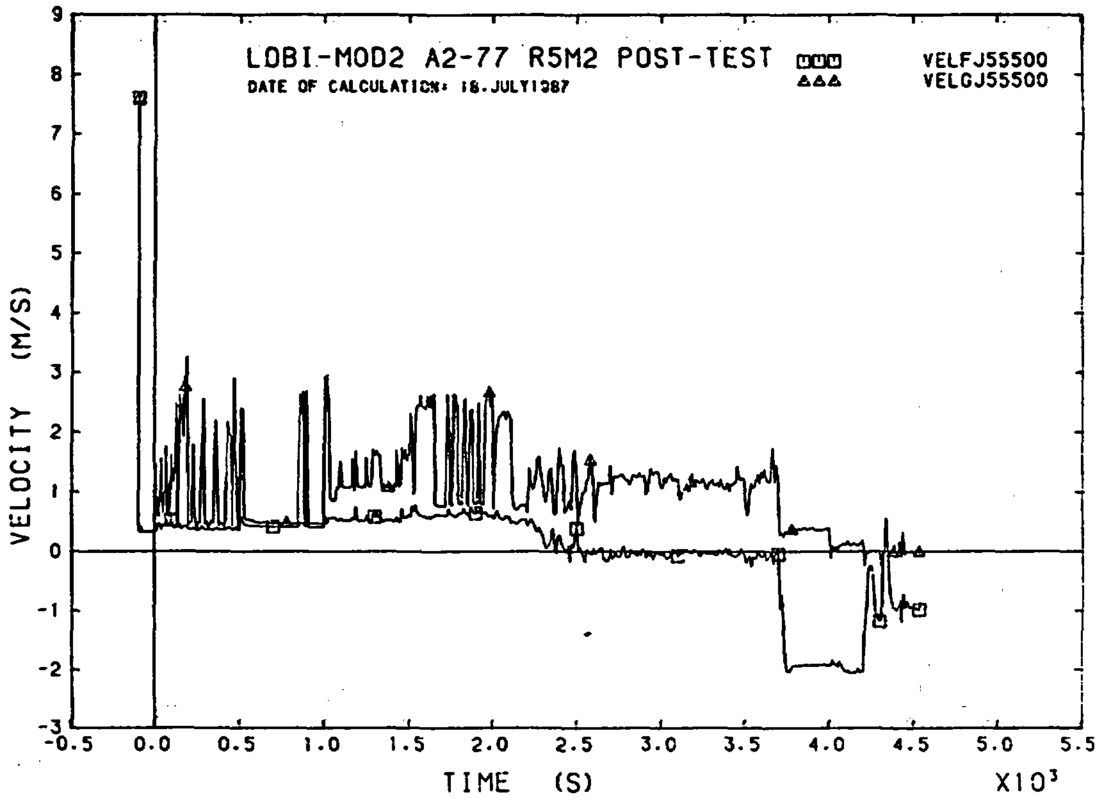

FIGURE D23 FLUID VELOCITIES IN I.L.S.G. INLET

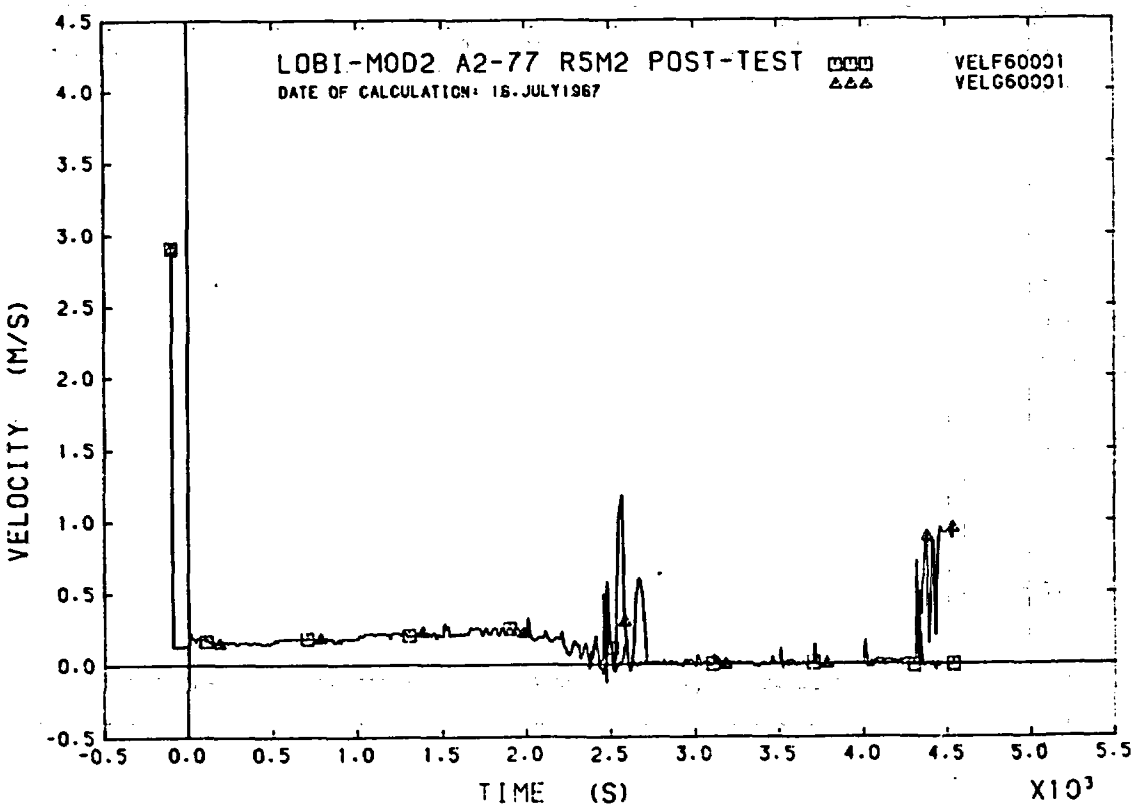

FIGURE D24 FLUID VELOCITIES IN I.L. PUMP INLET

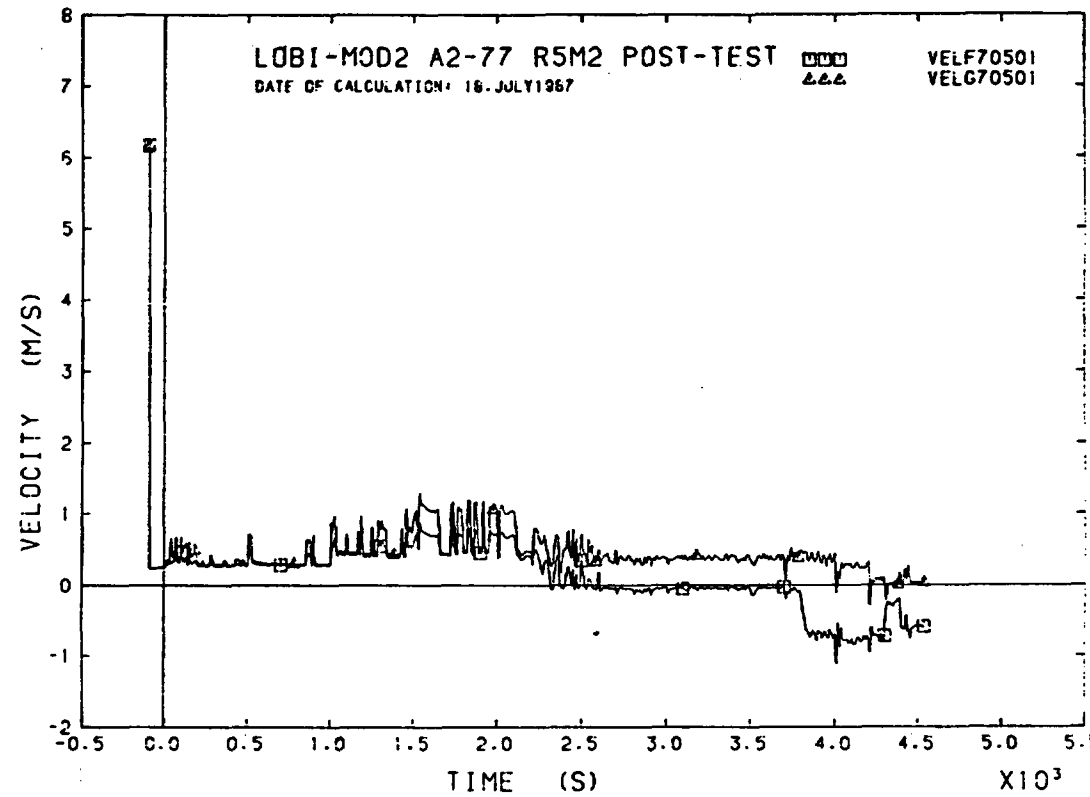

FIGURE D25 FLUID VELOCITIES IN B.L.S.G. INLET

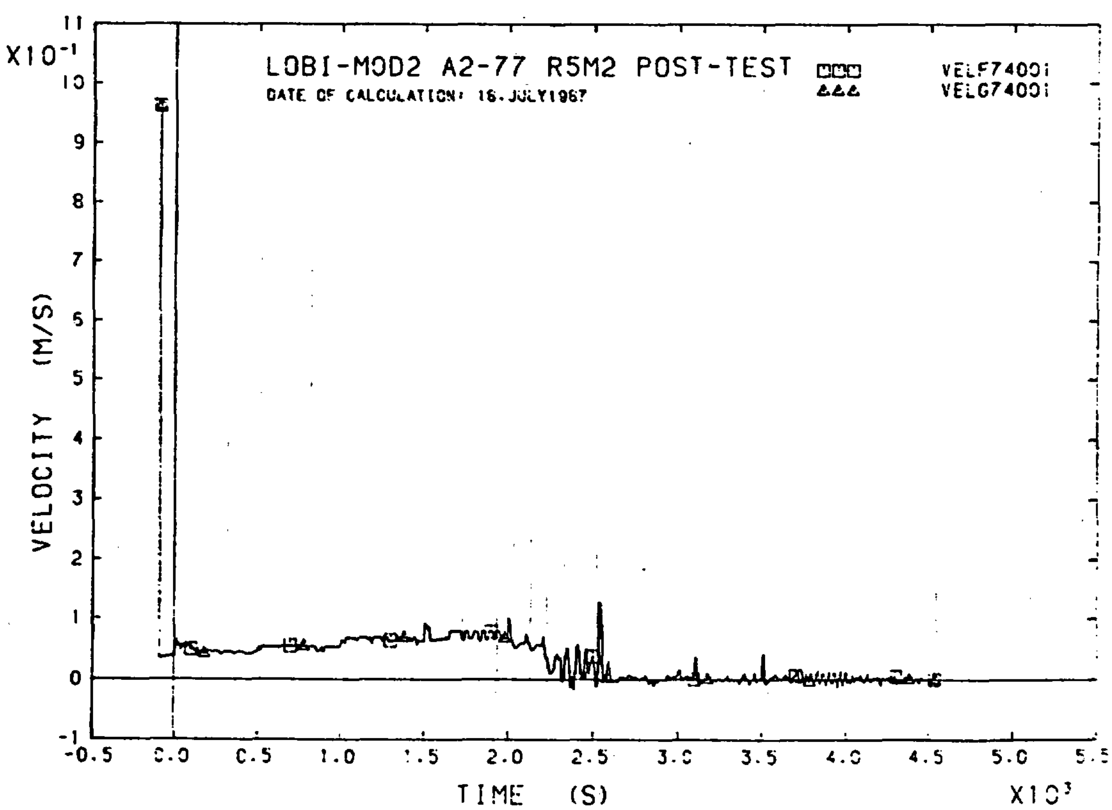

FIGURE D26 FLUID VELOCITIES IN B.L. PUMP INLET

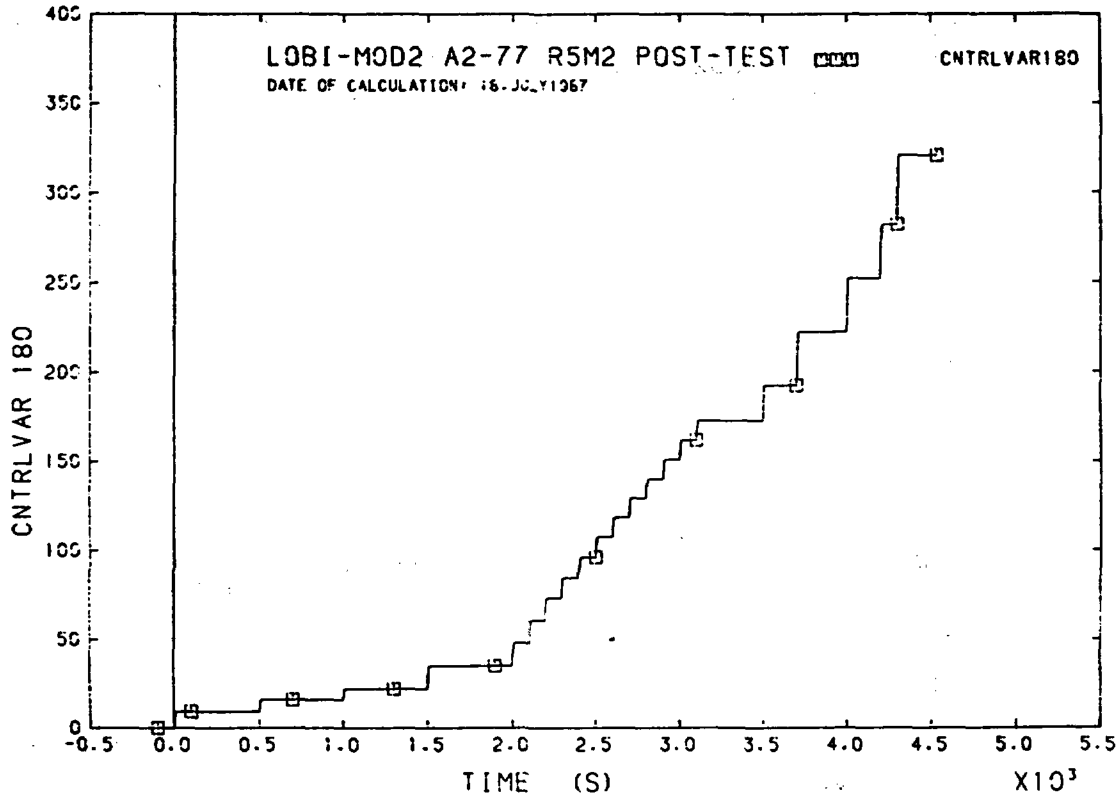

FIGURE D27 DRAINED MASS INTEGRAL

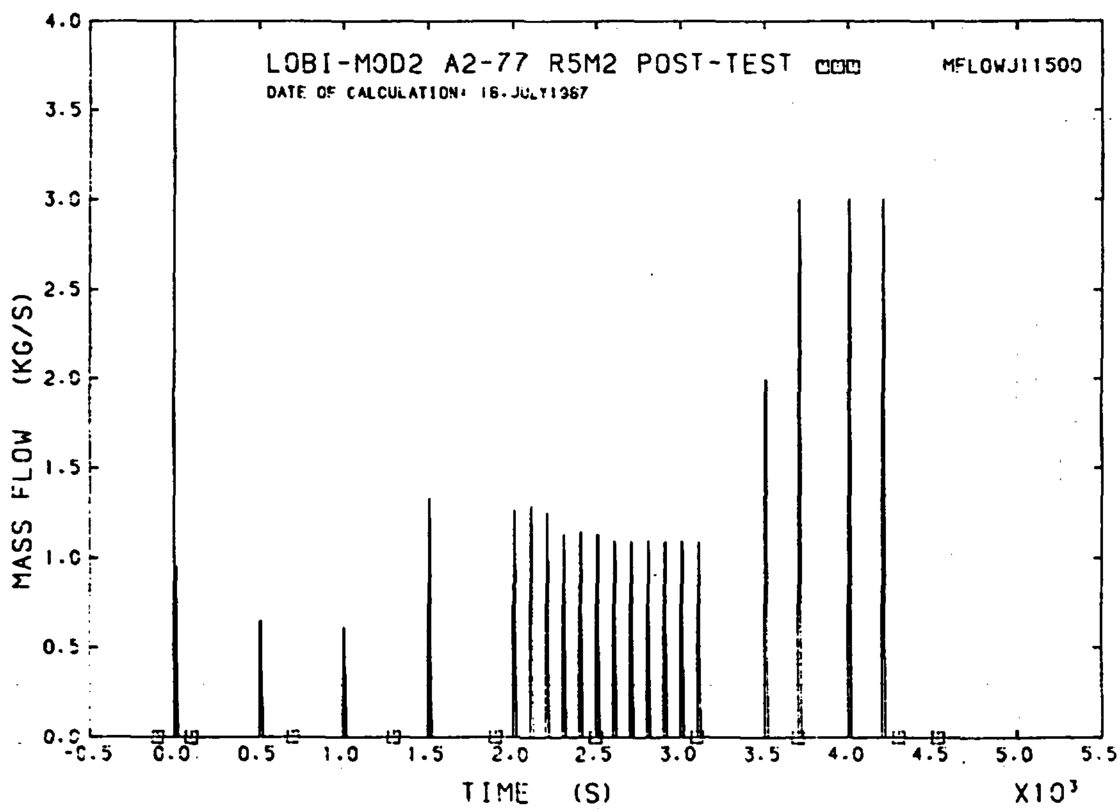

FIGURE D28 FLOWRATE DRAINED FROM LP

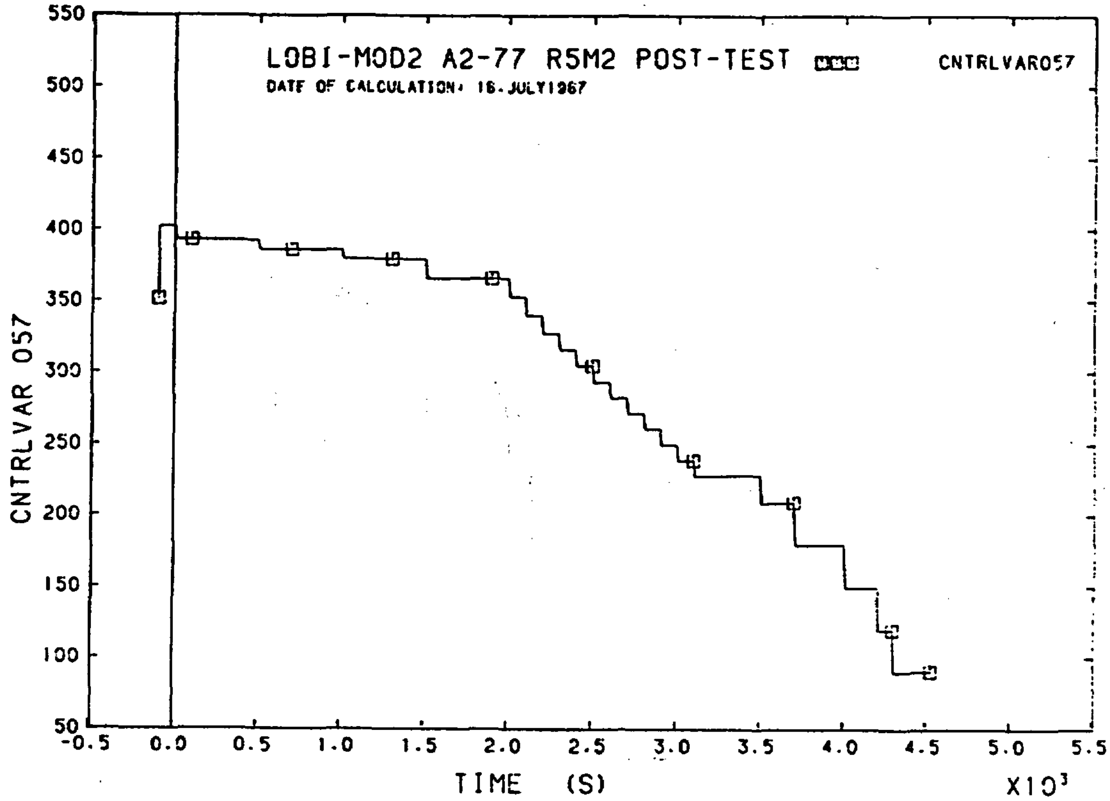

FIGURE D29 PRIMARY LOOP RESIDUAL MASS

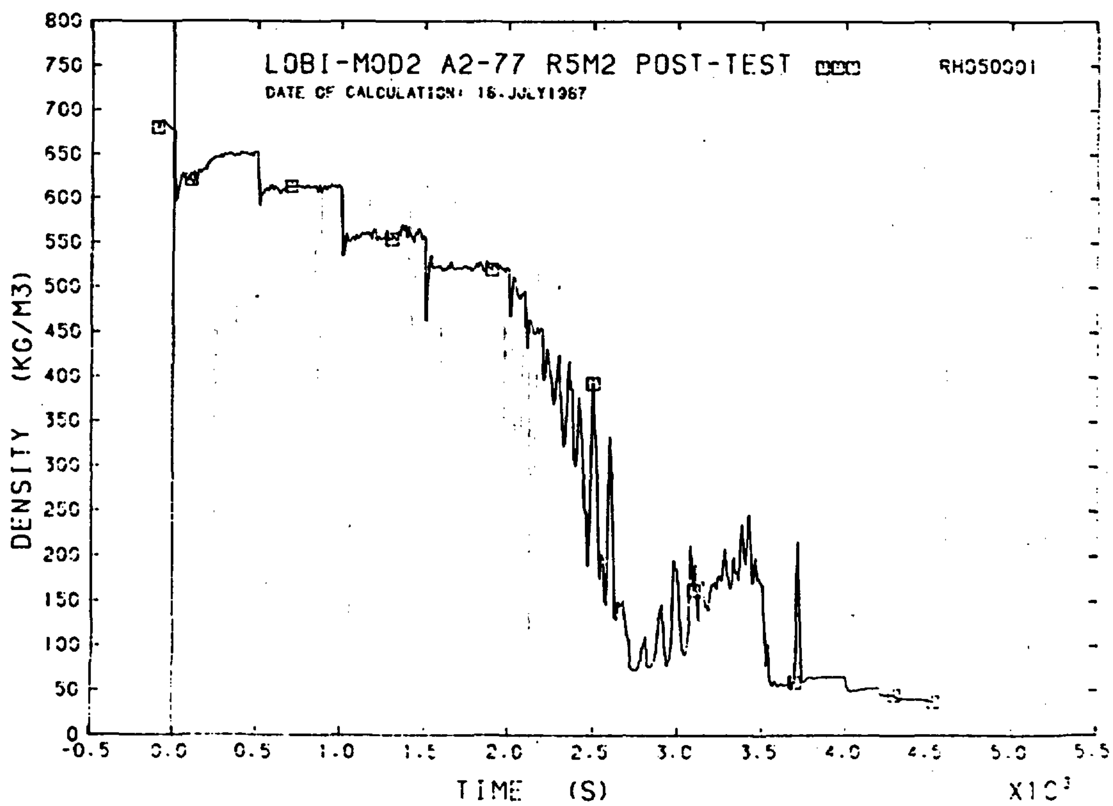

FIGURE D30 FLUID DENSITY IN I.L.-H.L. VESSEL OUTLET

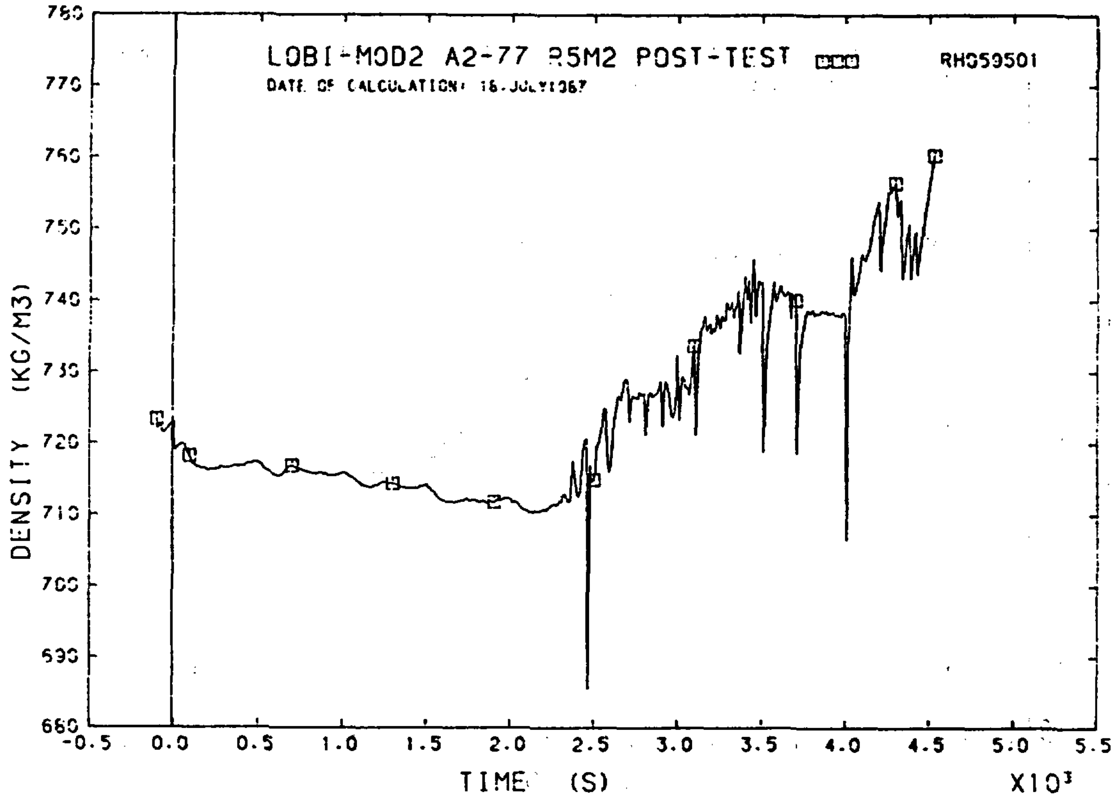

FIGURE D31 FLUID DENSITY IN I.L.-PUMP INLET

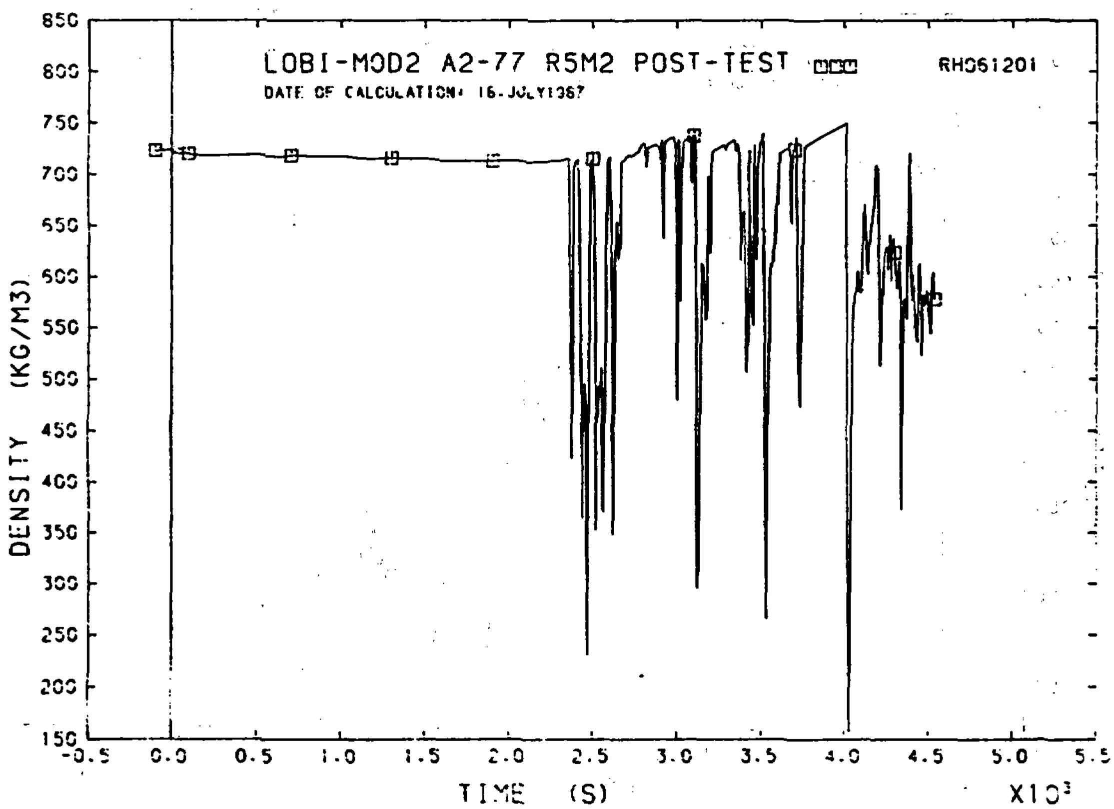

FIGURE D32 FLUID DENSITY IN I.L.-C.L. VESSEL INLET

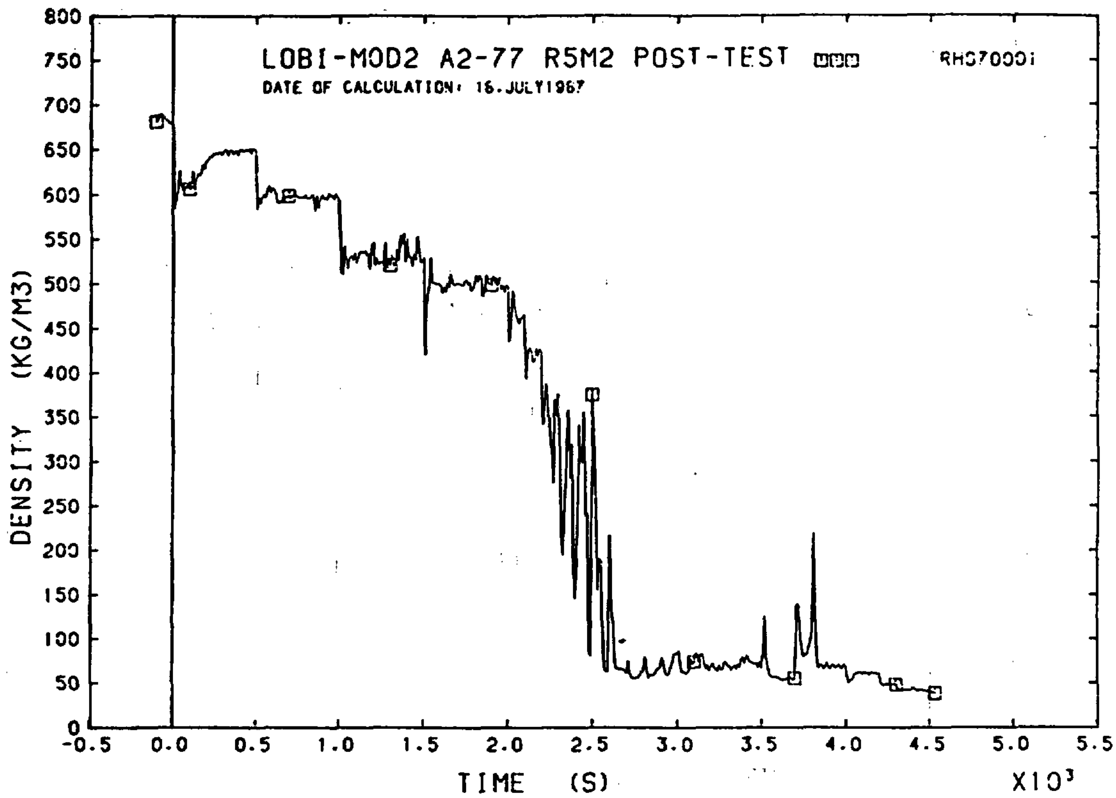

FIGURE D33 FLUID DENSITY IN B.L.-H.L. VESSEL OUTLET

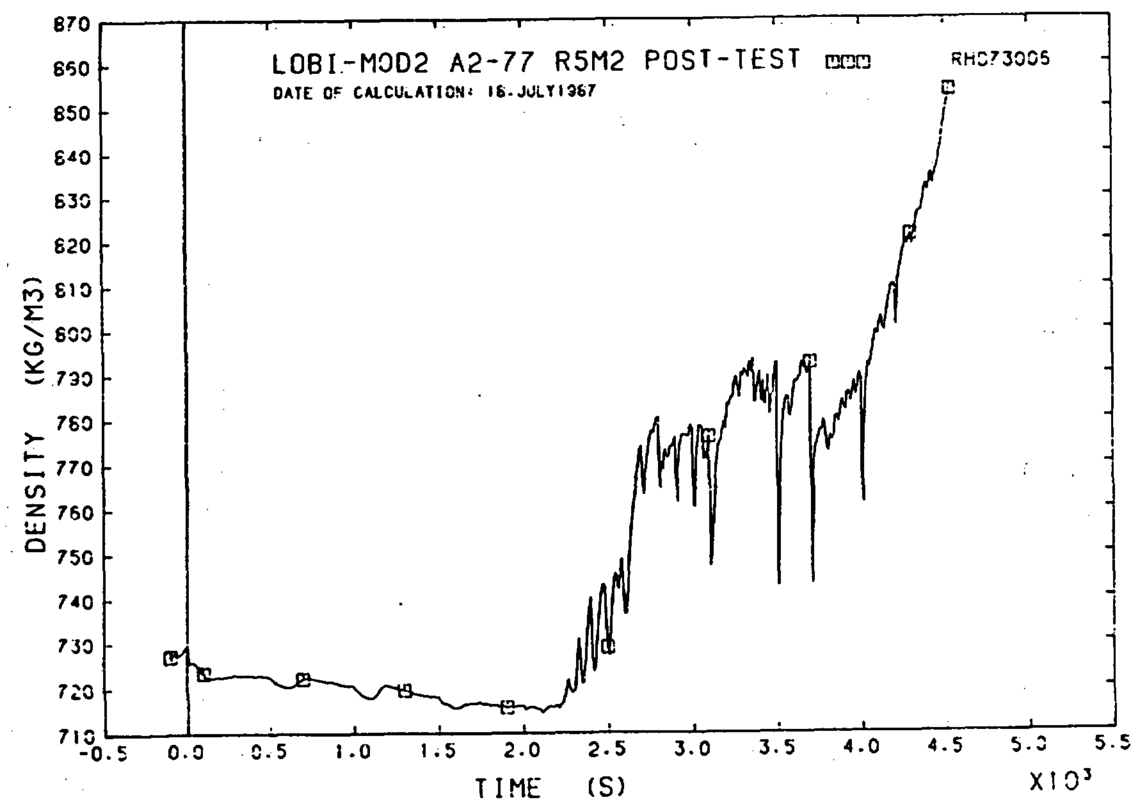

FIGURE D34 FLUID DENSITY IN B.L.-PUMP INLET

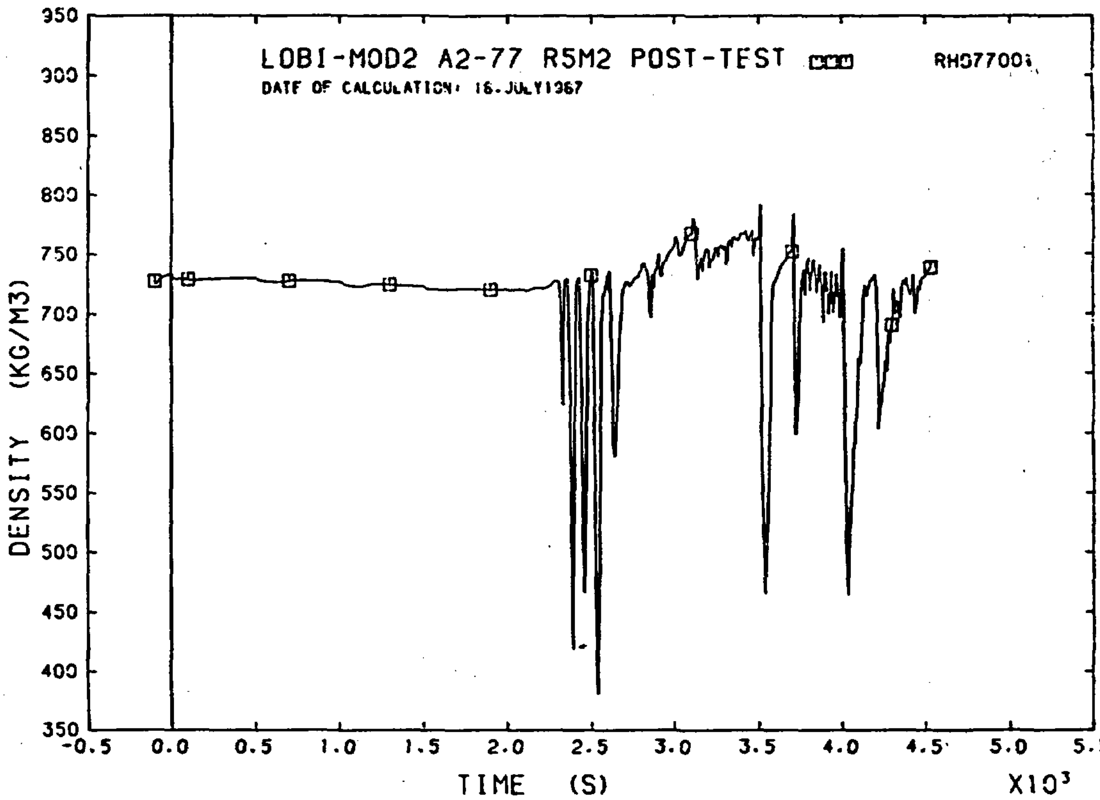

FIGURE D35 FLUID DENSITY IN B.L.-C.L. VESSEL INLET

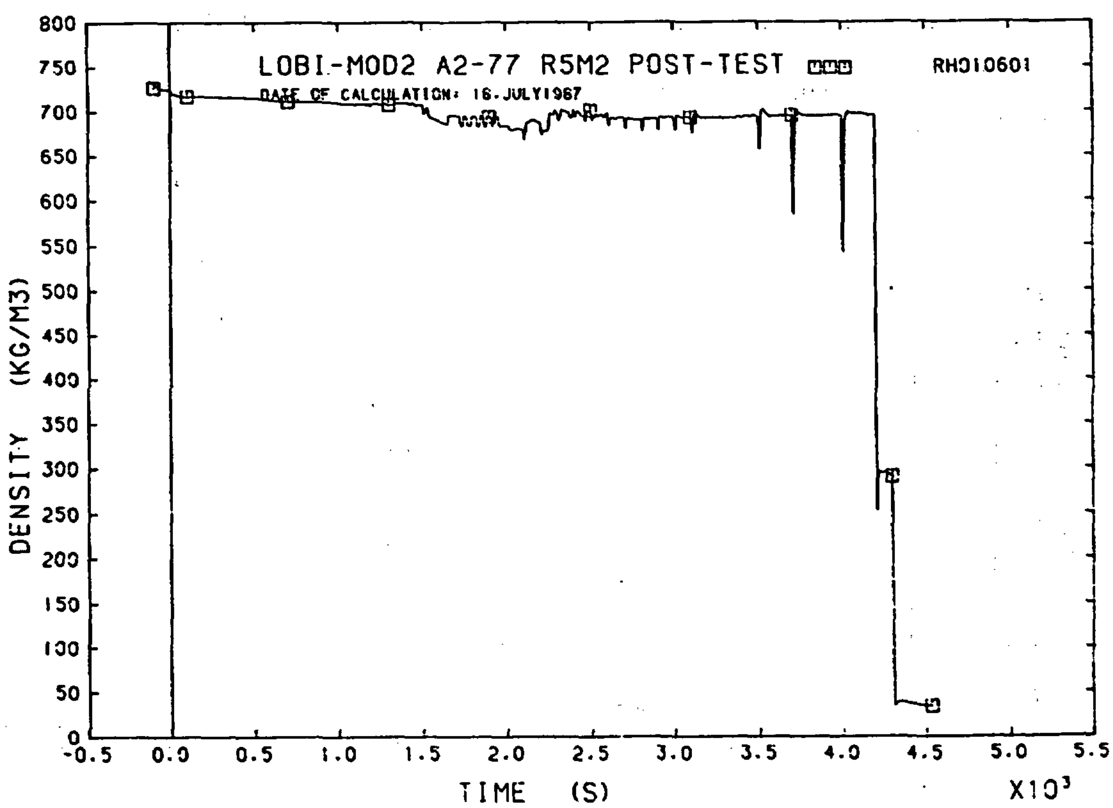

FIGURE D36 FLUID DENSITY IN PRESSURE VESSEL

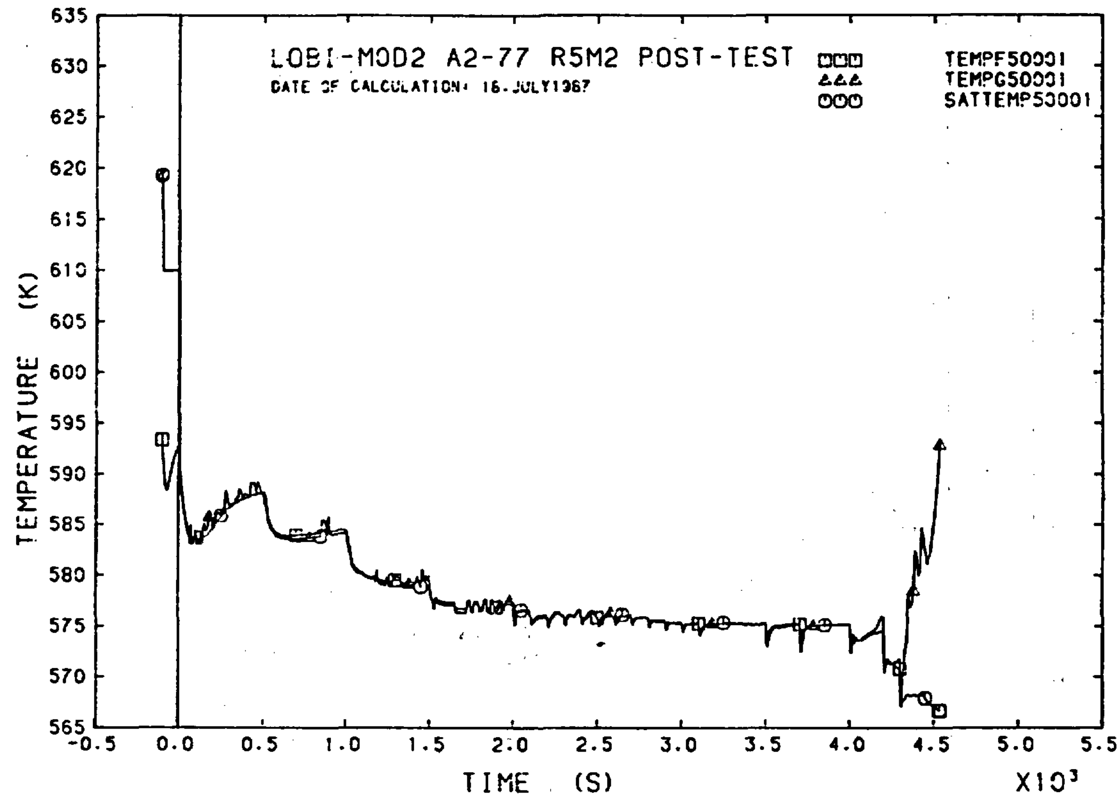

FIGURE D37 FLUID TEMPERATURE IN I.L.-H.L. VESSEL OUTLET

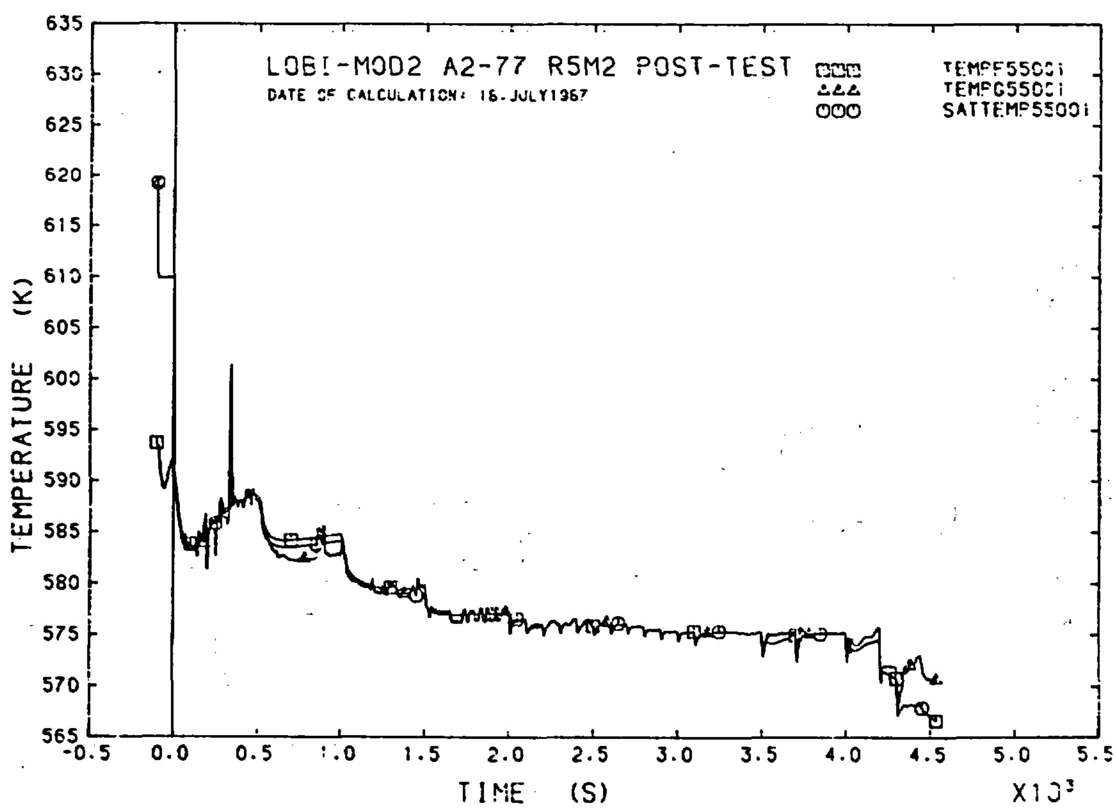

FIGURE D38 FLUID TEMPERATURE IN I.L.-S.G. INLET

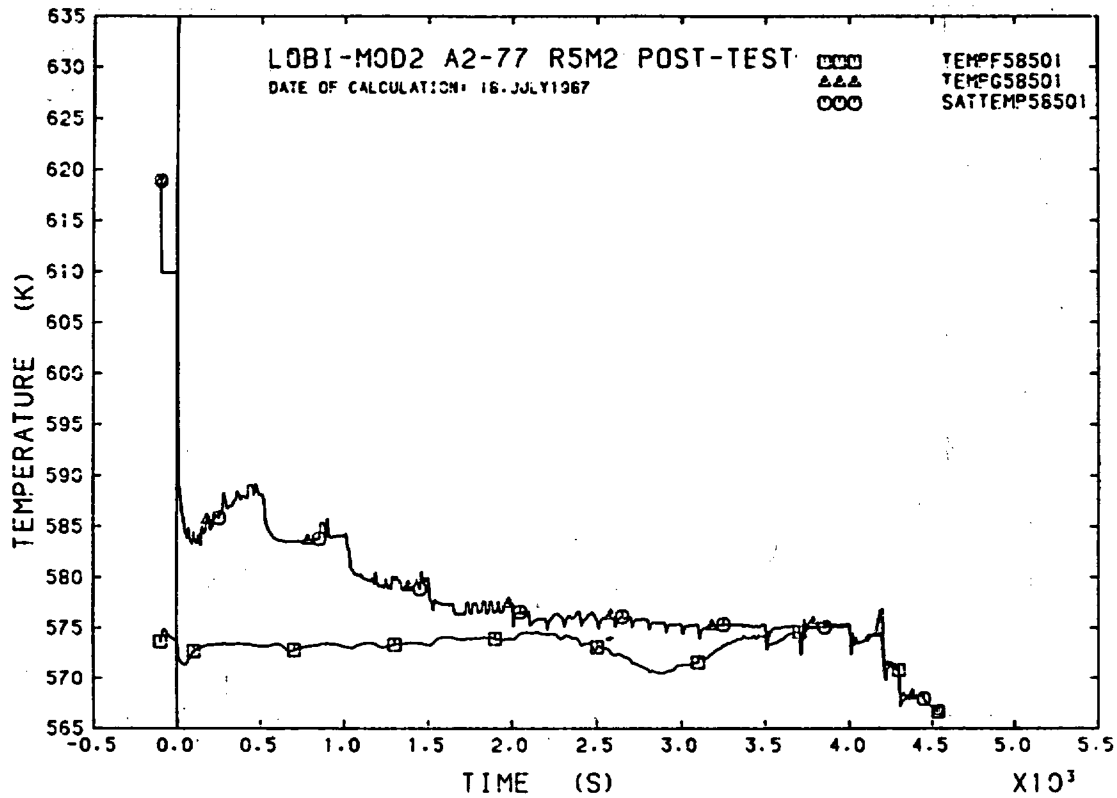

FIGURE D39 FLUID TEMPERATURE IN I.L.-S.G. OUTLET

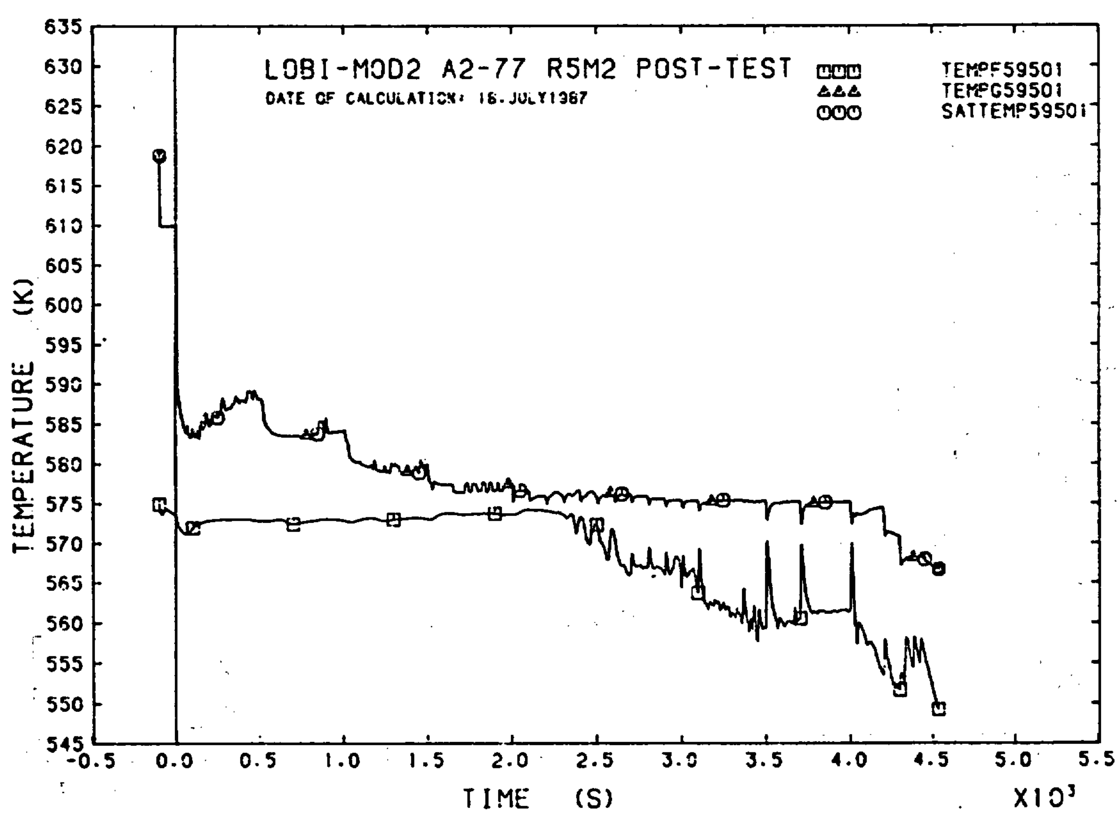

FIGURE D40 FLUID TEMPERATURE IN I.L.-PUMP INLET

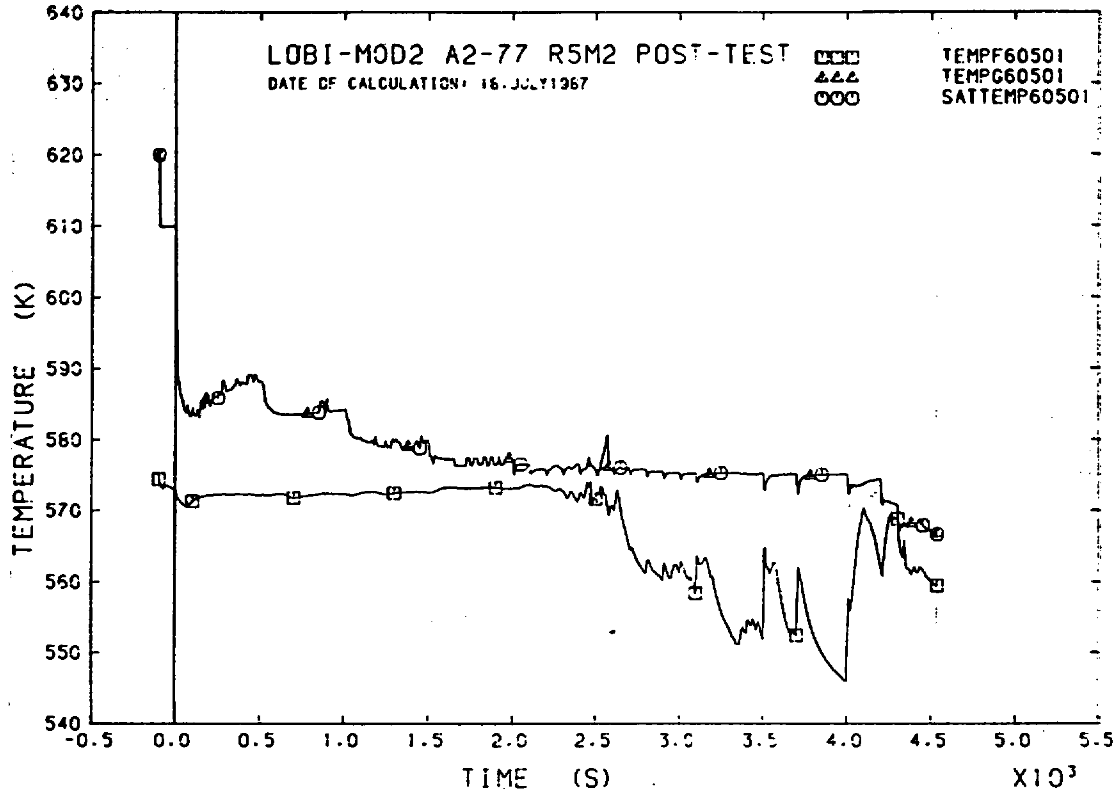

FIGURE D41 FLUID TEMPERATURE IN I.L.-PUMP OUTLET

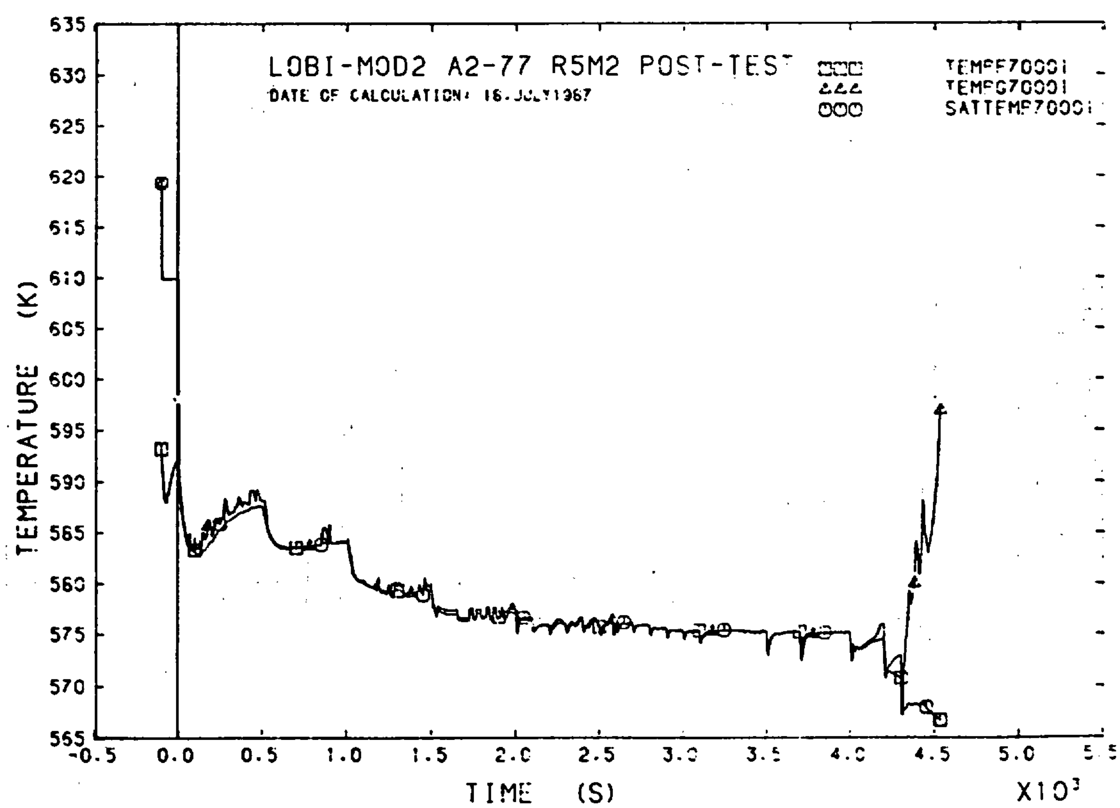

FIGURE D42 FLUID TEMPERATURE IN B.L.-H.L. VESSEL OUTLET

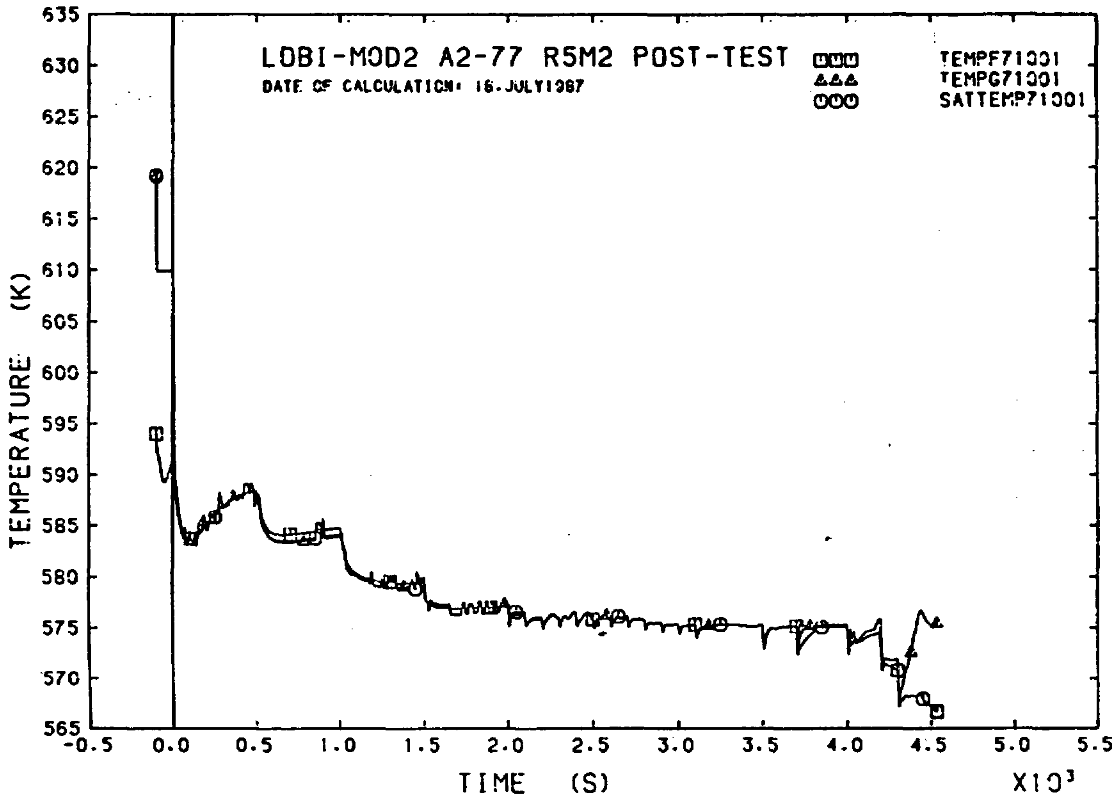

FIGURE D43 FLUID TEMPERATURE IN B.L.-S.G. INLET

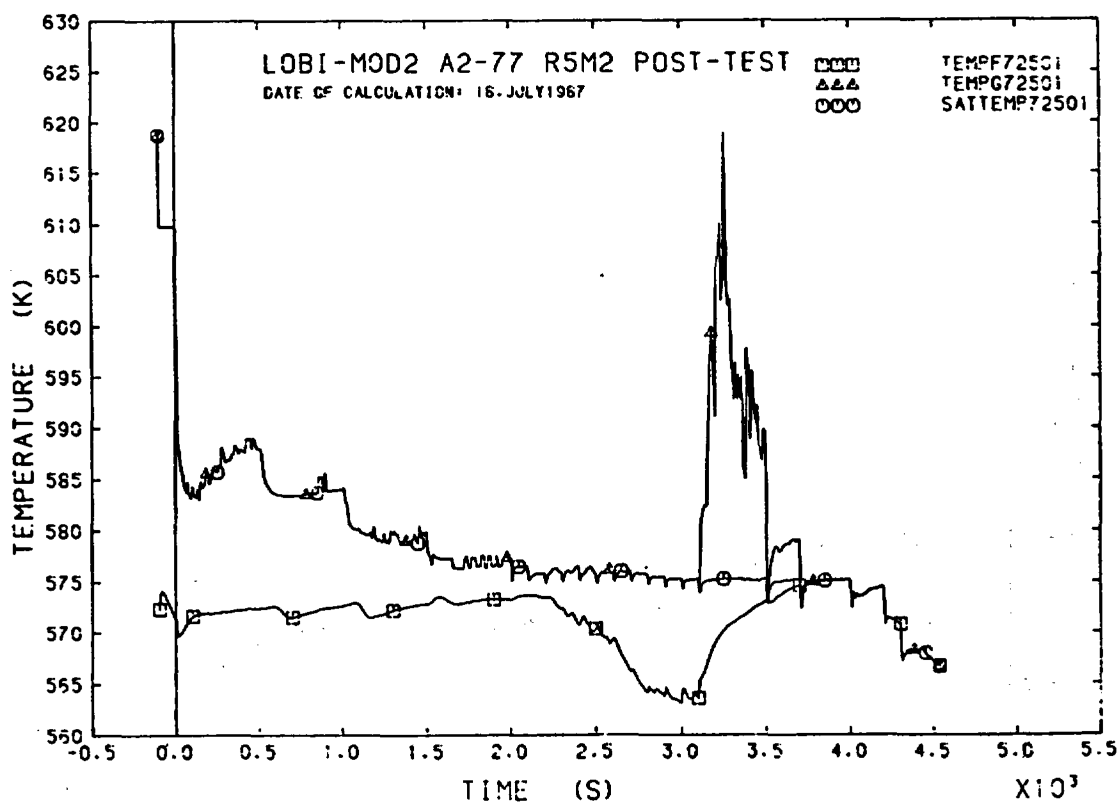

FIGURE D44 FLUID TEMPERATURE IN B.L.-S.G. OUTLET

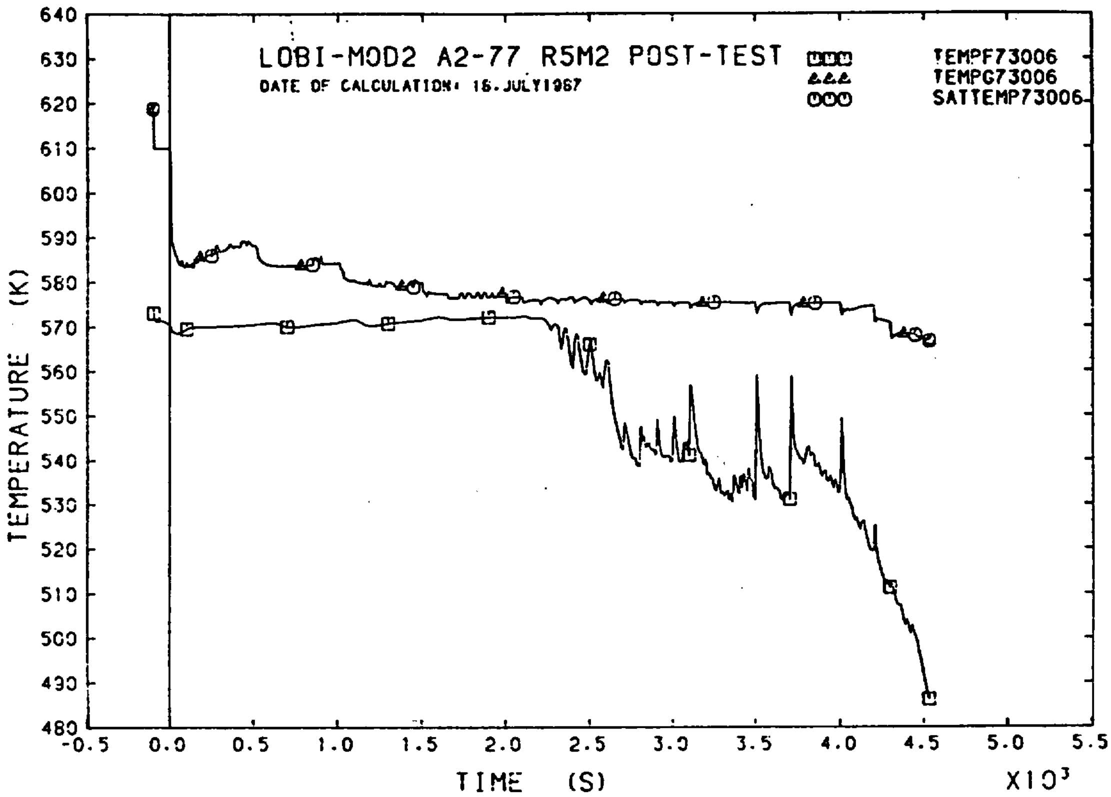

FIGURE D45 FLUID TEMPERATURE IN B.L.-PUMP INLET

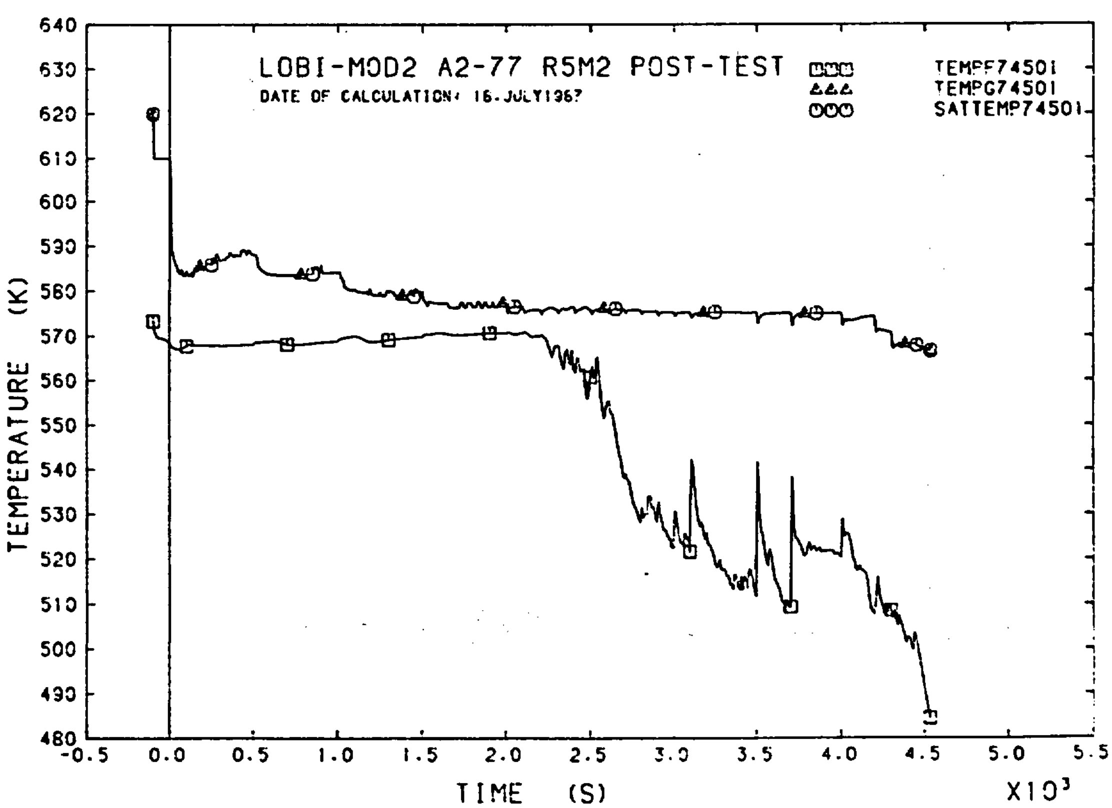

FIGURE D46 FLUID TEMPERATURE IN B.L.-PUMP OUTLET

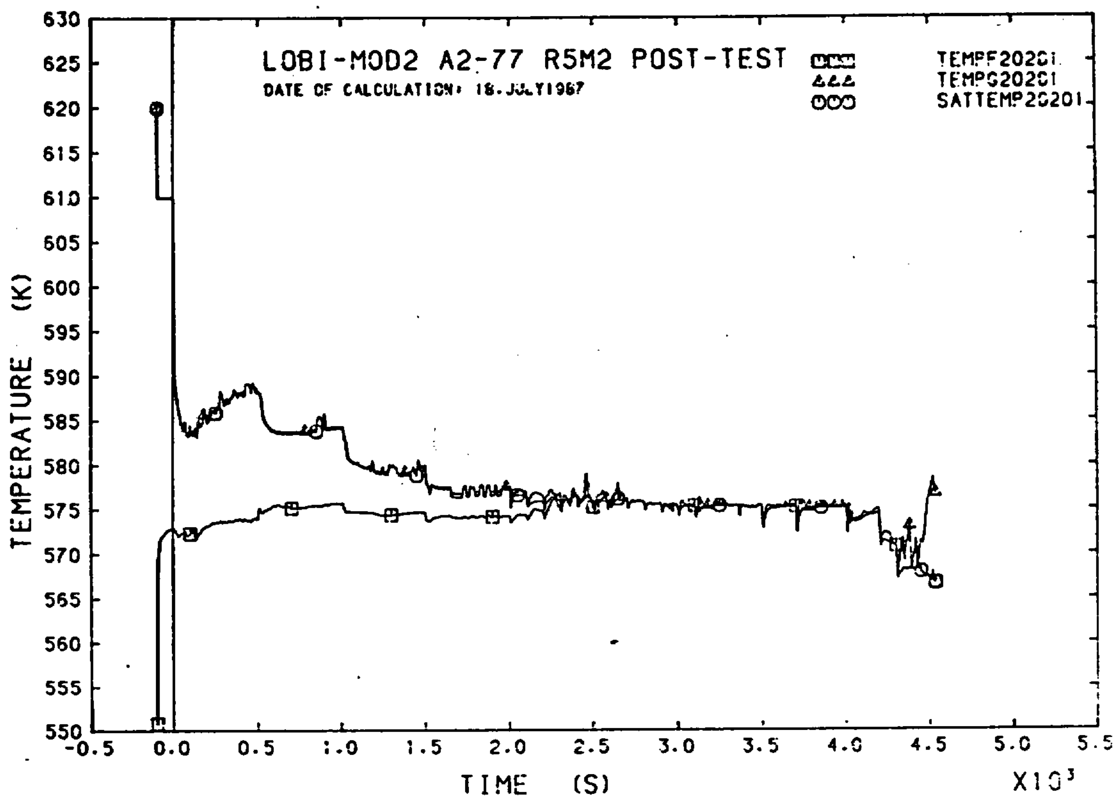

FIGURE D47 FLUID TEMPERATURE IN D.C. ANNULUS LOWER PART

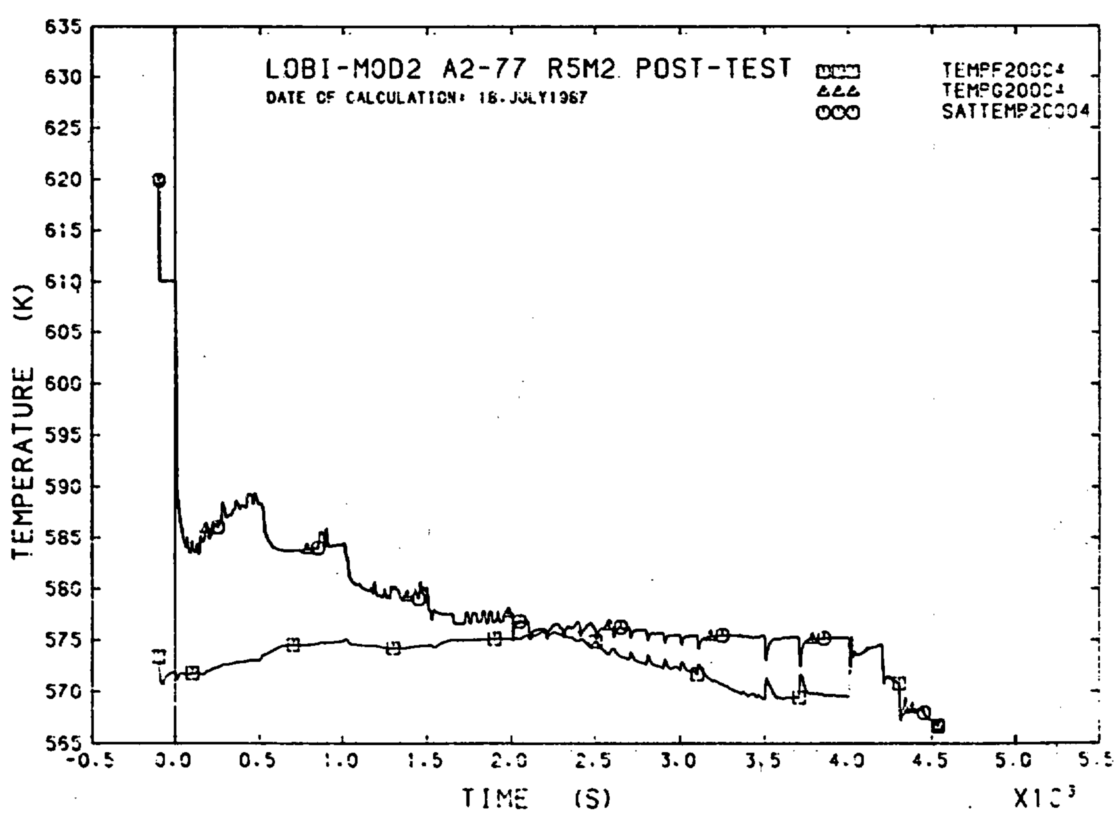

FIGURE D48 FLUID TEMPERATURE IN D.C. MIDDLE SECTION

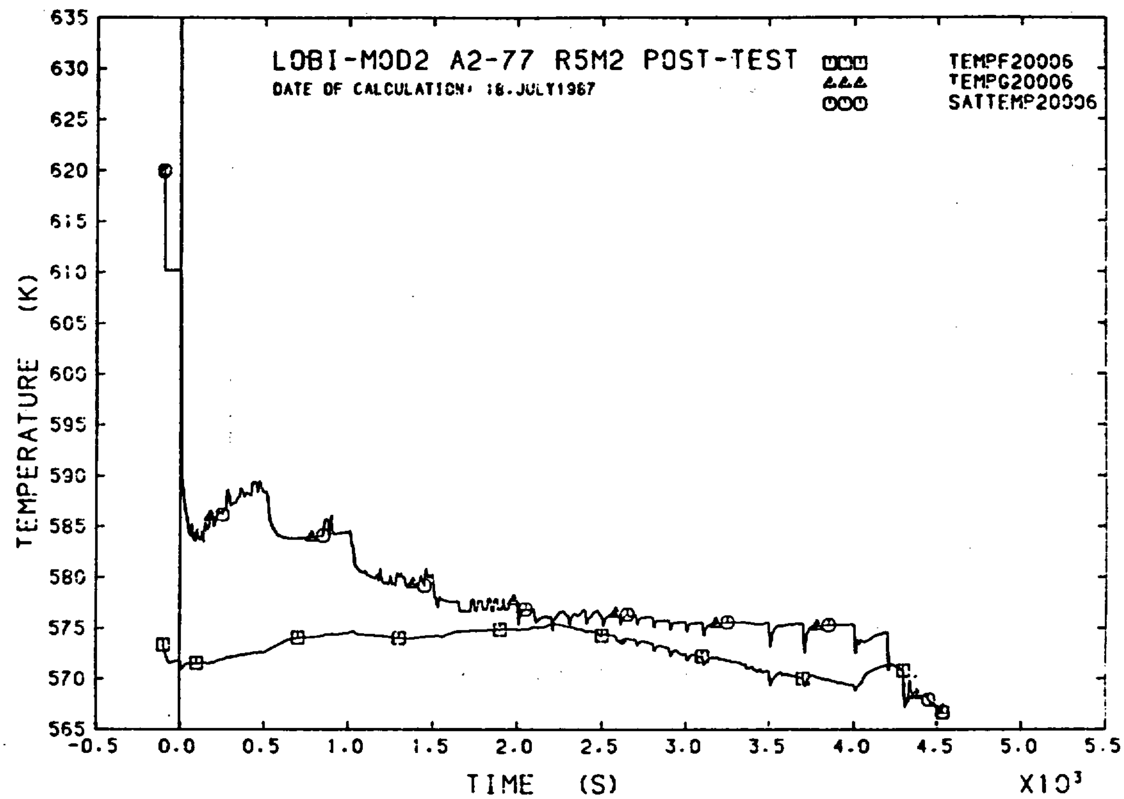

FIGURE D49 FLUID TEMPERATURE IN D.C. BOTTON

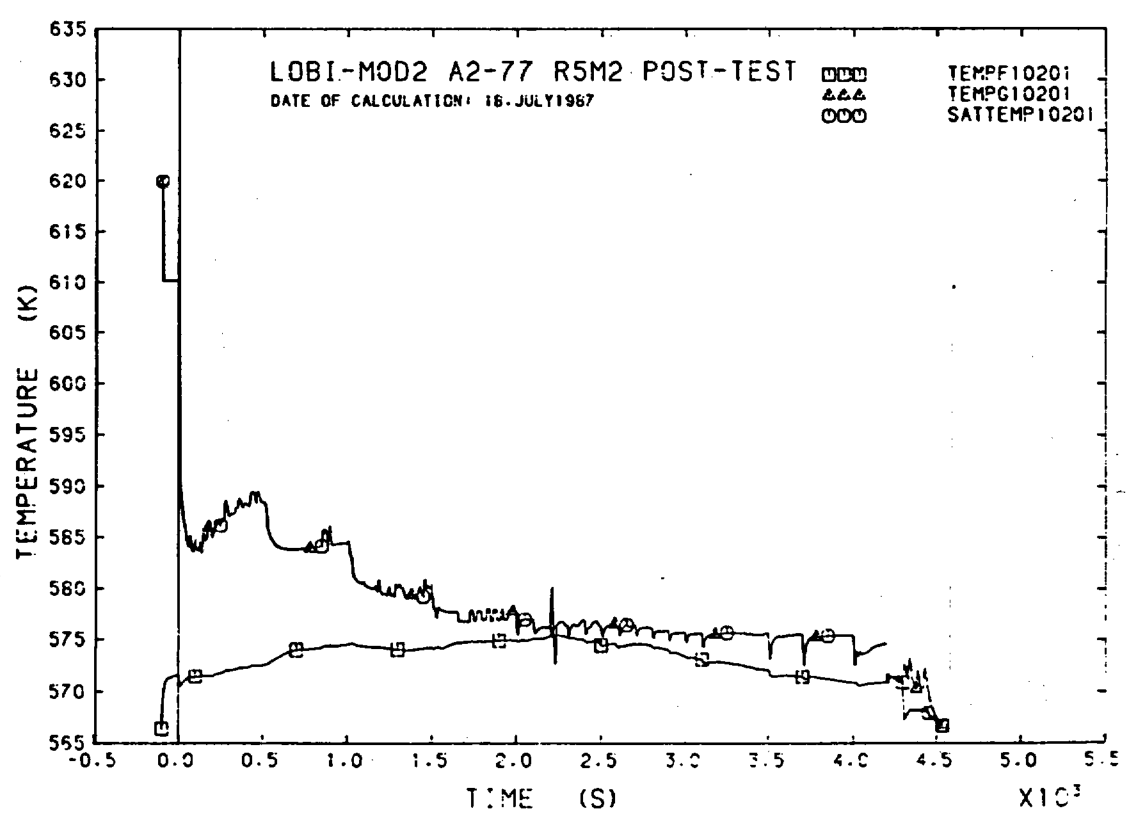

FIGURE D50 FLUID TEMPERATURE IN L.P.

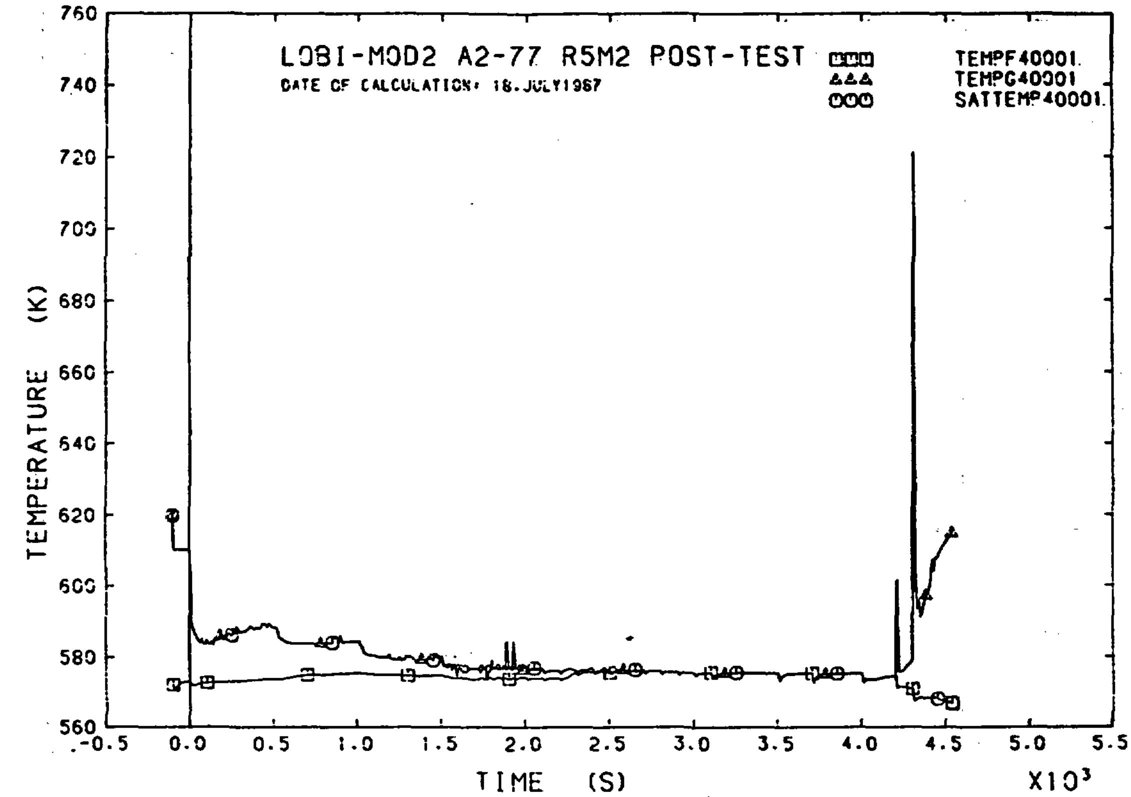

FIGURE D51 FLUID TEMPERATURE IN U.P.

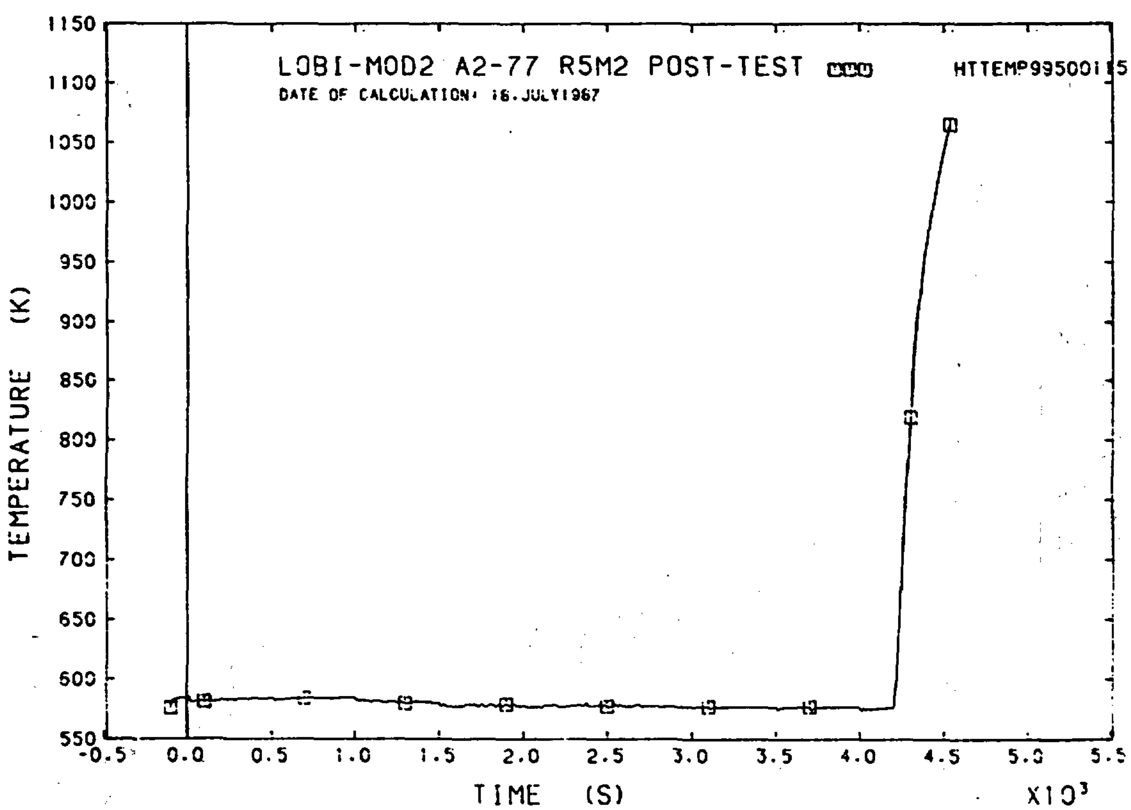

FIGURE D52 SURFACE ROD TEMPERATURE

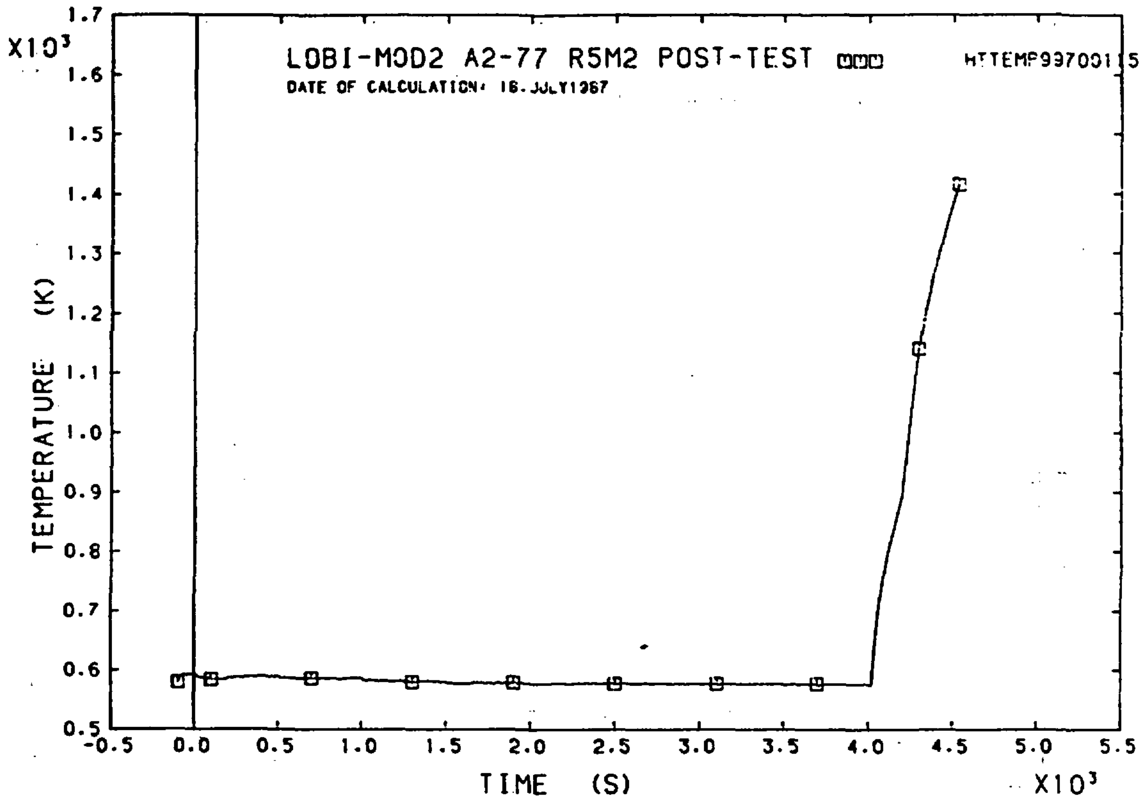

FIGURE D53 SURFACE ROD TEMPERATURE

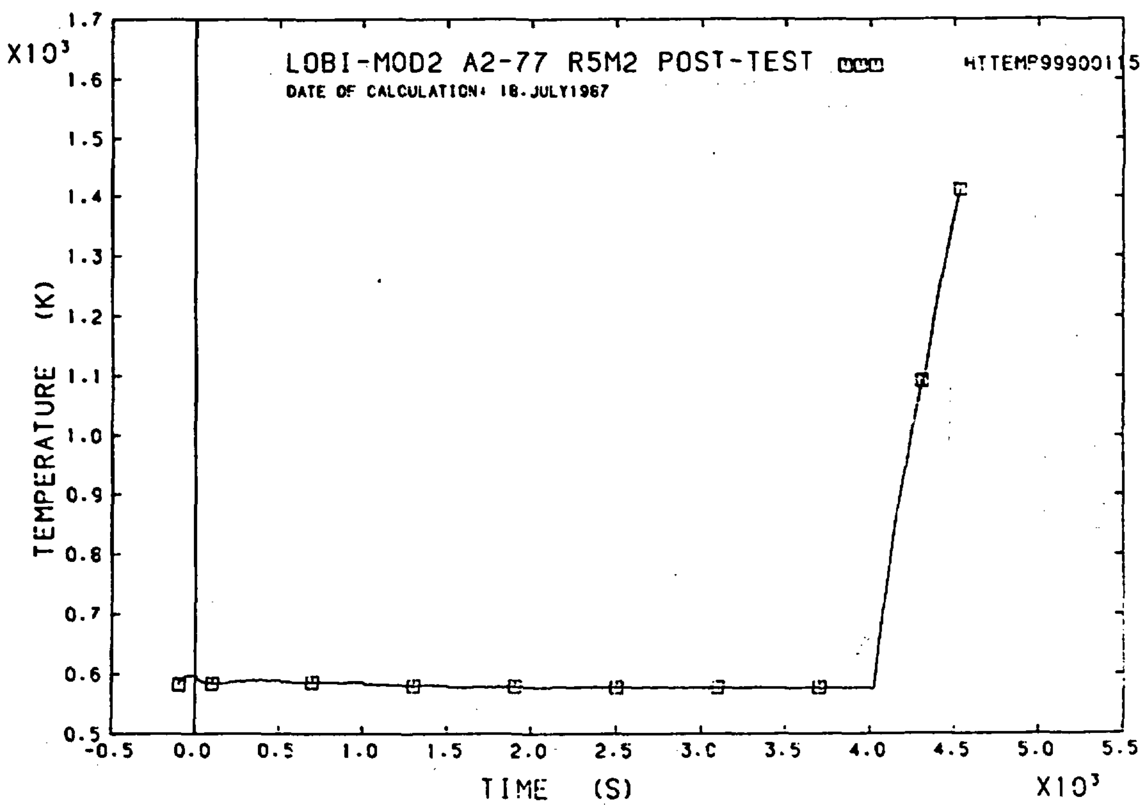

FIGURE D54 SURFACE ROD TEMPERATURE

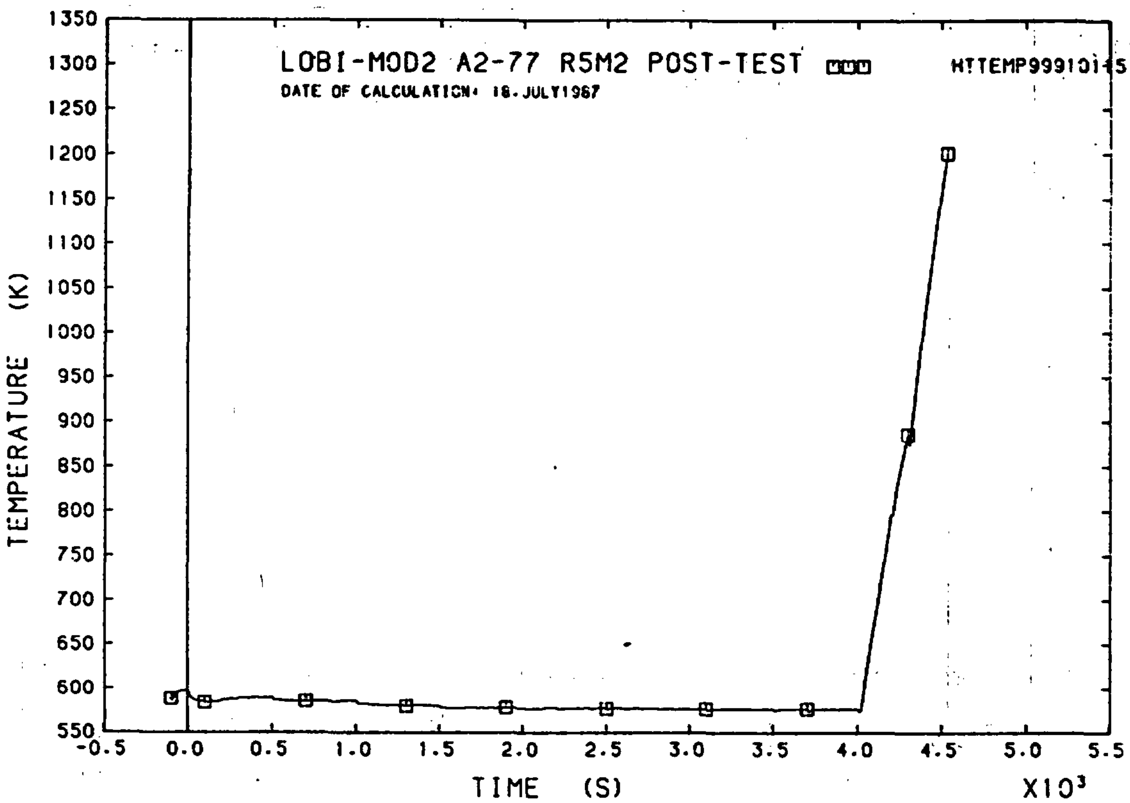

FIGURE D55 SURFACE ROD TEMPERATURE

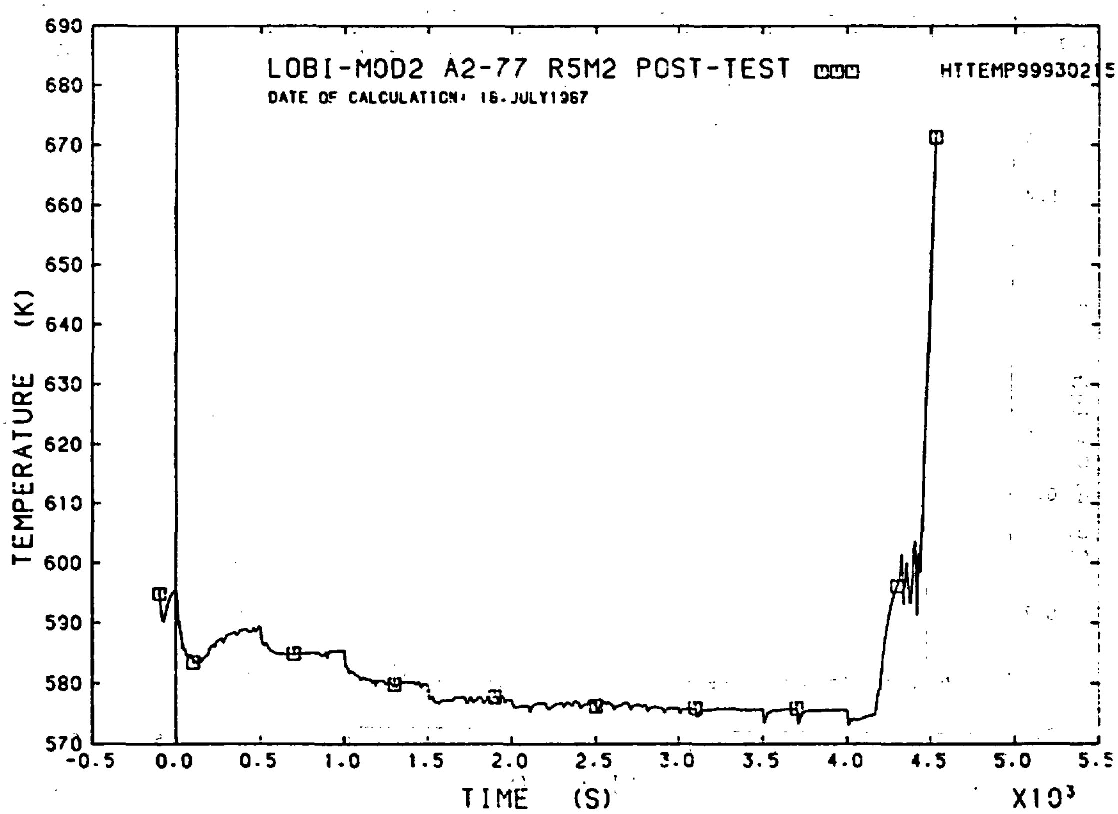

FIGURE D56 SURFACE ROD TEMPERATURE

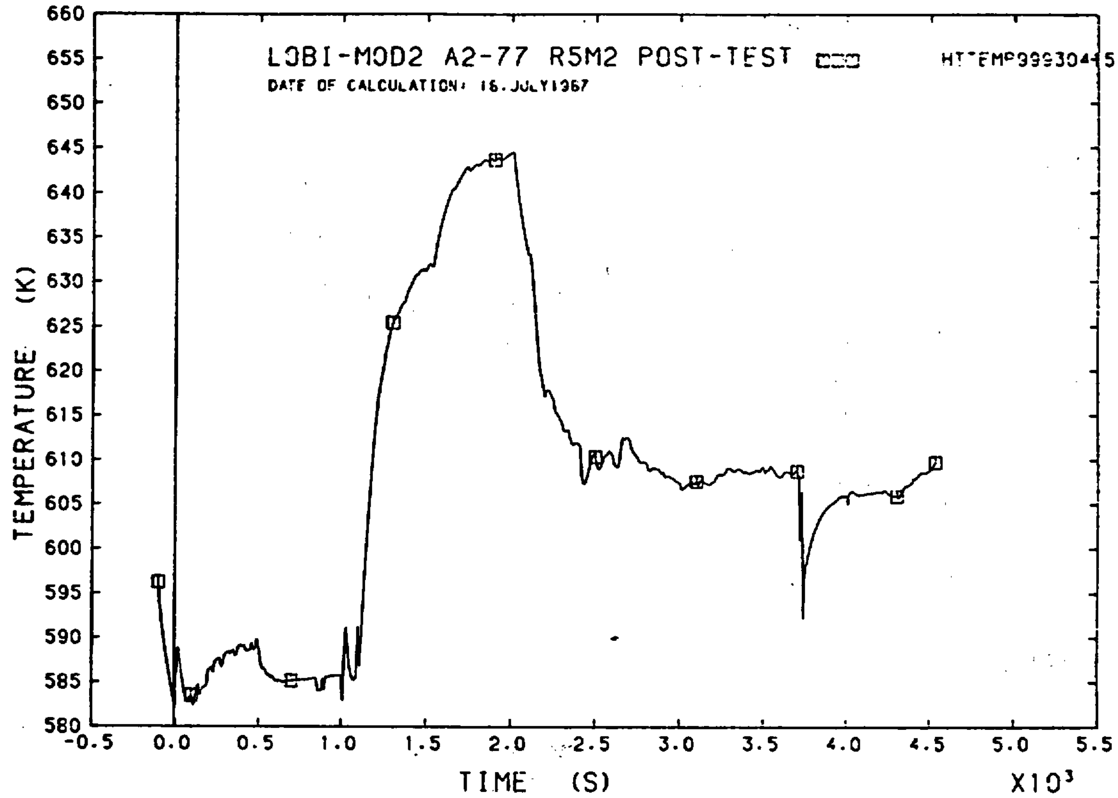

FIGURE D57 SURFACE ROD TEMPERATURE

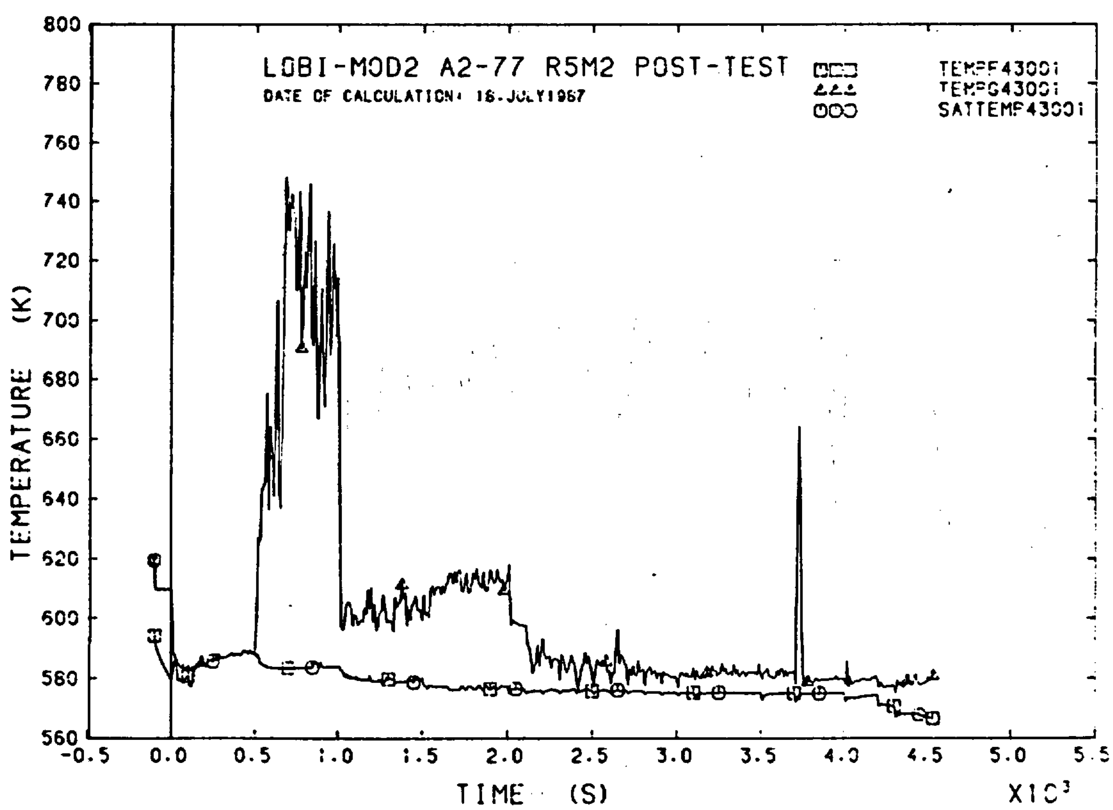

FIGURE D58 FLUID TEMPERATURES IN UPPER PLENUM

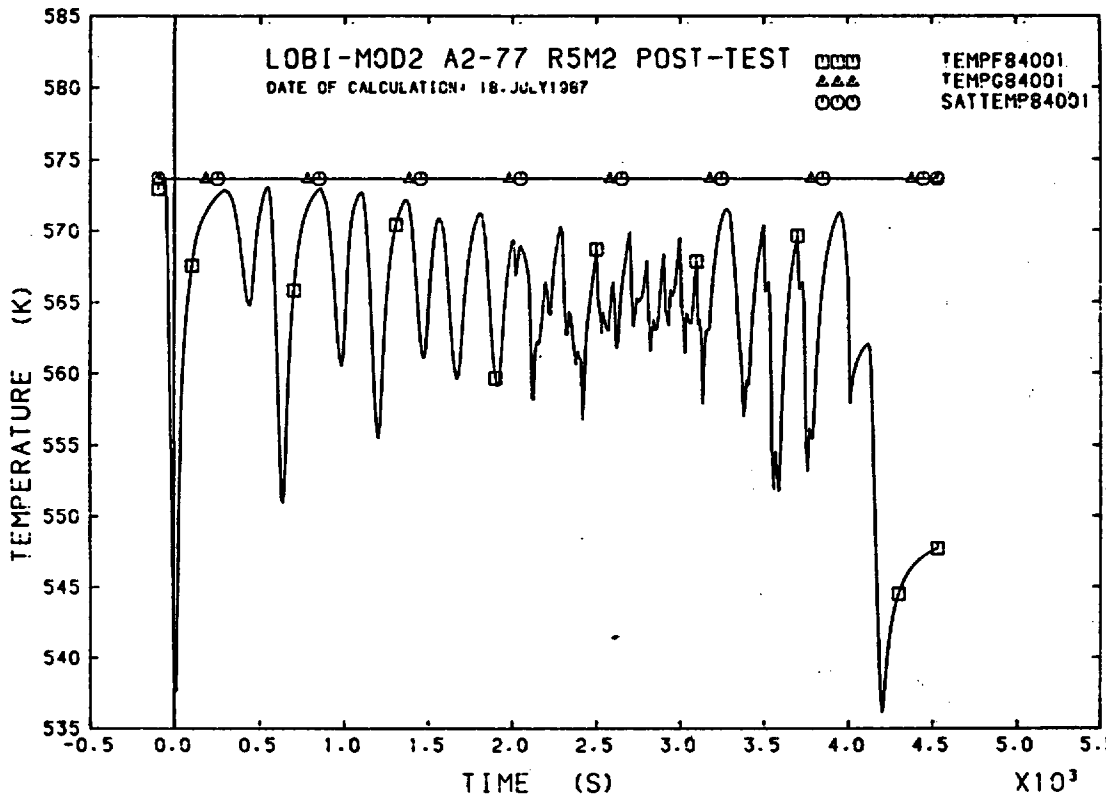

FIGURE D59 FLUID TEMPERATURES IN I.L. S.G. SECONDARY SIDE TOP

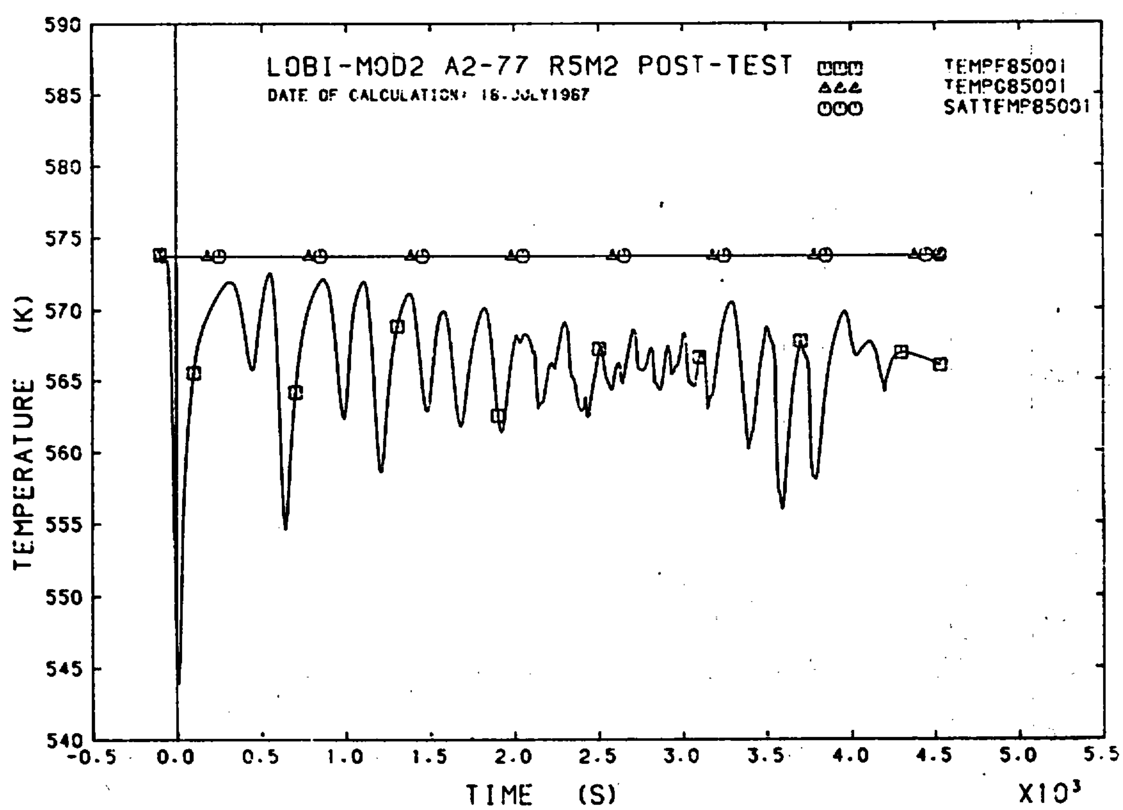

FIGURE D60 FLUID TEMPERATURES IN I.L. S.G. SECONDARY SIDE DOWNCOMER T.

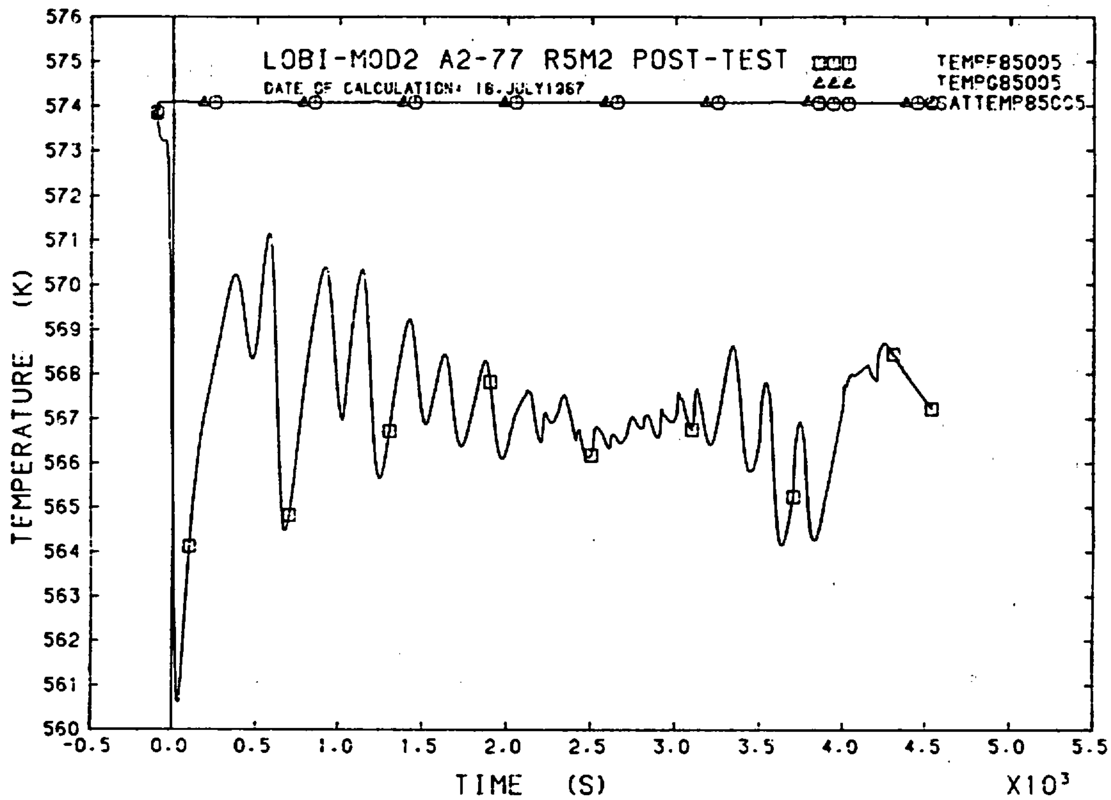

FIGURE D61 FLUID TEMPERATURES IN I.L. S.G. SECONDARY SIDE DOWNCOMER B.

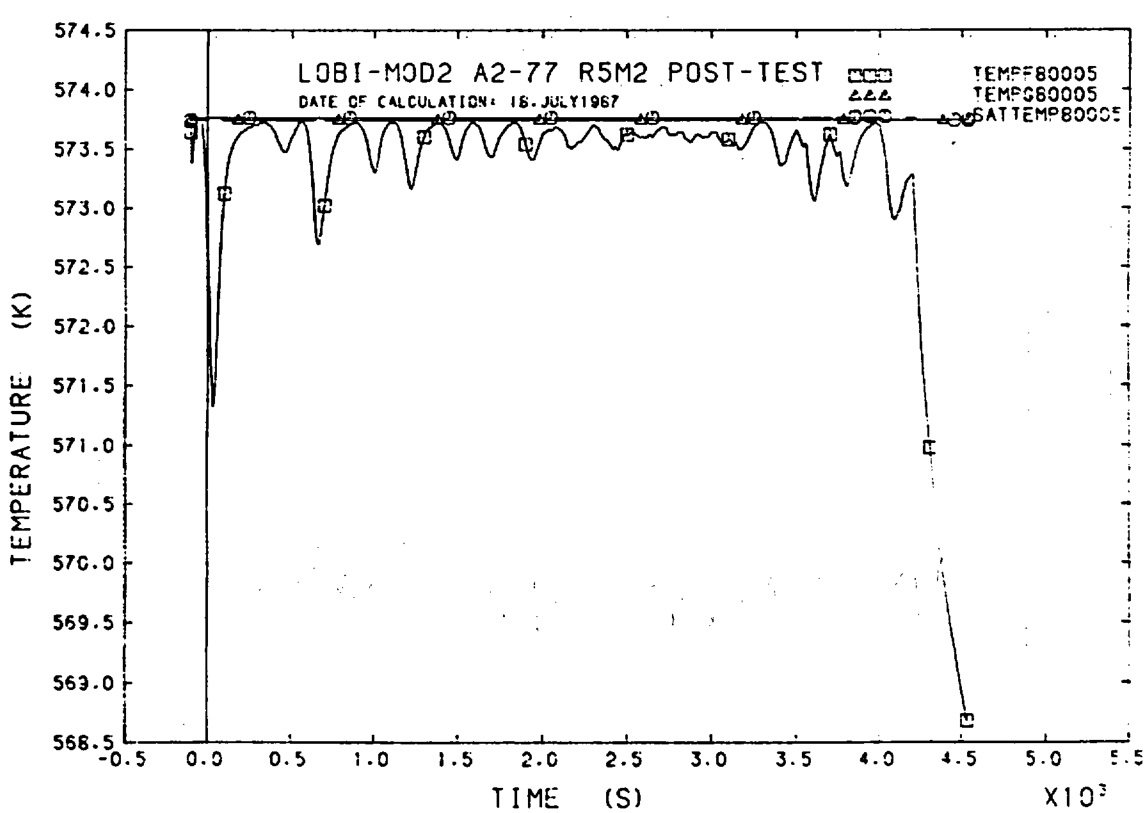

FIGURE D62 FLUID TEMPERATURES IN I.L. S.G. SECONDARY SIDE RISER

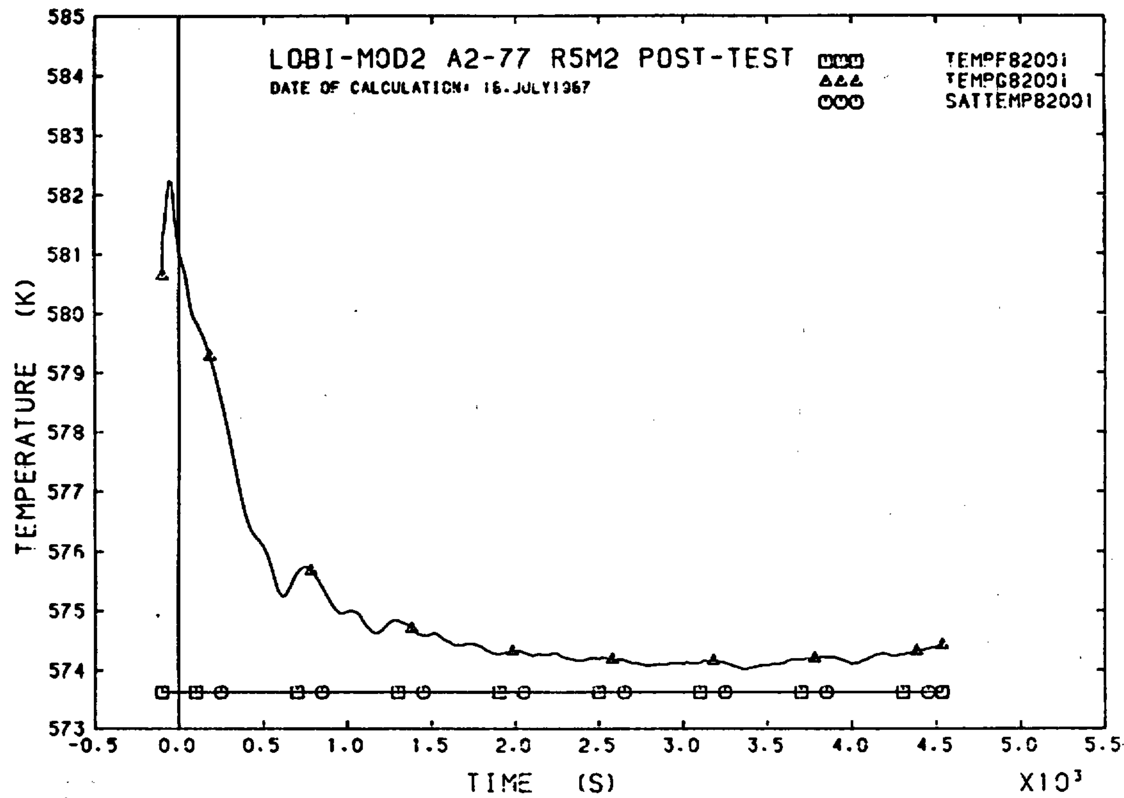

FIGURE D63 FLUID TEMPERATURES IN I.L. S.G. SECONDARY SIDE U-TUBES OUTLET

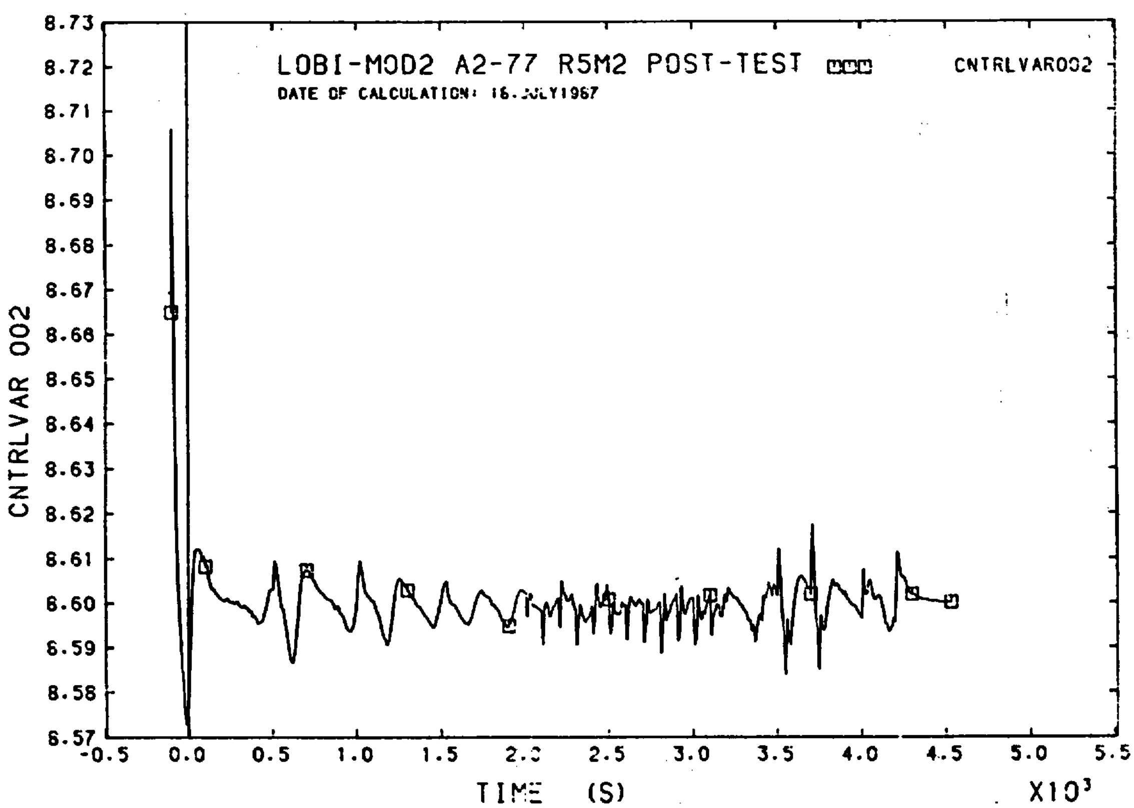

FIGURE D64 FLUID DOWNCOMER LEVEL IN I.L.S.G.

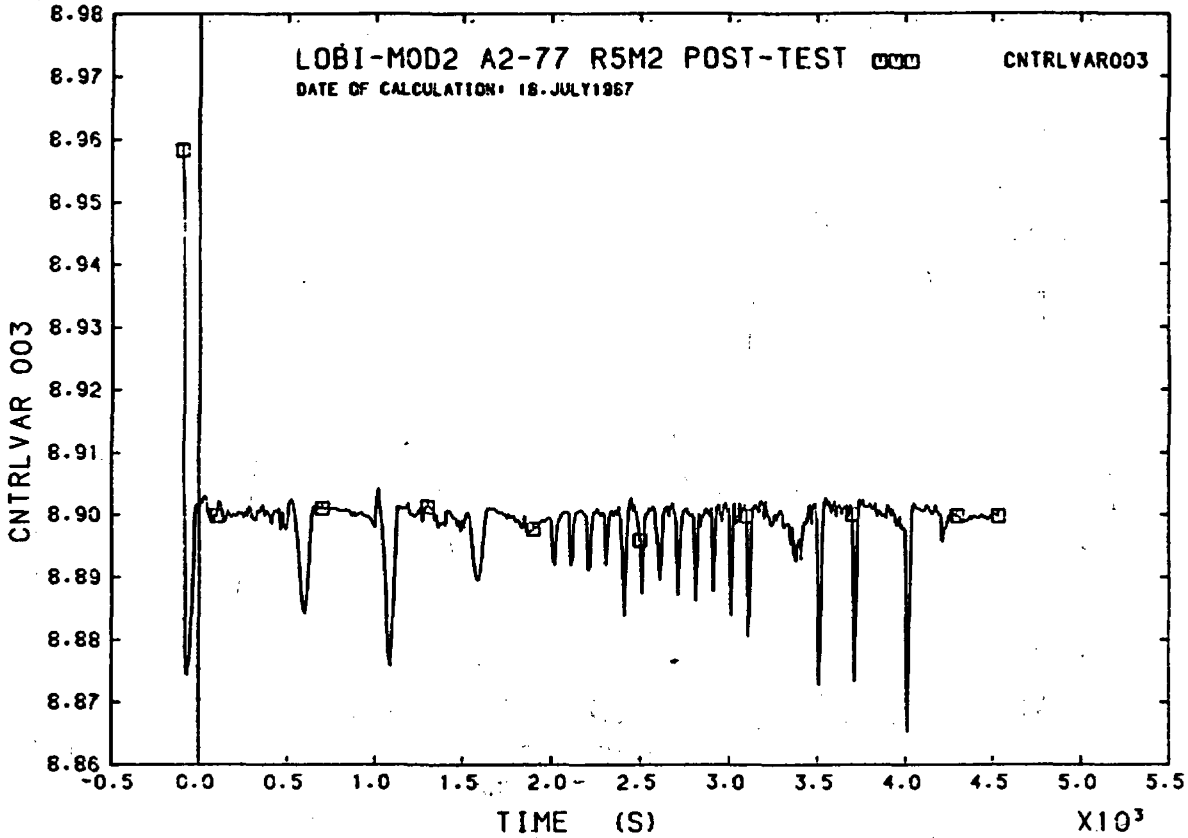

FIGURE D65 FLUID DOWNCOMER LEVEL IN B.L.S.G.

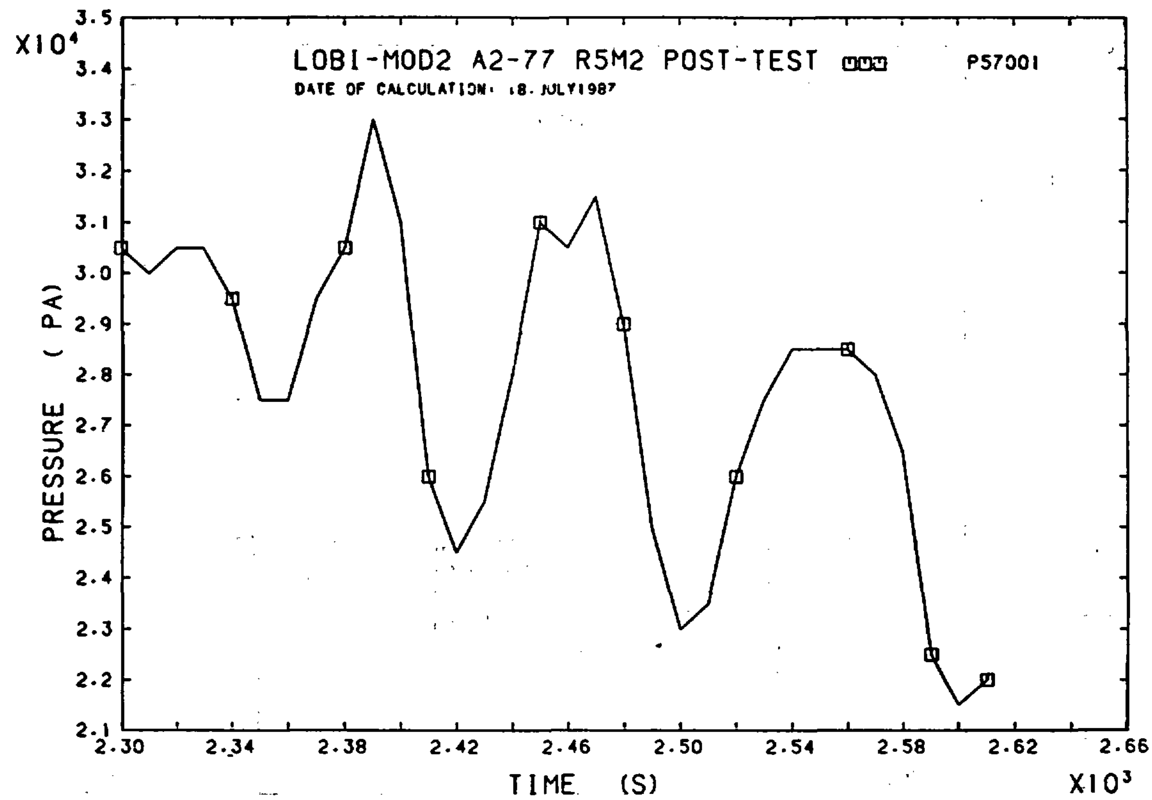

FIGURE D66 DIFFERENTIAL PRESSURE IN I.L. UT ASCENDING LEG UPPER TUBE

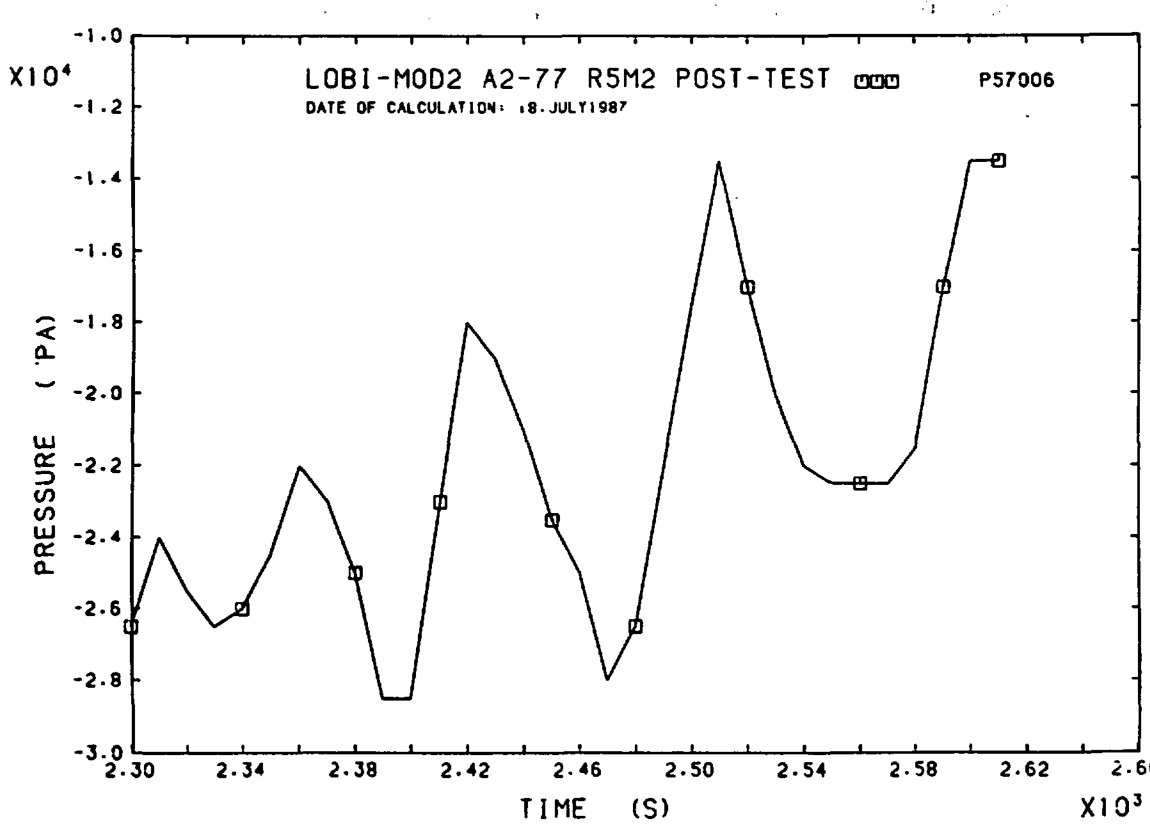

FIGURE D67 DIFFERENTIAL PRESSURE IN I.L. UT DESCENDING LEG UPPER TUBE

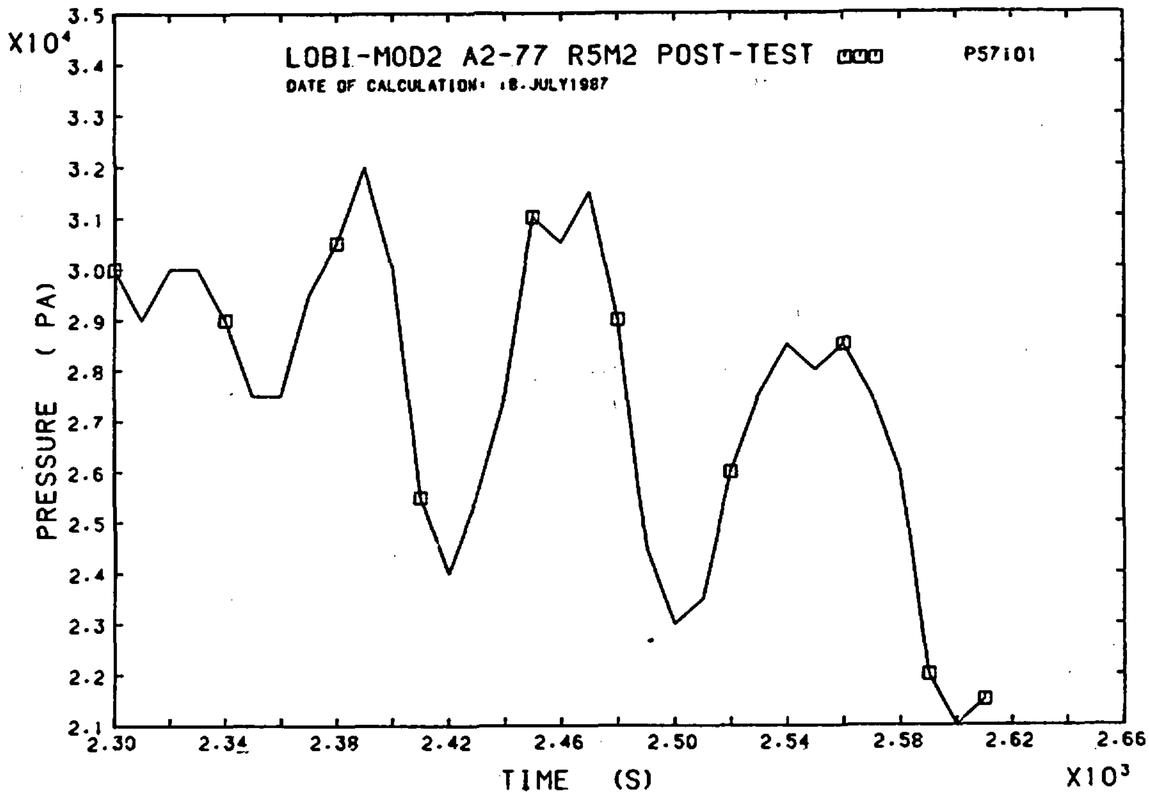

FIGURE D68 DIFFERENTIAL PRESSURE IN I.L. UT ASCENDING LEG LOWER TUBE

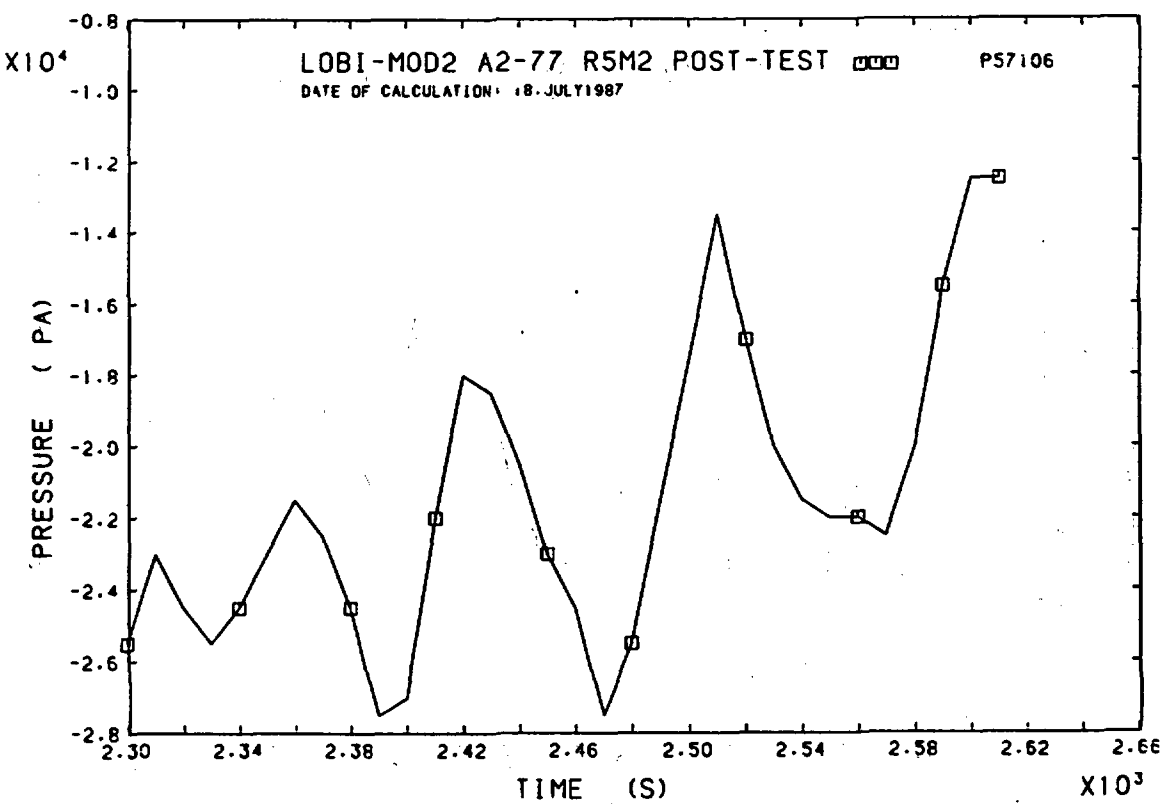

FIGURE D69 DIFFERENTIAL PRESSURE IN I.L. UT DESCENDING LEG LOWER TUBE

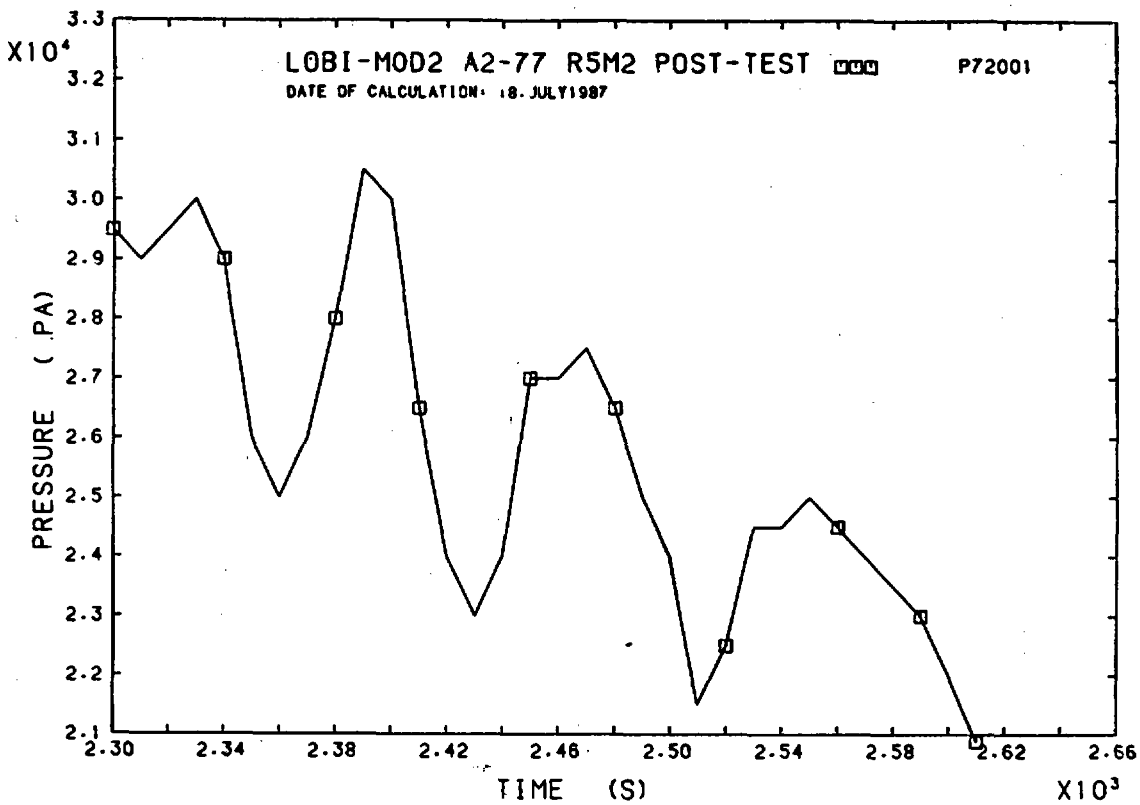

FIGURE D70 DIFFERENTIAL PRESSURE IN B.L. UT ASCENDING LEG UPPER TUBE

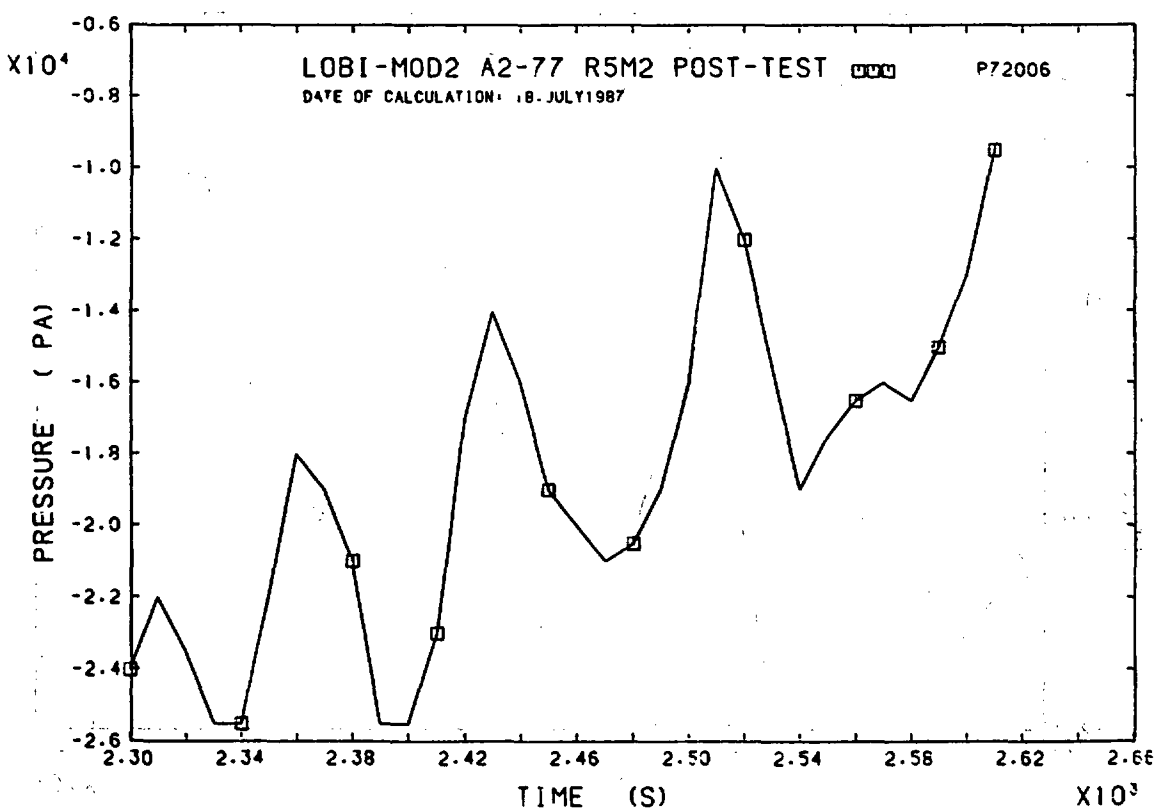

FIGURE D71 DIFFERENTIAL PRESSURE IN B.L. UT DESCENDING LEG UPPER TUBE

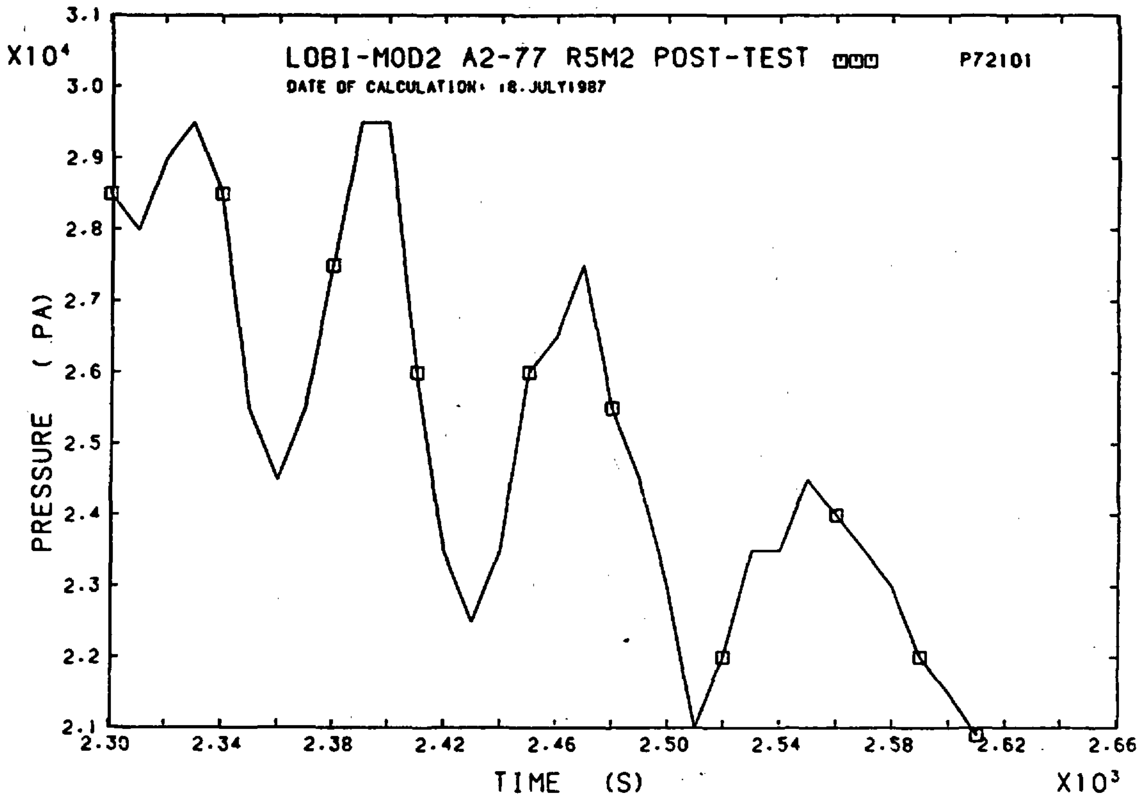

FIGURE D72 DIFFERENTIAL PRESSURE IN B.L. UT ASCENDING LEG LOWER TUBE

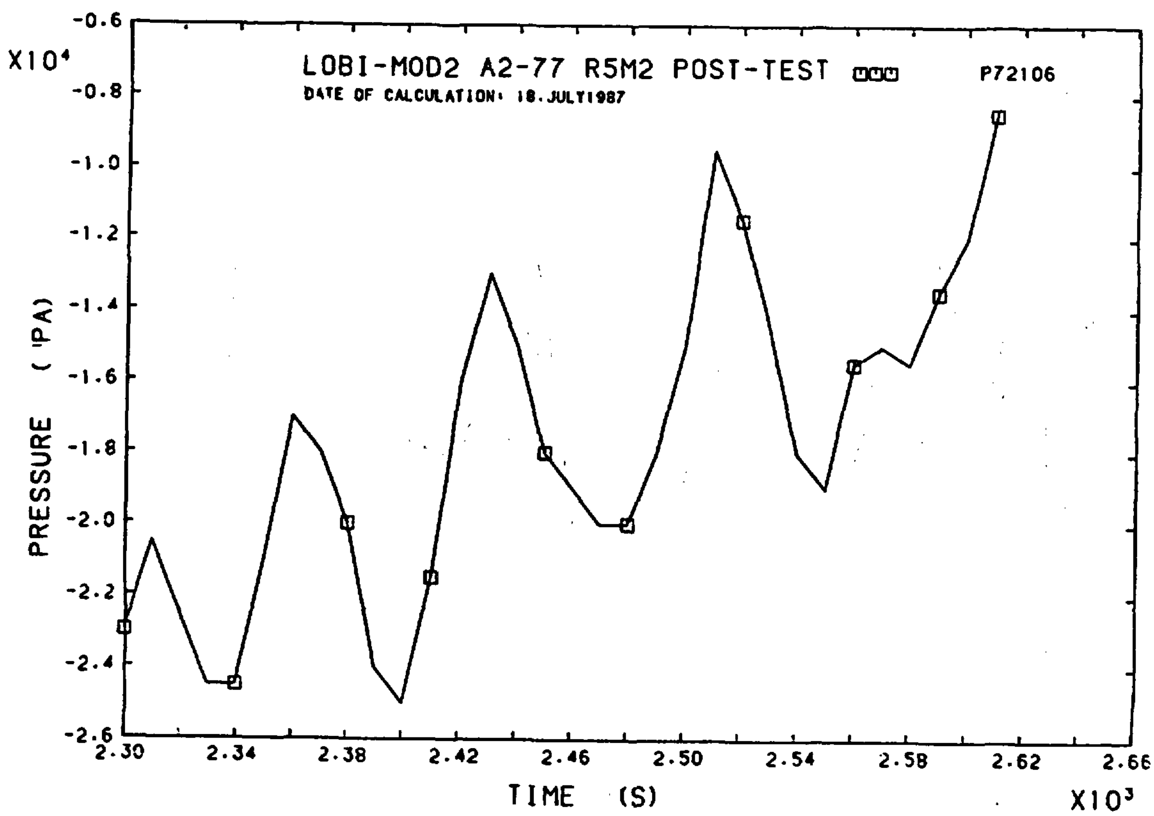

FIGURE D73 DIFFERENTIAL PRESSURE IN B.L. UT DESCENDING LEG LOWER TUBE

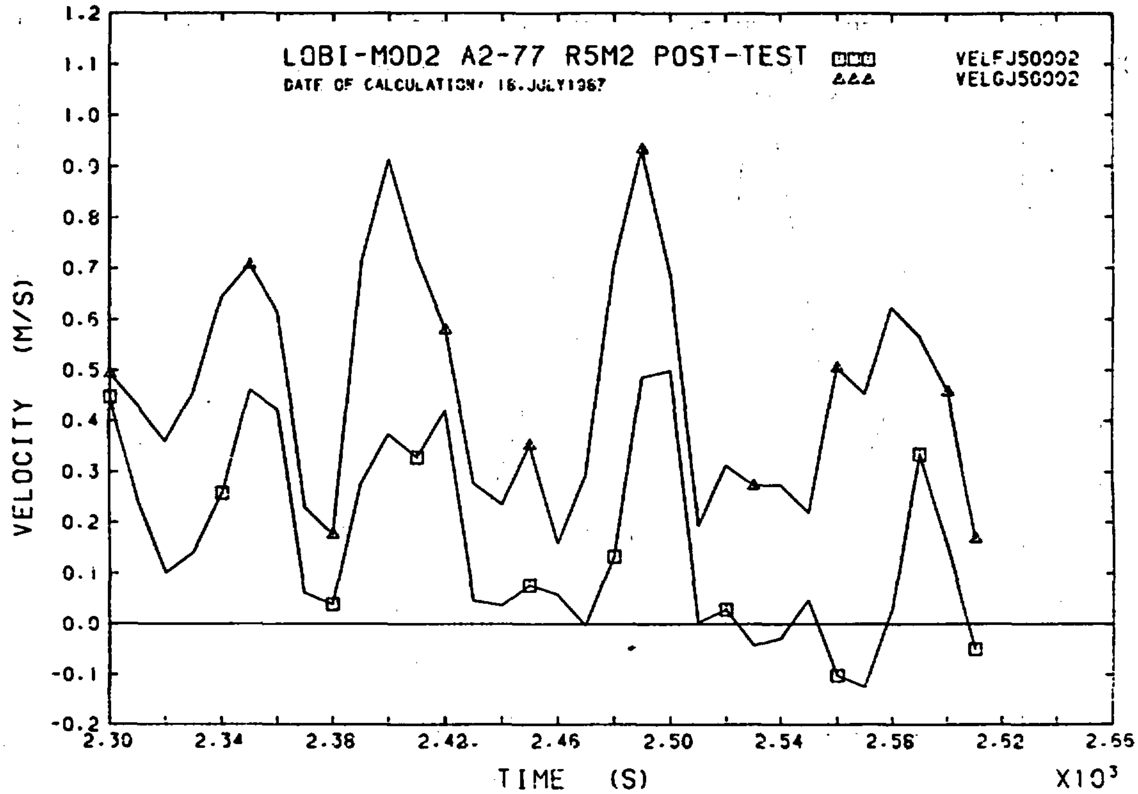

FIGURE D74 FLUID VELOCITIES IN TRIPLE LOOP H.L.

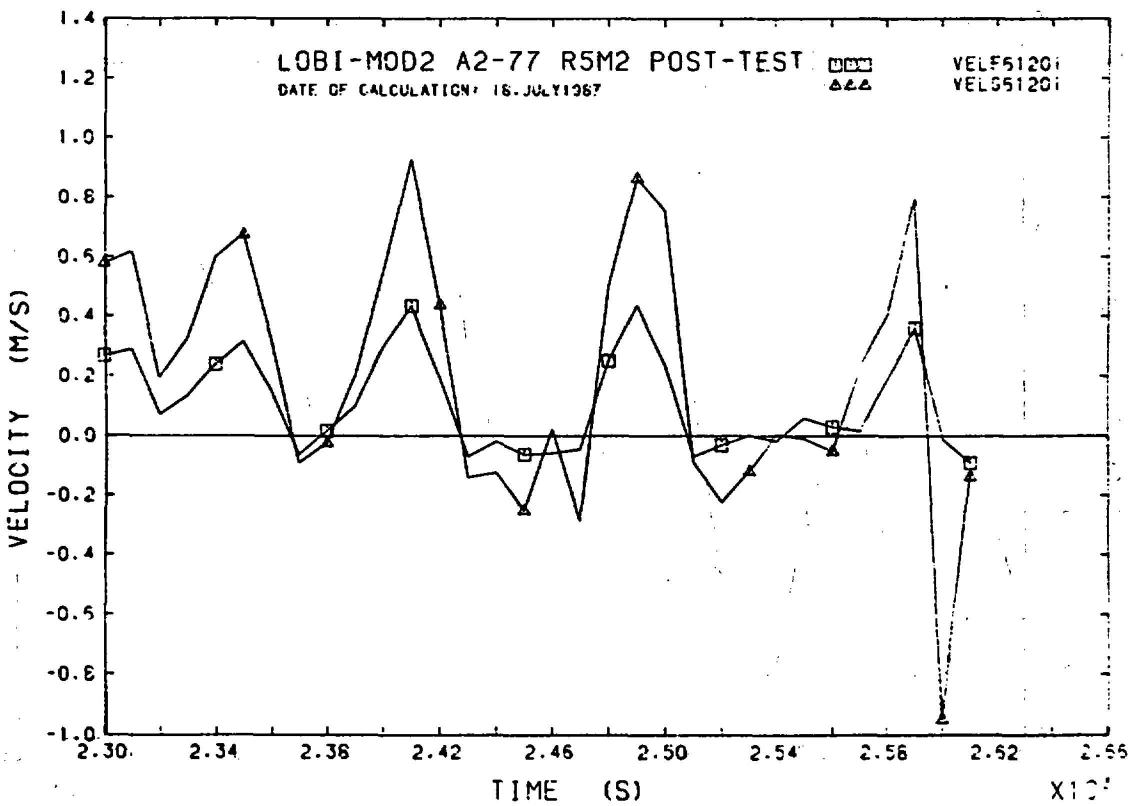

FIGURE D75 FLUID VELOCITIES IN TRIPLE LOOP C.L.

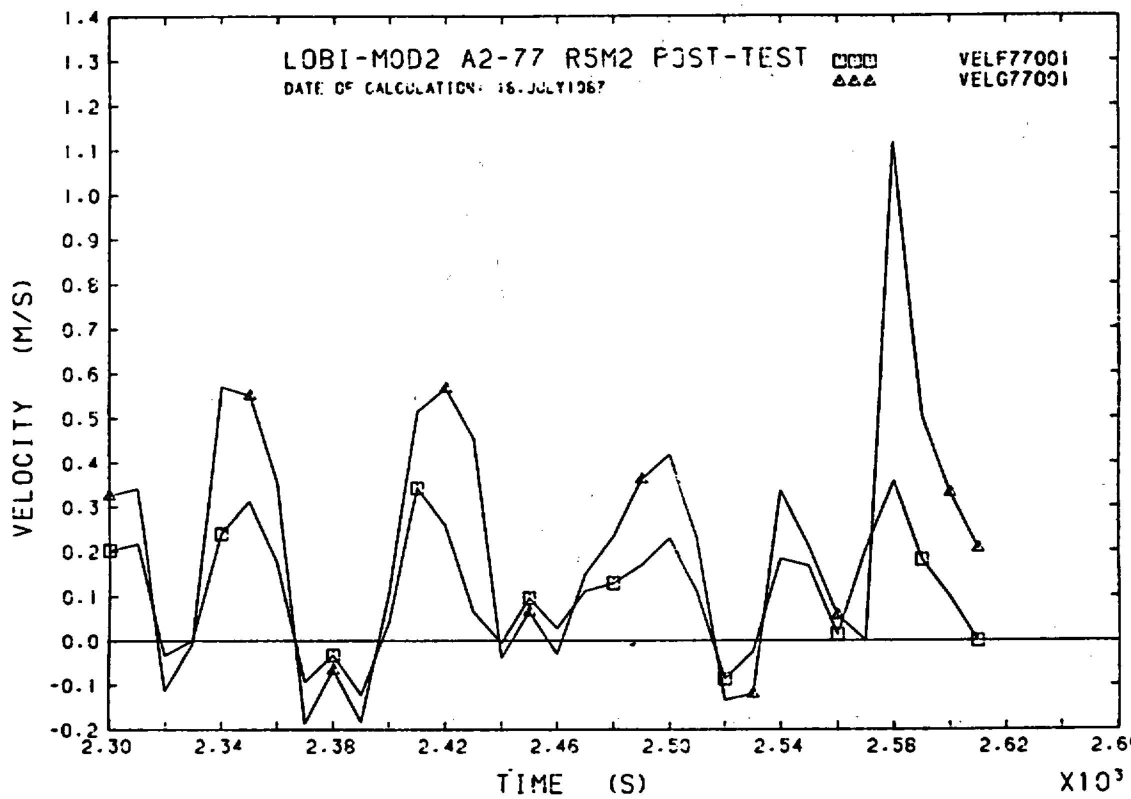

FIGURE D76 FLUID VELOCITIES IN SINGLE LOOP C.L.

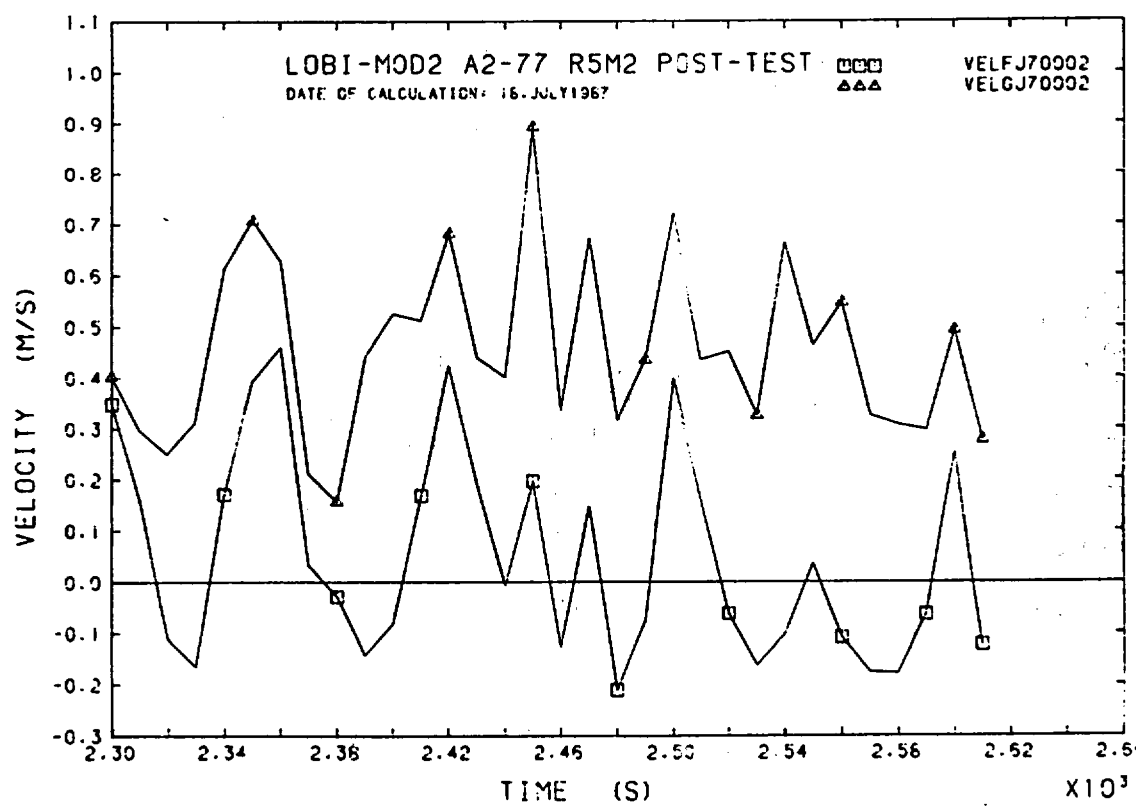

FIGURE D77 FLUID VELOCITIES IN SINGLE LOOP H.L.

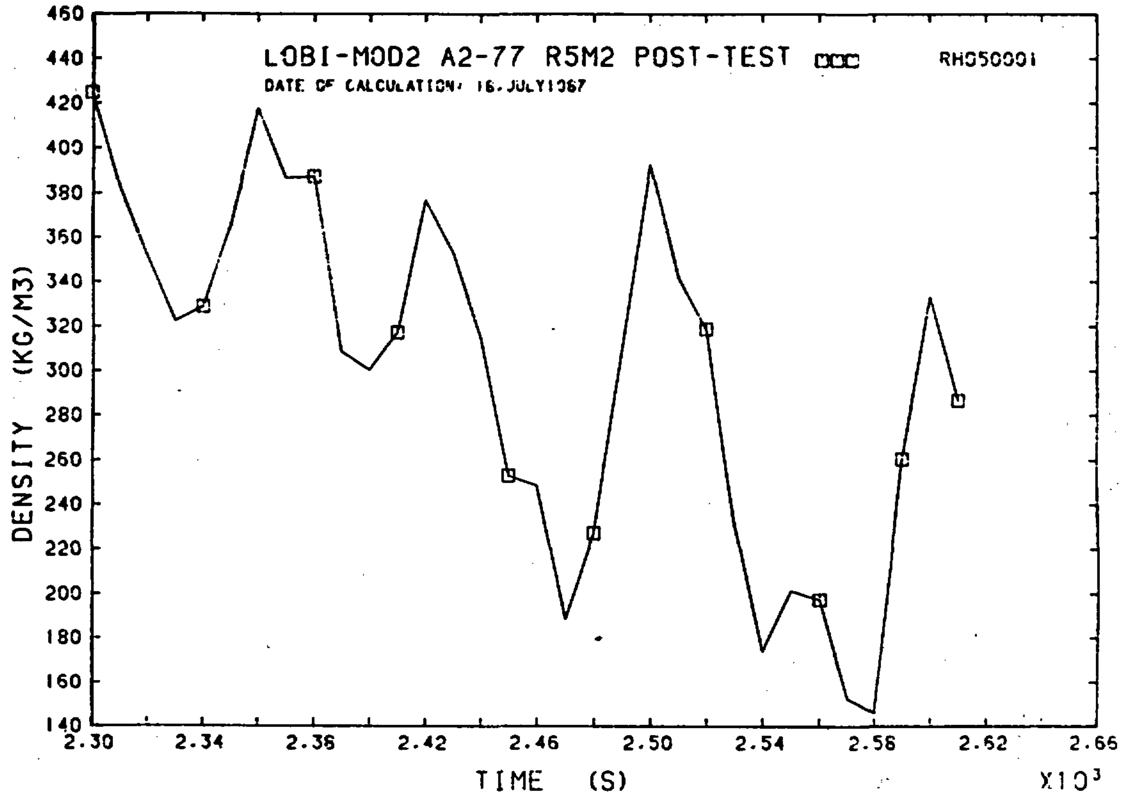

FIGURE D78 FLUID DENSITY IN I.L.-H.L.

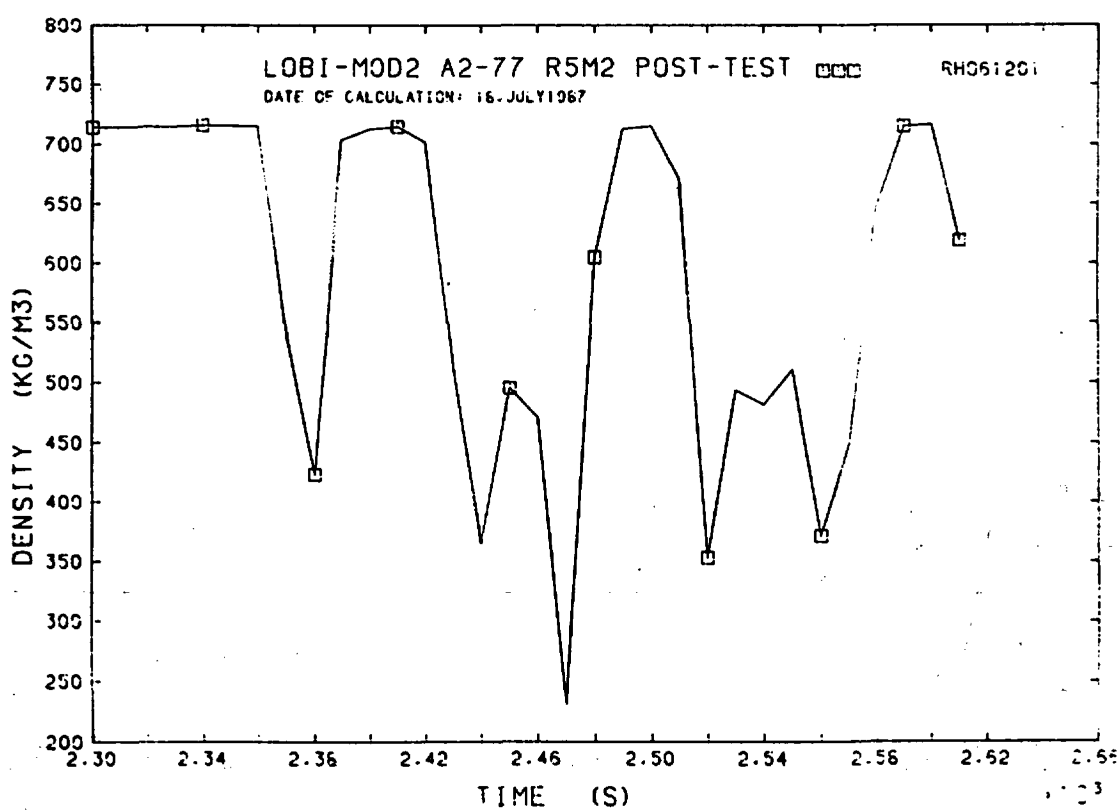

FIGURE D79 FLUID DENSITY IN I.L.-C.L.

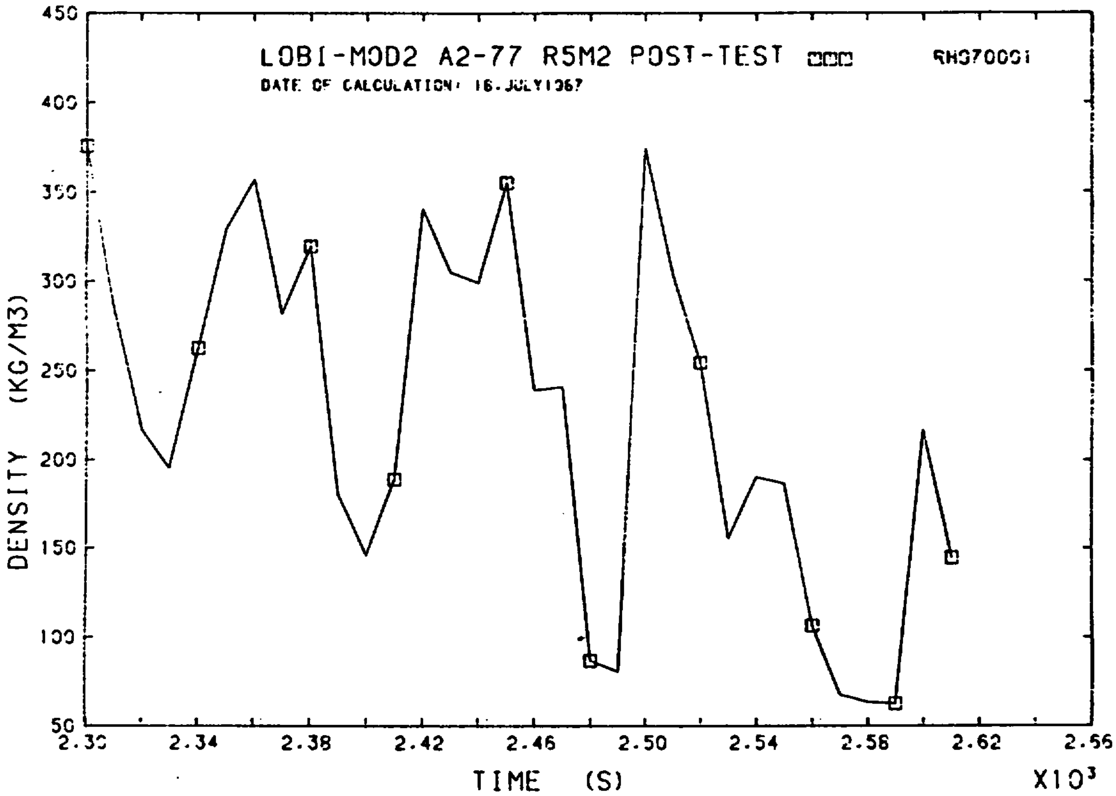

FIGURE D80 FLUID DENSITY IN B.L-H.L.

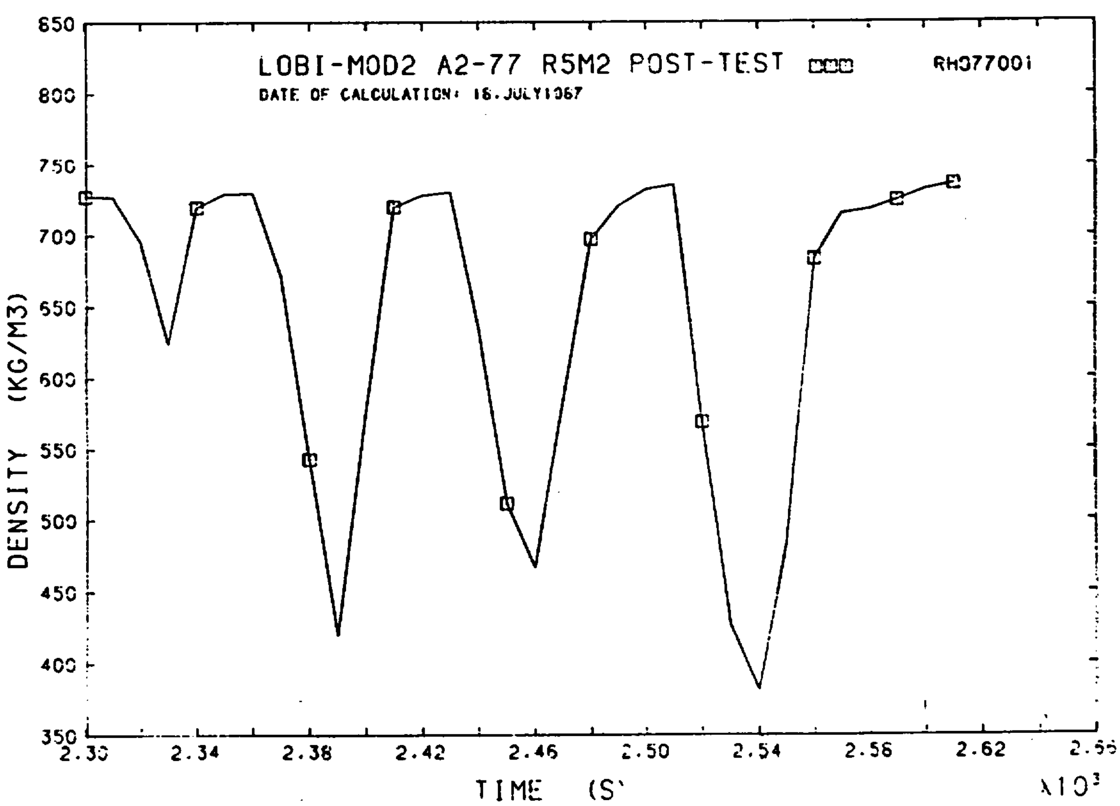

FIGURE D81 FLUID DENSITY IN B.L.C.L.

NRC FORM 335 (2-89) NRCM 1102, 3201, 3202

U.S. NUCLEAR REGULATORY COMMISSION

BIBLIOGRAPHIC DATA SHEET

(See instructions on the reverse)

1. REPORT NUMBER (Assigned by NRC. Add Vol., Supp., Rev., and Addendum Numbers, If any.)

NUREG/IA-0084
NT 163 (90)

2. TITLE AND SUBTITLE

Relevant Results Obtained in the Analysis of LOBI/MOD2 Natural Circulation Experiment A2-77A

3. DATE REPORT PUBLISHED

MONTH	YEAR
April	1992

4. FIN OR GRANT NUMBER

A4682

5. AUTHOR(S)

F. D'Auria, G.M. Galassi

6. TYPE OF REPORT

Technical

7. PERIOD COVERED (Inclusive Dates)

8. PERFORMING ORGANIZATION — NAME AND ADDRESS (If NRC, provide Division, Office or Region, U.S. Nuclear Regulatory Commission, and mailing address; if contractor, provide name and mailing address.)

Universita' Degli Studi Di Pisa
Dipartimento Di Costruzioni Meccaniche E Nucleari
Pisa, Italy

9. SPONSORING ORGANIZATION — NAME AND ADDRESS (If NRC, type "Same as above"; if contractor, provide NRC Division, Office or Region, U.S. Nuclear Regulatory Commission, and mailing address.)

Office of Nuclear Regulatory Research
U.S. Nuclear Regulatory Commission
Washington, DC 20555

10. SUPPLEMENTARY NOTES

11. ABSTRACT (200 words or less)

The present document describes the activities carried out at Pisa University to assess the RELAP5/MOD2 performance in the application to the natural circulation test A2-77A performed in LOBI/MOD2 facility. Sensitivity calculations have been performed in this context, with the attempt to distinguish the code limitations from the uncertainties of the measured conditions. The characterization of instabilities in two-phase natural circulation and the evaluation of the user effect upon the code results are special goals achieved in the frame of the A2-77A analysis. Both of these are discussed.

12. KEY WORDS/DESCRIPTORS (List words or phrases that will assist researchers in locating the report.)

RELAP5/MOD2
LOBI/MOD2
Natural Circulation Experiment A2-77A

13. AVAILABILITY STATEMENT

Unlimited

14. SECURITY CLASSIFICATION

(This Page)

Unclassified

(This Report)

Unclassified

15. NUMBER OF PAGES

16. PRICE

NRC FORM 335 (2-89)

THIS DOCUMENT WAS PRINTED USING RECYCLED PAPER

UNITED STATES
NUCLEAR REGULATORY COMMISSION
WASHINGTON, D.C. 20555

OFFICIAL BUSINESS
PENALTY FOR PRIVATE USE, $300

SPECIAL FOURTH-CLASS RATE
POSTAGE AND FEES PAID
USNRC
PERMIT NO. G-67